ABSTRACT

Title of Document: BILAYER LIPID MEMBRANE (BLM) INTEGRATION INTO MICROFLUIDIC PLATFORMS WITH APPLICATION TOWARD BLM-BASED BIOSENSORS

Louis Paul Hromada, Jr., Ph.D., 2007

Directed By: Associate Professor Donald L. DeVoe, Department of Mechanical Engineering

Bilayer Lipid Membranes (BLMs) have been widely used as an experimental tool to investigate fundamental cellular membrane physics and ion channel formation and transduction. Traditional BLM experimentation is usually performed in a macro-sized electrophysiology rig, which suffers from several well-known issues. First, BLMs have short lifetimes (typically on the order of tens of minutes to a few hours) and the laborious, irreproducible membrane formation process must be repeatedly applied for long-term testing. Second, stray capacitance inherent to traditional test rigs limits the temporal response leading, for example, to poor resolution in determining fast ion channel translocation events. Lastly, BLM testing is done within a single site format thus limiting throughput and increasing data collection time.

To mitigate the above drawbacks, BLM technology and microfluidic platforms can be integrated to advance the state-of-the-art of BLM-based biosensor technology.

Realization of BLM-based microfluidic biosensors can offer significant improvement towards sensor response characteristics (e.g. lower noise floor, increased time response). In addition, microfluidic biosensing chips can be fabricated with multiple BLM test sites that allow for parallel testing thus increasing data collection efficiency. Other benefits that microfluidics offer are: small reagent sensing volumes, disposable packaging, mass manufacturability, device portability for field studies, and lower device cost.

Novel polymer microfluidic platforms capable of both in-situ and ex-situ BLM formation are described in this work. The platforms have been demonstrated for the controlled delivery of trans-membrane proteins to the BLM sites, and monitoring of translocation events through these ion channels using integrated thin film Ag/AgCl electrodes. The detailed design, fabrication, and characterization of various micro-fabricated BLM platforms is presented in this dissertation.

BILAYER LIPID MEMBRANE (BLM) INTEGRATION INTO MICROFLUIDIC PLATFORMS WITH APPLICATION TOWARD BLM-BASED BIOSENSORS

By

Louis Paul Hromada, Jr.

Dissertation submitted to the Faculty of the Graduate School of the
University of Maryland, College Park, in partial fulfillment
of the requirements for the degree of
Ph.D.
2007

Advisory Committee:
Associate Professor Donald DeVoe, Chair
Assistant Professor Pamela Abshire
Professor Marco Colombini, Dean's Representative
Associate Professor Keith Herold
Assistant Professor Srinivasa Raghavan
Dr. Michael Gaitan, Special Member, NIST, Gaithersburg, MD.
Dr. John Kasianowicz, Special Member, NIST, Gaithersburg, MD.

Preface

A portion of this work was published in the Proceedings of the 10th International Conference on Miniaturized Systems for Chemistry and Life Sciences (μTAS), Tokyo, Japan, November 5-9, 2006.

Dissertation Organization

This dissertation is organized in the following way. In Chapter 1, the motivation behind developing BLM-based microfluidic biosensors is presented, which includes a brief introduction on how BLMs can be utilized for bio-sensing. In addition, issues associated with traditional BLM research are discussed followed by the potential advantages for leveraging microfluidics when conducting BLM research. Finally, a summary of the prior art that incorporates both BLM technology and microfluidics is given.

Chapter 2 provides additional background on BLM fundamentals, such as BLM structure and formation techniques. In addition, alpha hemolysin (α-HL) nanopores are introduced. Lastly, the BLM test chamber used at NIST (Gaithersburg, MD) is presented for modeling and comparison purposes.

Chapter 3 discusses BLM micro-device design, layout, and fabrication. Details such as choice of materials, microchannel sizes, and electrode layout are discussed. Finally, the micro-device fabrication procedure is outlined.

Chapter 4 summarizes the experimental results obtained from the BLM micro-devices. Details include BLM formation procedures, α-HL nanopore incorporation techniques, and PEG bio-sensing studies.

Chapter 5 presents contributions and offers future work suggestions towards BLM-based bio-sensors.

Finally, the appendices contain details on chip construction.

Dedication

To my beautiful wife, Erin, who supports me in every endeavor.

To my newborn son, Lucas, who shows me everyday why life is so amazing.

Acknowledgements

As with many endeavors, there are numerous people who provide "behind-the-scenes" support, whether it is academically, financially, emotionally, or all of the above. Many people helped out with this project, not because they had too, but because they wanted to see it succeed. In the end, it is this overwhelming support that truly makes a project successful.

First, I would like to thank my research advisor, D. DeVoe, and my NIST project leaders, M. Gaitan, and J. Kasianowicz, for their years of project guidance and for, of course, their financial support. Thanks to M. Colombini who provided some key insights and was always interested in hearing about the project. Also, thanks to P. Abshire, S. Raghavan, and K. Herold who participated on my committee.

A "big thank you" goes to my coworkers at the Maryland Microfluidics Lab. These are in no particular order: N. Sniadecki, C. Kimball, P. Kumar, J. Liu, L. Zhu, K. Tsao, J. Yang, J. Yi, K. Sahasrabudhe, and T. Ferguson. Also, thanks to REU summer students, D. Millard and J. Viren, whose hard work contributed greatly to the project.

My appreciation also goes out to the many NIST personnel who helped me. These are in no particular order: B. Polk, B. Nablo, J. Robertson, J. Reiner, E. Chan, M. Misakian, D. Reyes-Hernandez, L. Locascio, J. Wilkes, W. Vreeland, J. Shah, S. Forry, G. Mijares, C. McGray, and A. Jahn. Also, thanks to G. Henein and R. Hajdaj at the NIST AML who helped me with chip fabrication. Lastly, thanks to J. Anderson in the NIST glass shop for the glass brush fabrication.

Lastly, thanks to my mom and dad, my brother Tom, and his wife, Tiffany, who provided many years of behind-the-scenes support. Finally, thanks to J. Manzari, E. Crown, K. Kefauver, and D. Cantor, who provided many ideas and listened to my "issues" over the years without complaint. An additional thank you to K. Kefauver, who helped create the control electronics for the film hole burner.

Table of Contents

List of Tables

List of Figures

Chapter 1 BLM-Based Microfluidic Biosensors

Bilayer Lipid Membranes (BLMs) are considered the building blocks of life because many cell structures (e.g. cell walls, nucleus, mitochondria, etc) are composed of BLMs. BLMs are highly impermeable to ions, such as Na^+, K^+, Ca^{2+}, and Cl^-, yet critical cell functions rely on movement of these ions across the BLM. One way to facilitate rapid ion movement across the BLM is to incorporate trans-membrane channels. A trans-membrane ion channel, or nanopore, is an aqueous tunnel through the BLM thickness which allows contiguous connection between the opposing sides of the BLM. Research conducted with synthetic BLMs and ion channels have offered clues on how cellular functions and activities are carried out on a simpler scale, since cell walls tend to be complex in nature [1, 2]. This research has lead to realize BLMs and ion channels as possible biosensors capable of single molecule detection.

This chapter discusses the motivation for this research. First, an overview of biosensing with BLMs is presented. Next, traditional BLM experimentation issues are discussed followed by the advantages of conducting such research in microfluidic platforms. Lastly, prior art containing previously reported microfluidic works utilizing BLMs is presented.

1.1 Bio-sensing with BLMs

Consider a BLM, shown in Figure 1a, separating two distinct volumes of aqueous salt solution. Assuming the BLM acts as an ideal insulator, ion translocation will not occur in the membrane's native state. However, if an ion channel

incorporates within the membrane, a conducting and hydrophilic pathway across the membrane's hydrophobic interior is produced. Ion transport through the channel's nanopore can be due to diffusion or by electrokinetic actuation. When an electric field is applied, a steady-state conductance through the pore is realized as indicated by the green arrow in Figure 1a. After introducing analyte A into the salt solution left of the BLM, analyte A will pass through the nanopore if certain conditions are met. As analyte A passes though the nanopore, temporary states of lower conductance are created. These lower conductance states, known as blockades, appear as temporary changes in nanopore current like seen in Figure 1a.

If a different analyte is also present in the left volume, analyte B may translocate through the nanopore resulting in current blockades differing in depth and duration compared to analyte A, as shown in Figure 1b. Since each molecule produces different blockade depth and duration, molecular signatures may be used to identify specific analytes passing through the nanopore. Analytes too large to traverse the nanopore may also produce a blockade signature useful for identification by temporarily occluding the nanopore entrance.

A specific biosensor example that conducts base identification of single-stranded DNA (ssDNA) is shown in Figure 1c. In this case, ssDNA passes through the nanopore while the channel current is being monitored. Four conductance states, other then the baseline, result from the ssDNA bases passing through the pore, as described by Kasianowicz et al. [3-7], and others [8-18]. The above ssDNA biosensor is hypothetical and has not been realized due to multiple conductance states per base and poor temporal resolution in sequencing.

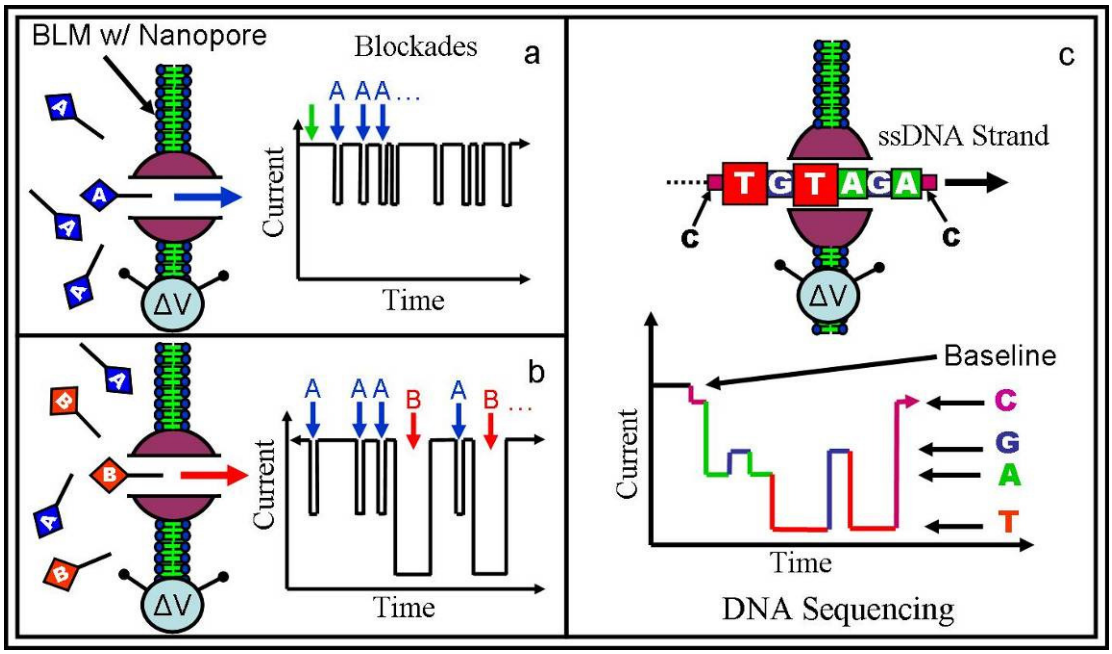

Figure 1: BLM biosensor examples. (a) A simple BLM biosensor with analyte A only, (b) Same biosensor later with analyte B introduced, and (c) A potential biosensor example showing ssDNA sequencing with a nanopore [6].

1.2 Traditional BLM Platform Issues

Traditional macro-scale BLM electrophysiology research suffers from several well-known issues: 1) BLM lifetimes are short. 2) BLM formation techniques are laborious and are subject to human variation, and 3) data collection throughput is limited. These are discussed below.

BLMs are marginally stable structures, thus BLM lifetimes are relatively short and depend on testing and environmental conditions including: 1) osmotic pressure difference across the membrane, 2) hydrostatic pressure difference across the membrane, 3) applied electrical field strength, and 4) choice of BLM composition, among others. As expected, BLM lifetimes reported in the literature vary widely. Under different testing conditions, reported BLM lifetimes range from 50 hours [19], 24 hours [20], 12 hours [21], < 8 hours [22], 1 hour [23], and 10-30 minutes [24].

Depending on the formation process, a BLM can take hours to form properly, thus some BLMs will rupture even before data collection starts.

BLM formation can be a laborious undertaking especially if long-term testing is required. If a BLM ruptures prior to completing a certain task, the experiment may have to be reset thus costing valuable testing time. In addition, BLM formation is usually done manually thus process variation is introduced further complicating the experimental challenge.

Data collection throughput is also limited since only a single experiment can be performed at a given time unless multiple test chambers are set up in parallel. Having multiple test chambers means: 1) more capital expenses spent on the associated electronics, 2) more real estate is required to house multiple test chambers, 3) more personnel to run multiple test chambers, etc.

1.3 Potential Advantages of Integrating BLMs into Microfluidic Platforms

Creating microfluidic platforms capable of sustaining BLM formation and testing has eight potential advantages. Table I, below, summarizes the advantages and then each advantage is explained in detail afterward.

Table I: Potential Advantages of Integrating BLMs and Microfluidics

1) Reduced Reagent Volumes
2) Disposable Chips and Mass Production
3) Device Specialization
4) Faster Dynamic Response
5) Reduction of System Noise
6) Improved BLM Stability and Lifetimes
7) All Inclusive Devices
8) Array Devices / Parallel Testing

1) Microfluidic devices provide small fluid volumes, in order of nanoliters, which could aid researchers when incorporating ion channels into BLMs. Typically, researchers only want a single ion channel to incorporate into a BLM and then the channel solution is flushed. The perfusion time required to flush the remaining ion channel solution in a microfluidic device will be much faster versus the macro-sized BLM test chamber, which typically has a volume on the order of milliliters.

2) Microfluidic devices can be mass produced (e.g. injection molding, hot embossing, etc) thus giving BLM researchers the option of using new devices for every experiment so as to prevent cross contamination of experimental solutions.

3) Microfluidic devices can be tailored to meet specific test requirements. For example, an injected reagent may need incubation prior to sending it towards the BLM site, or variable temperatures may be desired to study the kinetics of biopolymers threading through a nanopore. Incorporating a micro-heater into a microfluidic design may be more practical than doing so in a macro-scale chamber thus allowing localized heating and faster thermal response times.

4) The dynamic response of the BLM micro-device may be made superior to macro-scale BLM testing platforms because miniaturization techniques associated with microfluidic fabrication can create optimal design conditions previously unobtainable with macro fabrication methods. An increase in the system's bandwidth would allow transduction of fast gating events, such as DNA sequencing.

5) Reducing the system capacitance should, in theory, yield an improvement on noise signals according to Whitesides et al. [25] and Wonderlin et al. [26]. Whitesides identifies that BLM test platforms typically suffer from a combination of

shot noise, Johnson noise, 1/f noise, dielectric noise, thermal voltage noise, and headstage input voltage noise, where the first three components are considered small compared to the latter three. The supporting film capacitance is contributor to dielectric noise and headstage input noise, thus reducing its capacitance is beneficial. However, reducing the supporting film capacitance may not yield an overall reduction in noise because noise components sum in an RMS fashion where the largest component dominates the overall noise signal. Empirical testing will need to be done.

6) BLM integration into microfluidics will inherently produce smaller BLM sizes because a byproduct of MEMS research is to push miniaturization limits on making devices as small as possible. If smaller devices mean smaller BLMs, then BLM stability/lifetimes might improve because they are inversely proportional to BLM diameter. By marrying the two technologies (microfluidics and BLM testing), future researchers may be able to extend the limits of BLM research and electrophysiology.

7) System level benefits can be realized with microfluidic devices not possible with traditional BLM platforms. For instance, future microfluidic chips could house, deliver, and flush reagents to the BLM site when required and they could perform automated BLM formation if needed. Field deployment of microfluidic devices may be possible due to their portability, integrated electrodes, etc.

8) Additional advantages can be leveraged by utilizing microfluidic chips that house multiple BLM sites. For example, an analyte sample could be injected into a

multiple-site BLM microfluidic biosensor and divided up into N samples, where N equals the number of BLM detection sites. This would allow parallel testing of the same analyte as illustrated in Figure 2a. Two detection schemes could be utilized in this case. Each BLM site could be testing the analyte for different objectives or a primary BLM site could be testing and identifying the analyte. The extra BLM sites could be planned redundancy merely checking the validity of primary site's conclusion.

Another advantage a BLM array chip offers is the ability to perform parallel identification of multiple analytes. For example, an analyte cocktail consisting of three unknowns (A, B, & C) can be injected into a microfluidic biosensor, as shown in Figure 2c. Separation of the analyte cocktail into its individual constituents can be performed by electrophoresis, or other means. After the analytes are separated, each individual analyte plug could be towards a different BLM site. At this stage, each BLM site could perform the same tasks but on different analytes. Note, that once the analytes are directed to the respective channels post-electrophoresis, the new analyte plugs could be divided again as done in Figure 2a or b. In conclusion, the array design complexity is limitless provided that the necessary operations (plug division, electrophoresis, fluid control, and transduction) are reliable.

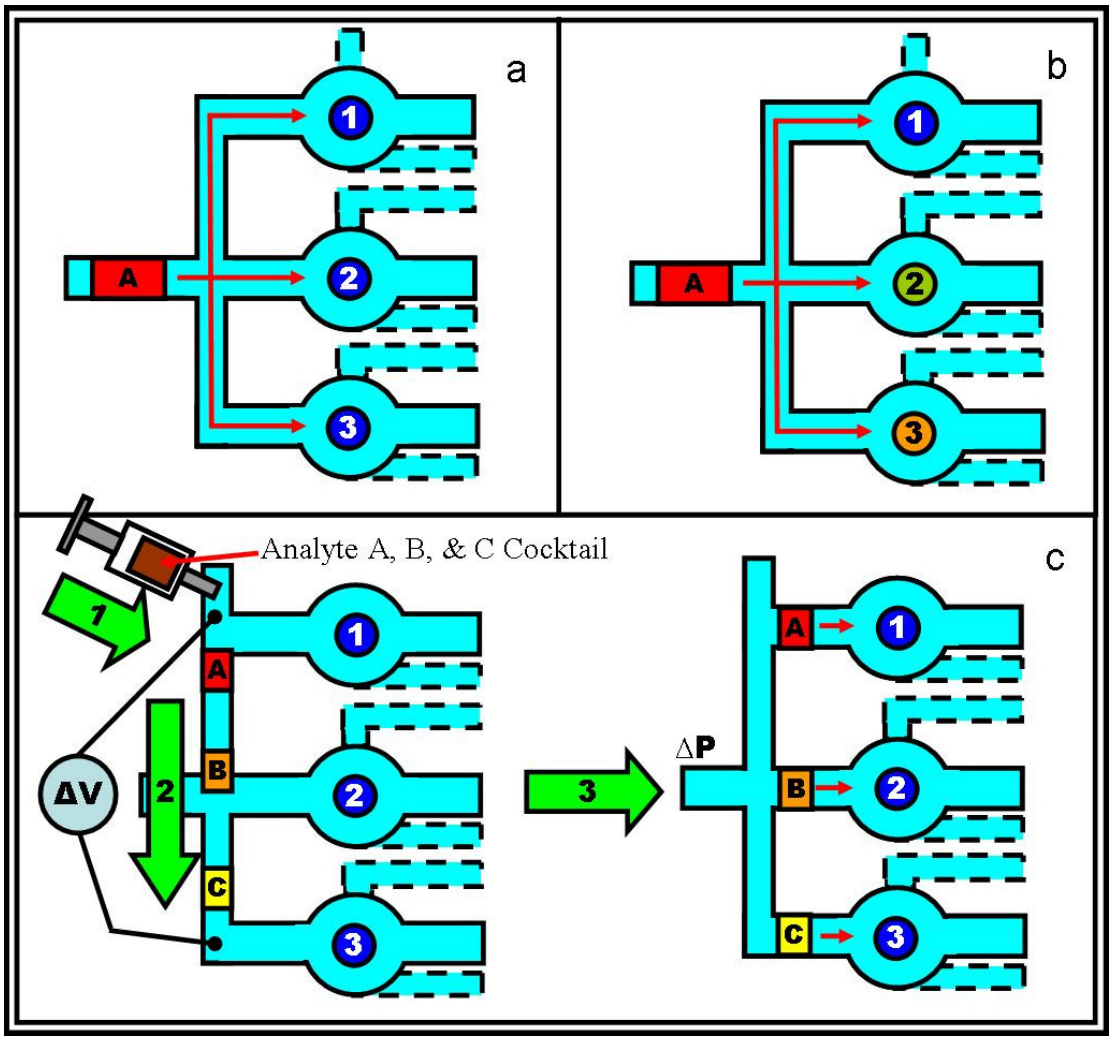

Figure 2: Illustrated advantages of BLM array devices. (a) Primary BLM site with two redundant sites testing analyte A for same objective, (b) Multiple BLM sites testing analyte A for different objectives, and (c) Multiple BLM sites testing various analytes post-separation from an analyte cocktail.

1.4 Prior Art of Microfluidic Works Utilizing BLMs

Suzuki et al. first reported in-situ BLM formation inside a microfluidic system in 2004 [27, 28]. Their system consisted of a silicon and glass sandwich as shown in Figure 3a. The same group demonstrated an open air array platform fabricated from silicon and glass (Figure 3b) and a similar system fabricated from polymethyl-methacrylate (PMMA) chip (Figure 3c).

The first Suzuki device reported, Figure 3a, consists of a glass/silicon/glass sandwich [27, 28]. Device fabrication is done using a combination of Deep Reactive Ion Etching (DRIE) and Tetramethylammonium hydroxide (TMAH) anisotropic etching to form channels on the front and back side of a Si wafer. The aperture, where the BLM formation occurs, is anisotropically etched hence is square in shape instead of circular. A Parylene coating is deposited over the machined Si wafer for electrical insulation and noise reduction. To complete the device, glass sheets, with patterned electrodes and via holes for fluid interconnects, are bonded to both sides of the machined Si wafer. This particular device contained multiple BLM sites (1 x 3).

Another array device [27, 28], shown in Figure 3b, is fabricated almost the same exact way as the first device. This particular device has a series of open air 3 x 3 wells where individual BLMs are created manually. To form BLMs, buffer solution is injected into the microchannels on the machined Si wafer underside, which are sealed by bonding a glass sheet. The buffer flows up to the etched aperture, but does not go through due to surface tension. A syringe pump is then used to manually pipe 10 nL of lipid solution into each well and the lipid is allowed to thin. A 1 mL drop of buffer is then placed manually over the lipid solution in each well to complete the BLM formation.

A PMMA chip [29] demonstrated by Suzuki et al. employs the same essential design as their previous Si/glass device. Overall device dimensions, especially channel dimensions, were not specified but channels appear to be 5 mm wide. The BLM supporting structure in this case is fairly thick PMMA sheet (2 mm). A drilling operation is performed to carefully create a conical well and aperture where the BLM

formation occurs. Incorporation of alamethicin [29], gramicidin [30], and α-HL [31] channels have been demonstrated in these PMMA devices. In a later work, Suzuki et al. demonstrates a similar chip with multiple BLM sites in a PMMA chip [32] as shown in Figure 3c. The same group has also reported a microfluidic device where a BLM can be formed along the microchannel length by contacting monolayers of lipid solutions [33].

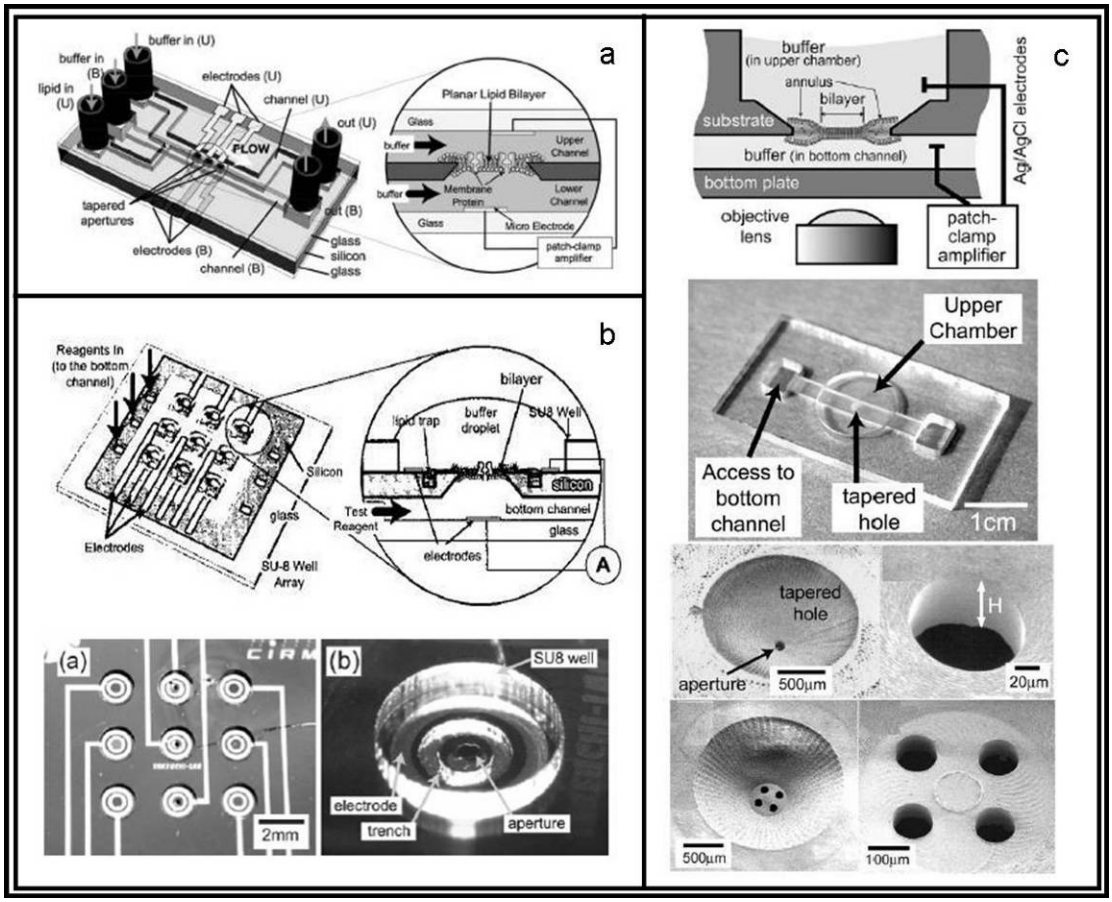

Figure 3: BLM microfluidic chips reported by Suzuki et al. (a) Multiple BLM array chip constructed from glass and silicon [27], (b, top) Well array chip (3x3) [28], and (b, bottom) details of Wells [27], (c, top and middle) BLM chip constructed from PMMA, and (c, bottom) Close-up of BLM formation sites [32]. Credits: (a and b, bottom) Reprinted with permission of The Royal Society of Chemistry. (b, top) © 2004 IEEE. (c) Reprinted with permission from [32], © 2006 American Chemistry Society.

In related work [34], Sandison et al. reported creating a 50 µm aperture capable of BLM formation in a Si/SiN wafer. After depositing a PECVD insulation layer, the wafer was then bonded to two pieces of glass to form an open well chip and Ag/AgCl wire electrodes were immersed into the fluidic reservoirs for electrical recordings. In addition, Sandison showed gramicidin nanopores incorporated in the BLM. However, Si-based substrates have limitations in that they are fragile and have large shunt capacitances due to the thin layers applied to insulate the aperture [35].

Sandison et al. [35, 36] demonstrated a polymer-based microfluidic chip utilizing hot embossed PMMA plastic films. Prior to chip assembly by solvent and thermal bonding, an aperture (50-100 µm in diameter) is fabricated in one of the embossed plastic layer by a laser. Electrical measurements were conducted by placing Ag/AgCl into the 500 µm wide microchannels. Sandison, also showed gramicidin nanopores incorporated into the BLM; however specifics such as gramicidin concentration and how the gramicidin was added were omitted. Building on their previous work, Sandison et al. show MthK channel incorporation in a BLM previously formed using a similar PMMA chip. The MthK channels were delivered to the BLM by a salt gradient across the BLM which promoted liposome fusion [37].

In the last work reported by Sandison et al [38], existing fabrication methods, set forth previously in [35, 36], are utilized to yield a PTFE/glass microfluidic chip. The embossed PTFE contains a laser-machined aperture at which BLM formation occurs, see Figure 4 for chip section. Electrode placement was not clearly defined but assumed to be immersed at the reservoirs as in previous work.

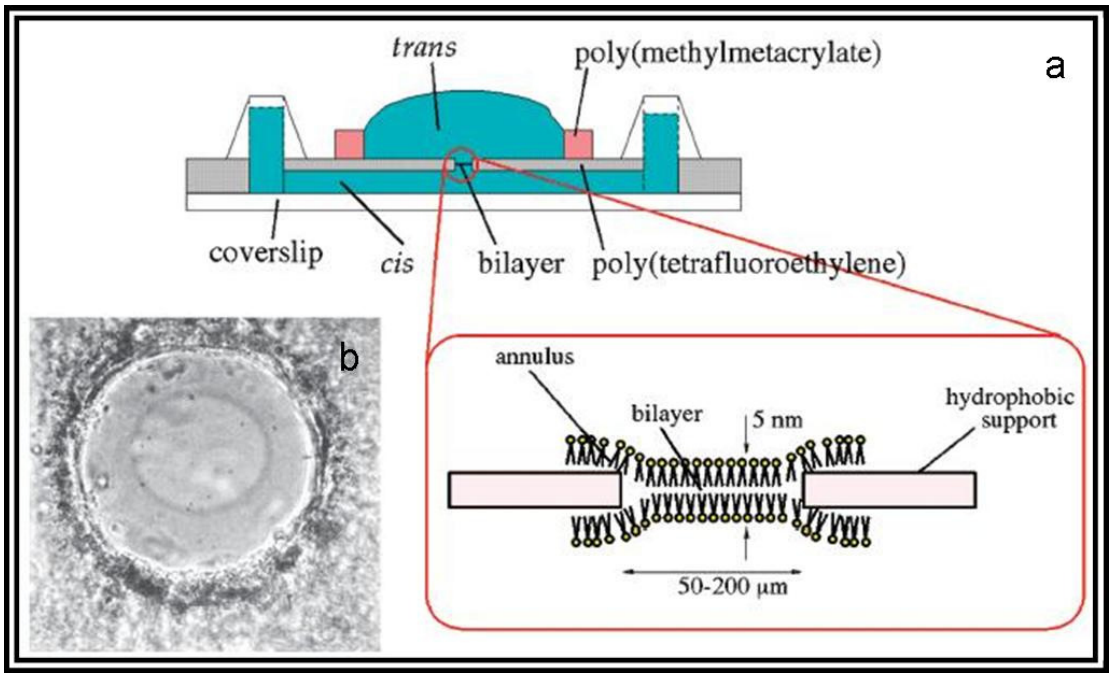

Figure 4: Microfluidic chip constructed by Sandison et al. [38]; Reprinted with permission from IEE Nanobiotechnology.

A different approach to BLM formation in a polymer microfluidic chip was developed by Malmstadt et al. [39, 40]. In this work, a Polydimethylsiloxane (PDMS) microfluidic device was used to reconstitute BLMs by absorbing excessive organic solvents into the bulk polymer, thus allowing BLMs to form automatically along the microchannel's length. Typically, BLMs formed through the painting method (discussed in Section 2.1.b) are plagued with poor formation repeatability mainly because excessive organic solvent prohibits proper BLM thinning. By leveraging PDMS's inherent solubility properties, Malmstadt carefully selects the lipid carrying organic solvent so that any remaining organic solvent will slowly diffuse away into the bulk PDMS microchannel surroundings.

Figure 5a illustrates the solvent extraction method reported by Malmstadt. Here, a plug of organic solvent dispersed with lipid is sandwiched between two aqueous phases as shown. Continually diffusing into the PDMS sidewall, the organic

solvent amount decreases with time. On the contrary, the lipid molecules cannot partition into the sidewall. After some time, a BLM forms as illustrated.

The PDMS device that Malmstadt created is shown in Figure 5b. This two layer device utilizes one layer for the microfluidic plumbing (blue lines), while the second layer houses means for fluid control by valve actuation (red lines) developed previously by Quake et al. [41, 42]. The elliptical-shaped microfluidic channels are 100 µm major width by 70 µm minor width. Ag/AgCl electrode wires are cast in place as the PDMS cures and their location is indicated by the number "4" in Figure 5b. BLM formation occurs to the right of the number "4", as indicated by the rectangular box. Finally, Malmstadt reported α-HL channel incorporation using an identical chip in [40].

BLM formation along a microchannel length has a few disadvantages: 1) Fluids cannot be streamed past the BLM as with other designs. If analytes were to be delivered to the BLM site, a diffusion process would govern how fast analytes would reach the BLM site, and 2) Any differential pressure across the BLM will cause the BLM to travel along the microchannel length.

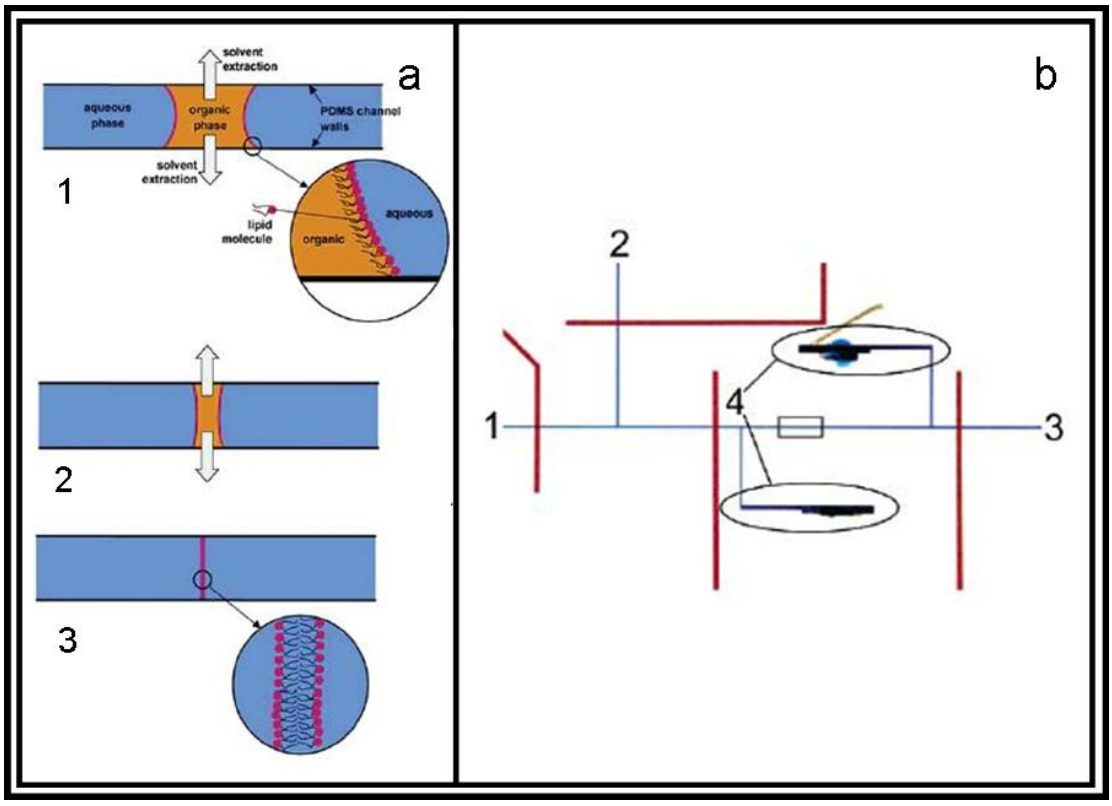

Figure 5: Work reported by Malmstadt et al. (a) Mechanism for BLM formation by solvent extraction method. See text for details, (b) Photograph of microfluidic device injected with food dye for clarity. Reprinted with permission from [39]; Copyright 2006 American Chemical Society.

1.5 Commercial BLM Testing Products

A survey of commercially available BLM testing products was conducted to ascertain the state of current products sold. Two companies (Harvard Apparatus [43], and Warner Instruments [44]) sold workstations designed specifically for planar BLM testing. These platforms, modeled after electrophysiology systems reported in the literature [45-47], are very similar to the test chamber employed by our NIST collaborators, which is discussed in Section 2.2.

The search turned up one viable commercial product made by Nanion Technologies, GmbH. Nanion claims that their product, Port-a-Patch NPC-1, is the world's smallest automated patch clamp setup [48] and is capable of performing

single-site testing with planar BLMs formed by painting or vesicle fusion [49]. The Port-a-Patch NPC-1 is shown below in Figure 6, having the dimensions of 17.5 cm x 9 cm x 7.5 cm, and weighs 1.42 kg according to [48]. The system utilizes lab vial caps for disposable test chips, which contain a glass substrate that has been micro-machined to create a micron-sized aperture where the BLM formation occurs. Caps are available with aperture sizes from 1 to 50 μm [49]. Fabrication details regarding the glass chips are provided by Fertig et al. [50-52] . Additional testing details when using the Port-a-Patch are provided elsewhere [53, 54]. Incidentally, Nanion offers a testing workstation, the NPC 16 Patchliner, which utilizes different disposable array chips containing microfluidic channels. The four-site array chips are a perfusion-based design utilizing <15 μL of solution and has interfacing for robotic pipetting [54, 55].

A Port-a-Patch NPC-1 was purchased by John Kasianowicz' group at NIST (Gaithersburg MD). Solely using the system for planar BLM testing, results have been elusive mainly due to BLM formation and lifetime difficulties. Creating BLMs via vesicle fusion has been problematic due to the inability to create appropriate-sized liposomes even when following Nanion's specifications. When using painting methods for BLMs formation, the traditional issues associated with painting methods still prevail (discussed in Section 2.1.b). So far, the Port-a-Patch NPC-1 has not alleviated the testing difficulties associated with BLM research [56].

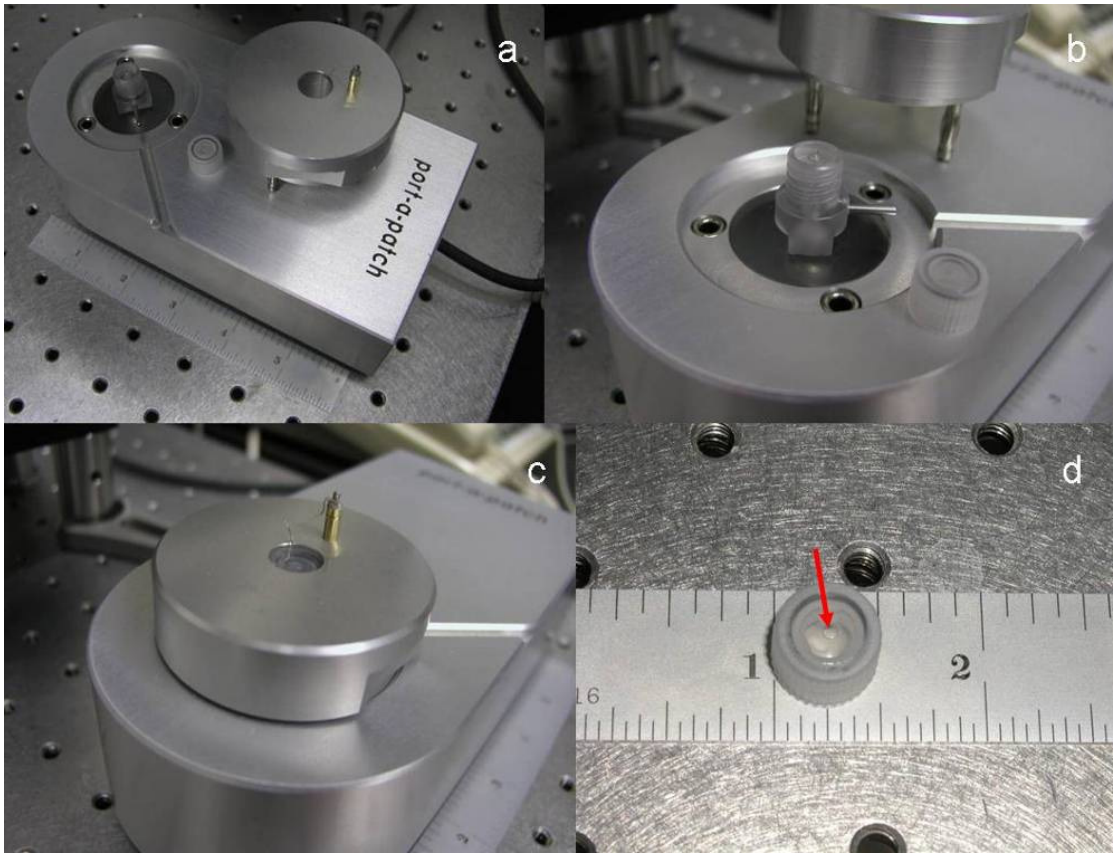

Figure 6: Port-a-Patch NPC-1 from Nanion Technologies, GmbH. (a) Iso-view of the Port-a-Patch with top and disposable chip removed, (b) Another iso-view showing detail of chip testing site with top removed, (c) Same view with top attached, and (d) Detail of disposable chip which contains a glass substrate with 20 µm diameter hole for BLM testing at red arrow.

Chapter 2 BLM Fundamentals

This chapter introduces BLMs basics, such as BLM definition, composition, and structure. Also presented are typical BLM formation techniques used by researchers. An overview of alpha-hemolysin (α-HL) nanopores is provided along with polyethylene glycol (PEG) which is used for testing the BLM micro-devices. Finally, the NIST test chamber is reviewed for comparison and modeling purposes.

2.1 BLM Background

2.1.a BLM Structure and Composition

Cells produce many lipids for various functions, but phosphoglycerides, commonly called phospholipids, are the major constituent of BLMs. As illustrated in Figure 7a, a BLM consists of many phospholipids arranged side-by-side forming a single monolayer which extends in all directions on the monolayer plane. When two monolayers are assembled together with their hydrophobic tails facing each other, a bilayer is formed [57, 58].

A phospholipid is shown in Figure 7b and c and each molecule consist of 4 parts [59]: 1) The non-polar fatty acid tails, 2) A phosphorous group, 3) A head group, and 4) A glycerol backbone connecting everything together. For example, the phospholipid shown in Figure 7 is Diphytanoyl Phosphocholine (DiPhyPC), which consists of two Phytanoyl tails and a Choline head group. There are many phospholipids but DiPhyPC is utilized in this research since DiPhyPC is reported in the literature for successful BLM formation [3, 4, 6, 60]. For information on DiPhyPC, see [61].

Phospholipids are amphipathic molecules having both hydrophilic (polar) and hydrophobic (non-polar) regions. Hydrophobic means "water hating" and hydrophilic is the opposite, (i.e. "water loving"). Phospholipids can be broken down into two major regions: 1) The hydrophobic fatty acid tails, and 2) the hydrophilic head group as shown in Figure 7c. For simplicity, a cartoon version of a phospholipid is shown in Figure 7d, where the round blue circle signifies the hydrophilic head group and the two black lines are the hydrophobic tails. Extending this cartoon model further, the cartoon bilayer is displayed in Figure 7e along with the associated regions of hydrophobicity. This cartoon bilayer will be used to represent BLMs in future figures.

Lipids tend to aggregate to avoid unfavorable contact of their hydrophobic regions with water. By associating together to minimize their energy, biological structures, such as planar BLMs, micelles, or liposomes, can be formed. Micelles are spherical lipid formations where the interior consists of hydrophobic media. Liposomes are also spherical lipid formations but have a hydrophilic interior. Due to the lipid's shape, certain structural formations are preferential over others. For instance, single tail lipids (conical packing shape) tend to aggregate into liposomes and double tail lipids (cylindrical packing shape) prefer to form planar BLMs [62].

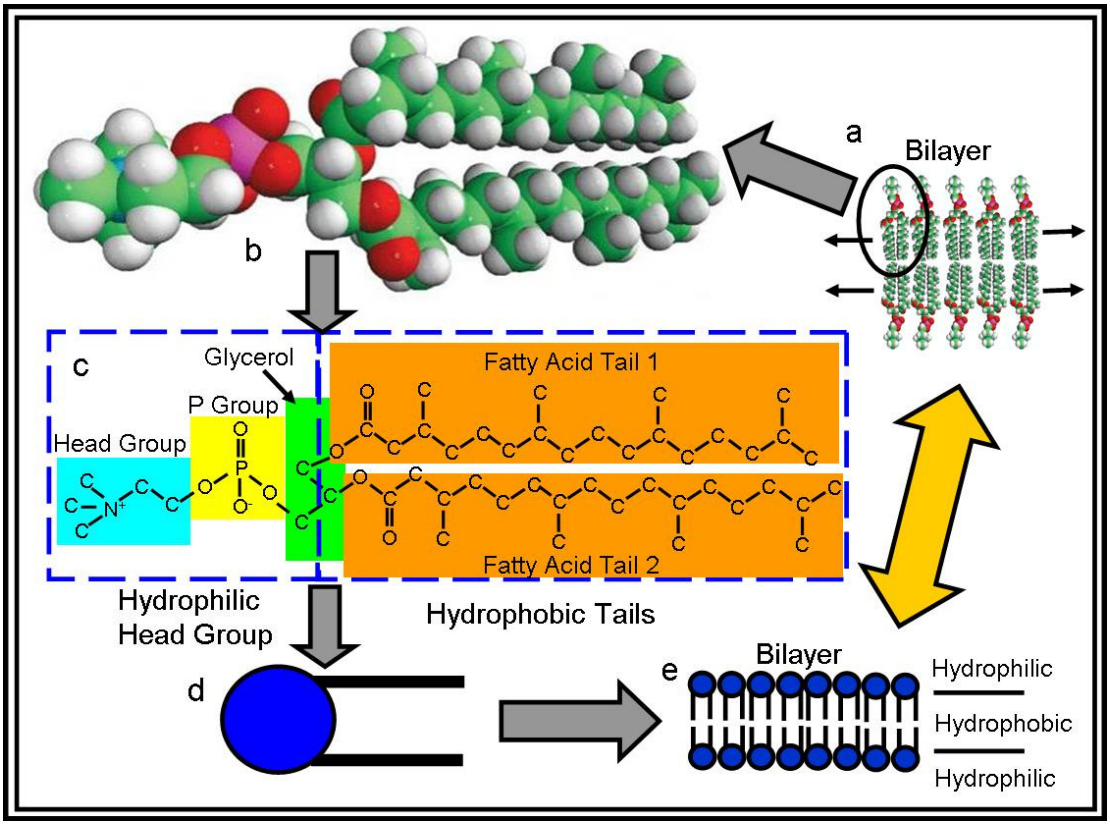

Figure 7: (a) An example BLM consisting of DiPhyPC, (b) Space-filled 3D model of DiPhyPC [61], (c) Kekule structure outlining the various groups, (d) A cartoon lipid molecule, and (e) Cartoon BLM.

2.1.b Traditional BLM Formation Techniques

When forming synthetic BLMs, many formation methods have been utilized. Two techniques, the painting method [63, 64] and the folding bilayer method [65], are commonly reported in the literature with each having advantages and disadvantages.

The painting method utilizes a paintbrush to paint lipid solution over a small aperture where BLM formation is desired. The paintbrush usually has all but one bristle removed so only a minute amount of lipid solution is delivered to the aperture. Painting is done submerged in aqueous buffer, thus increasing the method's difficulty. This method is highly susceptible to process variation: 1) too much lipid collected by the paintbrush, 2) too much lipid delivered to the aperture, 3) bristle

material used and its compliance, and 4) the painter's brushing technique. Researchers using this method must practice painting BLMs in order to achieve desirable results.

In the Figure 8, the painting technique is illustrated. First, a test chamber containing a septum with an aperture is shown in Figure 8a. BLM formation occurs at the aperture and the aperture's circumference is "pre-treated" (discussed later) with a hydrophobic solution as shown in Figure 8b. After conditioning the hole, the left and right bath reservoirs are filled with aqueous salt buffer solution until the hole is submerged as shown in Figure 8c and d. A single-bristle paintbrush, pre-loaded with lipid solution, is submerged until the bristle contacts the septum below the aperture and lays flat against the septum. The bristle is then rotated so that it would span across the hole's diameter transverse to the upward painting direction, The paintbrush is then carefully translated upward painting lipid solution over the hole as shown in Figure 8e.. With luck the BLM forms as illustrated in Figure 8f. Electrodes and voltage source, always present throughout the formation exercise, were omitted for clarity.

The Folding Bilayer, or "solvent free", method is probably the most common technique used to form BLMs because there is less process variation compared to painting BLMs. This method will be discussed later in Section 2.2.b since NIST prefers this approach.

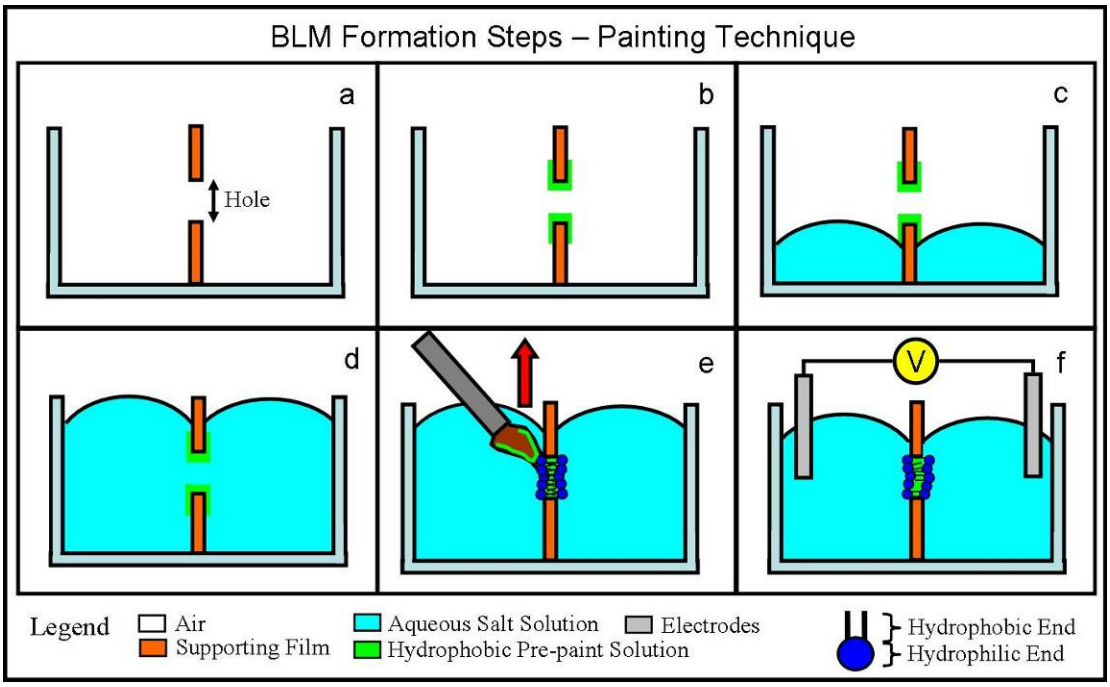

Figure 8: BLM formation via the painting method. See text for details.

2.1.c Alpha Hemolysin (α-HL) Nanopores

Many trans-membrane nanopores exist, only alpha hemolysin (α-HL) will be utilized in this research for the following reasons: 1) α-HL can be easily incorporated into a synthetic BLM. 2) α-HL is stable in the open configuration for long periods provided the right test conditions [66]. 3) α-HL's limiting aperture is relatively large compared to gramicidin [67]) thus making α-HL useful for bio-sensing larger molecules. 4) Dr Kasianowicz's research group at NIST utilizes α-HL for majority of their research work [3-6, 67, 68]. This provides comparison data when doing fledgling α-HL incorporation work with the BLM micro-devices.

α-HL, a toxin protein secreted by *Staphylococcus aureus*, binds to human red blood cells, monocytes, lymphocytes, and endothelial cells and causes cell lysis. Secreted as a monomer, α-HL is a water-soluble polypeptide with a 33.1 kDa molecular weight [67]. α-HL monomers readily incorporate into BLMs and

oligomerize into heptameric pore structures, with an approximate molecular weight of 232 kDa. Figure 9 illustrates an α-HL nanochannel with each monomer displayed by a different color ribbon. The hydrophobic stem of the α-HL heptamer is the portion that spans the BLM thickness and the rim portion helps anchor the heptamer. The trans-membrane stem is comprised of 14 anti-parallel β strands, two contributed from each monomer. If incomplete BLM formation occurs (i.e. not properly thinned), the α-HL stem will not span the entire BLM thickness, thus producing a partial pore. The hydrophilic α-HL heptamer cap portion, sticking proud of the BLM surface, will form on the BLM side that the α-HL monomer introduction occurs [69]. Once α-HL inserts into the BLM, it is firmly rooted and can only be removed with detergents.

The α-HL lumen varies from 14 to 46 Angstroms and houses hydrophilic solution thus making a contiguous connection between both sides of the BLM. The conductance path produced through the α-HL lumen has been shown to have linear dependence relative to solution conductivity that surrounds the BLM. An effective diameter of 11.4 Angstroms has been estimated. The above information was obtained from [69-71].

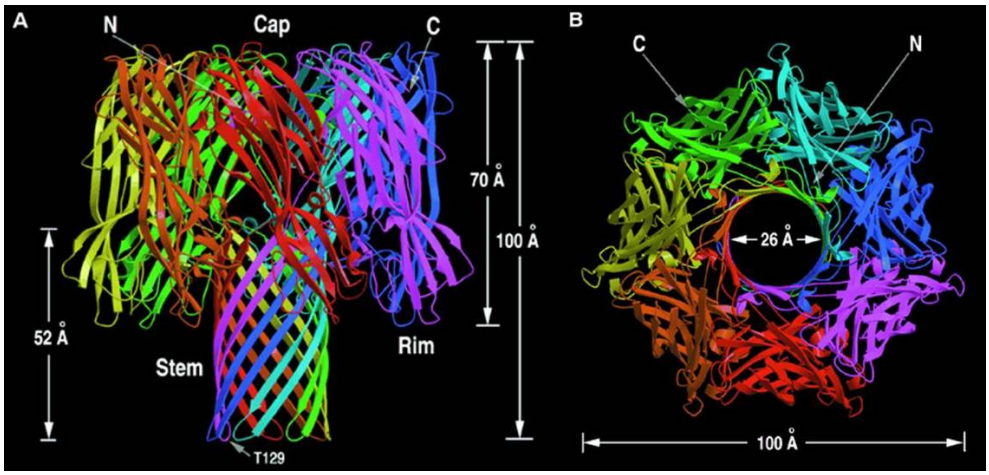

Figure 9: Profile and plan view (right) of α-HL heptameric channel shown as ribbons. Reprinted with permission from [70], © 1996 AAAS.

2.1.d Polyethylene Glycol

When initially testing bio-sensors, a sensor must first be calibrated to determine its sensitivity to a given analyte. This can be accomplish by injecting known analytes that have been detected in other works utilizing nanopores. According to the literature, a variety of analytes, such as H^+ [72], ssDNA [9], and other organics (Dextran [66], Polyvinyl Pyrrolidone [66], Anthrax toxins [73], Na Poly(Styrene Sulfonate) [18]), have been observed interacting with α-HL nanopores.

Polyethylene Glycol (PEG) has been shown to pass through α-HL channels in previous works [66, 72]. When PEG molecules thread through an α-HL channel, the ionic channel current decreases temporarily (blockades) as shown in Figure 1a. If these blockades are unique to certain PEG polymers then the sensor calibration can occur to distinguish between PEG polymers.

A PEG monomer, shown in Figure 10, consists of two ethylene molecules etherized together. This building block is stacked many times inline depending on the degree of polymerization, n. For example, if n = 28 then there are 28 monomers in a row before each end is terminated with a hydroxyl group.

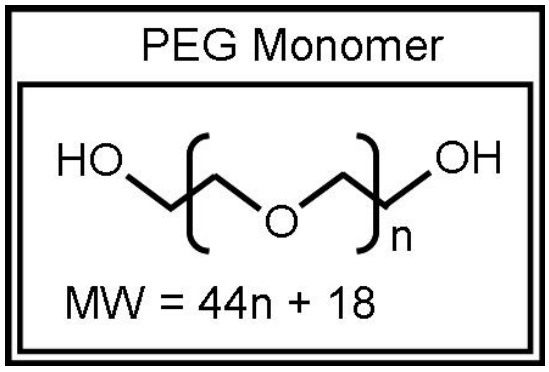

Figure 10: PEG molecule showing n degrees of polymerization.

The molecular weight of PEG can be calculated based on the formula given in Figure 10. For example, if n = 28, the molecular weight for that specific PEG polymer is 1250 g/mol. Commercially bought PEG samples can be mono-dispersed or poly-dispersed about a given molecular weight depending on the quality of the stock purchased. For information on PEG, see [74].

2.2 BLM Test Chamber at NIST

This section introduces the BLM test chamber, which is one of many electrophysiology setups located in Dr. Kasianowicz's lab at NIST (Gaithersburg, MD). Initially, the BLM test chamber was utilized for understanding the basics (i.e. BLM formation techniques, ion channel incorporation) and it was utilized in trying out key components (e.g. BLM formation on PVDC film) prior to implementation into the BLM micro-devices. The BLM test chamber is presented so readers not familiar with electrophysiology research can understand how fundamental BLM electrophysiology research is currently performed at NIST.

2.2.a BLM Experimental Setup (NIST)

The BLM test chamber, shown in Figure 11, consists of a multiple piece housing sandwiching a support film. Both housing and support film are constructed of PTFE which offers outstanding chemical resistance, electrical insulation, and hydrophobicity. The support film splits the housing volume thus two bathing wells are formed, the left and right bath. The support film contains a centralized micron-sized aperture for BLM formation. An Ag/AgCl electrode is placed in each bath so electrical measurements can be taken across the BLM.

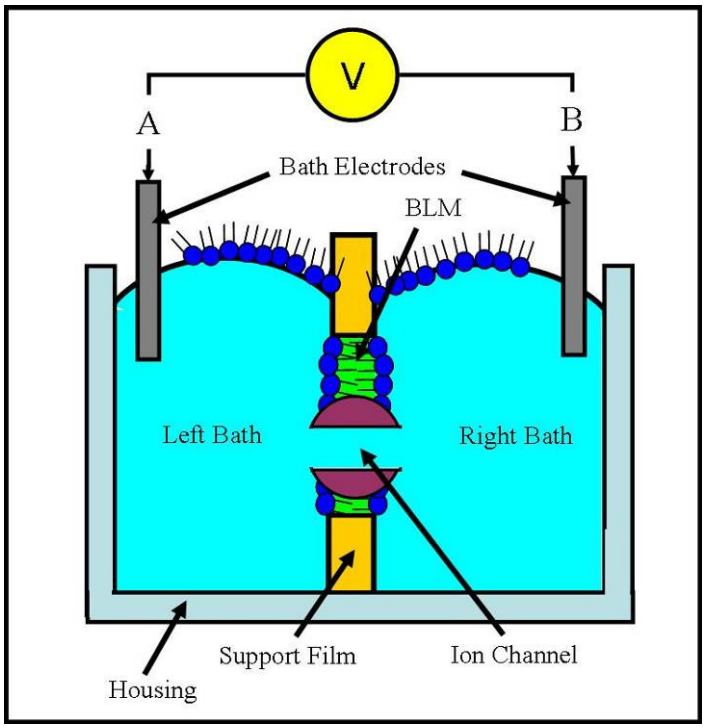

Figure 11: NIST BLM test chamber. See text for details.

Figure 12a shows a typical NIST BLM test chamber broken down while not in experiment. The test chamber dimensions are approximately 2 inches wide by 2.5 inches deep by 1 inch tall and each bath volume is approximately 2.5 mL. An aluminum frame compresses the housing together, thus forming a leak-proof seal around the supporting film. A plan view showing the BLM support film can be seen in Figure 12b. The preferred supporting film, used by NIST, is 25 µm thick, non-porous PTFE film (Goodfellow, UK) and the apertures (BLM formation site) are formed via hot needle and range in size from 90-150 µm in diameter.

The BLM test chamber sits inside a Faraday cage, constructed of µ-metal, which eliminates unwanted EMI pickup. In addition, the Faraday cage includes: 1) the headstage amplifier, which conditions the pico-ampere channel currents prior to sending outside the Faraday cage, 2) a syringe bank for injecting and withdrawing solutions from the test chamber bathing wells, and 3) control electronics for

miniature stirring bars (not shown). Outside the Faraday cage sits a side-looking microscope used in BLM formation. The entire setup sits on a vibration air table so that structural-borne vibrations are minimized. A detailed view and overhead isometric view of the experimental setup can be seen in Figure 12c and d.

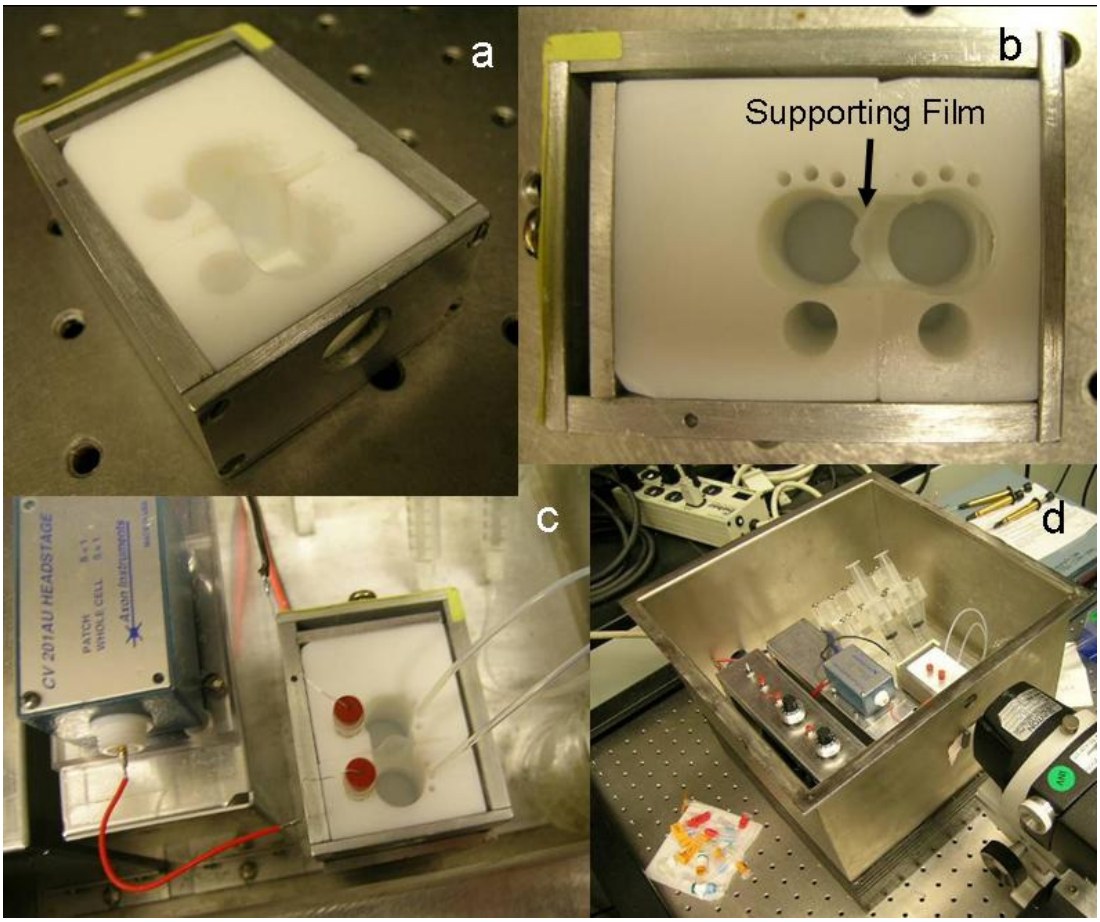

Figure 12: NIST BLM test chamber. (a) An isometric view of the test chamber, (b) Plan view of the test chamber showing the support film, (c) Same test chamber under testing conditions with electrodes and fluid supply hoses connected, and (d) Isometric view of the experimental setup.

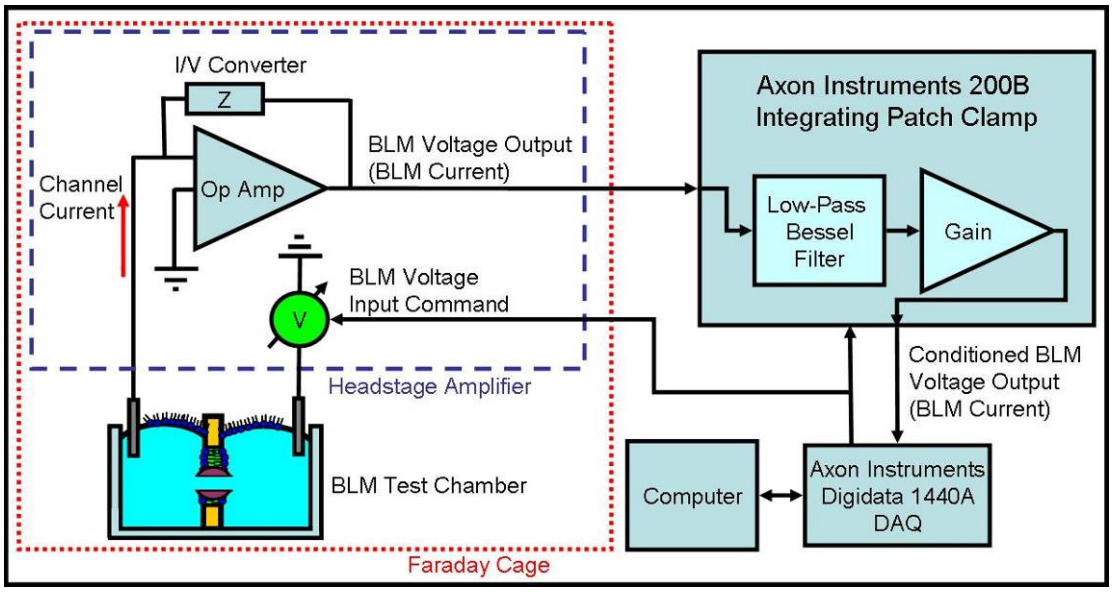

Figure 13: Block diagram of instrumentation used with the NIST text chamber. See text for details.

For successful low-noise ionic current measurements, NIST uses commercially bought patch clamp amplifiers, which have numerous built-in features, such as a 4-pole Bessel low pass filter, capacitance compensation, resistance compensation, and input command potentials. The Axopatch 200 series integrating patch clamp (Molecular Devices) is connected to a Digidata Data Acquisition (DAQ) box (Molecular Devices), which sends digitized signals to a computer for archiving. The DAQ box also provides analog outputs so user-defined input command signals can be applied to the BLM.

The Axopatch patch clamp utilizes a two amplifier setup with a headstage amplifier located adjacent to the testing chamber to maximize the signal-to-noise ratio. The headstage amplifier connects directly to the Ag/AgCl electrodes that are submerged in the NIST test chamber baths. The headstage amplifier performs two tasks: 1) It applies voltage across the BLM, and 2) It converts the measured ionic channel current into a proportional voltage output. For simplicity, the I-to-V

converter is shown as an op-amp in Figure 13. The voltage output produced by the headstage is sent to the Axopatch patch clamp main console, where the signal is filtered and amplified prior to being sent to the DAQ box.

2.2.b BLM Formation Technique Used (NIST)

The preferred BLM formation method used at NIST is the Montal and Mueller folding bilayer technique [65]. The formation process starts with the NIST test chamber shown in section (Figure 14a). In next step (Figure 14b), the aperture's periphery is coated, front and back, with 2 μL of "pre-paint", which consists of a 100 : 1 v/v pentane : hexadecane mixture. The pentane evaporates off seconds after application, leaving the hexadecane behind. Pre-painting of the aperture is important because: 1) It helps in annulus creation, the smooth transition from the nanometer-thin BLM to the supporting film which is ~1000x thicker, 2) It aids in arranging the lipid molecules as they are spread across the hole; keeping the molecules' hydrophobic tails inward, and 3) It aids BLM formation by allowing the excessive solvent to wick, or wet out, onto the surrounding support film periphery.

The next step is to fill both bath volumes with an aqueous salt solution and to raise the water levels just below the aperture, see Figure 14c. Typically, KCl and NaCl are used in varying ionic strengths (1 – 4 M) depending on testing conditions. Next, 15 μL of lipid solution (typically 10 mg of DiPhyPC, MW 846.27, suspended in 1mL pentane) is piped in both chambers. The lipid solution, immiscible in the aqueous buffer due to non-polar composition, floats on top of the buffer due to density differences. As the pentane evaporates off, the lipid molecules will orient so that the lipid's polar head group face the water interface, see Figure 14d. After 5

minutes, one side of the aqueous salt solution can be raised above the supporting film hole. This creates a lipid monolayer across the hole's span with the hydrophobic tails sticking inward, see Figure 14e. The right side can be raised subsequently completing the bilayer formation, see Figure 14f. Also, Ag/AgCl electrodes which were originally in the chamber are now shown for clarity.

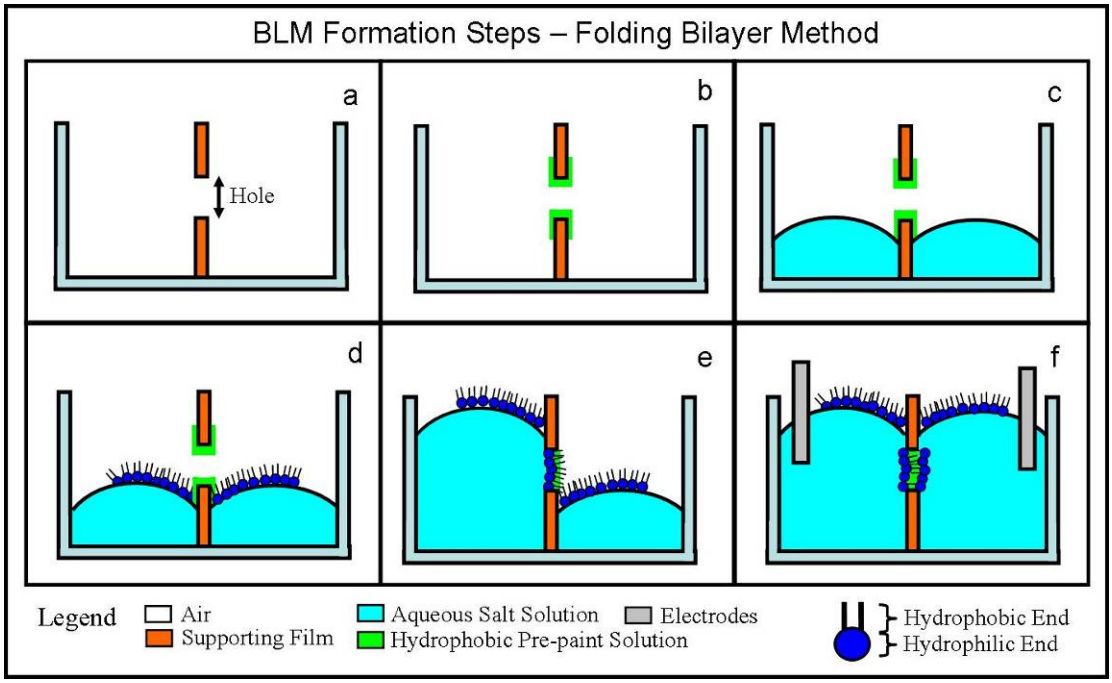

Figure 14: NIST BLM formation technique. See text for description of process.

While forming BLMs, current monitoring occurs in conjunction so BLM quality can be ascertained after formation. Initially, an AC potential (e.g. 20m$V_{p\text{-}p}$, 250 Hz triangular waveform) is applied across the electrodes. Prior to raising the bath levels, the current output appears as a squarewave whose gain is proportional to the support film capacitance. As the bath levels are raised for BLM formation, the current gain increases after successive BLM formation due to the additional capacitance introduced. If a BLM fails to form or pops prematurely, a lower than

expected resistive conductance occurs and a current overload occurs due to op-amp saturation.

2.2.c Ion Channel α-HL Incorporation (NIST)

Incorporation of α-HL ion channels into a previously formed BLM is illustrated in Figure 15 below. Figure 15a shows the NIST BLM test chamber ready for α-HL incorporation with a BLM formed previously. Next, 0.3 μL of ion channel solution (e.g. 1 μg α-HL per mL of 10mM MES, pH 7.5) is piped into the right bath as shown in Figure 15b. The chamber volume is then mixed with a magnetic stirring bar (not shown), and the monomers spontaneously interact with the BLM (see Figure 15c and d). A DC potential (40 – 200 mV) applied across the BLM allows for current monitoring. Prior to the α-HL solution injection, only small leakage current exists. When a single α-HL channel incorporates in the BLM, a noticeable current jump (tens of pA depending on input voltage) occurs and remains constant until other channels form or the original channel gates.

Injecting a higher concentration of trans-membrane solution will cause channel formation very rapidly, where the number of α-HL channels incorporated. is proportional to the current output amplitude. Typically, a single α-HL channel is desirable for bio-sensing so the remaining α-HL solution is flushed after the first channel has incorporated (see Figure 15e). Because the bath volume is a few milliliters, flushing occurs over minutes as care must be taken not to rupture the BLM. The possibility for additional α-HL channels to incorporate while flushing the ion channel solution remains. Figure 15f shows a BLM with single α-HL channel ready for future testing.

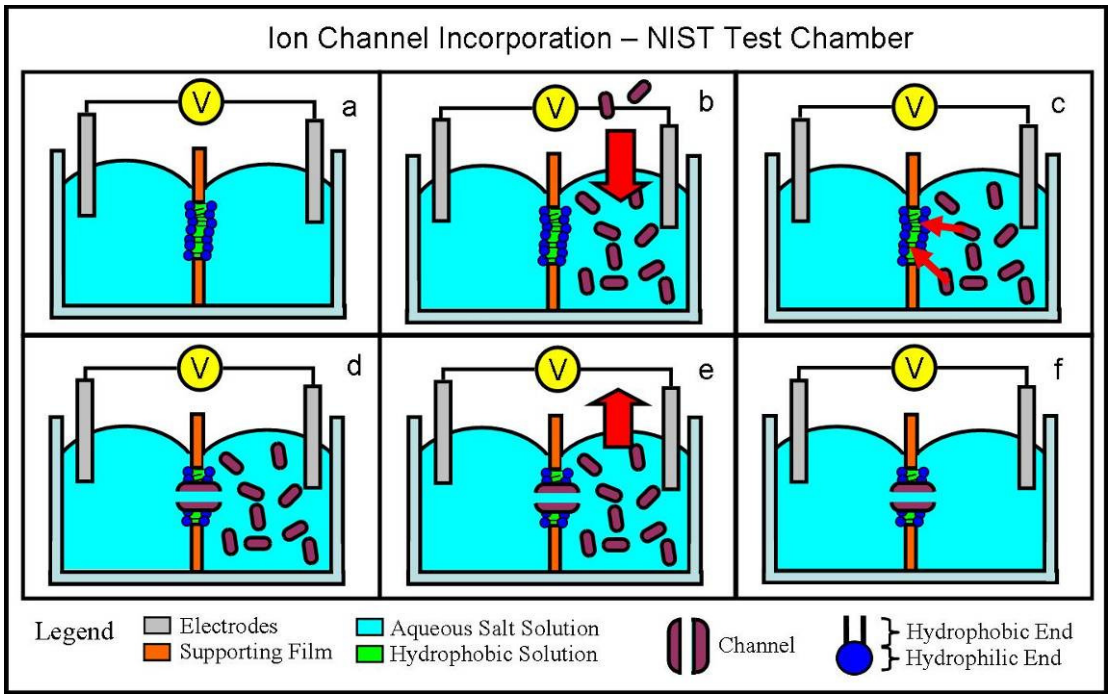

Figure 15: NIST α-HL channel incorporation technique. See text for description of process.

2.2.d PEG Sensing and Identification (NIST)

PEG sensing studies start with the NIST test chamber previously prepared with a BLM and single α-HL nanopore as shown in Figure 15f. First, the α-HL nanopore conductance must be established in absence of PEG for baseline comparison. This is done by applying a DC potential across the BLM and monitoring the ionic current. As seen in Figure 16a, the open channel baseline is 150pA with an applied 40 mV potential across the BLM, which is bathing in 4 M KCl, pH 7.5 buffer. Next, PEG molecules is added to the bath and blockades, on order of milliseconds, will start to occur as the PEG molecules interact with the α-HL nanopore, as seen in Figure 16a. Here, a poly-disperse PEG sample (MW_{avg} = 1500 g/mol) was added to the left bath from stock solutions (12 mg/mL) until the bath concentration was 45 µg/mL. Each blockade represents a PEG molecule passing through the α-HL nanopore into the opposing chamber. Blockade variation will occur because poly-

dispersed PEG contains various molecular weights hence translocation times will vary with PEG size.

The difference between mono-disperse and poly-disperse PEG is shown in Figure 16b. In separate experiments, a single α-HL nanopore, under identical test conditions except for the kind of PEG added to the left bath chamber, can provide unique PEG signatures. Figure 16b (top) shows a subset of the 10^5 blockades recorded for a poly-disperse PEG sample (MW_{avg} = 1500 g/mol) while to the right is a histogram plotting the frequency of the observed current blockade states. Another current trace and histogram is shown for a mono-disperse PEG sample (MW = 1294, n = 29) in Figure 16b (bottom). The mono-disperse PEG histogram indicates that two blockade current states were observed in addition to the baseline state. The rarer current state, indicated by the green arrow, is reasoned to be double PEG molecules passing simultaneous through the α-HL channel or sample contamination. Lastly, the common mono-disperse PEG current state is narrower than for poly-disperse PEG, thus proving a higher quality sample, albeit the possible contamination.

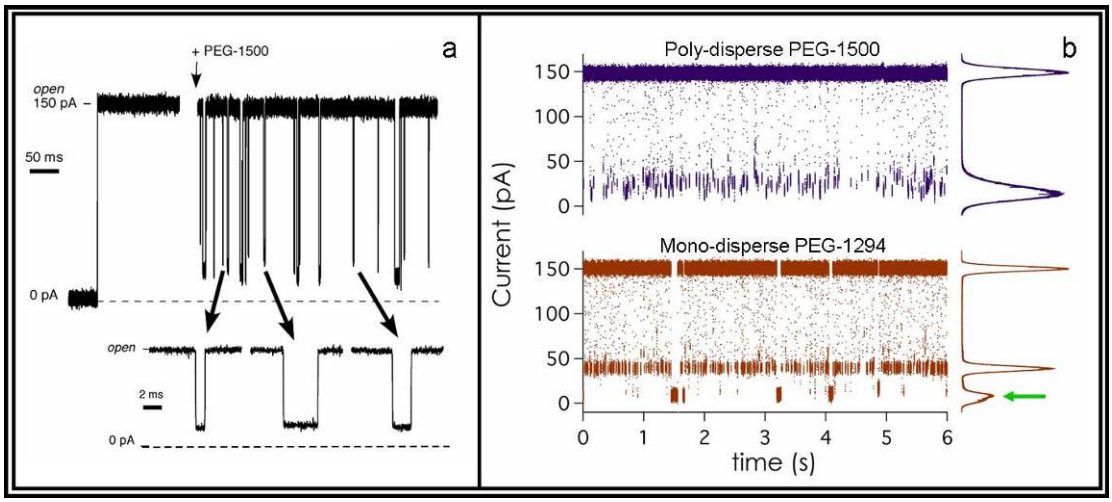

Figure 16: NIST PEG blockade data obtained from [75].

2.2.e Equivalent RC electrical Model (NIST)

The NIST test chamber is a mechanical system connected in series with outboard electrical circuitry capable of BLM electrophysiology research. An equivalent electrical system can be identified and substituted for the physical test chamber. By looking at the equivalent electrical model, the NIST test chamber can be modeled and the subsequent analysis can be utilized when designing the BLM micro-device.

In Figure 17, the NIST test chamber is again shown in section however equivalent RC electrical components have been superimposed over each mechanical part the electrical component represents. As shown, both baths can be converted into resistors since the buffer allows electrical charge movement from the submerged electrodes to the BLM interface and vise-versa. Likewise, the α-HL channel can be modeled as a resistor since it allows current to flow across the BLM. The support film and BLM act as a capacitor since it separates charge over a distance, which is the fundamental definition of a capacitor. Finally, note this is a simplistic equivalent RC model and a more complex RC model can be derived, if required, where leakage currents (i.e. electrode capacitance, BLM leakage and support film dielectric losses, etc) are taken into account.

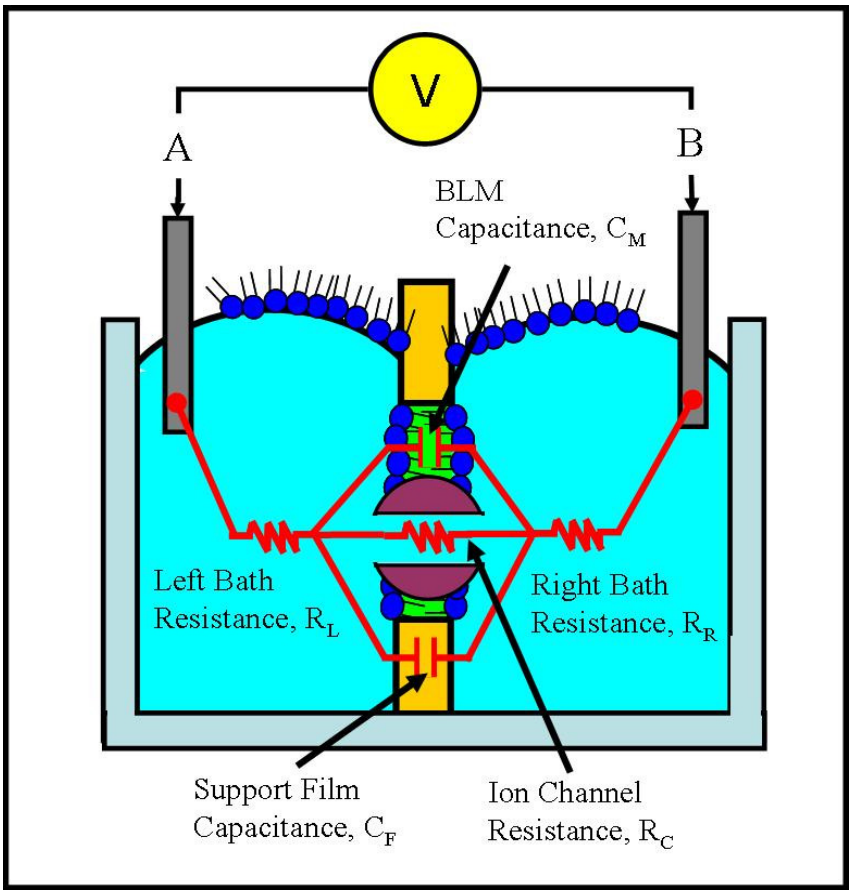

Figure 17: NIST test chamber with equivalent electronic components superimposed over their physical counterparts.

The RC circuit obtained from the NIST test chamber analysis can be transformed into a Thevenin equivalent circuit, which yields a simple series RC circuit that can be analyzed by inspection. Figure 18a-d details the Thevenin transformation of the BLM RC circuit.

One important RC circuit performance parameter is the time constant, τ, which measures how fast a system reacts to an input stimulus. A system with a small time constant settles to a new output state faster than a system with a large time constant. A biosensor that supposedly detects molecules traversing the BLM will need a time constant faster than the molecule's translocation time or detection will not occur.

Shown in Figure 18d, the equation for the NIST test chamber's time constant is provided and is the Thevenin impedance, Z_{th}, times the equivalent parallel capacitance of the BLM and surrounding support film, C_{eq}. Examining Z_{th}, the nanopore's resistance is much higher than bath's access resistance ($R_C >> R_U, R_L$) thus Z_{th} can be approximated as just the summation of the bath access resistances. To minimize the system's time constant, one would want to minimize the following: 1) the bath access resistances, 2) the BLM capacitance, and 3) the supporting film capacitance. These points will be utilized when designing the BLM micro-device and will be revisited.

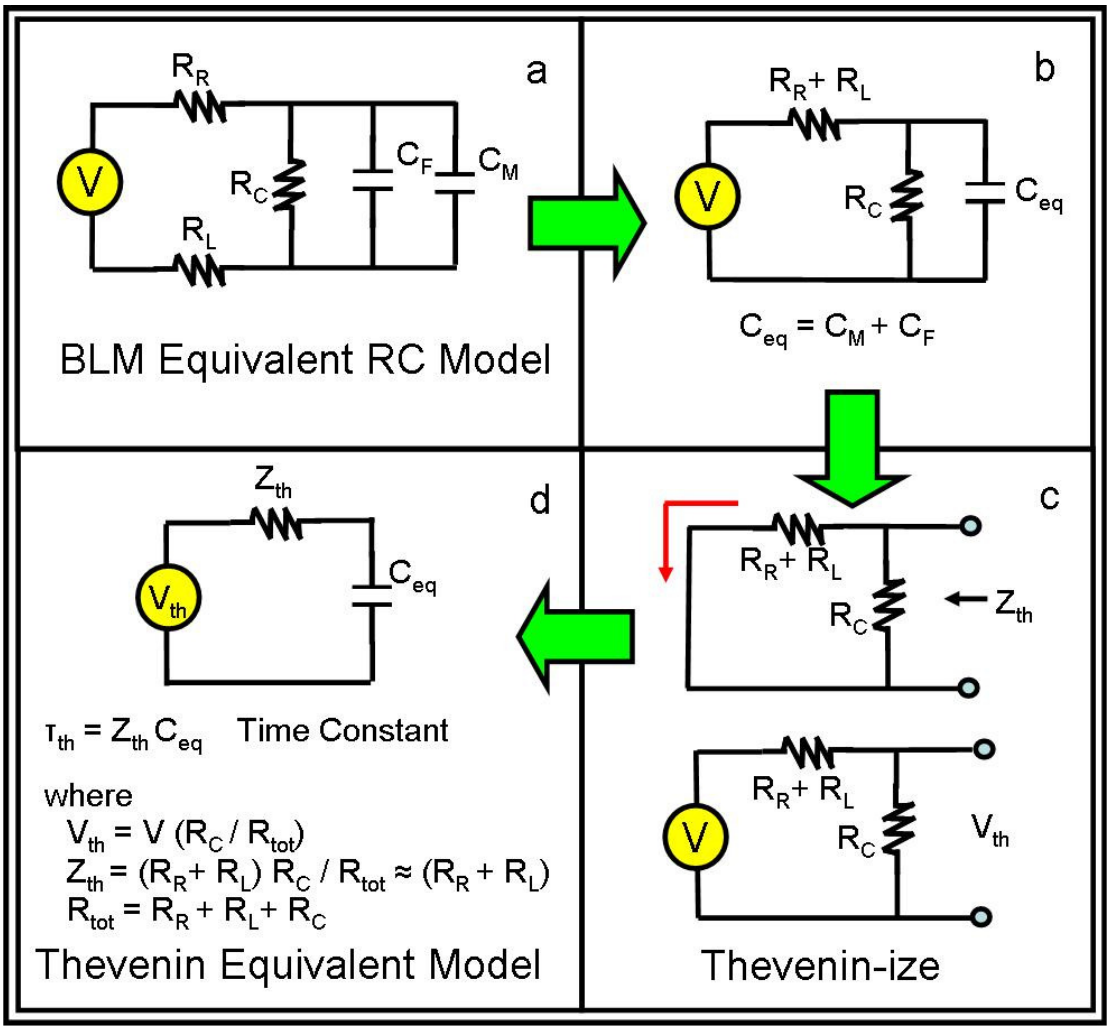

Figure 18: Thevenin equivalent model for the BLM RC circuit shown earlier.

NIST Test Chamber Bandwidth

Utilizing first principles to calculate resistances and capacitances, each element of the equivalent test chamber RC model can be estimated and the values are provided in Table II. Estimating the electrical components required the following assumptions:

- Since the bath volumes are more complex than pictured, the bath volume resistance was measured empirically. Due to symmetry, the left and right bath resistances are equal and were verified by an ohmmeter. Each bath contained 3 mL of 1M NaCl buffer solution, whose measured conductance was 79.7 mS/cm at room temperature.
- The α-HL resistance is calculated by assuming a right cylinder of constant diameter (26 Ang ID x 100 Ang long from [70]) filled with same 1 M NaCl solution.
- The BLM diameter is assumed to occupy the entire hole in the PTFE film, which is 120 µm. A specific capacitance of 0.7 µF/cm^2 [76] for solvent-free BLMs was used.
- When calculating supporting film capacitance, the BLM formation site was assumed to be located at film center with buffer raised just above the hole. The PTFE support film is 25.4 µm thick and has a dielectric constant, $\varepsilon = 2.1$.

Table II: Estimated Electrical Components for the NIST Test Chamber

Component	Description	Estimated Value
R_L, R_R	Left and Right Bath Resistance	1 kΩ
C_F	Support Film Capacitance	62.2 pF
C_M	Solvent-free BLM Capacitance, 120 µm Diameter	79.1 pF
R_c	α-HL Channel Resistance	0.29 GΩ

Substituting the above values into the equation given in Figure 18, the time constant for the NIST test chamber is estimated to be 0.283 µsec. Taking the inverse, the bandwidth is estimated to be 3.5MHz. In reality, the NIST test chamber probably

has a much lower bandwidth when the associated electronics (headstage, leakage capacitance/resistance compensation circuitry, etc) are considered. From Figure 16, PEG blockades last on the order of milliseconds.

2.3 BLM Formation Methods in Other Microfluidics Works

This section summarizes successful BLM formation techniques with relevance to microfluidic chips reported by the three groups (Suzuki et al., Sandison et al., and Malmstadt et al.) mentioned in Section 1.4. Reviewing the literature is very valuable and provided insight towards the work reported in this dissertation.

2.3.a BLM Formation Techniques by Suzuki et al.

Suzuki et al. reports filling the upper well with 50 µL of 10 mM KCl buffer [32]. Due to surface tension, the buffer does not wick into the lower microchannel as shown in Figure 19-(1). Next, lipid solution, 20 mg/mL of asolectin in n-decane, is injected into the lower channel coating all interfaces; see Figure 19-(2). The remaining lipid solution is then collected, via absorption, by placing cotton wading in the inlet thus air remains in the lower channel as in Figure 19-(3). Buffer is then injected into the lower channel as shown in Figure 19-(4). External pressure is applied from the top side to cause the remaining lipid solution to thin down into a BLM (see Figure 19-(5)). Additional testing solutions can be injected via the bottom channel. Similar formation techniques are also reported by Suzuki et al. [30, 31]. In earlier works, the technique lacks the top side chamber for pressure equilibration in [27-29].

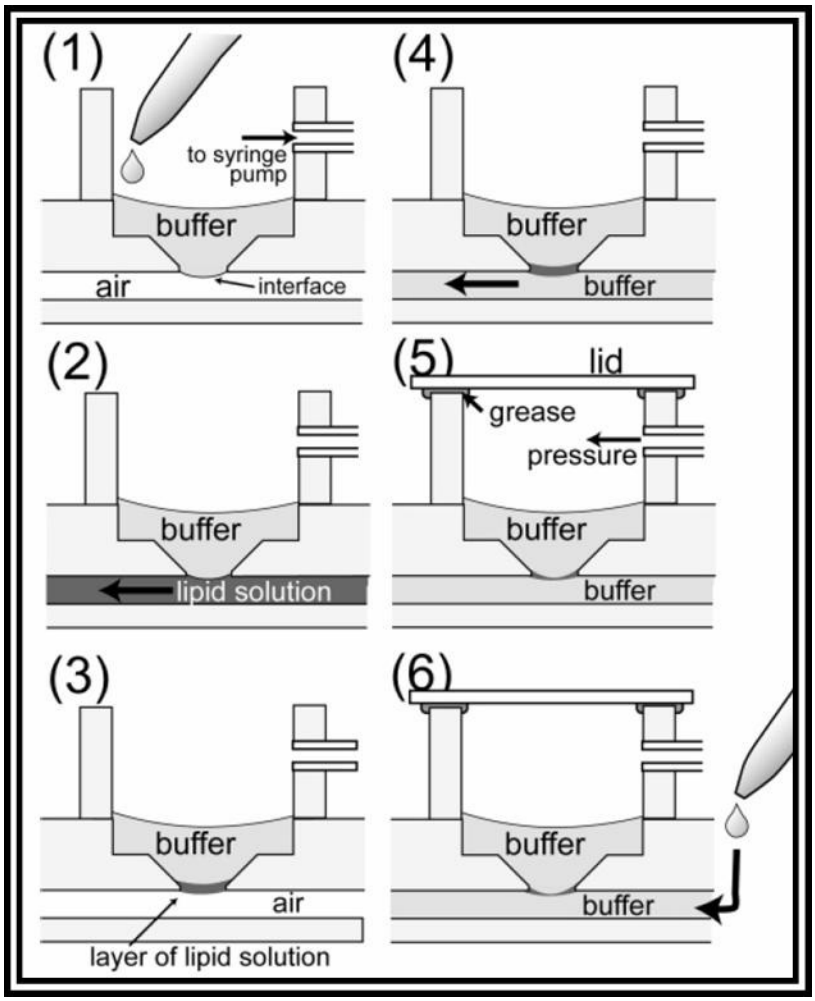

Figure 19: BLM formation method presented by Suzuki et al. See text for details. Reprinted with permission from [32], © 2006 American Chemistry Society.

2.3.b BLM Formation Techniques by Sandison et al.

Sandison et al. reports various techniques when forming BLMs in their microfluidic devices. Sandison states that one microfluidic channel was typically filled with 1 M KCl (or a 2% agarose with 1 M KCl) electrolyte leaving the second microchannel still containing air [35]. A plug of lipid solution, 2 mg/mL DiPhyPC in n-decane, immediately followed by identical electrolyte, is then flowed across the aperture. If the BLM does not thin spontaneously, the electrolyte in one of the microchannels is pumped to encourage thinning.

In another work, Sandison et al. started by filling the entire chip with buffer solution and then the upper well is emptied [37]. An ~1 µL volume of lipid solution, 10 mg/mL 7 : 3 POPE : POPC in n-decane, is piped over the aperture and allowed to drain before buffer is injected into the upper well again. The upper well is drained for the second time thus leaving lipid film spanning the aperture exposed to air for approximately 30 seconds. After air exposure, the upper well is filled with buffer again while monitoring the BLM optically and electrically. At this point, the buffer concentrations in the cis and trans side of the BLM are 150 mM and 720 mM KCl, respectively with 8 mM HEPES, pH 7.4. Concentration differences are to induce liposome –to-BLM fusion as discussed in [37].

In another work, Sandison et al, reports BLM formation by painting the same lipid solution stated above (except 20mg/mL) over an aperture in PTFE film using a brush. The same buffers mentioned above were used [38].

2.3.c BLM Formation Technique by Malmstadt et al.

Malmstadt et al. reported a BLM formation technique which removed extraneous solvent by a diffusion process into the surrounding bulk PDMS [39]. Figure 20 illustrates the Malmstadt reported BLM formation process, where the process begins with filling the entire PDMS device with buffer (1 M KCl, 5 mM HEPES, pH 7.0). Next, a 2 nL plug of lipid solution, 0.025% w/v DiPhyPC Lipid in 1 : 1 n-decane/squalene with 50 ppm v/v perfluorooctane, is injected at 15 – 45 µL/hr using a syringe connected to a syringe pump. After moving the lipid plug toward chip center (box indicated in Figure 5b), the lipid plug is allowed to sit so diffusion of the extraneous solvent can permeate into the bulk PDMS. Some time later, the lipid

plug minimizes into a BLM as can be determined by electrical signal analysis. A time sequence of this event is shown below in Figure 20.

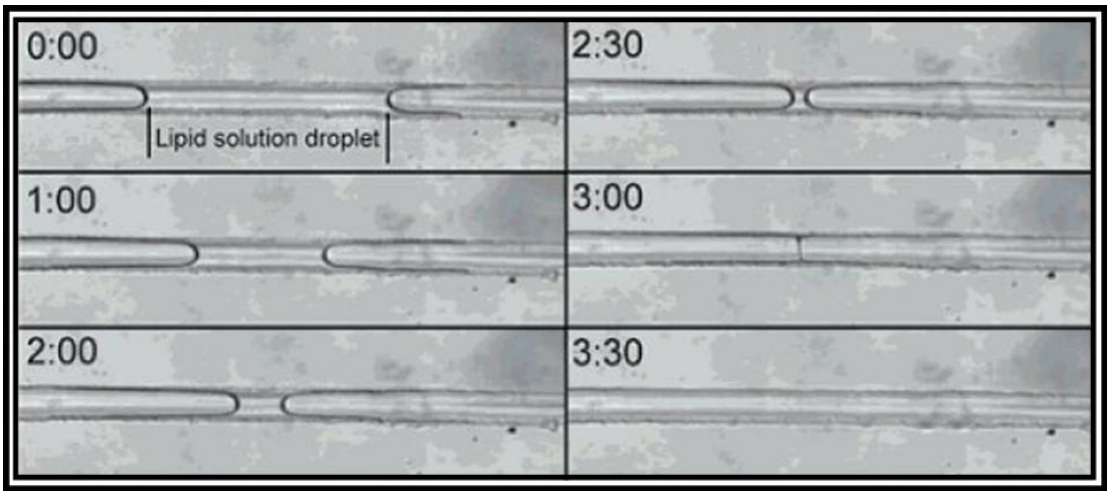

Figure 20: Photograph series showing BLM formation in a microchannel reported by Malmstadt et al. Here, the microfluidic channels are 100 µm wide by 70 µm deep. Time in upper left corner is in minutes : seconds. Reprinted with permission from [39]; Copyright 2006 American Chemical Society.

Chapter 3 BLM Micro-Device Design and Fabrication

This chapter introduces the BLM micro-devices and discusses design methodology and fabrication. Particulars, such as material choice, microchannel size, and electrode layout, are discussed along with other design issues. Next, an overview of micro-device fabrication is given. Fabrication details are limited for brevity, but can be found in Appendices A-C.

3.1 BLM Micro-Devices and Design

This dissertation yields a fabrication method capable of constructing two similar micro-devices. One type of micro-device is a closed device meaning that the BLM formation site cannot be accessed by hand, whereas the other type is an open well device in which the BLM formation site can be accessed for manual BLM interaction. Both micro-devices are shown in Figure 21 and will be discussed in turn. Following micro-device introduction, design methodology and issues will then be discussed.

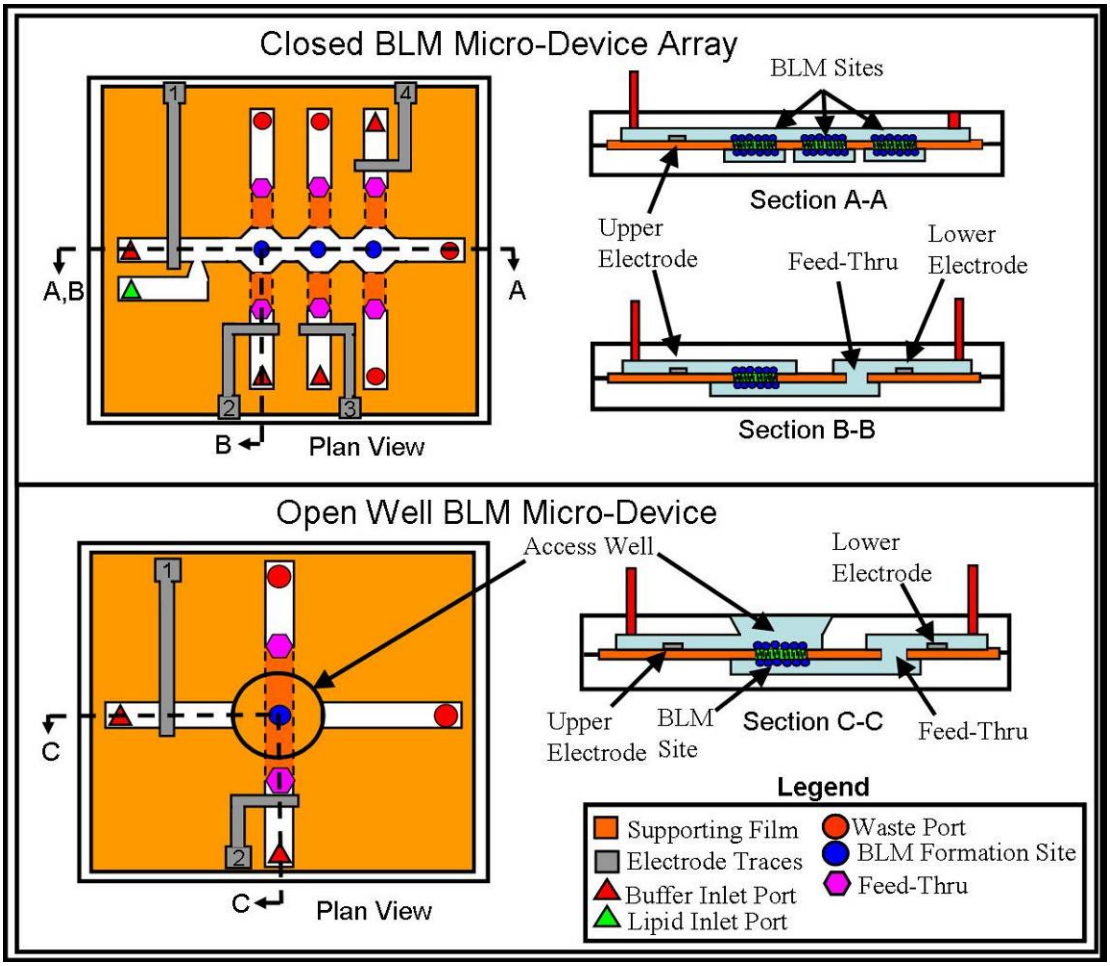

Figure 21: The BLM micro-devices. At top is the closed 1 x 3 micro-device array. At bottom is the open well micro-device. See text for details.

3.1.a BLM Micro-Device Array (Closed)

The BLM micro-device array, shown in Figure 21, is a closed design where the BLM site cannot be accessed manually thus BLM formation occurs under remote conditions. The micro-device, roughly 5 cm square, is of sandwich construction where two pieces of polycarbonate (PC) are separated by a piece of Polyvinylidene-chloride (PVDC) support film. The primary purpose of the PVDC supporting film is to sustain BLMs at the BLM formation sites. The BLM formation site is a micron-sized hole burned into the PVDC supporting film. The BLM micro-device design allows up to three BLM formation sites per chip, hence the design shown above is a 1

x 3 array. If a 1x3 array is not warranted due to test conditions, the BLM formation holes need not be created so a single site (1 x 1) or a double site (1 x 2) array can be created.

Each PC piece, 3/32 inch thick, contains a network of microfluidic channels, where nominal channel dimensions are 50 µm square. The microchannels in the top wafer are isolated from the microchannels in the bottom wafer. Only at the BLM formation sites do the top and bottom microchannels intersect so fluid interfaces exist on both sides of the BLM, see Section A-A of Figure 21. For the array sites to be electrically isolated from one another, each bottom microchannel is isolated from its neighbor. Fluidic ports, either inlet or waste, are located at the end of each microchannel. An auxiliary microchannel exists in the upper microfluidic network and aids in lipid solution delivery to the BLM formation sites.

Metal electrode traces are fabricated on top of the PVDC film prior to chip assembly thus are embedded between the PC layers. The primary electrode, No. 1, allows electrical connection to the upper microchannel, whereas the other electrodes, No. 2-No. 4, allow electrical connection to the bottom microchannels. If all three BLMs are present at the array sites, the bottom electrodes are isolated from one another. If the first array site were to be queried then electrodes No. 1 and No. 2 are used. If second array site were to be queried then electrodes No. 1 and No. 3, etc.

Feed thrus exist along the length of the bottom microchannels and are incorporated into the design because the electrode traces exist only on one side of the PVDC film due to fabrication limitations. For the bottom microchannels to be connected electrically, the bottom microchannel is diverted into the top wafer, via a

pair of feed-thrus, see Section B-B of Figure 21. Pictures of a BLM micro-device array chip are shown in Figure 22.

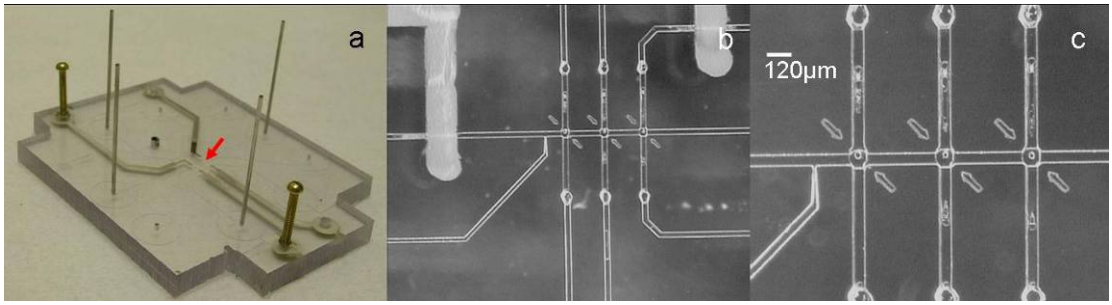

Figure 22: Pictures of the BLM micro-device array. (a) Iso-view of chip where the red arrow denotes the location of the 1 x 3 array, (b) Plan view of 1 x 3 array with upper Ag/AgCl electrode to left and 3rd array site electrode on upper right. Note, 1st and 2nd array site electrodes are out of view, and (d) Detail of the BLM array sites.

3.1.b Open Well BLM Micro-Device

The open well BLM micro-device, shown in Figure 23, is an extension of the closed design, presented earlier. This design has an access port, or open well, that is constructed prior to chip assembly as shown in Section C-C of Figure 21. This open well allows direct access to the BLM site during testing whether it is for manually forming a BLM or for delivery of additional testing solutions. The open well micro-device has a single BLM formation site, but can be converted to an array design in future chip generations. All other chip aspects are identical to the closed BLM micro-device. Pictures of an open well BLM micro-device are shown in Figure 23.

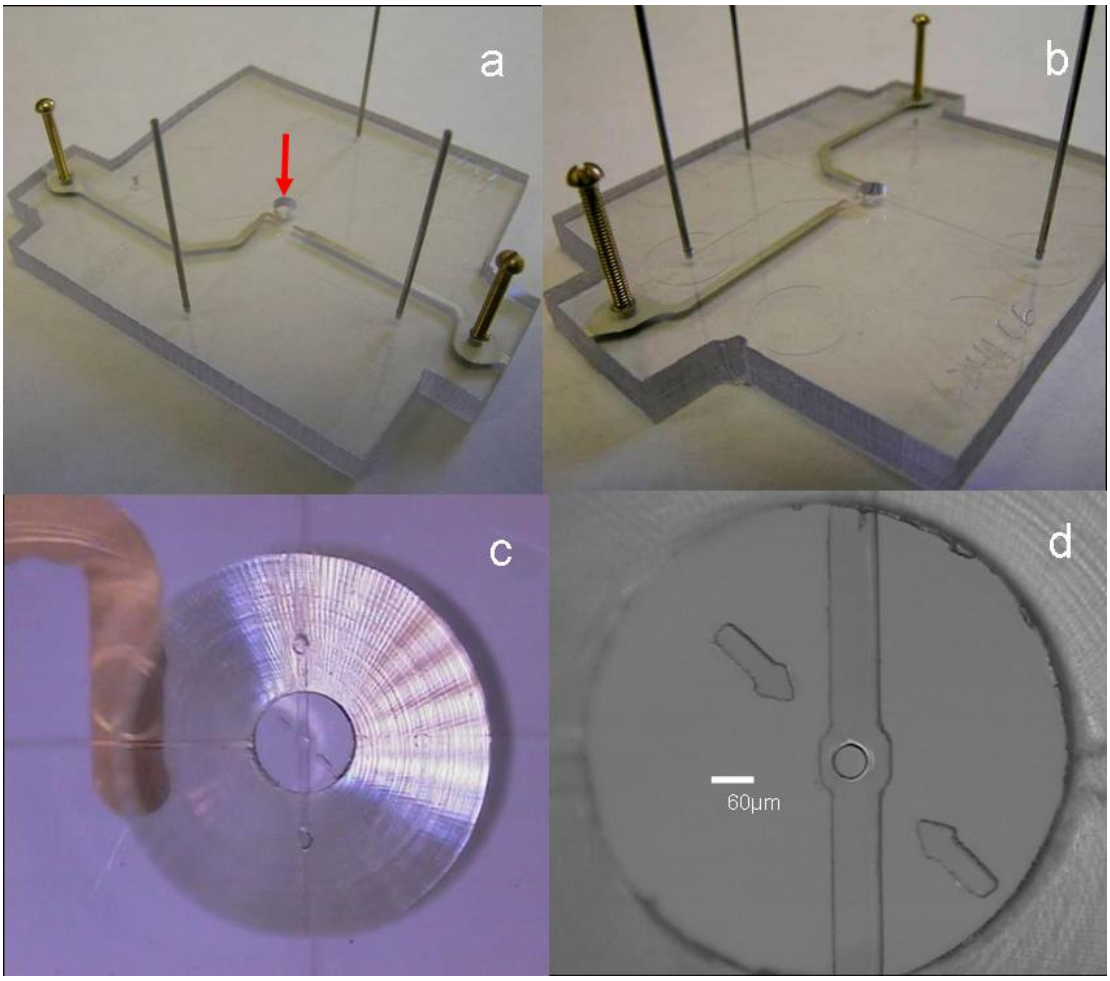

Figure 23: Pictures of the open well BLM micro-device. (a) and (b) Two iso-views of chip where the red arrow denotes the open well, (c) Plan view of open well with upper Ag/AgCl electrode to left, and (d) Detail of BLM formation site and lower microchannel.

3.1.c Designing BLM Micro-Device via Electrical Model

Similar to the NIST test chamber, the BLM micro-device's physical system can be transformed into an equivalent RC circuit. Figure 24 shows the BLM micro-device in section with the equivalent electronic components superimposed over its physical embodiment. The microchannels can be converted to resistors because the microchannels are filled with conductive buffer. Another resistor can be inserted for the ion channel since it allows a conductive path between the top and bottom

microchannels. Lastly, capacitors are substituted for the support film and the BLM, since they separate charge over a distance.

When designing the BLM micro-devices, the concepts gathered from analyzing the NIST test chamber's RC electrical model will be leveraged (See Section 2.2.e). The micro-device's bandwidth can be maximized by minimizing: 1) the microchannel's access resistance, 2) the BLM capacitance, and 3) the supporting film capacitance. These concepts will be discussed in turn.

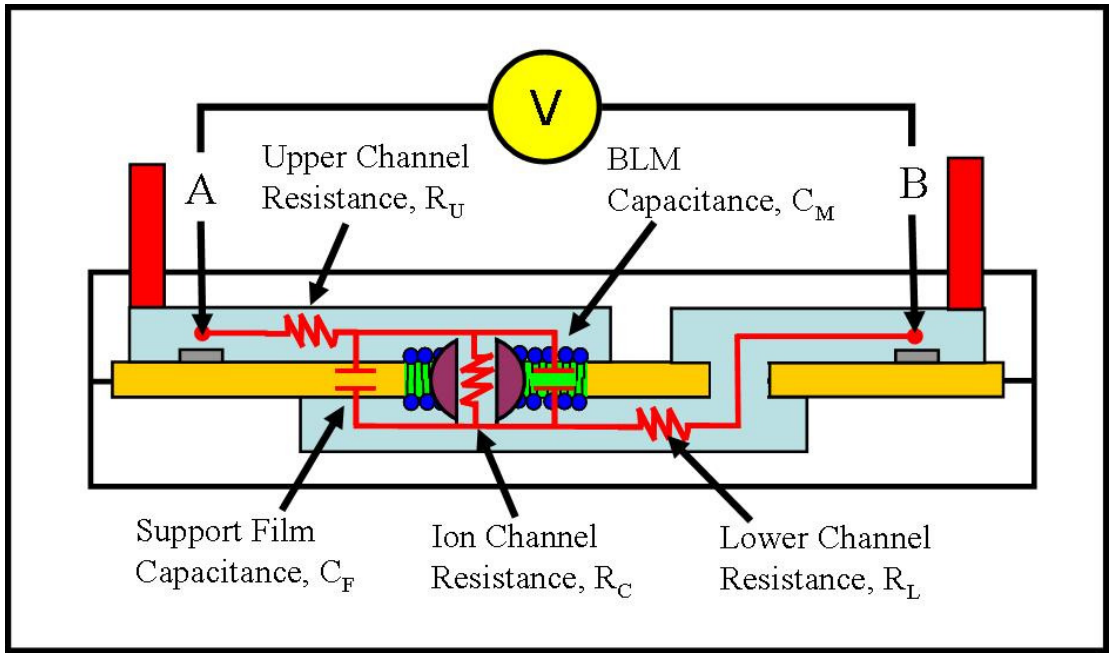

Figure 24: Cross section of BLM micro-device showing electrical components superimposed over their physical counterparts.

Minimizing Microchannel Access Resistance

The following equation is used for calculating the resistance of microchannel filled with conductive buffer: $R = L / (A G)$, where R is resistance, G is the electrolytic conductivity, L is microchannel length, and A is microchannel cross sectional area. Based upon the above equation, the following is recommended: 1) Placing the electrodes close to BLM formation site as possible thus reducing the

microchannel length between the electrode and BLM site. 2) Maximizing the salt concentration in the buffer thus increasing conductivity (e.g. 1 M versus 0.1 M). 3) Increasing the buffer's conductivity by utilizing a salt with inherently higher ion mobility (e.g. KCl versus NaCl), and 4) Maximizing the microchannel's cross sectional area by increasing the height and width of the microchannels.

Some recommendations cannot be implemented due to physical constraints, manufacturing limitations, etc. For example, the microchannel width cannot be increased over 100µm wide because it was found that the supporting film would sag and seal the channel during the chip bonding process. Likewise, the microchannel height cannot be increased due to fabrication limitations when imprinting the microchannels. Additionally, if the microchannel height and width were increased dramatically to reduce the access resistance, one inherent advantage of using microfluidic systems is lost; namely. small reagent volumes.

Minimizing Supporting Film Capacitance

The following equation is used for calculating the capacitance of a parallel plate capacitor: $C = (\varepsilon_o \varepsilon A) / t$, where C is capacitance, A is the area, ε_o is the permittivity of free space, ε is the support film's dielectric constant, and t is the dielectric, or film, thickness. Based upon the above equation, the following is recommended: 1) Use a film with lower dielectric constant (e.g. PTFE versus PVDC). 2) Decrease the exposed area of supporting film, and 3) Increase the film thickness.

Again due to manufacturing constraints, material limitations, some of the above recommendations cannot be followed. For example, PTFE could not be used

as the support film because of micro-device bonding issues incurred due to its inherently high glass transition temperature. On the other hand, PVDC has a lower glass transition temperature thus allowing the film to solve multiple fabrication problems: 1) PVDC is known to support BLM formation [60, 65]. 2) PVDC heat seals well thus providing leak-proof microchannels, and 3) PVDC offers superior bond strength after chip assembly and bonding. Finally, the area of exposed supporting film is limited by current fabrication methods and film thickness is limited to commercially available products.

Minimizing BLM Capacitance and Aspect Ratio

The same equation for parallel plate capacitance can be examined and applied to minimizing the BLM capacitance. Unfortunately limitations exist again as only the BLM area can be minimized because the dielectric constant and BLM thickness cannot be altered.

BLM maximum diameter is physically constrained by the hole diameter in the supporting film assuming that the BLM annulus is infinitely small. On the other end, BLM minimum diameter is constrained by meeting minimum energy requirements set forth by the volume of lipid solution delivered, the boundary conditions and the hole's aspect ratio (D/t) in the supporting film [77]. The aspect ratio is important as if in extreme, the BLM will not spontaneously thin thus resulting in a thick lipid plug. Hole aspect ratio ranging from 3.2 to 6 have been successful in forming BLMs in the NIST test chamber.

Micro-Device System Bandwidth

Like the prior NIST test chamber analysis, resistances and capacitances can be estimated with the values are reported in Table III. Estimating the electrical components required the following assumptions:

- The microchannels are filled with 1 M NaCl, whose conductance of 79.7 mS/cm was experimentally measured at room temperature.
- The current BLM micro-device design was used. The microchannel dimensions are nominal 60 µm wide x 50 µm deep.
- The upper and lower microchannel channel resistances are not equal. The distance from the lower electrode to the BLM site is approximately three times longer than the distance from the upper electrode to the BLM site.
- The upper channel resistances are different for the open well chip versus the closed chip due to the well.
- The BLM diameter is assumed to occupy the entire hole in the PVDC film, which is 40 µm. A specific capacitance (0.4 $\mu F/cm^2$ [76]) for painted BLMs was used.
- When calculating the supporting film capacitance, the intersect area between both microchannels was used for the closed chip device. The intersecting area between the lower channel and open well (1mm diameter) was used for the open well devices. The PVDC supporting film is 12.5 µm thick and has a dielectric constant, $\varepsilon = 3$.

Table III: Estimated Electrical Components for the BLM Micro-Device

Component	Description	Estimated Value
R_u	Upper Channel Resistance, Open Well Chip	32 kΩ
R_u	Upper Channel Resistance, Closed Chip	51 kΩ
R_L	Lower Channel Resistance	163 kΩ
R_c	α-HL Channel Resistance	0.29 GΩ
C_f	Support Film Capacitance, Open Well Chip	0.13 pF
C_f	Support Film Capacitance, Closed Chip	0.02 pF
C_M	Painted BLM Capacitance, 40 μm Diameter	6.32 pF

Substituting the above values into the equation given in Figure 18, the time constants for the BLM open well and closed micro-devices are estimated to be 1.25 and 1.35 μsec, respectively. Taking the inverses, the bandwidths are estimated to be 0.80 and 0.74 MHz. Clearly, the open well has marginally better performance versus the closed chip. When comparing the above time constants to the NIST test chamber, the NIST test chamber's time constant is over four times better.

By comparing the calculated resistance and capacitance values for the micro-devices and the NIST test chamber (Table III versus Table II), the reason for poor micro-device performance can be seen. The total capacitance (support film plus BLM) for the closed micro-device is 6.34 pF versus 141.3 pF for the NIST test chamber; an approximate 22 times reduction. On the other hand, the total access resistance for the close micro-device is 214 kΩ versus 2 kΩ for the NIST test chamber; an approximate 100 fold increase. Reduction of system capacitance is a big advantage for micro-devices compared to the NIST test chamber, however the biggest challenge when utilizing microfluidics will be to keep the access resistance low.

Incidentally, the micro-device original design intended for a BLM formation site of 20 µm in diameter. However after poor BLM formation results, the hole site was increased to 40µm in diameter to produce a more favorable aspect ratio. This doubling of the diameter led to a four times the increase of BLM area used in the calculation, and hence the BLM micro-devices have a time constant four times slower compared to the NIST test chamber.

3.1.d Device Design Fabrication Issues

Before BLM micro-devices were fabricated, time was invested to learn how BLMs were formed in the NIST test chamber. The design was reverse engineered with hopes of leveraging past experiences in reducing the learning curve and design iterations when working with the BLM micro-devices. That first generation design was far from perfect and many design issues were prevalent, such as: 1) choice of materials, 2) polymer-to-solvent compatibility, 3) BLM supporting film choice, 4) microchannel sealing, 5) and supporting film hole fabrication.

Original scope for this project called for a micro-device capable of performing BLM studies with focus on utilizing polymer materials as the primary construction material. With that in mind, the choice came down to which polymers for which parts. Given the micro-device's sandwich structure, one polymer needed to be selected for the microchannel-imprinted wafers and a second polymer for the support film.

The supporting film initial choice was PTFE because this was successfully used by NIST in forming BLMs and was prevalently used by others in the BLM research community according to the literature [5, 19, 25, 47, 60, 65, 67, 68, 78-80].

However, PTFE quickly fell from grace since the non-porous type required was impossible to thermally bond to other polymers. As a result, mechanical bolting of the first generation devices was performed, which created more problems than solved. Figure 25 shows photographs of the first generation BLM micro-device. Channel leakage became a real problem especially when highly wettable pentane was injected into the system. In addition, supporting film holes were difficult to make in PTFE because of the higher temperature required to melt the polymer. After a frustrating period, PTFE was abandoned for polyvinylidene chloride, or PVDC. PVDC was suggested by Dr. Colombini of UOM Biology Department as a possible film choice since he used PVDC film for past BLM studies. After some further research, others in the literature use PVDC [60, 65] also successfully. PVDC solved many problems relatively quick: 1) Channel leakage was no longer a problem since devices could now be thermally bonded together thus sealing the channels, and 2) Creating small micron-sized holes in PVDC for BLM formation was also easier compared to PTFE. While having higher dielectric constant and poorer hydrophobicity compared to PTFE, the benefits gained in chip construction made PVDC the choice material for the supporting film. More details regarding supporting film hole formation is discussed in Appendix A.

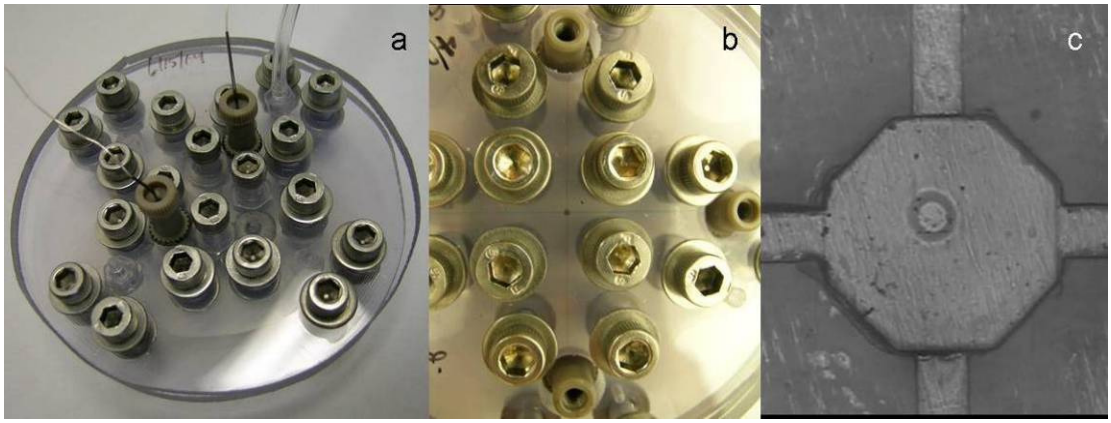

Figure 25: First generation BLM prototype. (a) Iso-view of bolted prototype utilizing PTFE support film, (b) Plan view of bolted prototype where the microchannels have been filled with blue and red dye indicators, and (c) Close-up of channel intersection and BLM formation site (70 µm diameter).

Material selection for the two imprinted wafers came down to two choices: polymethyl-methacrylate (PMMA) and polycarbonate (PC). These plastics were front runners because standard imprinting recipes for both exist due to their extensive use in other MEMS projects conducted at MML. PC was ultimately chosen overall due to its higher glass transition temperature (T_g = 150ºC) versus PMMA (T_g = 100ºC). The higher T_g is vital since PVDC has a T_g of 140ºC, thus the chip can be thermally bonded using the PVDC as an adhesion film without worry of melting the previously imprinted microchannels in the PC.

A paramount design concern is solvent compatibility between all the solutions required for BLM experimental testing and the materials used in the micro-device. For instance, phospholipids (i.e. DiPhyPC) typically used for BLM formation are soluble in both pentane and chloroform. Pentane does not dissolve polycarbonate or PVDC, whereas chloroform is acceptable with PVDC but dissolves polycarbonate. Chloroform would be a poor choice as a lipid carrier inside a polycarbonate device. All solvents used in the BLM micro-devices need solvent compatibility verification

either by checking solubility parameters given in the literature or by experimental confirmation.

3.2 Device Fabrication Overview

In constructing the BLM micro-devices, the fabrication steps are numerous. While fabrication details are important for successful chip construction, an overview is given here so the major fabrication steps can be highlighted. The fabrication details can be found in Appendices A-C.

The fabrication process can be split into three major categories: 1) preliminary micro-device fabrication, 2) Ag/AgCl electrode fabrication, and 3) final assembly and post-bonding operations. These will be discussed in turn.

3.2.a Preliminary BLM Micro-device Fabrication

The process starts with two blank polycarbonate (PC) wafers, one for the top microfluidic network and one for the bottom microfluidic network. Both wafers are imprinted with the appropriate microfluidic network by hot embossing, as shown in Figure 26a. Hot embossing involves placing blank PC wafers into a heated press, where they are pressed against a master template (mold) that has the negative microfluidic pattern of interest. Master templates are created by photolithography, where SU-8, a negative tone photo-polymer, is patterned on silicon wafers. These master templates are placed in a hot press prior to the blank PC pieces. Once everything is arranged in the press, an optimized heat and pressure recipe is implemented and the outcome is an embossed PC wafer with microfluidic channels mimicking the master template, just inverted. See Appendix A for details on hot embossing (e.g. hot press set up, imprinting recipes, SU-8 photolithography, etc)

After the PC wafers are imprinted with microchannels, machining operations are performed individually to the top and bottom imprints. First, a series of mounting holes are drilled so the wafers can be held by mechanical fixtures in future fabrication steps. Next, via holes are drilled in the top wafer, which allow for later fluidic and electrical connections after the device is finished. All holes are drilled using a drill press as illustrated in Figure 26b. If an open well micro-device being is constructed, the well is machined at this point.

Next, a pre-cut piece of PVDC film is placed on the bottom PC wafer covering the microchannels. To avoid application problems, such as creases, air bubbles, etc., a film application method has been developed which involves sliding a piece of PTFE from underneath the PVDC and then smoothing the PVDC out on the bottom PC imprint, as shown in Figure 26c.

The last step in this fabrication section is hole creation in the PVDC film as shown in Figure 26d. Feed-thru holes that connect the upper to lower microchannels are created first, followed by the hole which becomes the BLM formation site. The feed-thru holes are about 120 µm in diameter, whereas the BLM formation holes are approximately 40 µm in diameter. A specialized device, called the film hole burner, was constructed in order to create these micron-sized holes in PVDC film. Precise location of the feed-thrus and BLM formation sites are required since these features need to be located inside micron-sized features. The Film Hole Burner accomplishes all of these tasks and is discussed further in appendix A.

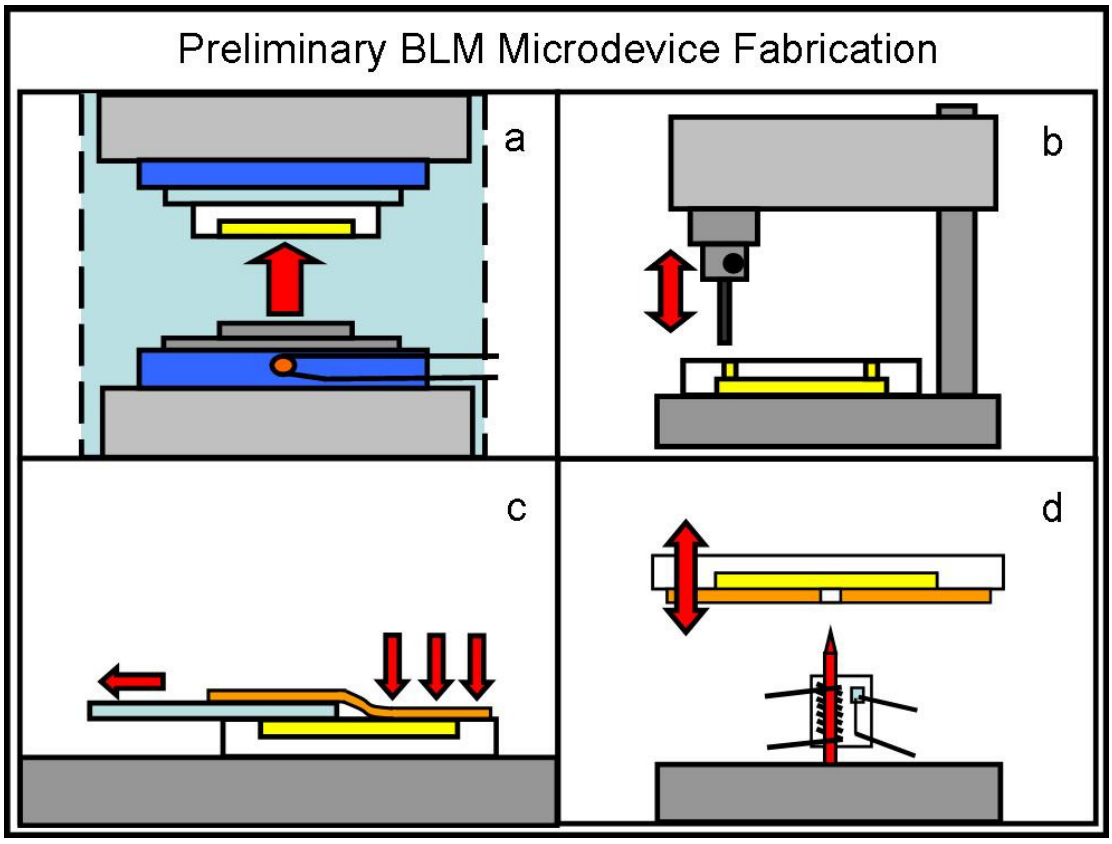

Figure 26: Preliminary BLM micro-device fabrication steps. (a) Using the hot press to imprint microchannels into polycarbonate wafers, (b) Using a drill press to drill holes that perform various functions in the imprints, (c) Applying the PVDC film to the bottom imprint, and (d) Burning the BLM formation site and feed-thrus in the PVDC film.

3.2.b Ag/AgCl Electrode Fabrication

The next phase of chip construction consists of Ag/AgCl thin film electrode fabrication on top of the PVDC film by using a combination of evaporation and electroplating techniques. This process is illustrated by Figure 27.

A brass shadowmask is mounted over the PVDC film during evaporation so select areas are metal coated, see Figure 27a. Prepared in lots of six, the wafers have layers of Cr, Au, and Ag thermally evaporated onto them with nominal deposition depths of 100 Ang, 100 Ang, and 1000 Ang, respectively as shown in Figure 27b-d. The brass shadowmask is subsequently removed revealing patterned metal traces.

To increase electrode performance, e.g. stability and lifetime, the Ag thickness is increased using an electroplating technique. After placing each wafer onto a homemade electrochemistry rig, each trace to be electroplated is covered with plating solution (0.35 M $AgNO_3$ in aqueous 1M NH_3) followed by submersion of a Pt counter electrode overhead. A constant current (~mA) is then applied across the counter electrode and the Ag working electrode trace, thus causing Ag to plate onto the existing Ag trace, as shown in Figure 27e. Electroplating is performed until the Ag trace thickness is nominally 2 μm thick and each trace is electroplated separately.

The final step in the electrode fabrication is to chloridize the Ag traces tips where they extend into the microchannels. This is done by piping an oxidizing solution, 30 mM $FeCl_3$, onto the trace tip, and waiting 1 minute for the reaction to occur. The reaction is self-terminating due to the amount of exposed Ag reducing over time. After one minute, a AgCl layer exists over the pure Ag trace, as shown in Figure 27f. The electrodes are complete and the final stage of the chip fabrication can begin.

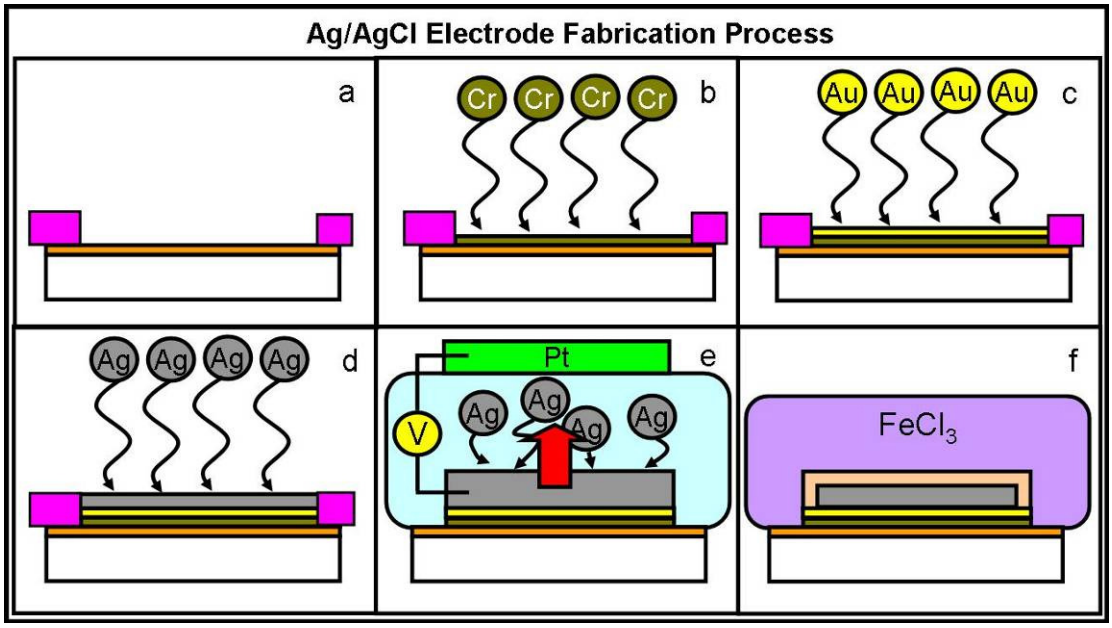

Figure 27: Ag/AgCl electrode fabrication overview. (a) A brass shadowmask is mounted over the bottom PC wafer, (b) Chromium is evaporated onto the PVDC, (c) and (d) Followed by gold and silver, (e) The Ag layer is thickened by a secondary electroplating process, and (f) Electrode traces extending into the microchannels are chloridized.

3.2.c Final Assembly and Post-Bonding Operations

The PC wafers are ready for assembly into devices. The first step is wafer alignment, where microchannels in the top imprint are carefully mated to the ones in the bottom imprint. Microchannel alignment needs to be within 10 µm or device functionality will be compromised. To achieve such tight positioning tolerances, an alignment jig was constructed as illustrated in Figure 28a. The alignment jig attaches to a probe station, thus utilizing its inherent translational and rotational capabilities to help align the top to the bottom wafer. The alignment process is performed with aid of a microscope.

After alignment, the wafers are temporarily pinned together, removed from the alignment jig, and then placed into the hot press for thermal bonding, see Figure 28b. An optimized heat and pressure recipe is used which causes the PVDC film to

function as an adhesive layer. Upon cooling, the top and bottom wafers become an integral micro-device. Process details on device thermal bonding can be found in appendix C.

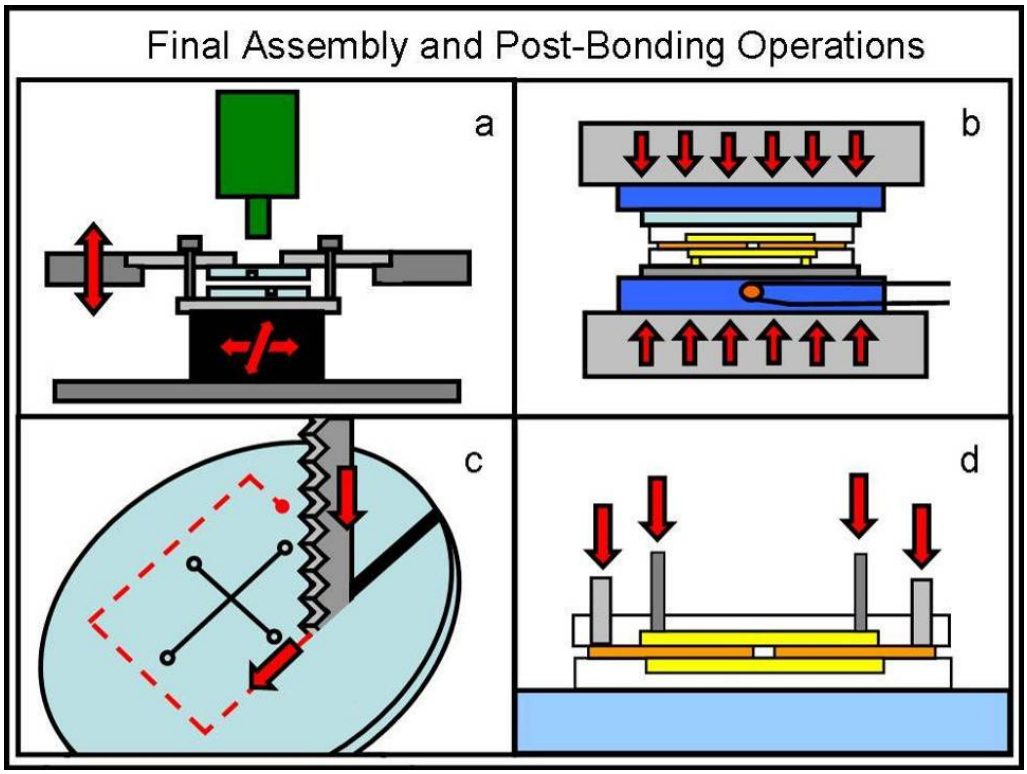

Figure 28: Chip assembly and post-bonding operations. (a) Prior to thermal bonding, the top and bottom wafers are aligned. (b) Thermal bonding of device in the hot press. (c) Extracting the micro-device using a band saw, and (d) Readying the micro-device for testing by adding fluidic ports and electrode terminals.

The next step involves removing the micro-device from its now useless surrounding. Using a band saw, the chip is extracted by cutting around the chip's designated boundary as demonstrated in Figure 28c. The final step in the micro-device fabrication process is to prepare the chip for testing which consists of inserting the needle ports for fluidic I/O and attaching electrode terminals for electrical I/O, which is illustrated in Figure 28d. The fabrication process concludes and the micro-device is ready for testing.

Chapter 4 Micro-Device Experimental Testing and Results

This chapter discusses experimental testing and results regarding the BLM micro-devices. First, the experimental setup is reviewed along with instrumentation used in a typical test. Next, test results for the open well BLM micro-device are discussed followed by results for the BLM micro-device array chip. Testing procedures (i.e. BLM formation, etc) will be presented for each chip.

4.1 Experimental Setup and Instrumentation

The BLM micro-devices are tested while sitting on the translational stage of a Zeiss Axiovert 200 inverted microscope. The microscope, with BLM micro-device, sits on a vibration isolation table with a Faraday cage overhead to minimize noise pickup. The microscope has a side-mounted camera, Zeiss Axiocam MRm, which feeds video to a DAQ computer. A commercial software program, Zeiss AxioVision, allows the user to view or archive the video feed.

For fluidic I/O, a bank of Harvard Apparatus PHD 2000 Infuse/Withdrawal syringe pumps are adjacently located to the microscope and are also connected to the DAQ computer for remote control. The syringe pump control electronics are housed outside the Faraday cage whereas the syringe pump stepper motor are inside the Faraday cage. Typically, the three syringe pumps are connected to the micro-device as shown in Figure 29. Buffer solution, α-HL solution, and PEG-containing solution need to be hooked up to the chip. The syringe pumps are controlled by a homemade software program, called *Pump-inator 2006*, which is discussed briefly in Appendix D.

For electrical I/O, the micro-device's integrated Ag/AgCl electrodes are connected as shown in Figure 29. Membrane input command potentials, applied via the lower microchannel, are controlled by using the Axopatch 200B amplifier. The primary Ag/AgCl electrode, which connects to the open well, is connected to the high impedance headstage (CV203BU). Inside the headstage, the membrane current is converted to a proportional voltage output signal (I / V converter) prior to sending the signal outside the Faraday cage to the main Axopatch amplifier. The output signal is then filtered using an onboard 4-pole Bessel Low-Pass filter (f_c = 10kHz) and subsequently amplified prior to being digitized by a Digidata 1440A (Molecular Devices) Digital-to-Analog converter at a sampling rate of 50kHz (20 µsec).

All electrical signals (voltage input and current output) from the micro-devices are recorded on the computer via DAQ software, Clampex 10 (Molecular Devices). The digitized electrical signals are displayed visually on screen along with syringe pump conditions and microscope video feed so real time testing conditions are known. All data displayed on the computer desktop is then screen captured with Snag It 8 (TechSmith Corp, MI) software for later analysis.

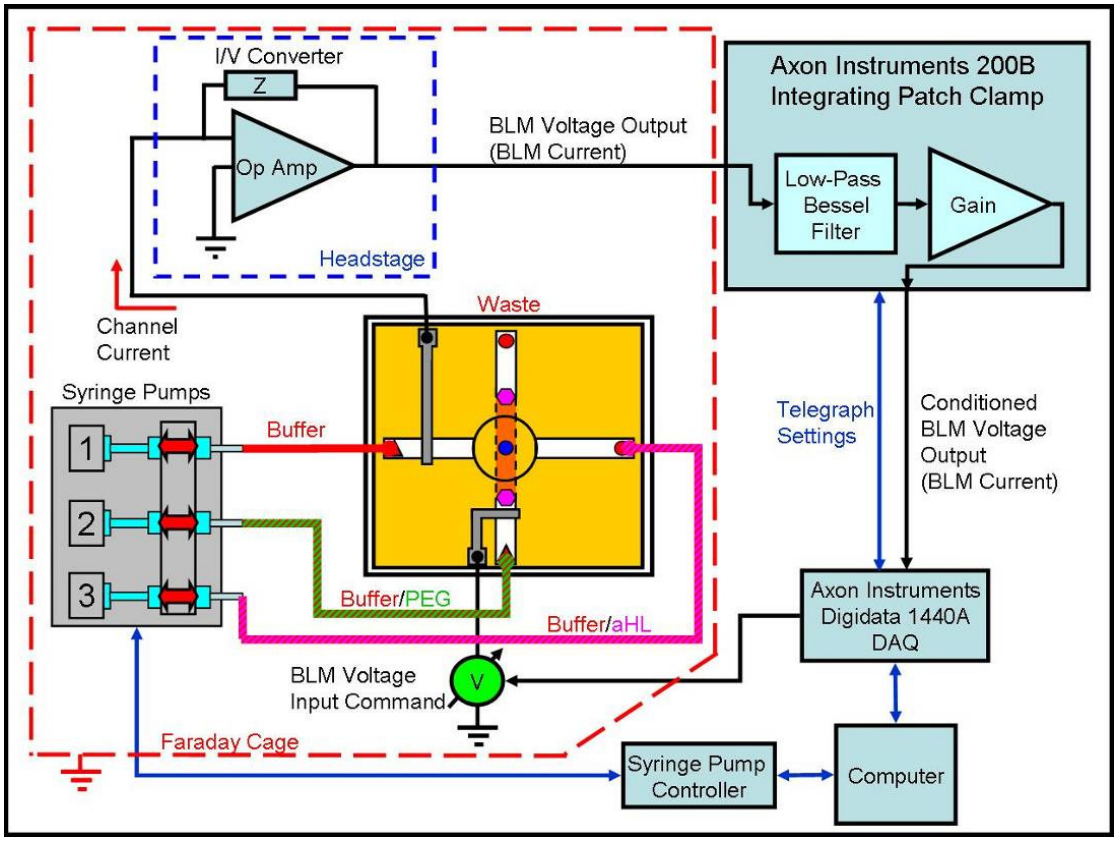

Figure 29: Open well BLM micro-device experimental block diagram. The BLM micro-device array chip is tested in a similar manner. See text for details.

4.2 Open Well BLM Micro-Device Results

4.2.a BLM Formation Technique

This section discusses the diffusion painting technique used to form BLMs in the open well micro-devices. First, the background and issues that led to diffusion painting development are discussed. Next, the physical procedure is presented on painting a BLM in the open well micro-devices. Lastly, a method for checking BLM quality is reported which can be used for both micro-devices.

Open Well BLM Formation

Recall the two common BLM formation techniques: 1) Folding Bilayer and 2) Painting. Both were discussed earlier in Sections 2.1.b and 2.2.b, respectively, and both were tried on the open well BLM micro-devices without success.

Initially, the folding bilayer method seemed like a feasible technique to try in the open well micro-device because it could be adapted easily from the NIST test chamber standard procedures. However after a few attempts, the BLM would never form as the second aqueous phase was carefully pumped over the supporting hole. The top buffer solution would always snap through the BLM formation site thus mating up with the bottom buffer. While this technique still holds future promise, a suitable technique for forming BLMs in the micro-devices via the folding bilayer technique has yet to be perfected.

Traditional painting of BLMs, on the other hand, is an art because one needs to have: 1) the "right" paintbrush with all but one bristle cut off, 2) the "right" amount of lipid solution on the single bristle, 3) the "right" amount of hand-eye coordination that borders on exceptional, and 4) the "right" amount of delivered lipid solution so that the lipid tends to thin and not plug the hole. Clearly, if one of these "rights" is wrong than the process becomes extremely unsuccessful with the common outcomes being a hole plugged with too much lipid solution or nothing at all. BLM formation via painting can be frustrating and takes patience and practice. Based upon the two most common outcomes, the painting method is very sensitive to the amount of lipid solution delivered. If the traditional paint method can be modified so that the amount of lipid solution delivered factors less in the overall outcome of BLM formation, then this technique will be improved.

BLM Diffusion Painting

The idea of using diffusion to rid extraneous lipid solvent is not a new one. Recall, Malmstadt et al. [39, 40], carefully chose a lipid solvent so that it would diffuse into the surrounding PDMS thus forming a BLM. A similar lipid solvent can be designed where the extraneous lipid solvent diffuses away into the bulk aqueous phase. Diffusion painting of BLMs is based on this concept.

Traditional lipid solutions used for BLM painting usually consist of an alkane or alkene (e.g. n-decane, n-hexadecane or squalene) as found in the literature [20, 24, 25, 76, 81-83]. Alkanes are mainly chosen because they are hydrophobic and immiscible in water, thus perfect choices for lipid solvation and annulus composition. Longer chain alkanes are utilized to keep the BLM thin as lower chain organics can partition into the BLM from the annulus [84]. The annulus, while making up a large part of the BLM's total volume, is small compared to the volume of the BLM formation site hole in which the BLM occupies. Based on this, the alkane solvent which comprises the annulus needs only to be in sparing amounts.

In diffusion BLM painting, the traditional lipid solution that is immiscible in the aqueous buffer phase is replaced in part by a lipid solution that is partially miscible. By using a lipid solution that consists of an immiscible solvent in ratio to a miscible solvent, the excessive miscible solvent can be driven off via diffusion while the immiscible solvent will remain behind in the BLM annulus. The miscible solvent will act primarily as a lipid carrier since it will diffuse away once the lipid solution is painted at the BLM formation site.

When selecting the miscible solvent, it must be: 1) able to dissolve the lipid molecules, 2) miscible with the immiscible solvent, 3) compatible with the

surrounding polymers, and 4) able to diffuse into the surrounding bulk aqueous phase at a controllable rate. An alcohol-based solvent was chosen since it meets the conditions set forth above. For the immiscible solvent, hexadecane will be used since it is a traditional solvent for BLM painting.

Table IV provides solubility data for a few simple alcohols. As expected, this data shows that the alcohol solubility in water decreases as chain length increases. However, the data presented does not indicate how fast the alcohols diffuse into an aqueous phase containing salt. Because the alcohol diffusion rate is unknown and is the ratio of alcohol-to-alkane, empirical testing was performed to determine the best alcohol to use as the miscible solvent in the lipid solution. Alcohol-to-hexadecane ratios (v/v) starting from 10^3 : 1, 10^2 : 1, 10 : 1, and 1 : 1 were tried. Lipid concentrations of DiPhyPC were held constant with traditional painting concentrations at 15 mg/ml.

Table IV: Alcohol Solubility Limits in Water

Alcohol	Water Solubility[85]
Methanol	∞
Ethanol	∞
2-Propanol	∞
n-Butanol	80 g/L at 20ºC
n-Pentanol	22 g/L at 22ºC
n-Hexanol	6 g/L at 25ºC
n-Heptanol	2.85g/L at 100ºC

After a few initial tests, Methanol through n-Butanol were found to diffuse away too quickly as little lipid solution would be remain on the glass brush just after submersion in the open well. On the other hand, a lipid solution containing n-Heptanol took over an hour to diffuse away, thus leaving n-Pentanol and n-Hexanol as possible choices. Subsequent tests with both alcohols, found that a 10 : 1 alcohol-

to-hexadecane ratio performed the best while still using DiPhyPC lipid concentrations around 15 mg/ml.

Novel BLM Diffusion Painting Formation Technique

Forming a BLM in the open well micro-device by using the diffusion painting method starts with filling the chip with buffer. Figure 30a illustrates the steps of BLM formation in the open well micro-device and Figure 31 shows a series of still photos taken during an actual BLM formation process. In this case, 4 M NaCl with 10 mM MES (pH 7.5) buffer was used to fill the chip. Next, a Pyrex glass "brush" is used to paint the lipid solution over the BLM formation site as shown in Figure 30b. Made from 3/16 inch in diameter rod stock, this glass brush consists of a thermally drawn neck down with a fire-polished ball end whose diameter is in the hundreds of microns (~300 μm). A small portion of the lipid solution (~1 μL of 15 mg/ml DiPhyPC in 10 : 1 v/v n-Hexanol : n-Hexadecane) is dispensed onto a clean glass microscope slide and is gathered up with the glass brush's ball end using a rolling motion.

After coating the brush with lipid solution, the brush is submerged into the open well until the ball end touches the supporting film just adjacent of the BLM formation hole. The brush is then slid over the BLM formation site to the opposing side supporting film before the brush is lifted from the film. A good painting motion will cause a temporary occlusion of the BLM formation site, which can be seen by the change in electrical signal (saturated triangular waveform to squarewave) as the brush moves over the hole. If a painting attempt has been successful, the temporary occlusion squarewave will turn back into a triangular waveform with finite amplitude.

Sometimes a few tries are needed to successfully apply lipid to the BLM formation site. The first attempts may be "pre-treating" the formation site for subsequent painting tries and / or the lipid solution is stripped off the brush by the buffer's high surface tension as the brush is submerged.

After a successful painting attempt, the lipid solution spans the BLM formation site as shown in Figure 30c. The alcohol portion of the lipid solution starts to diffuse away into the bulk buffer phase and the output current signal is triangular with its gain shrinking with time. Diffusion time will again depend on a few factors, mainly the alcohol's molecular weight and the volume of delivered lipid solution. Observations made during experiments have indicated alcohol diffusion time becomes slower in higher salt buffers but this has not been formally studied. After the alcohol diffuses away completely, the output current signal will transform itself from a triangular wave into a squarewave signifying that the BLM has formed as illustrated in Figure 30d.

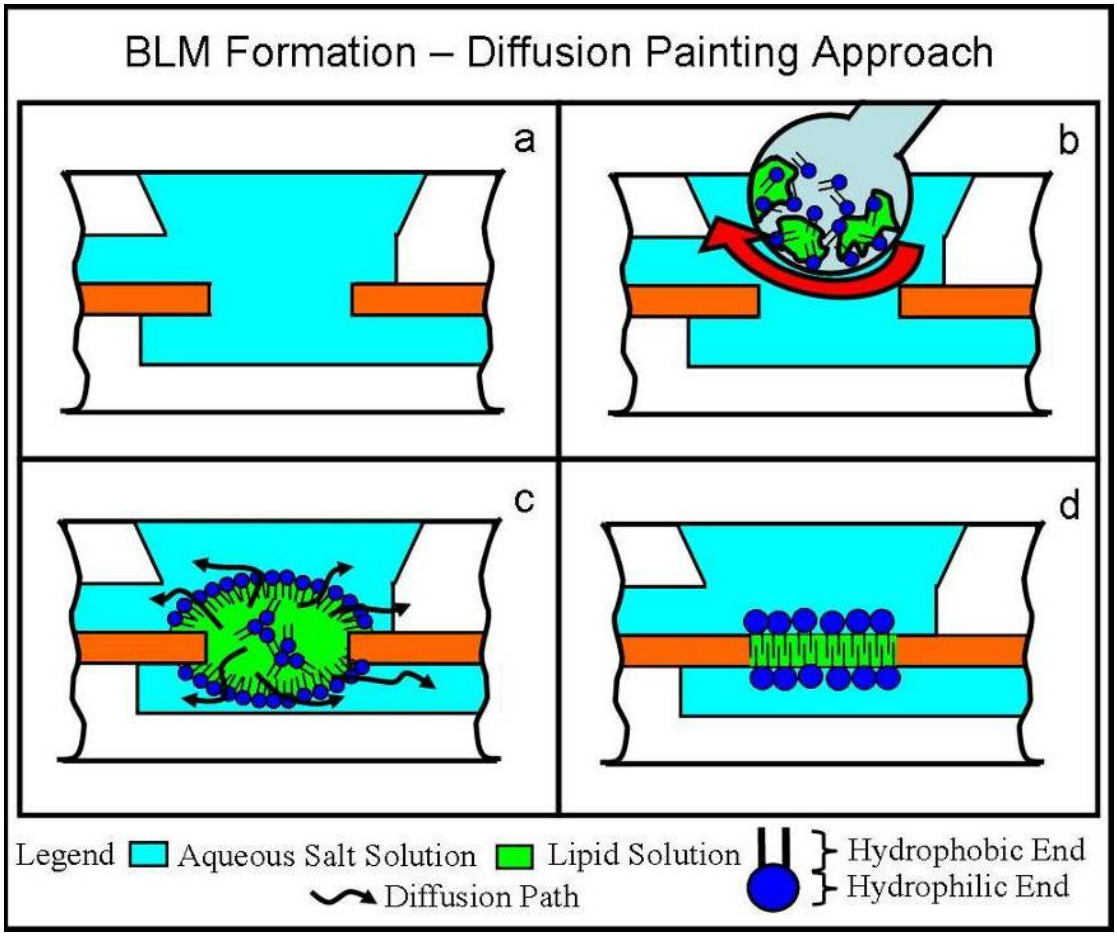

Figure 30: BLM formation method utilizing diffusion of extraneous lipid solution into the surrounding aqueous buffer. See text for details. Not to scale.

Ascertaining BLM Quality and Lifetimes

After the BLM is formed and thinned, the process turns to ascertaining whether the formation spanning the hole is truly a BLM and if so, of what quality. There a few items to check: 1) The output current waveform should be a squarewave provided that the input is a triangular waveform. 2) When 40 mV DC is applied, current should not be excessively noisy or drift erratically or have substantial leakage current. A good BLM will have a leakage current < 1 pA [76]. Substantial leakage usually indicates a leaky annulus (dirty chip, etc). 3) The squarewave amplitude is required to fall into an acceptable range. This process is discussed in detail next.

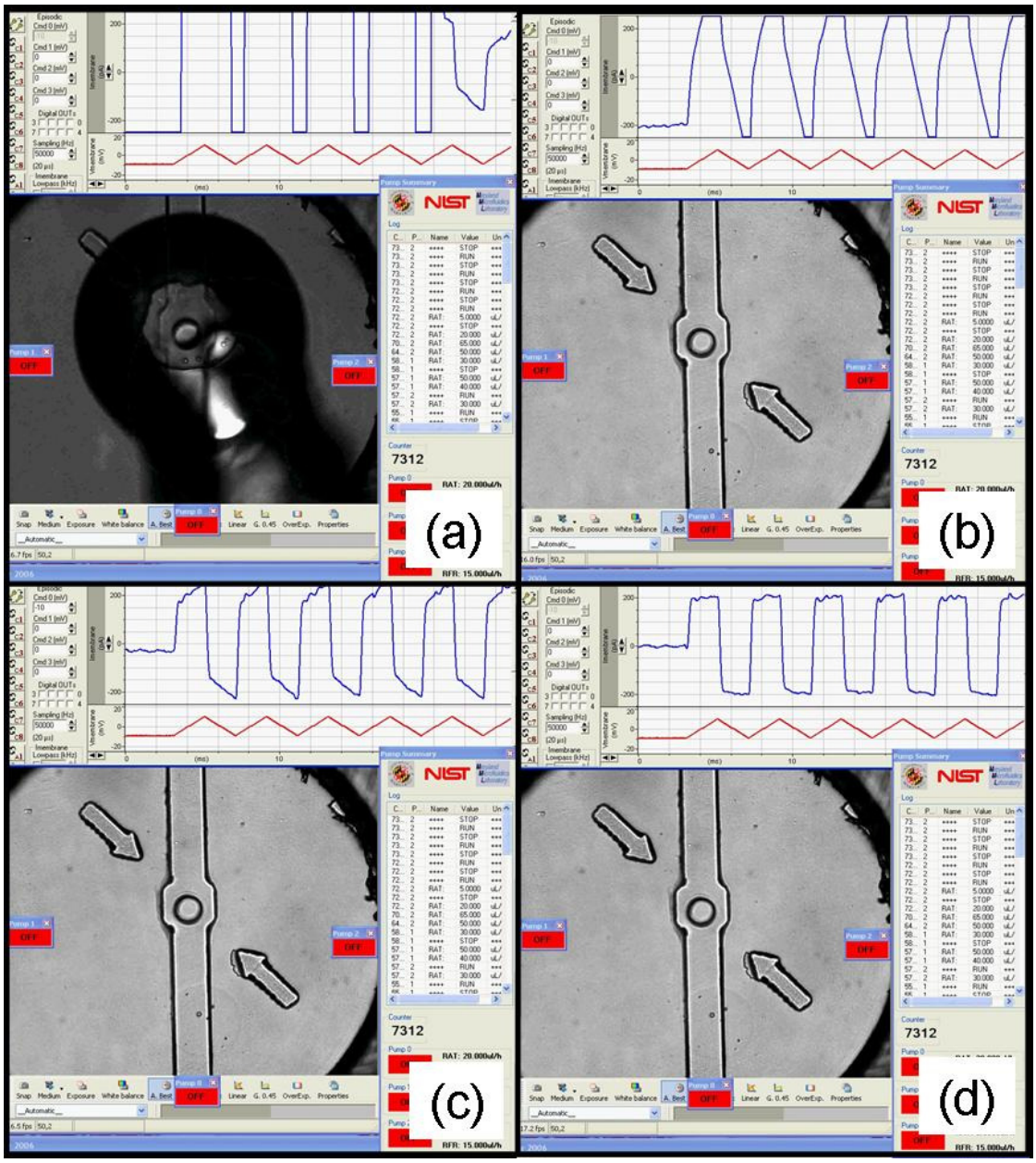

Figure 31: BLM formation method by diffusion painting. (a) A glass brush paints lipid solution over the BLM formation site. Electrical I/O signals depicted above where blue waveform is output current and red is input triangular waveform at 20mVp-p, 250 Hz. (b) Later, current waveform gain shrinks slowly transforming into a squarewave. (c) Later, the squarewave is becoming more pronounced, and (d) Resulting squarewave for the current output signifying that the BLM has formed. The entire process took approximately two minutes.

Verification of BLM Quality

BLM diameter varies from test to test, thus following a quality assurance protocol will guarantee that each passing BLM is acceptable for further testing. The BLM quality protocol verifies that the output current squarewave amplitude is in an acceptable range provided that the input is a 20 mVp-p, 250 Hz triangle wave. As an example, the BLM formed in Figure 31d is spanning a hole in the PVDC that is ~45 µm in diameter and the output current amplitude reads ~200 pA. A BLM diameter can range from 0 µm < BLM Diameter < 45 µm where 0µm would be a thick lipid plug and 45 µm would be the maximum diameter constrained by the hole diameter.

Figure 32 compares output current squarewave amplitudes obtained empirically versus the BLM diameter range discussed above. Shown are three lines that indicate various BLM specific capacitances, C_{BLM}, given in the literature [76]. The blue line represents theoretical ideal BLM specific capacitance (1 µF/cm^2), whereas the red line represents folding bilayer specific capacitance (0.7 µF/cm^2) and the black line represents painting bilayer specific capacitance (0.4 µF/cm^2) all plotted versus BLM diameter. The following equation was used to determine the output current squarewave amplitude:

$$i_{BLM} = (C_{BLM} A_{BLM} + C_{stray}) dV/dt$$

where i_{BLM} is the output current, A_{BLM} is the BLM area, dV/dt is the time derivative of the input voltage, and C_{stray} is the chip's background capacitance. The input voltage waveform was provided earlier, thus dV/dt equals 10 V/sec and the stray micro-device capacitance, C_{stray}, was empirically measured from a "no-hole" BLM micro-device. A "no-hole" micro-device is a chip without the BLM formation hole burned into the PVDC film. Filling a no-hole BLM micro-device with buffer and

applying an identical input will yield a squarewave that identifies the chip's stray capacitance. Electrical measurements from a "no-hole" micro-device conclude that the open well BLM micro-device's stray capacitance is ~10 pF.

As Figure 32 shows, if a BLM diameter occupies the entire BLM formation hole (i.e. 45 µm) than the maximum current output squarewave will be approximately ~260 pA if using the blue line, ~210 pA if using the red line, and ~165 pA if using the black line for BLM specific capacitance, respectively. Since the output current amplitude in Figure 31d is ~200 pA, the BLM falls in an acceptable range 165 pA < 200 pA < 260 pA. Also note the BLM formed in Figure 31d falls between the specific capacitances given for the folding bilayer and painting methods thus lending more credibility that the BLM formed is of high quality. If the measured current amplitude tends toward the ideal case (210 -- 260 pA or higher), the BLM curvature should be suspected to be non-planar due to some external influence. This BLM should be ruptured and reformed.

On the other hand, suppose the BLM diameter is small compared to the BLM formation hole. According to Figure 32, as the BLM diameter tends toward 0 µm, the output current squarewave amplitude tends toward 100 pA. This current amplitude would signify a thick lipid plug occupying the BLM formation hole, which was determined empirically earlier with the "no-hole" chip (100 pA / (10 V/sec) = 10 pF). By experimental observation, if a newly formed BLM had an output squarewave amplitude of ≤ 140 pA, the BLM should be rejected. BLM diameters on order of the supporting film hole radius tend to shrink with time thus thick lipid plugs result.

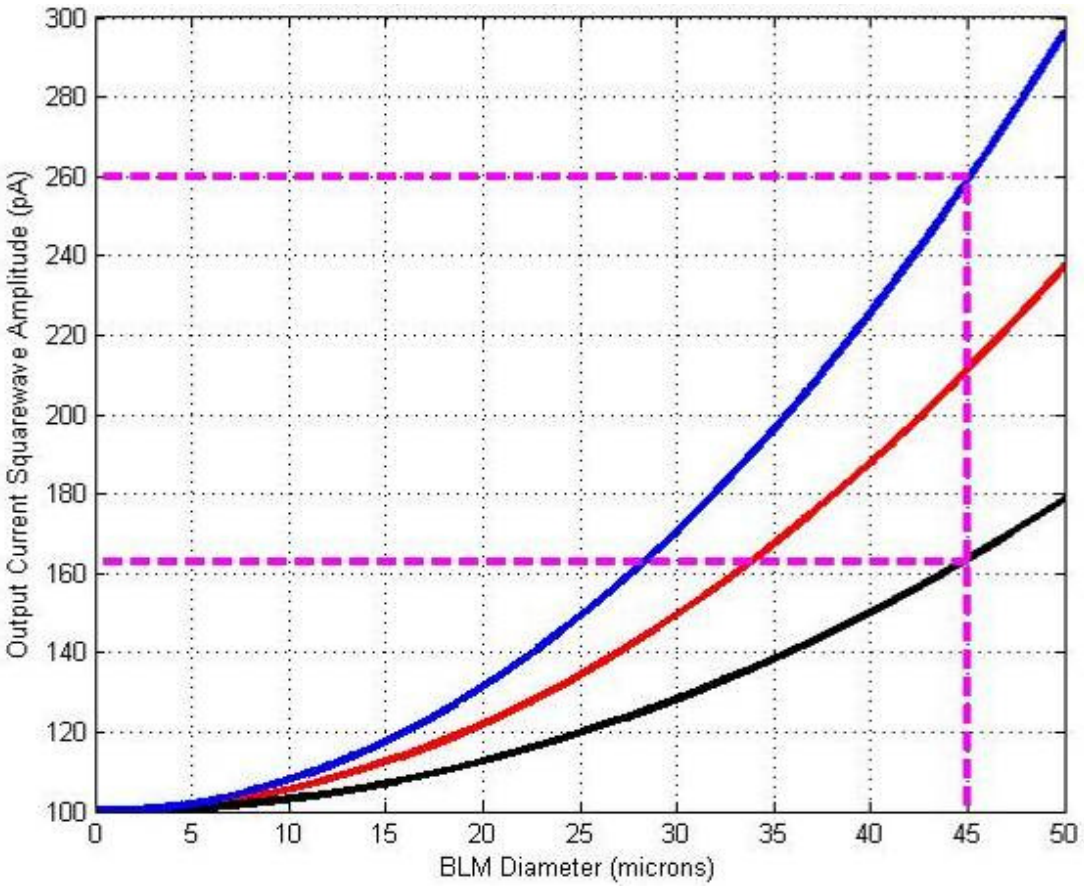

Figure 32: Output current squarewave amplitude versus BLM diameter determined empirically.

4.2.b Trans-membrane Channel Incorporation

Three different methods were attempted when incorporating α-HL channels into BLMs formed in the open well micro-devices: 1) Syringe injected via the top microchannel, 2) Syringe injected via the bottom microchannel, and 3) Manually piped into the top well as shown in Figure 33. Each method has its advantages and disadvantages. For instance, piping α-HL solution into the top well (Method 3) is a very quick delivery process. However diffusion of the α-HL protein can be slow without the aid of bulk convective mixing. On the other hand, injecting the α-HL solution via a syringe (Methods 1 or 2) constitutes a very slow (~μL/hr flow rates)

delivery process since the BLM is pressure sensitive, but this process effectively delivers the protein directly to site with minimal diffusion distance.

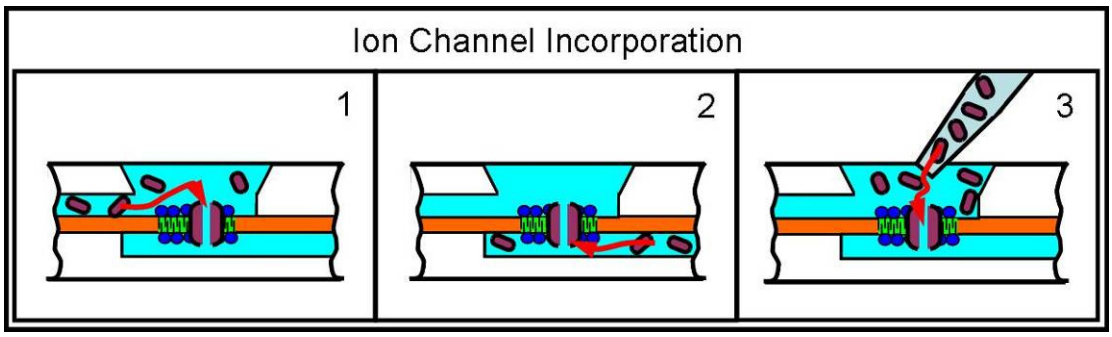

Figure 33: Ways to incorporate ion channels into the open well BLM micro-device. See text for details.

Each delivery method was performed with some being successful and others being unsuccessful. Piping 1-2 µL of 50 µg/mL α-HL solution into the open well directly produced numerous experiments with successful α-HL incorporation usually after 20 - 40 minutes. One difficultly with piping α-HL solution into the open well was that BLM rupture was common upon solution delivery.

When trying α-HL incorporation via lower microchannel injection, attempts were unsuccessful. Concentrations of α-HL solutions were varied from 25 – 500 µg/mL and the solution was pulse pumped for very long times (hours at ~3 µL/hr) to guarantee the α-HL solution reaching the BLM site. One possible explanation may be that the α-HL molecules are coating the microchannel walls and are never reaching the BLM site. Another possible explanation may be that an electrokinetic attraction/repulsion is occurring between the α-HL molecules and the Ag/AgCl electrode housed in the lower microchannel. This might be possible since α-HL is zwitterionic with an isoelectric point (pI = 8.5 [86]) and the α-HL solution pH used for experiments is approximately 7.2. Since the solution pH differs from α-HL's pI, α-HL is a charged molecule. With applied clamping voltages of +/- 40mV DC, it is

unclear if α-HL's electrophoretic mobility is problematic when testing inside the micro-device since the electric field is small.

Lastly, injecting α-HL solution via a top microchannel that did not house an Ag/AgCl electrode was successful. Again, α-HL solution concentrations varied from 25 – 500 µg/mL with pump rates between 5 – 15 µL/hr. Successful α-HL incorporation is shown in Figure 34. In this test, α-HL solution (500 µg/mL) was pulse pumped at 15 µL/hr into the open well until current jumps occurred. With an input clamping voltage of +40 mV DC, four distinct current jumps were observed after some time. Table V, below, provides the associated statistics for the four current jumps. Three of the four current jumps have close Δ mean current values of approximately 40 pA, which is expected for each α-HL channel incorporated at +40 mV applied potential. Each α-HL channel provides approximately 1 Siemen of conductance under 1 M KCl salt, pH 7.5 per [87]. However, α-HL channels can exhibit more than one conductance state at a given pH [67], which probably explains the third current jump outlier. In the next section, I-V data and rectification ratio will be discussed to help verify that α-HL channels did indeed incorporate as shown.

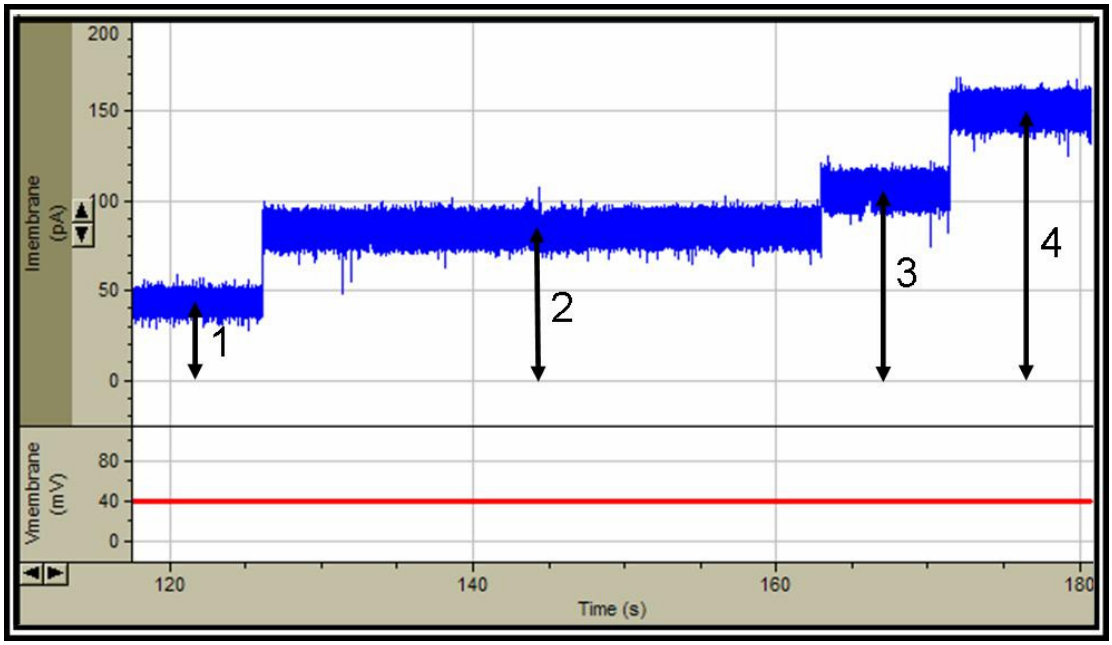

Figure 34: Data recordings showing four distinct α-HL current jumps (top, blue) and corresponding input clamp voltage at +40 mV DC (below, red). Current data filtered with an 8-pole Bessel low pass filter (f_c = 1 kHz). BLM bathed in 1 M NaCl buffer, pH 6.92.

Table V: Statistics for α-HL Current Jumps Shown in Figure 34.

Current Jump	Mean Current (pA)	Standard Deviation (pA)	Δ Mean Current (pA)
1	43.27	3.51	43.27
2	85.00	4.69	41.73
3	106.52	4.64	21.52
4	151.17	5.01	44.65

4.2.c I-V Curves and Rectification Ratio

Successful α-HL channel incorporation into a BLM can be verified by studying the current-voltage (I-V) relationship. α-HL channels exhibit a non-linear, rectifying, pH dependant I-V relationship as reported in [67, 88]. The degree of rectification can be determined by comparing the ratio of current magnitudes at equivalent positive and negative potentials (e.g. $| I(V_{-120mV}) / I(V_{120mV}) |$).

In Figure 35 below, multiple I-V curves are plotted for the α-HL channels incorporated into the BLM shown earlier in Figure 34. Note: the I-V relationship is ohmic for negative applied potentials whereas this is not the case at positive potentials. Additional, drops in current magnitudes at high positive potentials (i.e. +170 mV and +190 mV) for some data sets are due to the α-HL channels gating real time. The inset, shown in Figure 35, shows an I-V curve for an earlier single α-HL channel experiment recorded in the NIST test chamber with near identical test conditions (1 M NaCl, pH = 7.5) [67]. Note, the two sets of I-V curves look similar in shape, but have differing slopes due to the number of α-HL channels incorporated in each experiment. By comparing current values for negative voltages only, the number of α-HL channels incorporated during the open well micro-device test can be estimated at 7. Lastly, the rectification ratio at 120 mV for the I-V data collected with the open well micro-device is ~1.3 which compares favorably to the ratio reported in [67].

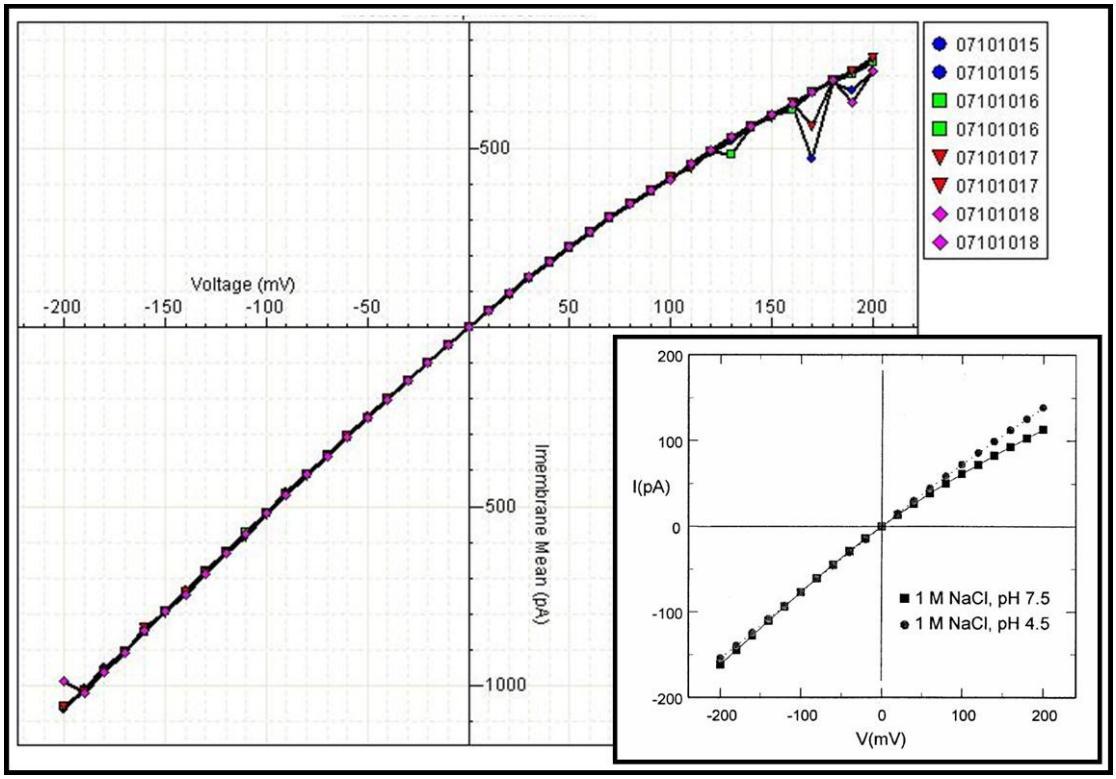

Figure 35: Multiple α-HL channel I-V data collected from an earlier experiment reported in Figure 34. Inset shows I-V data for single α-HL channel at 1 M NaCl, for pH 4.5 and 7.5. Inset from [67] with reprint permission granted by Springer-Verlag.

4.2.d PEG Biosensor Experiments

To show that biosensing can be performed with the BLM open well micro-device, PEG samples can be delivered to the BLM site similarly to α-HL channel delivery, as depicted in Figure 33. As with delivering α-HL solutions, some methods were successful in PEG delivery and others not. Multiple tests were conducted where mono-disperse PEG-29 solutions (MW = 1294 g/mol, 50 µM) were injected via a syringe into the top and bottom microchannel without success.

Due to time constraints, experiments were conducted where mono-disperse PEG-29 solution (50 µM in 4 M NaCl buffer) was "pre-loaded" into the open well prior to BLM formation. By pre-loading the open well, PEG blockades should occur immediately after BLM formation since the PEG is already on site. Shown in Figure

36a, a current trace shows an α-HL channel incorporating into a BLM bathed in 4 M NaCl, pH 7.52. Immediately after α-HL incorporation, current blockades occur as the PEG interacts with the channel. Details showing three other PEG blockades are in Figure 36b and c. Lifetimes of these blockades are on order of half a millisecond, which is expected for PEG threading through the α-HL channel head side first. PEG blockade lifetimes are known to be 10 times longer when the PEG threads through the α-HL tail side first due to the nanopore's asymmetry [56].

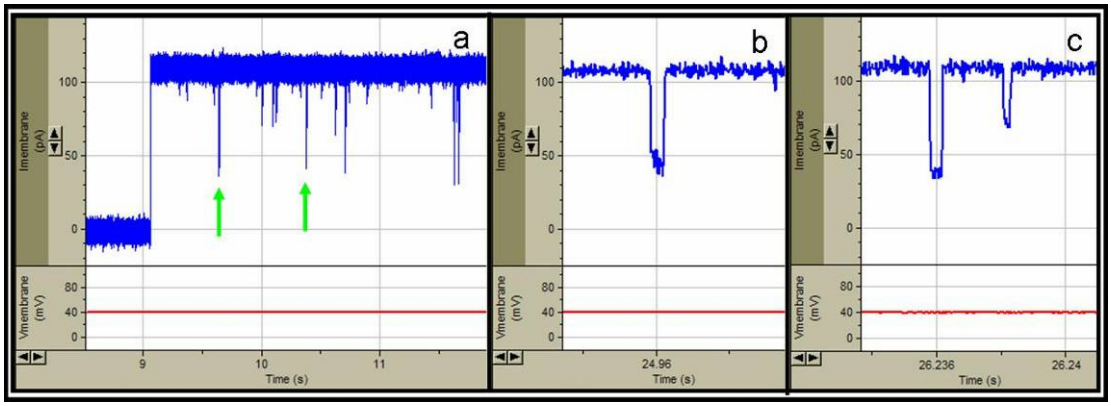

Figure 36: (a) Data recording showing single α-HL current jump of ~110 pA and immediate PEG-29 blockades (green arrows), (b) and (c) Close-up of three blockades with lifetimes in order of half a millisecond. Corresponding input voltage is +40 mV DC (red line), data sampling rate is 50 kHz, and filtered with a 4-pole Bessel low pass filter at 10 kHz. BLM bathed in 4 M NaCl, pH 7.52.

4.2.e PEG Blockade Analysis

Raw current signals need to be analyzed for PEG blockade recognition and to extract meaningful blockade information that ultimately could lead to PEG identification if given as an unknown analyte. Below in Figure 37, a 20 millisecond snippet of raw α-HL current data is provided containing a single state PEG blockade. In this example, the open channel current is ~110 pA and the PEG blockade current is ~50 pA. Since the open channel current has inherent noise, an open channel mean and standard deviation, C_m and C_σ respectively, can be calculated assuming a

Gaussian distribution. A noise floor, depicted by the green line, can then be determined by taking a user-defined number of standard deviations away from the mean (typically 4 - 6σ). Blockades are now defined by the current dropping below the noise floor for a minimum set of consecutive data points (typically > 5), which is set by the current sampling and filtering frequency used.

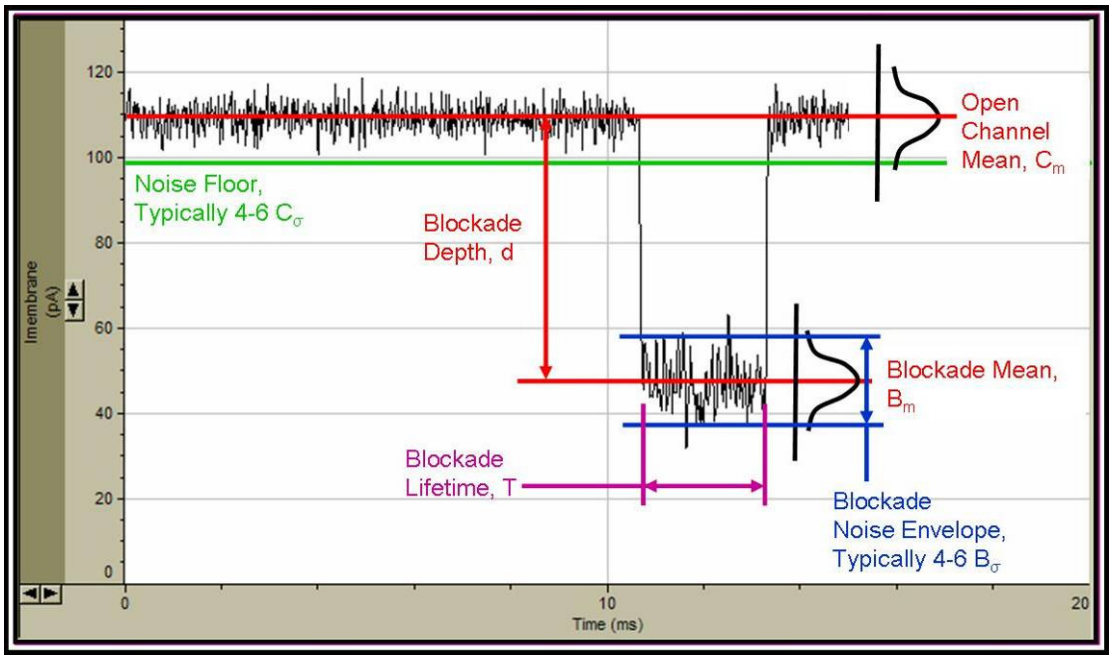

Figure 37: Sample PEG blockade analysis. See text for details.

For each blockade, the blockade mean and standard deviation, B_m and B_σ respectively, can be calculated. Again, a user-defined noise envelope (typically 4 – 6σ) around the blockade current can be utilized to extract outliers. The blockade depth, d, can then be measured which is the difference between the open channel mean and the blockade mean. Finally, the blockade lifetime, τ, is calculated by the absolute time difference between the first and last blockade data point within the blockade noise envelope. Analyzing many blockade events (typically > 10^5) will lead to a distribution of blockade depths and blockade lifetimes, which can be plotted as histograms.

4.2.f PEG Blockade Histograms

Implementation of the above analysis on thousands of blockade events can be daunting. To automate the process, a computer program was written in *Matlab* that accepts blocks of raw current data. The program analyzes the data for PEG blockade mean currents and lifetimes. The *Matlab* program outputs two histograms: 1) frequency of blockade mean currents, and 2) frequency of blockade lifetimes.

The entire current trace of Figure 36 was analyzed using the above *Matlab* program and the histogram output is provided in Figure 38. The top histogram shows the frequency of PEG-29 blockade mean currents, and the bottom histogram shows the frequency of PEG-29 blockade lifetimes. The blockade analysis on the 40 minute data set yielded 6773 blockades that were below the noise floor (6σ away at ~74 pA) and greater than 0.1 milliseconds in lifetime. As can be seen, there are three distinct mean blockade current peaks at approximately 35, 43, and 65 pA. Mono-disperse PEG-29 blockade data, obtained by using the NIST test chamber, was shown in Figure 16b, lower. Direct comparison of NIST data may not be logical since different buffer salt was used. NIST used 4 M KCl, pH 7.5 whereas the experiment discussed here was performed in 4 M NaCl, pH 7.52. Due to the difference in salt conductivity and how ions hydrate the PEG molecules [89], one would expect similar histogram shapes but with different values. Note, the same triple hump signature is evident when comparing the NIST PEG-29 data in Figure 16b to what is shown in Figure 38.

Looking at the blockade lifetime histogram, an exponential decay is seen versus lifetime, with an approximate decay time constant of 0.3 msecs. Quicker events occur around 0.1 msecs, whereas rarer events last 1-3mSecs in duration. NIST comparison data is not shown but PEG-29 blockade lifetimes show a similar

exponential decay but with a time constant of 3.2 msecs [90]. Blockade lifetimes observed by NIST are 10 fold longer, which could be an artifact of the testing conditions. PEG was allowed to interact with the α-HL channel via the tail side, whereas in the experiment discussed here, PEG was allowed to interact with the α-HL channel via the head side. α-HL electrostatic asymmetries are probably the reason for the different blockade lifetimes based upon channel entrance. This unpublished observation concludes that PEG blockade lifetimes are approximately 10 fold longer if PEG enters the α-HL channel tail side as opposed to head side [91].

4.2.g Open Well Micro-Device Testing Issues

Many issues were prevalent when testing the open well BLM micro-devices. The major issues include: 1) Too much lipid solution delivery even if the diffusion painting approach is used when forming BLMs. 2) Evaporation of buffer solution from the open well and lower waste reservoir which could lead to osmotic and hydrostatic pressure differences across the BLM. 3) Air bubbles especially at the fluidic inlet ports, and 5) electrostatic discharge rupturing the BLM if delivering solutions manually in the open well.

4.3 BLM Micro-Device Array Results

This section reports the results obtained when testing the BLM micro-device array chips. First, BLM formation inside the closed micro-device will be reported. Finally, issues regarding testing the BLM micro-device arrays will be discussed.

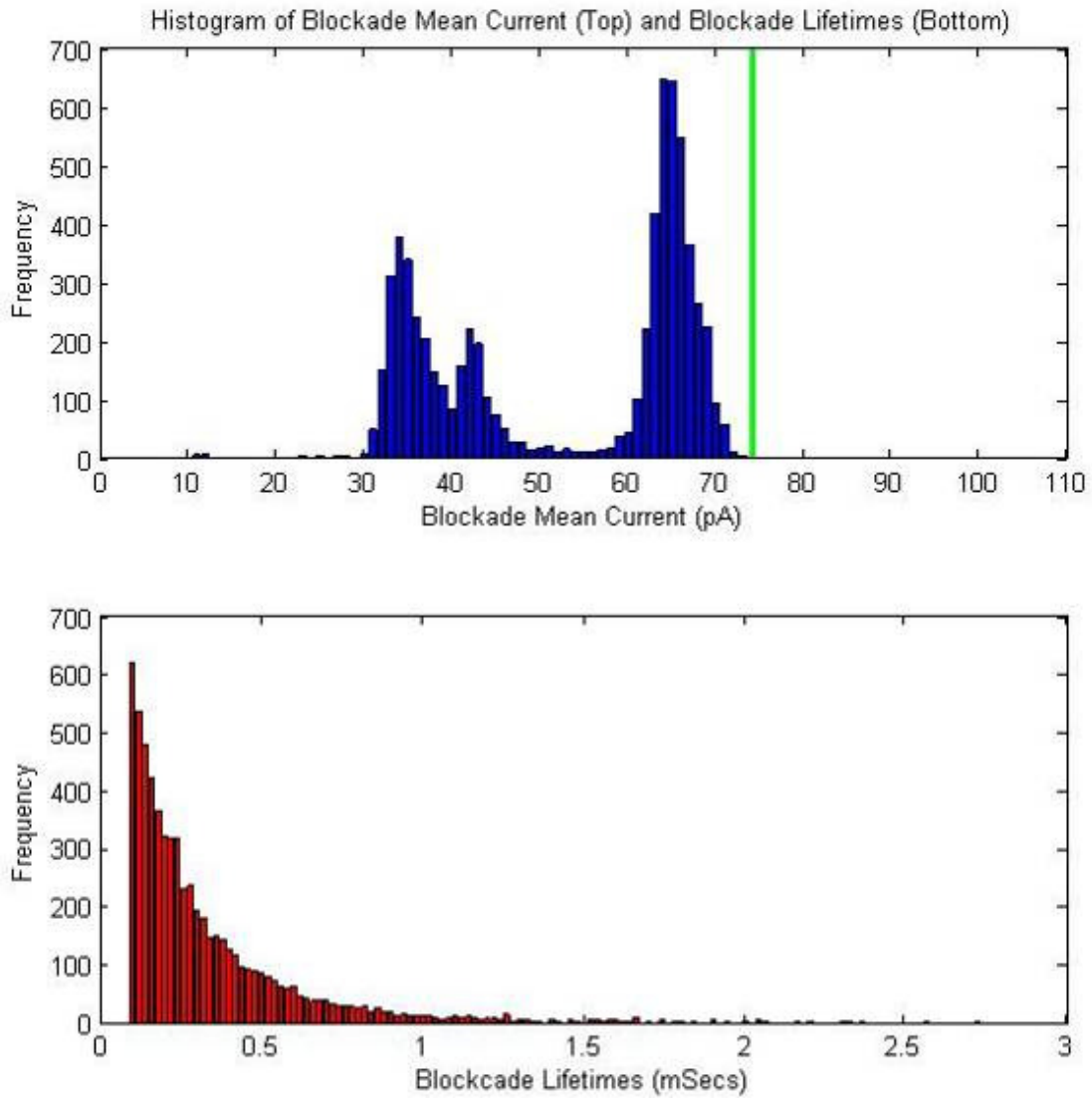

Figure 38: Histograms for the PEG-29 blockade data shown in Figure 36. (top) Histogram of blockade mean current, and (bottom) histogram of blockade lifetimes. The green line represents the noise floor (74 pA).

4.3.a BLM Formation Technique

BLM formation inside the closed array micro-device consists of precise fluidic movements. Initially, the entire chip would be filled with buffer solution (typically 1 M KCl, 5 mM MES, pH 6.7) starting with initial filling of the lower microchannel. Because of surface tension, the buffer will not flow through the BLM formation site as indicated by opposing arrows in Figure 39. Next, the upper microchannel is flooded with buffer and an electrical test is performed to check

electrode performance and buffer continuity. Lipid solution, consisting of 10 mg/mL DiPhyPC in n-hexadecane, is carefully pulse pumped into the main upper microchannel via a side channel at 1 μL/hr. Figure 39a shows the lipid solution entering the main channel as indicated by the red "1". After enough lipid solution enters the channel, buffer continuity is broken and the current output signal transforms into a squarewave. Some time later, the lipid solution volume slowly increases, spreading in both directions, and eventually passing over the BLM formation site as shown in Figure 39b. Occasionally, the lipid solution will recede back into the side channel from which it emanated from if fluid pumping was carefully performed as shown in Figure 39c. Some lipid solution delivered to the BLM formation site remains behind since current signal remains a squarewave, thus indicating a possible BLM formation. On other testing occasions, the lipid solution will not retract automatically and the lipid solution becomes stagnant in the main channel. In this case, buffer is injected into the upper microchannel to displace the lipid solution towards the waste well as shown in Figure 39d. As the lipid remaining within the 25 μm diameter hole thins, the square wave amplitude increases which is characteristic of capacitive lipid membrane formation. For the experiment shown in Figure 39d, post-BLM formation analysis of accompanying electrical signals yields a BLM capacitance of 2.5 pF. When dividing by the BLM area, a 0.5 $\mu F/cm^2$ specific BLM capacitance is achieved which compares favorably to other reported ranges of specific BLM capacitances [27, 32, 33, 35, 63, 81].

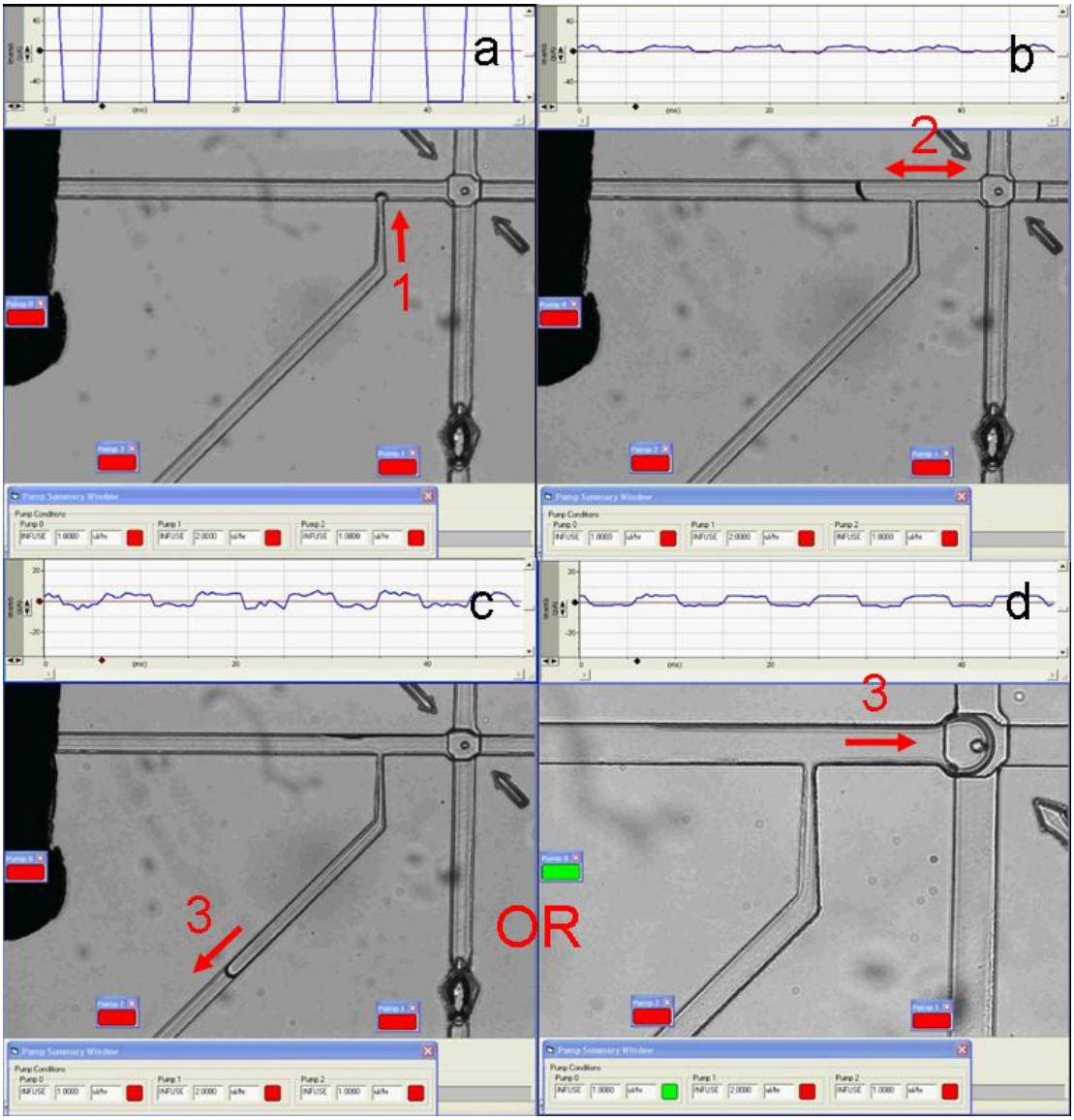

Figure 39: Typical BLM Formation Strategies for the BLM Micro-Device Array. See Text for Details.

4.3.b BLM Micro-Device Array Testing Issues

Many issues were prevalent when testing the BLM micro-device array chips. The major issues include: 1) Poor fluidic control when pumping the lipid solution into the chip for BLM formation. 2) The complexity of chip testing with more than a single site active, and 3) Air bubbles trapped inside the microfluidic device especially at the fluidic injections ports. Each issue will be discussed in turn.

Fluidic Control Issues

Because of its closed design, the ease of BLM formation is governed strictly by how well the fluids in the microchannel network are controlled and manipulated remotely. In a new micro-device array chip, a common problem is that lipid solutions tend to not act "plug-like"; meaning the lipid solution wicks everywhere due to its low surface tension and polymers inherent hydrophobicity. As shown in Figure 40, lipid solution is being pulse pumped toward the main channel. However before the main lipid front has reached the main channel, lipid solution has managed to wick along the microchannel walls preceding the lipid front. This wicking action causes lipid solution to collect in places not desirable as shown. To make issues worse even if the lipid solution were to be withdrawn back down the side channel, the lipid solution would eventually wick to the same places in a seemingly oscillatory way.

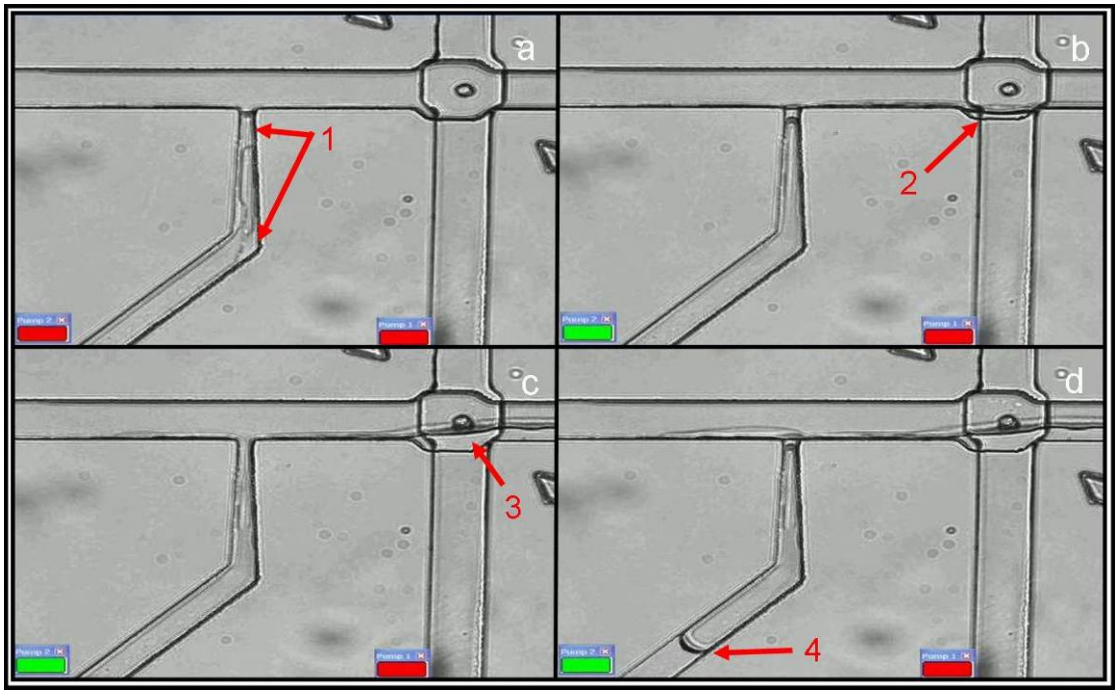

Figure 40: BLM formation attempt in a single site BLM array chip. (a) Lipid solution wicking along microchannel wall and collecting at microchannel neck down as indicated by no. 1. (b) Lipid solution running along main channel wall and fills trough at BLM formation site as indicated by no. 2. (c) Trough continues to fill as indicated by no. 3. (d) Main lipid front finally comes into view on side channel as indicated by no. 4. Note, lipid front curvature and long lipid solution trails along wall.

UV-Ozone Treatment

To improve fluidic movements inside the array chip, an UV-ozone surface treatment was performed to the PVDC film and mating PC wafer. The UV-ozone process is discussed in Appendix D. The effect of UV-ozone surface treating the upper microchannel can be seen in Figure 41. Initial results of new UV-ozone treated chips were promising as the lipid solution acts plug like (no wicking) when advancing into the main channel as shown in Figure 41a. However, benefits of UV-ozone treatment do not last long as once the lipid solution coats the surroundings, fluidic control seems to degrade especially if that portion of the microchannel was coated with lipid previously. In Figure 41b, buffer is being pumped into the chip so it

displaces the lipid solution towards the upper channel waste. However, the buffer overrides the lipid solution passing it by. Eventually, fluidic behavior in the UV-ozone treated array chip mimics a native array chip as shown in Figure 41c and d.

Due to material and process limitations, UV-ozone surface treatment can lead to a microchannel with very different wetting properties. In a treated micro-device design, the PVDC film (floor of microchannel) is more hydrophobic than the PC walls and ceiling, as reported in Table XIV of Appendix D. This difference in hydrophobicity causes the lipid solution to wick along the microchannel floor under certain conditions. Because UV-ozone treated chips quickly revert back to a chip with native-like fluidic control, UV-ozone surface treatment was not deemed worth the effort to perform on future chips.

Multiple Array Site Testing

When initially working with the BLM micro-device array chips, the chips were fabricated and tested with 1 x 3 array configurations. The idea was to be able to have three chances per chip per test to form BLMs. Since instrumentation was not available to electrically monitor all three BLM sites simultaneously, only the first (left most) array site was monitored with the other two sites left floating (lower channel electrodes No. 3 and No. 4 open). However, tests proved that additional BLM sites added too much system complexity as shown in Figure 42. Majority of the BLM micro-device array chips tested thereafter were of single BLM formation site configuration (1 x 1). Once the testing procedures for the single-site micro-device were proven, the idea was to increase system complexity again by adding in the remaining BLM formation sites.

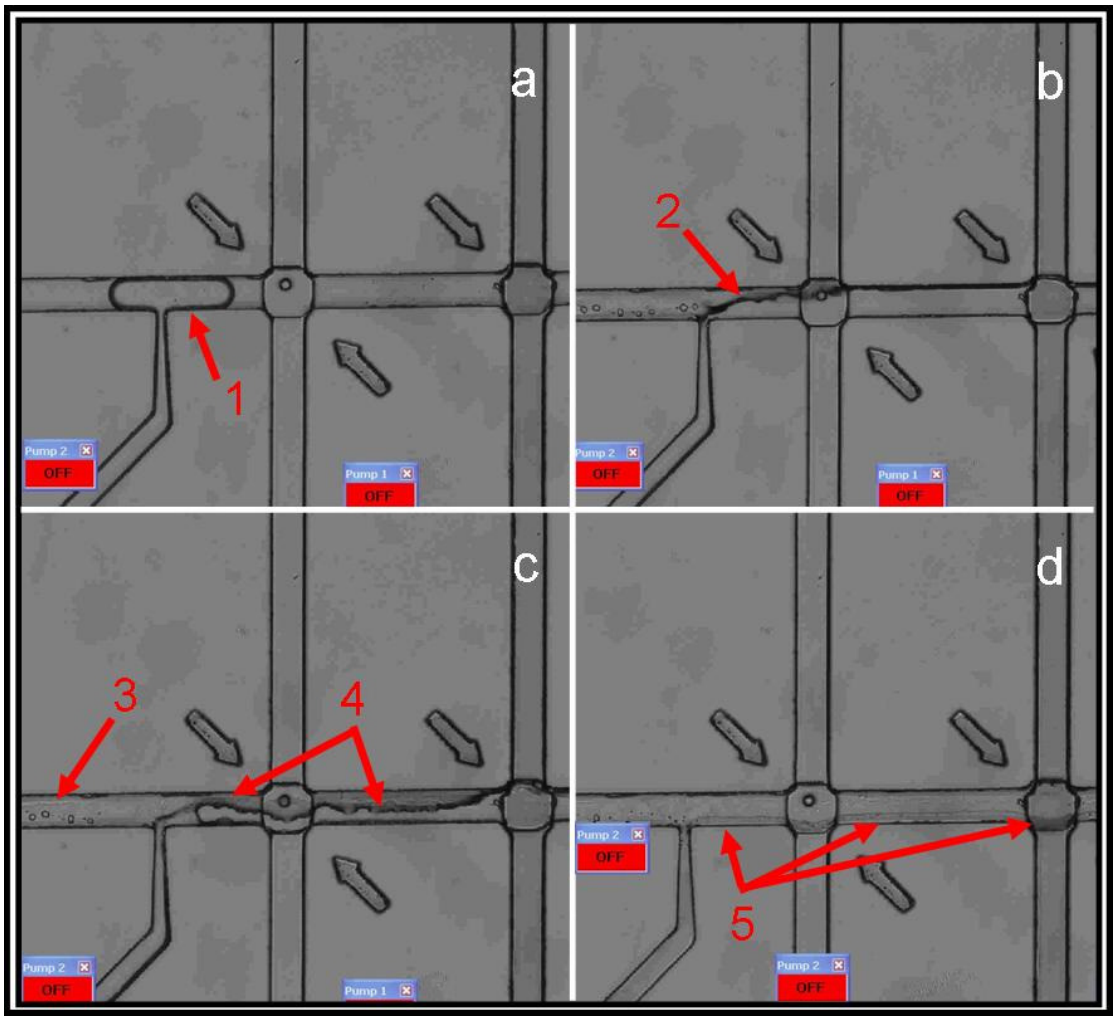

Figure 41: BLM formation in single-site, UV-Ozone treated, BLM array chip. (a) At no. 1, lipid solution is entering the main channel for first time. Note, shape of lipid front. (b) Buffer solution injected to displace lipid solution across BLM formation site toward waste. At no. 2, buffer solution is overriding lipid solution. (c) At no. 3, lipid solution puddles remaining behind, and at no. 4, lipid solution running along PVDC film. (d) At no. 5, lipid solution proceeding to wick along main channel wall filling up trough at array site 1 and further down the main channel.

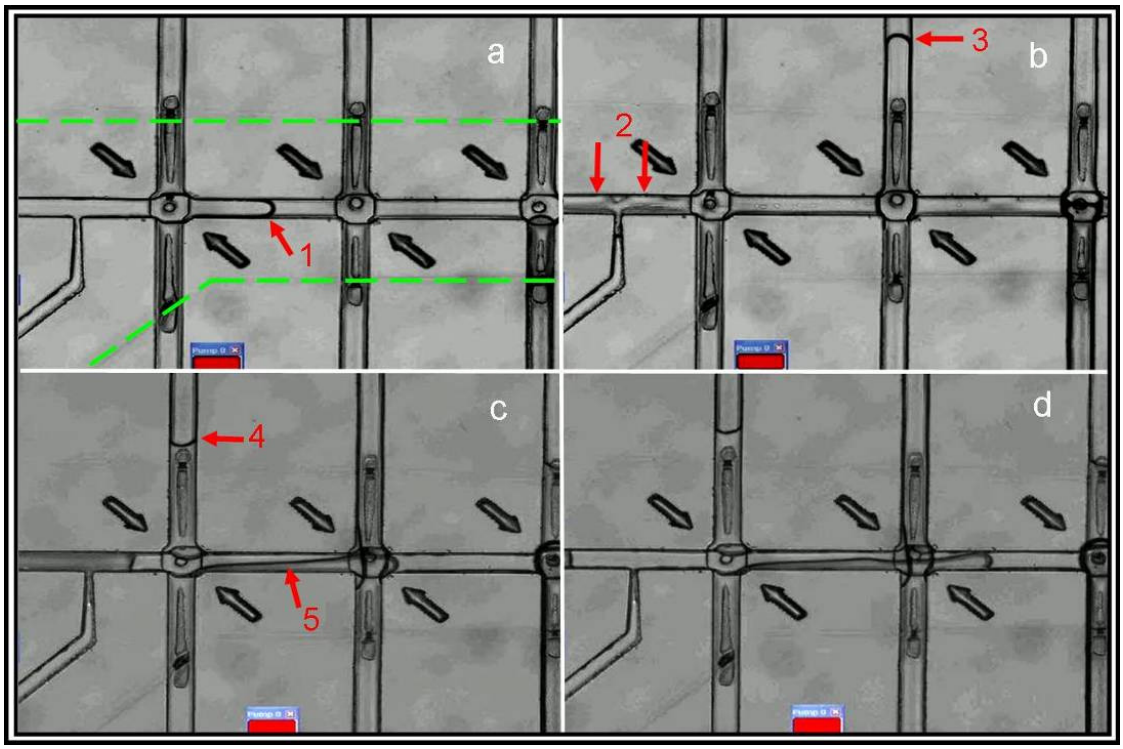

Figure 42: BLM formation attempt in a 1 x 3 site UV-Ozone treated BLM array chip. (a) At no. 1, lipid front filling main channel proceeding to coat array site 2 and 3. Green dotted lines represent area of microchannel UV-Ozone treated. (b) At no. 2, lipid solution running along PVDC film or floor of microchannel and at no. 3, lipid solution entered lower microchannel of array site 2. (c) At no. 4, lipid solution entered lower channel of array site 1 and at no. 5, lipid solution is wicking along main channel walls. (d) Lipid solution wicking along main channel.

Chapter 5 Contributions and Future Work

This final chapter sums up the contributions provided to the BLM research community and offers suggestions for future work in advancing the BLM micro-devices platforms discussed in this dissertation. Finally, a conclusion summarizes the work presented within.

5.1 Contributions

Work presented in this dissertation is novel. Significant contributions of this work are:

- A manufacturing plan to fabricate microfluidic devices capable of performing electrophysiological studies utilizing BLMs.
- The realization of an open well single-site BLM microfluidic device capable of rudimentary BLM biosensing studies.
- The realization of a multiple-site BLM microfluidic device to leverage inherent advantages, such as parallel testing and/or multi-analyte testing.
- A painting method to form BLMs based on excessive solvent removal via diffusion into the surrounding bulk phase.
- The adaptation of an existing electrode fabrication method on semiconductor substrates for successful electrodes construction on polymer substrates.
- An imprinting method for hot embossing microchannels into polycarbonate plastic using SU-8 on Si master templates.
- A fluidic interfacing technique, utilizing hypodermic needles, for leak proof plumbing connections to off chip fluidic sources.
- A software program, *Pump-inator 2006*, that allows remote actuation of syringe pumps during micro-device test situations.

5.2 Prior Art Comparison

Below, Table VI summarizes and allows comparison of the Open Well BLM Micro-Device to the prior art devices discussed in Section 1.4. The following points can be made: 1) Only two polymer-based micro-devices have integrated electrodes. They are the Open Well BLM Micro-Device and the PDMS device constructed by Malmstadt et al. [39]. 2) Polymer-based micro-devices constructed by Suzuki et al. [27, 28, 32, 33] and Sandison et al. [37, 38] have electrodes placed in the fluid reservoirs, thus their microchannel sizes tend to be larger so as to keep the access resistance low, and 3) The Open Well BLM Micro-Device is pushing the state-of-the-art for BLM micro-devices by having integrated thin film electrodes, the smallest BLM formation site size, and microchannel size.

5.3 Future Work

This section suggests topics for future work regarding BLM micro-devices. Topics are discussed in turn.

5.3.a Experimental Setup

The current experimental setup used to conduct micro-device testing has limitations. As described in Section 4.1, the micro-device sits on the stage of an inverted microscope. In turn, the microscope sits on a vibration isolation table left of which sit a bank of syringe pumps used for fluid I/O to the micro-device. Around the periphery of the vibration isolation table is a Faraday cage used to reduce noise pickup while collecting data. Thus the problem becomes apparent; sources of noise (i.e. syringe pump stepper motors, and microscope power cord) are housed inside the Faraday cage thus compromising it.

Table VI: Comparison of Prior Art to Open Well BLM Micro-Device

Work	BLM Site Size	Microchannel Size	Integrated Electrodes	Well Size	Major Disadvantage
Open Well BLM Micro-Device	40 µm	Nominal 50 µm W and H	Thin Film Ag/AgCl	3 mm	Evaporation
Suzuki et al. [27]	150 µm	500 µm W x 100 µm H	Patterned on Glass	N/A	Noise, Fragile
Suzuki et al. [27, 28]	200 µm	Omitted	Cr/Au Patterned on Glass	1.5 mm	Evaporation Same as Above
Suzuki et al. [32]	100 µm	2 mm x 0.5 mm	No, In Reservoirs	8 mm	Array Chip Not Independent Sites
Suzuki et al. [33]	100 µm BLM Dia.	1 mm x 0.5 mm	No, In Reservoirs	N/A	BLM Forms Along Microchannel
Sandison et al. [37]	50 - 100 µm	500 µm wide	No, In Reservoirs	Omitted	Evaporation
Sandison et al. [38]	50 – 200 µm	Omitted	No, In Reservoirs	50 µL	Evaporation
Malmstadt et al. [39]	70 µm x 100 µm	70 µm x 100 µm	Ag/AgCl Wire Cast in Place	N/A	BLM Forms Along Microchannel

To currently achieve low noise data collection, the microscope has to be unplugged and the power cord removed from the Faraday cage. Running experiments without use of a microscope for optical observations makes testing difficult. The syringe pumps, on the other hand, only emit noise when actuated, see Figure 43. When pumping conductive solutions into the chip, syringe pumps need to be carefully cycled on and off so that the BLM current signal could be observed periodically. For example, if α-HL solution is being injected into the lower microchannel, one would have to make the decision of observing the electrical signal for potential α-HL channel incorporation or pump the α-HL solution into chip. One cannot pump

solution into the chip and observe the electrical signal simultaneously, which is a major drawback.

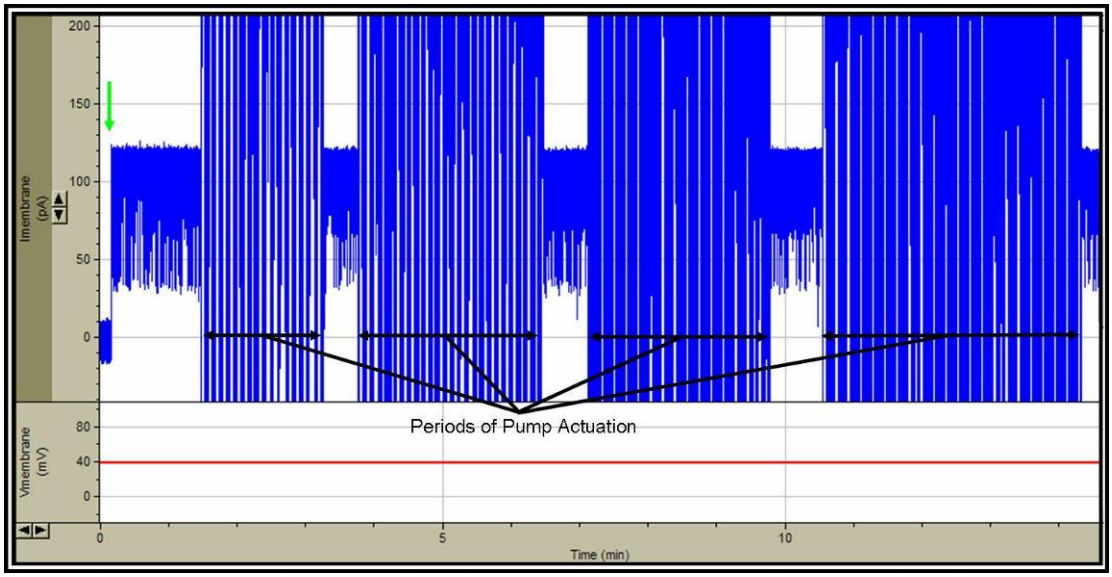

Figure 43: Current trace after α-HL incorporation (green arrow) showing the effect of synchronous noise emitted from the syringe pump stepper motors. Near-term solution is to pulse pump solutions into the micro-devices thus stopping periodically to check electrical signals.

To remedy the problem, the experimental setup needs a major overhaul. All noise sources need to be outside the Faraday cage with no exceptions. Some recommendations are: 1) The syringes containing conductive solutions need to isolated electrically to reduce capacitive-coupled noise pickup. 2) In addition, the syringe pumps need to be isolated from the remaining structure to minimize structure-borne noise pickup. Placing the syringe pumps on rubber mounts for vibration control would an acceptable option. 3) Use a smaller Faraday cage so that the microscope power cord does not compromise the Faraday cage's integrity thus allowing optical measurements at all times during the experiment.

A new experimental setup was constructed based upon the above recommendations and is shown in Figure 44. This setup utilizes a smaller Faraday

cage, constructed from brass perforated sheet, which encloses the micro-device and associated fluidic capillaries. The syringe pump stepper motors are now located outside the Faraday cage. Non-conductive fiberglass plunger rods, connected to the syringe pumps, make mechanical connections to the syringes inside the Faraday cage for remote solution injection or withdrawal. The syringes sit on a non-conductive ultra-high molecular weight (UHMW) polyethylene housing inside the Faraday cage to minimize noise introduction into the capillary. Shown in Figure 44d, the BLM micro-device is located close to the Axon Instrument head stage amplifier to minimize electrical lead distances. In addition, the micro-device is clamped down to the microscope stage.

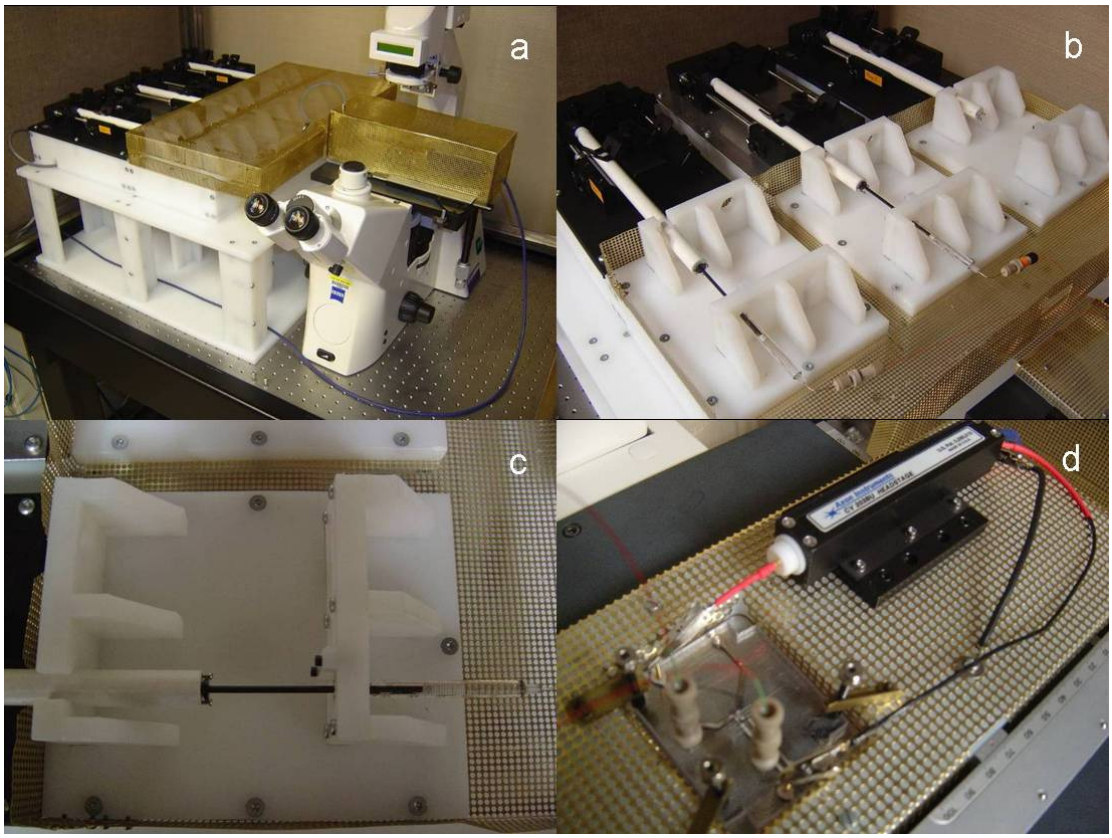

Figure 44: Pictures of newly constructed experimental setup for BLM micro-device testing. See text for details.

A power spectrum analysis (PSA) was conducted for both the old experimental setup and new experimental setup described in Figure 44. The resulting PSA plots, shown in Figure 45, were conducted under similar test conditions. A "no-hole" micro-device, described in Section 4.2.a, was filled with 2 M NaCl (old setup) and 2 M KCl (new setup) buffer solution. All other conditions were identical (e.g. capillary length, number of capillaries, syringe types, filtering rate, amplifier gain, pumps actuated, microscope on). The PSA for the old setup, Figure 45a, shows peaks of interest at 120 Hz and its multiples. The PSA for the new setup, Figure 45b, shows two plots: one PSA with the syringe pumps on (blue) and one PSA with the syringe pumps off (red). Peaks of interest around 40 and 80 Hz are probably mechanical resonances as they do not change as the syringe pump are actuated. Some noise pickup is still experienced with the syringe pumps actuated and at this time, it is unclear if this is caused by electrical noise pickup or if it is primarily structural-borne noise pickup. Finally, the broadband PSA for the new setup is almost two decades lower than the old setup so this is a drastic improvement, which should allow real time electrical monitoring while pumping solutions into the BLM micro-device.

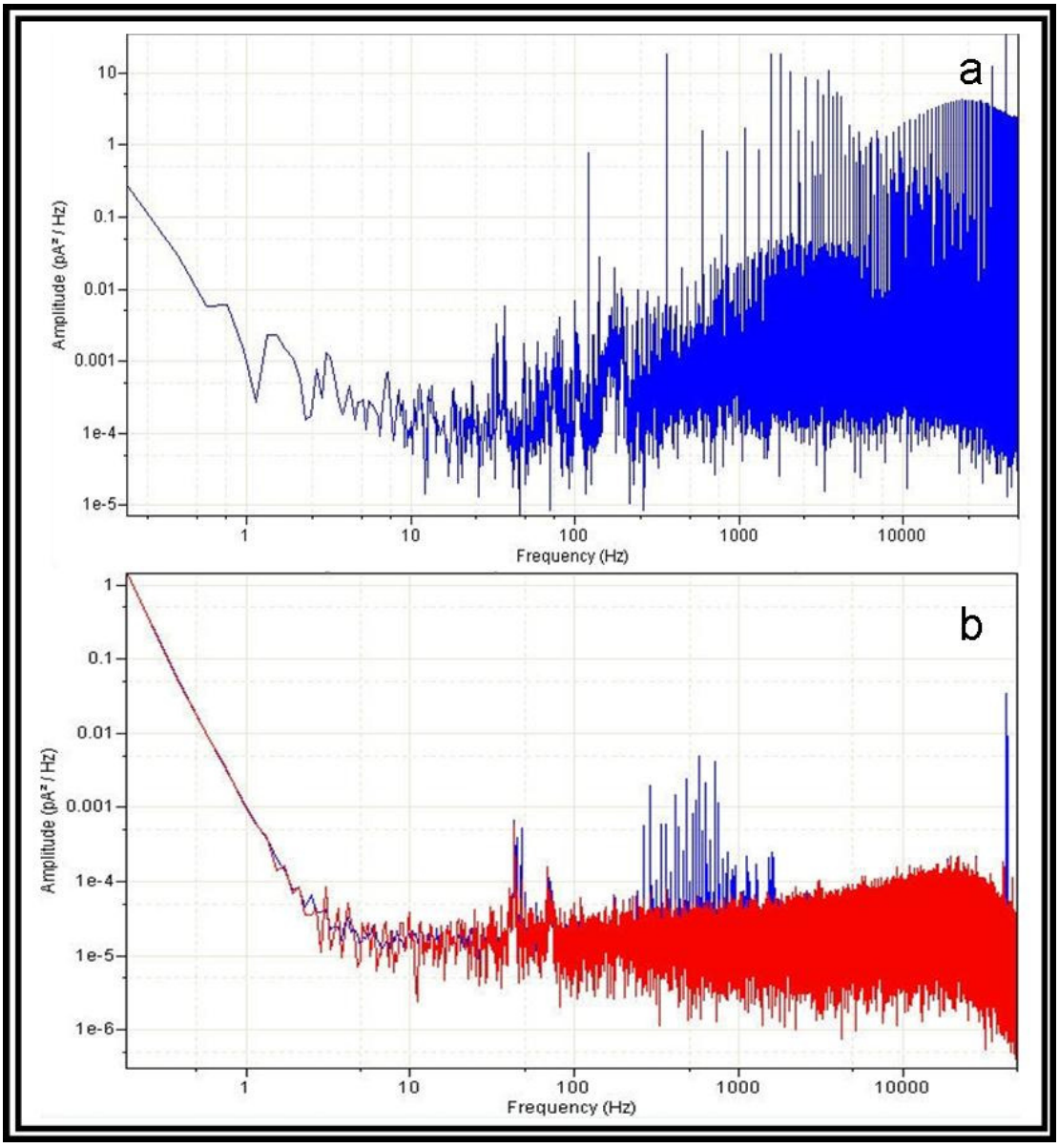

Figure 45: Power spectrum analysis (PSA) plots comparing experimental setups. (a) PSA of old experimental setup as described in Section 4.1 with syringe pumps on. (b) PSA of newly constructed setup pictured in prior figure. Red PSA is with syringe pumps off, whereas blue PSA is with syringe pumps on. See text for details.

5.3.b BLM Micro-Devices

The current BLM micro-device design has limitations and can be improved upon. One issue is that the temporal response of the current micro-device is slower than its macro counterpart, the NIST test chamber. In Section 3.1.c, conclusions state that minimizing access resistance and system capacitance are important to maximizing device bandwidth. The current micro-device design shows great promise in reducing system capacitance but suffers from higher access resistance when compared to the NIST test chamber.

The next generation BLM micro-device should be designed with the aim of decreasing access resistance. Clearly, the easiest way to meet this goal is having the electrodes as close as possible to the BLM site. The current electrode fabrication technique limits electrode-to-BLM site distance. Improvements in electrode fabrication, such as: 1) higher precision shadowmask machining would allow for closer spaced features, and 2) tighter positional tolerances on shadowmask alignment would allow closer electrode proximity to the BLM site. In addition, an alternate fabrication method may be more advantageous if electrodes can be constructed on both sides of the PVDC support film, so as to eliminate the need for the lower microchannel feed thrus.

Another aspect for improving BLM micro-device performance would be to introduce valving mechanisms so that solutions are pre-loaded on-chip, thus eliminating the need for fluidic capillaries which constantly inject noise into the chip. As discussed earlier, a PDMS chip reported by Malmstadt et al. [39] has integrated valving means. Fabrication of valve mechanisms in a rigid polymer device will take a concerted effort.

5.3.c Open Well BLM Micro-Device

One way to specifically improve the open well BLM micro-device would be to increase the open well accessibility. By improving the accessibility, external tools capable of aiding in automated BLM formation can be introduced. One such tool is the Eppendorf FemtoJet Microinjector [92], which can deliver femtoliter (10^{-15} L) volumes by ultra-fine glass capillaries. This tool can be used to deliver femtoliter quantities of BLM formation solution directly to the BLM site, thus automating the process and removing the human variation element that plaques traditional BLM painting techniques. Additionally, the FemtoJet could be used to deliver femtoliter volumes of analytes locally to the BLM site.

Another future goal of the open well BLM micro-device would be to transform it from a single-site design to chip capable of multiple site testing. Based upon how adaptable the manufacturing plan is for the current micro-device, this should not be difficult to perform.

5.3.d BLM Micro-Device Array

With regards to difficulties of fluid control as discussed in Section 4.3.b, an idea for future work would be to design a microchannel network that utilizes the microchannel's material inherent wetting properties along with optimized channel geometry so that BLM formation occurs naturally. One such concept is illustrated below in Figure 46. Here, the micro-device basic design is kept as in Figure 21, except that the upper channel contains numerous dead-end channels emanating radially form the BLM formation site. Upon filling the chip, the lower microchannel is filled first with buffer as shown in Figure 46a. Next, buffer solution is injected into

the upper microchannel and depicted by the number 1 in Figure 46b. Since the device is constructed from hydrophobic plastic, the buffer only travels up so far into the dead-end microchannels thus creating pockets of entrapped air. Next, a precise volumetric plug of lipid solution (green) is injected into the upper microchannel and is pumped toward the BLM formation site. As the lipid plug displaces the buffer out of the BLM formation site, the lipid solution is wicked into the dead-end microchannels as shown in Figure 46c. If the microchannel geometry is optimized, the entire lipid plug can be wicked away by the dead-end microchannels thus pulling all excess lipid solution away from the BLM formation site. Being able to manipulate the excess lipid solution around the BLM formation site periphery, the BLM should thin properly as illustrated in Figure 46d. With some computer simulations and optimization, this idea may be realized. Lastly, if the dead-end microchannels are modified so that they are connected to a pressure source instead, the trapped lipid solution can be forced back and forth as needed for reoccurring BLM formation.

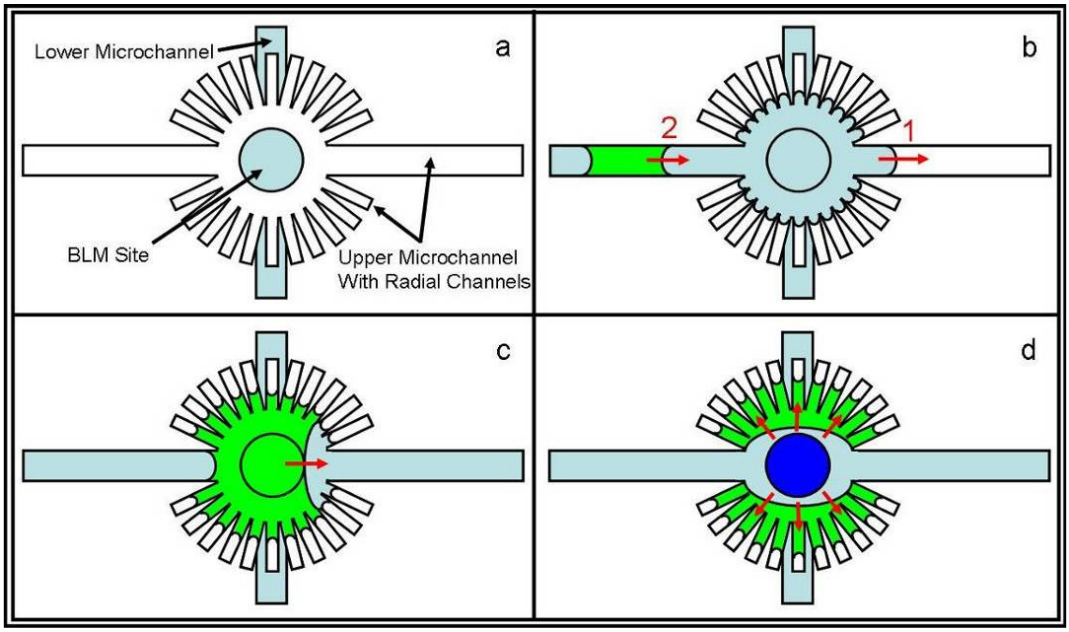

Figure 46: Possible BLM Formation Scheme for a Closed Microchannel Network. See Text for Details.

5.4 Conclusion

Two microfluidic devices, having integrated thin film Ag/AgCl electrodes, capable of performing BLM electrophysiology studies have been realized. One micro-device consists of a single BLM test site that is accessible to manual intervention via an open well, while the other micro-device is an enclosed chip with multiple BLM test sites.

The open well BLM micro-device was shown to support BLM formation by a novel diffusion painting approach. α-HL ion channel incorporation into the BLM was conducted multiple ways including injecting via microchannel and piping into the open well. Conductance jump magnitudes as the ion channels incorporated were favorable to data reported elsewhere. Finally, rudimentary sensing of polyethylene glycol molecules traversing the ion channel was shown.

The closed BLM array chip also supported BLM formation by remote lipid solution injection via a microchannel network. Fluidic control issues prevented any further experimentation with incorporating ion channels and bio-sensing.

The micro-devices explored here comprise a first step toward advanced BLM biosensors capable of single molecule detection. The work disclosed within offers plenty of potential avenues for next generation micro-devices including, but not limited to: 1) electrophoretic transport of trans-membrane proteins to populate individual BLMs, 2) electrophoretic analyte separation prior to delivery to the sensing sites, or 3) liposome delivery of analyte packets to BLM sites.

Appendix A

Preliminary BLM Micro-device Fabrication

This appendix provides details on BLM micro-device fabrication, part 1 of 3. Covered in this appendix is: 1) hot embossing of PC wafers and associated details, 2) post-machining operations (i.e. drilling, etc) of imprinting PC wafers, and 3) PVDC film application and associated details. These will be discussed in turn.

Polymer Wafer Imprinting

This section reports the procedures for imprinting microchannels into polymer wafers. First, master template fabrication, or SU-8 lithography, is discussed followed by the hot embossing recipe. The hot embossing recipe, discussed here is for PC, but other polymers (COC and PMMA) can be imprinted using the same embossing jig with modifications (Si wafer on stainless steel plate). Other polymers will require recipe modification of the temperature, pressure, and dwell time parameters.

Master Template Fabrication (SU-8 Lithography)

Master template fabrication utilizes conventional lithographic procedure in accordance with SU-8 manufacturer's specifications (Microchem, MA). As much detail as possible has been provided below, since it is known that the resulting product (i.e. sidewall profile, and substrate adhesion) is very sensitive to process parameter variation. The procedure given below will yield features approximately 50μm tall provided that SU-8 2050 formulation is used. It is assumed that the SU-8 processing specifications provided by Microchem have been reviewed. It is also

assumed that persons following this procedure are familiar with chemicals and equipment associated with photolithography.

Wafer Pre-Processing

Bare Si test wafers are used for master template fabrication. Virgin wafers are cleaned with an acetone-methanol-DI water rinse followed by N_2 air drying. Next, wafer dehydration follows in a convection oven at 120 °C for a minimum of 8 hours (overnight) prior to spinning on SU-8.

Recycling Previously Used Wafers

Used wafers can be recycled by carefully scraping off old SU-8 structures via a razor blade held at an incline to wafer surface. Wafer submersion in a Nanostrip (Cyantek, CA) bath removes the remaining SU-8. Heat Nanostrip bath to just under boiling for faster etch rates. Dip times are approximate 5 - 7 minutes if SU-8 is mostly scraped off prior to heated Nanostrip bath. Etch is complete when all SU-8 is removed, which is identified by the Nanostrip bath turning clear again from a purplish-black. Multiple Nanostrip baths (i.e. three beakers) are typically done in parallel if cleaning a lot of wafers at once. Decanted Nanostrip amount is typically just above wafer thickness.

Upon removing wafers from Nanostrip bath, dip wafers in a beaker of DI water for 10 seconds. Remove wafer from DI water bath and then rinse both sides with DI water for 20 seconds. Follow remaining cleaning and dehydration regiment for virgin wafers as discussed previously.

SU-8 Spinning and Pre-exposure Bake

A day prior to SU-8 lithography, take the appropriate amount of SU-8 2050 from the source bottle, which is located in the cleanroom refrigerator. Pour the appropriate amount of SU-8 in a sealed amber bottle suitable for dispensing at the spinner. By doing this, the SU-8 viscosity will be approximately the same every time yielding repeatable feature thickness and trapped air bubbles will come out of the SU-8 allowing for perfect application.

After removing the Si wafers from the oven, cool for 5 minutes. Place a piece of tape, folded over on itself, on the wafers edge as shown in Figure 47. This tape is very helpful as when the tape is removed later on, an uncoated spot will exist for comparison during development. SU-8 application occurs on a Specialty Coating Systems G3P spincoater (Cookson Electronics Co, IN) with the spinning parameters provided in Table VII. Detailed instructions for using the SCS G3P spinner can be found on the MML website. After all wafers are coated, wafer baking follows on a level digital-controlled hotplate.

Pre-exposure bake is conducted at 65 °C for 4 minutes followed by ramping up to 95 °C (7 minutes) on same hotplate. Avoid using two hotplates because transferring wafer from lower temperature to higher temperature can cause adhesion problems due to thermal shock. A hotplate ramp rate of 555 °C/hr (maximum ramp rate achievable) is used. Once 95 °C is obtained, dwell for 6 minutes before starting to cool back down to 65 °C. Cooling ramp rate is slower, so ramp down time is approximately 12 minutes. All times (baking and dwell) and associated temperatures were ascertained from the Microchem specification sheet. Note: Cheating on bake

times usually always yield an unsatisfactory product (poor sidewall or poor substrate adhesion). After soft-bake ramp cool down to 65 °C, the wafer can be removed from the hotplate. Prior to UV exposure, a wafer cooling period of 5 minutes concludes the bake operation. Remove the tape placed on the wafer during the previous step prior to UV exposure.

Table VII: Spincoater Settings for 50µm Tall Features Using SU-8 2050

Step	RPM	Ramp	Dwell	Dispense
0	0	0	0	4
1	500	5	5	--
2	3000	8	22	--
3	1000	2	1	--

Photolithography Mask Generation

Depending on application, either a film emulsion (transparency) or chrome masks can be used to pattern SU-8. Chrome masks are superior in two ways: 1) Cr masks offer finer line resolution and 2) Cr masks will yield features with better side wall roughness, which is important for some applications. Of course, Cr masks are more expensive versus film emulsion masks. Lastly regardless of mask choice, SU-8 is a negative photoresist so this calls for a dark-field mask.

NIST provides Cr mask generation but development is left up to the user. The steps required are: 1) Develop the Shipley 1812 photoresist, 2) Etch the Cr layer, and then 3) Remove the photoresist. In developing the photoresist, either 351 Microposit (Rohm and Haas, MA) or AZ400 (1:4) (AZ Electronic, NJ) developer can be used. Replenish with fresh AZ400 often since etch rates seem to decrease fast compared to 351 Developer. Photoresist thickness has never been measured, but development times can range from 5 – 10 minutes. Photoresist removal continues until exposed Cr

layer appears gold. Line resolution should be checked as well as total photoresist removal from all desired areas. Next, the Cr layer is etched using a Cr etchant (Type 1020, Chemtrec, MA). Cr development is quick and takes approximately 1 minute. Development of the Cr layer ceases when one can see through the glass. Cr thickness has never been measured nor compared to manufacturer's specifications. The last step is to remove the unwanted photoresist, which can be done by using acetone or photoresist remover. A final cleaning with acetone, methanol, and DI water will yield a clean Cr mask.

SU-8 Exposure and Post-exposure Bake

The PRX-1000 UV source (Tamarack Sci, CA), primarily emitting i-line (365nm) radiation, is used to initiate cross-linking in the SU-8 photopolymer. By allowing the UV lamp a 5 minute warm-up period guarantees that the lamp power will not fluctuate when dosing the wafer. Detailed instructions for using the Tamarack PRX UV source can be found on the MML website.

In Figure 47e, the wafer is shown being exposed. The PRX has a typical intensity output from 20-30 mW/cm^{-2} depending on bulb's age. The bulb intensity can be measured by using the IL1400 radiometer (International Light, MA) with photo detector (XRL-340A) designed for UV wavelengths (340 - 420 nm). For 50 µm feature thickness, desirable results are usually obtained with three 40 second exposures (2 minutes total). Rest periods, usually 30 seconds, between each exposure period helps avoid excessive heat buildup in the SU-8 layer thus minimizing excessive T-topping. Note: According to above exposure time, the dose given to the wafer is approximately 4 J/cm^2. Use caution, the PRX intensity value given above

does not include radiation attenuation due to mask glass and other filter glasses. Suspected actual dose to wafer is more like 2.6 J/cm^2. If comparing to Microchem dosing specifications for 50µm feature thickness, the above adjusted dose is about 6.5 times higher. Previous results show that more exposure time is beneficial for substrate adhesion and sidewall profile, thus dosage requirements stray from Microchem's specifications.

Shown in Figure 47e, the wafer is sandwiched above by a transparency mask (attached to float glass) and a piece of UV filter glass. Below the wafer are five cleanroom wipes and a piece of aluminum (5 inch x 5 inch x 1/8 inch) to stiffen the assembly. All pieces are held together using binder clips so shifting will not occur during exposure. The amber cutoff filter glass (aka Ghodssi Filter), with unknown properties, is used to block unwanted incident UV radiation that leads to excessive feature T-topping. Since certain types of filter glasses generate heat when absorbing radiation, a glass holder has been constructed (not shown) so the filter glass can be placed above the wafer (hence, avoiding heat conduction into the SU-8 layer) being exposed.

Post-exposure bake is conducted just like the pre-exposure bake except that bake times are altered. In this case, dwell time at 65 °C is 2 minutes followed by an 8 minute dwell at 95 °C. Ramping between the temperatures remains the same (7 minutes up and 12 minutes down). The wafer can be removed from the hotplate and then a wafer cooling period of 5 minutes concludes the baking operation prior to development.

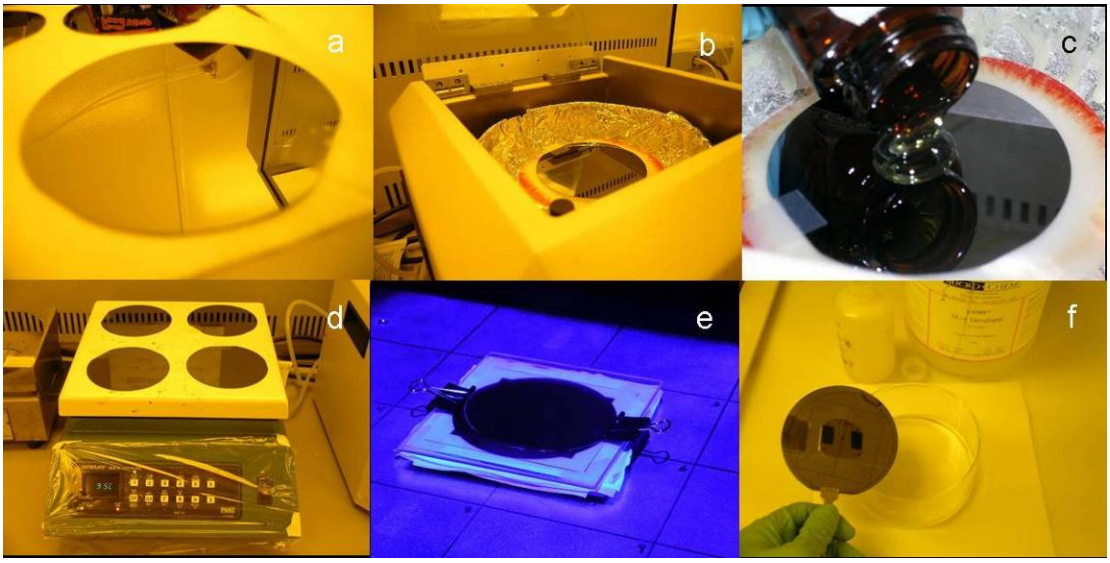

Figure 47: SU-8 photolithography in pictures. (a) Pre-cleaned Si wafer with tape ready to go, (b) Wafer placed in spin coater, (c) Pouring of SU-8 onto Si wafer, (d) Soft baking wafers on hotplate, (e) Exposing wafers under UV source, and (f) Wafer development.

SU-8 Development, Rinsing, and Hard Bake

Wafer development starts with 40 mL of fresh SU-8 developer (Microchem, MA) decanted in a 5 inch beaker. Development initiates by submerging the previously exposed wafer into the beaker. The developer is constantly agitated while the unexposed SU-8 is being removed. Development ceases visually by comparing the bare Si field (where the tape was during SU-8 application) to a field of unexposed SU-8. Typical time for development is 1 minute, 20 seconds for 50µm feature thickness.

Upon removing the master template and rinsing with DI water, a SU-8 residue will remain. To clean up the template post-development, a repeated DI water/fresh developer/DI water rinse is performed until all residues are removed from both wafer sides. This typically takes 2 - 5 cycles. Fresh developer, approximate 2 mL, is piped onto the wafer using a pipette.

Generally, ceasing development early and cycling with DI water/developer rinse to remove the final bit of SU-8 seems preferable rather than to overdevelop. Overdeveloping almost always leads to feature delamination from the Si substrate. Note: Features that have started delaminating during development can be "saved" if the wafer is immediately placed on a hotplate (120 °C) following the final rinse cycle. Heating the wafer drives off remaining developer and the delaminated features suck back down to the substrate, almost magically. Warning: Once you place your wafer on the hotplate for solvent drive off, do not remove it. Thermal shock will cause built up stresses in the SU-8 layer to totally delaminate. Following solvent drive off, hard bake each master template for a minimum of 2 hours at 200 °C. Hard-baking allows: 1) further SU-8 cross linking to occur, 2) annealing of thermal stresses in the SU-8 layer, and 3) maximum substrate adhesion.

Feature Verification via PDMS Casting

This section discusses how to verify SU-8 feature height/thickness and feature sidewall profile without using the stylus profilometer. This technique is beneficial because SU-8 features, typically abrupt in nature with its vertical sidewalls, can damage the profilometer stylus, if care is not taken. As a note, if you do use a profilometer to measure SU-8 feature height, always step down and never step up.

After fabricating SU-8 master templates, a few drops of PDMS are poured onto the feature of interest and cured. The PDMS can then be peeled from the template and placed on a piece of plastic or other compliant material for sectioning. The PDMS guillotine cutter, as shown in Figure 48a, can be used to make very straight cuts perpendicular to the PDMS surface. Two parallel cuts, approximately 1-

2 mm apart, completely through the PDMS thickness will suffice. Using tweezers, the PDMS sample can then be removed and flipped 90 degrees so that the SU-8 feature can be analyzed under a microscope. Height and width measurements can be made by a calibrated microscope reticule.

Prior to placing a PDMS section down on a microscope slide for analysis, a few IPA drops on the slide surface is helpful. The IPA temporarily negates the PDMS stickiness, thus allowing the elastic PDMS section to be placed down without feature distortion. Prior to microscope inspection, let the IPA evaporate since it will have collected in the microchannel cross section due to capillary action. Figure 48e and f show a few PDMS cross sections that ultimately illustrate a poor (excessive T-topping) and good microchannel cross section. Recall, that PDMS castings yield the negative of the molded feature.

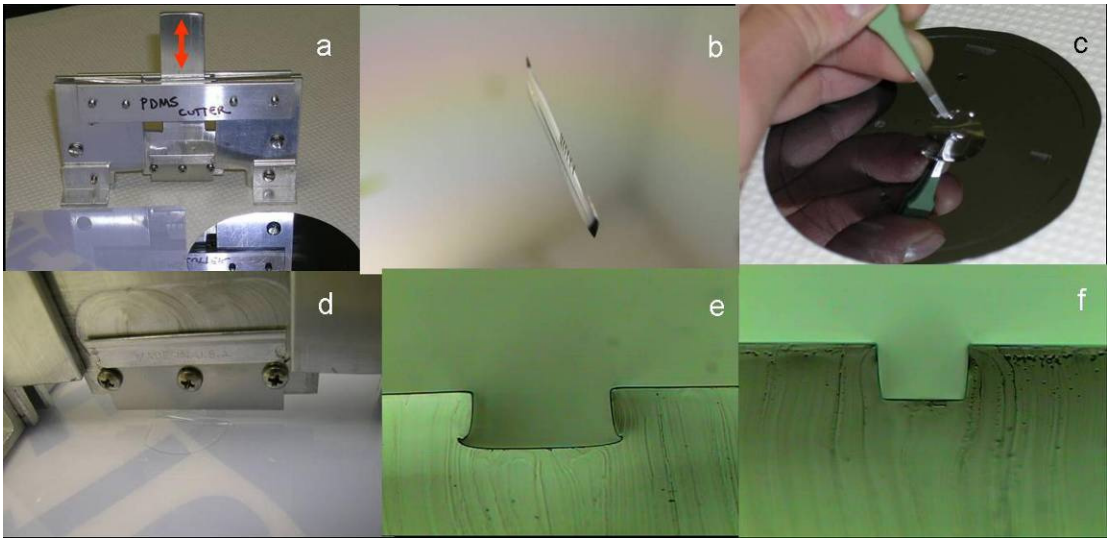

Figure 48: SU-8 feature verification via PDMS casting and sectioning. (a) PDMS guillotine cutter, (b) Sectioned PDMS waiting for inspection, (c) PDMS sample being peeled from Si template, (d) Close-up of guillotine, (e) and (f) PDMS sections showing poor and good sidewall profiles, respectively.

SU-8 Photolithography Issues

The above optimized SU-8 recipe resulted from many trials. Issues, such as poor SU-8 application during spin coating, poor feature resolution, SU-8 residue remaining after development, and poor feature adhesion / delamination were prevalent during early lithographic trials. Table VIII reports possible causes and solution to the common issues associated with SU-8 photolithography.

Table VIII: Common Issues Associated with SU-8 Photolithography

Bonding Issue	Possible Cause	Solution
Poor SU-8 Application During Spin Coating	1) Air Bubbles in SU-8 2) Too Little SU-8 Applied to Wafer	1) Let SU-8 Sit at Room Temperature Overnight 2) Increase SU-8 Volume
Features Smaller Than Mask Dimensions	1) Exposure Time Too Short 2) Over Development	1) Increase Exposure Dose 2) Decrease Development Time
Features Larger Than Mask Dimensions	1) Exposure Time Too Long 2) Under Development	1) Decrease Exposure Dose 2) Increase Development Time
SU-8 Residue Remaining After Developing	1) Development Bath Contaminated with Dissolved SU-8	1) Rinse with Fresh Developer
Poor Feature Shape	1) Over Exposure 2) Heat Build Up During Exposure	1) Reduce Exposure Time 2) Break Exposure Time Into Periods
Poor Feature Adhesion / Delamination	3) Under Exposure or Over Development 4) Soft Bake Times Short 5) Lack of Hard Bake	3) Increase Exposure Time 4) Increase Bake Time 5) Perform Hard Bake

Hot Embossing of Polymer Wafers

SU-8 imprinting utilizes hot embossing techniques well documented in the literature. As much detail as possible has been provided below, since it is well known that the resulting product (i.e. imprint sidewall profile, imprint depth and master template damage) is very sensitive to process parameter variation. The procedure

given below, if followed correctly, will yield numerous imprints from one master template without visible damage or wear. It is assumed that persons following this procedure are familiar with equipment associated with hot embossing.

Embossing Setup and Overview

A Carver AutoFour/15 Press (Carver, IN) was utilized to create PC imprints from SU-8 master templates, described earlier. Schematically shown in Figure 49, the hot press consists of a stationary upper platen and a hydraulically driven bottom platen with a 15 ton load capacity. Both platens are capable of temperature control, via heating and water-cooling, with digital readouts on the control console. Platens were checked for parallelism prior to embossing so that induced shear forces upon loading and unloading does not cause microchannel deformation and/or possible master template feature delamination.

An embossing fixture, shown in Figure 50b, was constructed to aid in the embossing and mold removal operation. The embossing fixture, consisting of an upper and lower half, aids the operator to accurately measure local imprint temperature during the embossing procedure. The lower half of the embossing fixture was fabricated from aluminum plates in which a thermocouple has been embedded with high-temperature epoxy. This thermocouple is used as the primary temperature readout when setting temperature set points for the embossing procedure described next. The upper half consists of an aluminum plate/glass combination bolted onto the upper platen. Glass plates (Precision Glass and Optics, CA) are mechanically fastened to the upper fixture and are used to keep the opposing imprint surface smooth and optically clear during imprinting. More importantly, the

embossing fixture assists in mold removal by taking advantage of the press's inherent vertical motion. The fixture's lower portion has a mechanical means to securely hold down the master template to the aluminum plate. Upon platen separation, the upper and lower fixture plates move in conjunction with the upper and lower platens, respectively. The PC imprint naturally adheres to the glass plate due to Van-der-Waals attraction thus the PC imprint removal occurs automatically at the end of press cycle. Once cooled, the PC imprint can then be removed from the upper glass plate with minimal effort by wafer tweezers.

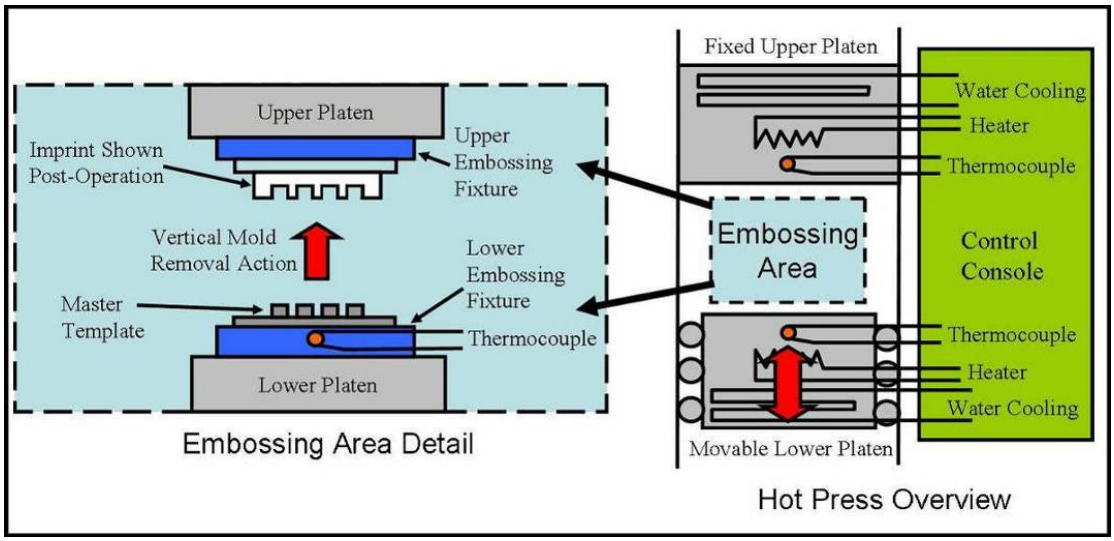

Figure 49: Schematic of hot press along with detail of embossing area.

Embossing Procedure

This procedure was developed by performing a series of imprinting trials until the best product was produced. By following this procedure, imprints with 10 to 75 µm feature depth have been obtained in PC wafers with 3/32 inch thickness. Recipe modification maybe required if the master template design becomes extreme, such as smaller feature size, larger amount of features, or if features height is greater than 75 µm. As features or thickness increase, frictional forces along the feature sidewall

increase during de-molding thus preventing imprint separation from the master template. In addition, this recipe will need to be adjusted if polymer surface modifications, such as UV-ozone treatments, are utilized.

Polycarbonate Wafer Preparation

Before embossing, PC wafers, 3.5 inches in diameter are cut from a larger PC stock sheet (McMaster-Carr, NJ, P/N 8574K25). Both sides of the PC wafers are deburred using a block plane. The white protective film is then removed from both sides so that wafer cleaning can take place. Wafers are rinsed with DI water and then blow dried with ionizing N_2 air. The clean wafers are stacked inside a beaker and then covered. The covered beaker is then placed in a vacuum oven for dehydration (100 °C) for a minimum of 8 hours. When needed for embossing, a PC wafer is removed from the vacuum oven, cleaned again with the ionizing N_2 air gun, and then inserted into the press for embossing.

Embossing Jig Preparation and Installation

Prior to embossing, the desired master template must be installed into the bottom embossing jig. This is accomplished by removing the 8 flat head screws that anchor the steel hold-down plate to the bottom aluminum bottom plate. Remove the hold-down plate and center the master template onto the aluminum bottom plate. Make sure to blow dust and debris away from the aluminum bottom plate and from the master template underside to avoid possible master template damage upon tightening of hold-down plate. Replace the hold-down plate and the 8 flat head screws, making sure not to tighten excessively. Note, the hold-down plate is keyed for rotational orientation.

Once the master template is installed, the embossing jig (upper and lower) can be installed into the press. The upper embossing jig should be installed first followed by the lower embossing jig. Make sure both are centered in the press and do a dry run to make sure alignment is ok and no interference exists. Use a wipe with IPA to clean the glass on the upper fixture prior to initial imprinting. Figure 50 shows a series of pictures documenting the embossing process.

Embossing Recipe

The hot press is run under temperature control, where all temperature measurements are read from the lower embossing jig's thermocouple. At the beginning of each embossing run, the press platens are programmed for a 177 °C (350 °F) setpoint. Warm-up period takes approximately 20 minutes. At a reading of 130 °C (266 °F), place a cleaned 3.5 inch diameter PC wafer on top of the master template and close the press until a small gap remains between the wafer and the upper embossing jig. This allows for the PC wafer to heat up evenly to the surrounding platen temperature.

At a reading of 150 °C (302 °F), which is the T_g for PC, close the press at the slowest pump speed (15 %) and apply an initial force of 700 pounds. Keep the loading constant until the wafer temperature reaches 160 °C (320 °F) and then increase the applied load to 2700 pounds. At a reading of 166 °C (331 °F), initiate water cooling. Carefully monitoring the master template thermocouple, open the press when the temperature reaches 147 °C (297 °F). Upon press opening, mold removal occurs as the PC imprint should remain affixed to the overhead glass plate. Allow the PC imprint to cool to 135 °C (275 °F) before scraping it off using wafer

tweezers. The process can then be repeated with cycle times approximately 20 minutes. After the imprinted wafer is removed, immediately cover the microchannels with blue dicing tape (Semiconductor Equipment Corp, CA) and place the wafer in a wafer boat.

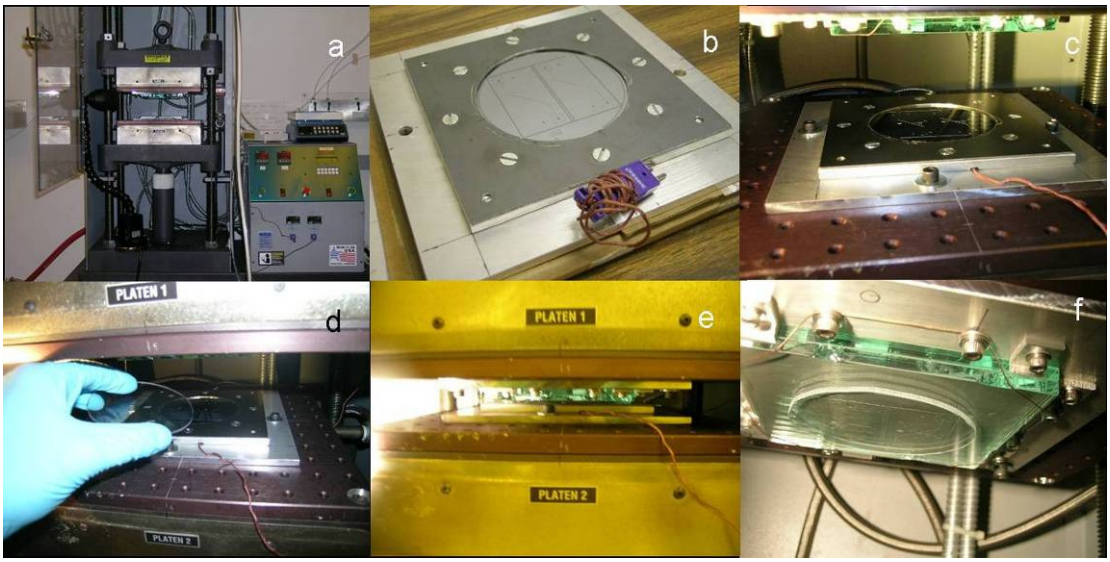

Figure 50: SU-8 imprinting in pictures. (a) The Carver hot press, (b) Lower embossing fixture with master template installed, (c) Upper and lower embossing fixture installed in press, (d) Inserting blank polycarbonate wafer, (e) Imprinting the wafer, and (f) Press opening and mold removal.

Microchannel Imprinting Issues

The above optimized microchannel hot embossing recipe resulted from many trials. Many issues, such as template feature delamination, poor microchannel definition, PC wafer flatness, and/or PC wafer will not release from template were prevalent during early device bonding. Table IX reports possible causes and solution to the common issues associated with hot embossing.

Table IX: Common Issues Associated with Hot Embossing

Bonding Issue	Possible Cause	Solution
Template Feature Delamination or Deformation	3) Imprinting Temperature Too Low 4) Excessive Shear Force During Imprinting 5) Wafer Not Releasing from Template After Press Opening 6) Poor Feature Adhesion Strength to Template	3) Increase Press Closing Temperature Above Polymer T_g 4) Check Hot Press Platen Parallelism 5) See Below 6) Consult Lithography Issues.
Poor Microchannel Definition or Uneven Across Wafer Imprint	3) Imprinting Temperature Too Low 4) Imprinting Pressure Too Low 5) Microchannel Features Too Flexible 6) Press Platens Not Parallel	3) Increase Press Closing Temperature Above Polymer T_g 4) Increase Imprinting Pressure to Reported 5) Dimensions Must Be < 100 µm H x W 6) Check Press Platen Parallelism
Poor PC Wafer Flatness or Deformed	2) Removing PC Wafer Too Early 3) Bonding Temperature and Pressure Too High; Squashing Wafer. 4) Debris Between PC Wafer and Template	2) Increase Cool Down Time Prior to Wafer Removal. 3) Reduce Both Max Temperature and Pressure. 4) Use N_2 Ionizing Gun to Clean Prior to Imprinting
PC Wafer Will Not Release from Template	6) Too Many Features Increasing Release Force 7) Press Open Temperature Too Low	6) Open Press at Higher Temperature. 7) Use Simpler Design or Alternate Imprinting Method

Post-Imprinting Fabrication Operations

This section discusses post-imprinting fabrication operations performed to the newly imprinted PC wafers. First, the operations that are common to both the top and bottom PC wafer are reported, such as drilling holes, deburring holes, and wafer cleaning. Next, the operations that only the bottom wafer receives are discussed in

detail, namely PVDC film application and BLM supporting hole formation. Finally, the section concludes with information on the Film Hole Burner and associated details.

Machining Operations

First discussed are machining operations common to both the top and bottom PC wafers.

Hole Location and Identification

Holes drilled into the PC wafers can be classified into 4 categories: 1) alignment holes, 2) electrical I/O holes, 3) mounting holes, and 4) fluid I/O holes. Approximate hole locations can be found in Figure 51 along with a legend identifying the purpose of the hole. A cross designating a hole's physical location is imprinted on each PC wafer. Each type of hole will now be discussed in turn.

Alignment holes receive spring pins, which in turn hold the assembled devices together prior to thermal bonding. A No. 52 diameter drill is used for drilling these holes. The number of alignment holes drilled is actually half the number shown in Figure 51 since the PC wafers are assembled at the time of drilling. More details on the device alignment, alignment hole drilling, and spring pin insertion are given later.

Electrical I/O holes receive the terminal screws which connect the Ag/AgCl electrodes to external circuitry. These holes are threaded so that a mating 0-80 UNF machine screw can be received after device bonding. A 3/64 inch tap drill is used when drilling these holes.

Mounting holes are used to attach the wafers to all of the jigs used throughout the remaining fabrication process. For example, the mounting holes are utilized to

attach the bottom wafers to the substrate holder when evaporating metals for electrode fabrication. The mounting holes are also used when aligning the top and bottom wafer during device assembly. These holes are threaded to receive a mating 0-80 UNF machine screw. A 3/64 inch tap drill is used when drilling these holes.

Finally, the Fluid I/O holes receive the fluidic needleports, which in turn allow fluids to be injected into the chip in a controlled fashion. These holes are thru holes and are drilled using a No. 71 drill bit. It is important that these holes are drilled at the microchannel's end so precise location is required. Since these holes are small and the microchannel even smaller, a microscope is used as an aid when drilling. Since this is not a normal drilling practice, this drilling procedure will be outlined next.

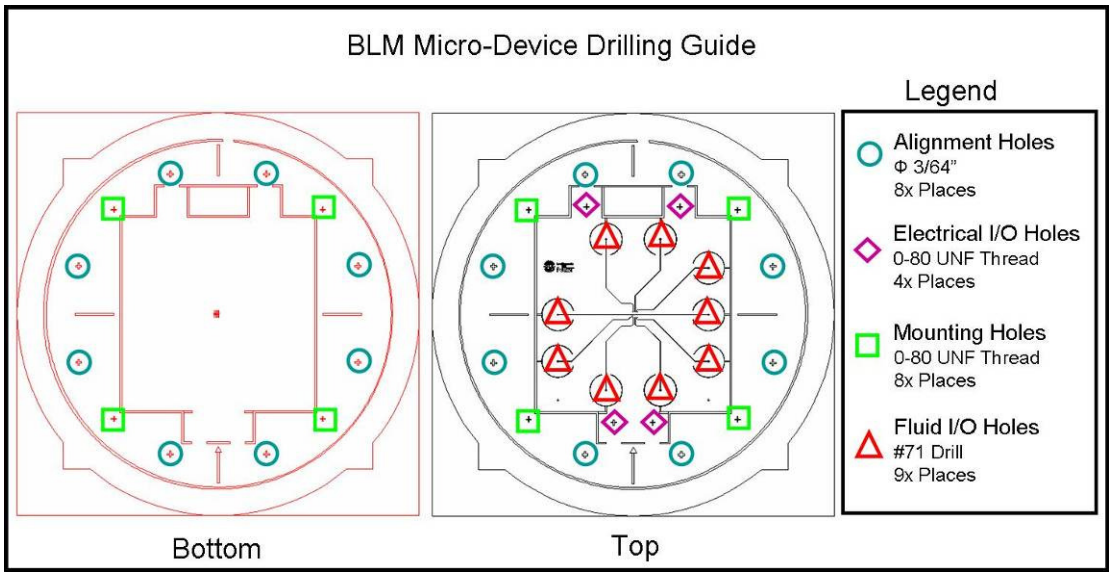

Figure 51: Location and identification of holes drilled in the top and bottom PC wafers. Note, alignment holes are drilled later during device assembly so actual number of alignment holes is half of number shown.

Drilling and Deburring Operation Details

Discussed here is the procedure for drilling the fluidic I/O holes. Since these holes required precision location at the end of a microchannel's run, an inspection

microscope is used to help locate the drill bit prior to creating the hole. The microscope is setup like shown in Figure 52a. Since PC is reflective, this is beneficial in locating the drill bit tip. When the inverted image of the reflected drill bit tip meets up with the physical tip, the drill bit will be touching the surface of the PC. The holes are then drilled as shown in Figure 52b. Be sure to firmly hold the substrate while drilling. After drilling, deburr the exterior side of the fluidic I/O holes with an O-flute countersink deburring tool (Figure 52c). Incidentally, all holes on this project are drilled with tungsten carbide drills where possible. These drills (Drill Bit City, IL) provide the best finish when drilling into plastics.

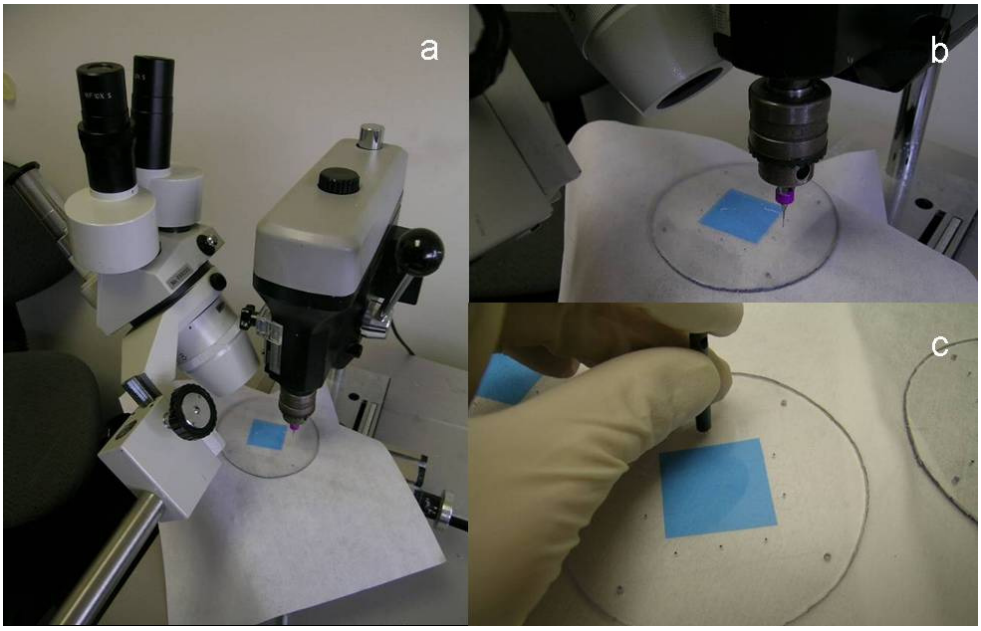

Figure 52: Hole drilling and deburring in pictures. (a) Close-up of the drilling setup, (b) The drilling setup consists of a miniature drill press and inspection microscope, and (c) Using an O-flute countersink to deburr the holes.

Wafer Cleaning

A lot of dust and debris is created when drilling holes, which left on the wafers would be very detrimental to device function during testing. It only takes one encapsulated dirt particle during bonding to foul testing by blocking a channel or

flowing downstream and eventually lodging itself at the most critical device portion. Many hours goes into making a single device, so cleanliness is paramount. Since drilling and other machining cannot be done in the cleanroom, devices must be removed from the cleanroom setting, machined, and then returned back into their original state of cleanliness. Future fabrication operations will be done inside a cleanroom setting, so wafer cleaning must be performed for that reason as well.

The first step is to blow off all visible dust and debris after drilling/machining before entering the cleanroom. Once inside the cleanroom, the wafers can be cleaned with a squirt of IPA and then washed with DI water. A vigorous DI water rinse is performed for at least 20 seconds making sure that the DI water jet gets into all drilled holes, especially the tapped holes. After rinsing, a N_2 blow gun is used to blow off all remaining DI water. Again, make sure all holes are cleaned with the ionizing N_2 gun. Finally, the cleaned wafers are placed in a covered wafer boat for air drying.

BLM Support Film Application

This section discusses issues dealing with Polyvinylidene chloride, PVDC support film application on the bottom PC imprint. Specifics, such as the film itself and application of film, are reported. Film hole burning to create the BLM formation site and feed thrus are also discussed. Lastly, information on the Film Hole Burner is provided.

PVDC Application History

After cleaning the wafers, the next step is to apply the PVDC film to the bottom imprint. Over the course of this project, PVDC application has varied quite a bit. PVDC film is electrostatically charged so it is very clingy and attracts an

unbelievable amount of dust. Both wet and dry methods were tried in applying the PVDC and each has advantages and disadvantages. For example, a wet method of applying PVDC is to float the PVDC on DI water (or IPA) and then to displace the water from underneath the PVDC by a squeegee. This method works great for eliminating static dust attraction and entrapped air bubbles during the PVDC application. However, the wafers have to be dehydrated for days afterward before placing in the evaporator for electrode fabrication. On the other hand, dry methods do not require a dehydration period but air entrapment and dust attraction can be problematic. Because time is always a factor, a dry method was ultimately used and is discussed below.

PVDC Film

The BLM support film utilized in the micro-devices is polyvinylidene chloride having a trade name of Saran (Dow Plastics, MI). In purchasing PVDC, one has to be careful that the correct formulation of PVDC is being bought. PVDC wrap currently sold in the grocery stores is polyethylene, which is not equivalent even though it has the Saran trade name. PVDC used in this project is Saran 8 grade, which is 12.5 μm thick. It was purchased in roll form (12 inch wide x 2000 ft) from Filcon (Clare, MI), who has a license to manufacture Saran from Dow Plastics. The PVDC is an amber-colored vapor barrier film that is typically used in protecting food in wrapping or heat sealing applications. PVDC has a melting temperature of 172 ºC and a glass transition temperature of -15 ºC [93].

PVDC Application Procedure

PVDC application starts with a word of warning. Dust buildup due to electrostatic charge is a big problem as is the PVDC wanting folding up on itself. Rule number one is to always use the ionizing N_2 gun to blow off the dust prior to each and every step. If a lull in the procedure presents itself, always restart by using the ionizing N_2 gun to blow off the dust before proceeding. From here on out, it is understood that the ionizing N_2 gun will be used to clean the PVDC and mating parts between each step in the process. Needless to say, this work is all done in the cleanroom where airborne dust particles are minimized.

The first step is to cut the PVDC into 82.5 mm (3.25 inch) diameter circles, which are slightly smaller than the 88.9 mm (3.5 inch) diameter imprinted PC wafers. To aid in doing this, a stretcher was constructed from ¼ inch PC sheet so that the PVDC film could be held about its periphery without it folding up on itself (See Figure 53a). After the film is placed on the stretcher, binder clips are used to hold the PVDC. Next, a 4 inch by 8 inch piece of silicone (McMaster, NJ, P/N 8632K422) is placed on the table as a cutting pad. The PVDC is laid on top of the silicone followed by a circle template, as shown in Figure 53b. A sharp scalpel is then used to follow the template edge when cutting out the circles. Two circles are cut at one time (side by side) and then the template and remaining PVDC, still on the stretcher, is placed aside.

After the circles have been cut, it is time to ready the PC imprint. Start by removing the protective blue dicing tape and then place the PC wafer, imprint side up, on a clean wipe. Next, place a piece of PTFE (30 mils thick) over the PC imprint. Carefully, remove a PVDC circle that was previously cut on the silicone pad. Place

the PVDC side that was facing up on the silicone pad face down on the PTFE. Starting from right to left, slowly remove the PTFE while using your finger to smooth out the PVDC onto the PC wafer. If an air bubble is formed or the PVDC creases, retrace your steps by moving the PTFE back to the right and repeating the smoothing process. After the PTFE sheet is removed, the PVDC film should be completely smoothed out onto the PC wafer. A completed PC wafer with PVDC is shown in Figure 53f and is now ready for electrode fabrication. Air bubbles entrapped after PVDC application do disappear after a few days, so waiting a day or two before electrode fabrication will yield best results. Figure 53 shows the above steps in pictures.

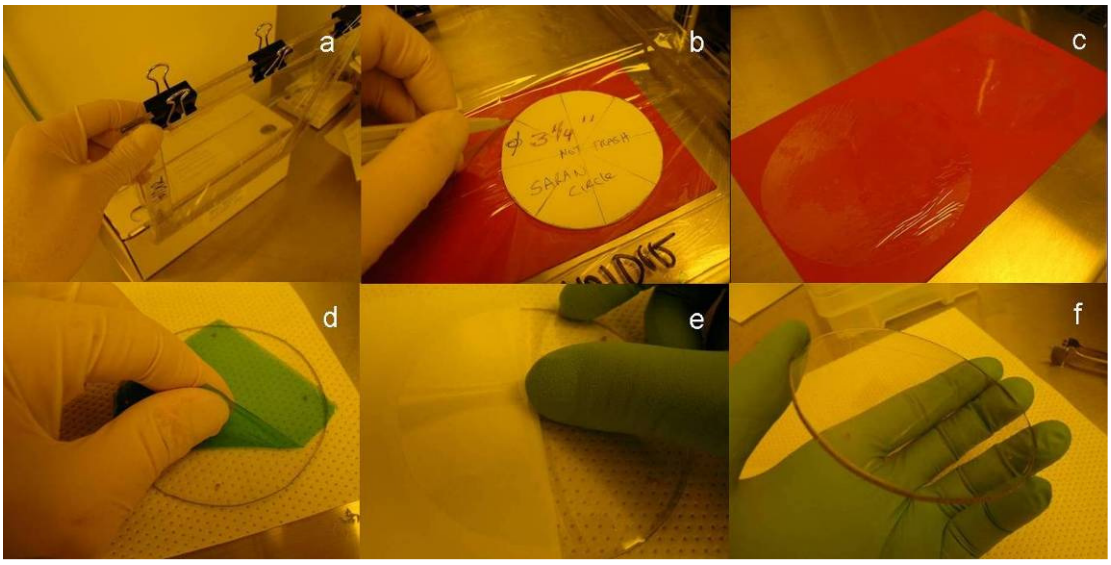

Figure 53: PVDC application steps in pictures. (a) PVDC being placed on the film stretcher, (b) PVDC being cut with a scalpel, (c) Two PVDC cutouts ready to go, (d) Preparing the PC wafer for PVDC application, (e) Smoothing out the PVDC film, and (f) the finished bottom PC wafer with PVDC film applied.

Hole Burning in PVDC Film

The discussion now turns to burning the micron-sized holes required for BLM formation and for the lower microchannel feed thrus. Since both are created similarly, this discussion will focus on the BLM formation hole only since it is of critical importance. Additional points dealing with burning the feed thru holes will be added when needed.

Recall, the size, location, and shape of these holes are very important. The preferred hole diameter for the BLM formation site can be determined since PVDC film thickness is known and the aspect ratio for BLM formation is given in the literature [77]. Also, these holes must be located precisely inside a microchannel which adds to the fabrication difficulty. The Film Hole Burner was created to aid in locating the holes and is discussed later. Finally, the shape of the hole is very important and it is discussed next.

Hole Quality

BLM formation depends highly on the quality of the hole obtained. A perfect hole must be free of debris, especially any debris that projects into the hole's interior. The rim of the hole must be smooth with a graceful transition where the BLM annulus contacts the hole periphery. An ideal hole would be perfectly round as well, but this is probably the least important factor. Hole out-of-roundness is more tolerable than hole rim quality. Figure 54 below shows a series of holes either burned in PVDC or PTFE. Going from left to right, the hole quality in terms of BLM formation capability deteriorates. The holes on the right are the most undesirable holes (BLM formation not likely) to the most desirable holes on the left (BLM

formation likely). In the same figure, some SEM images were collected of holes burned in PVDC film. Prior to imaging, the holes were coated with 250 Angstroms of Ag using thermal evaporation.

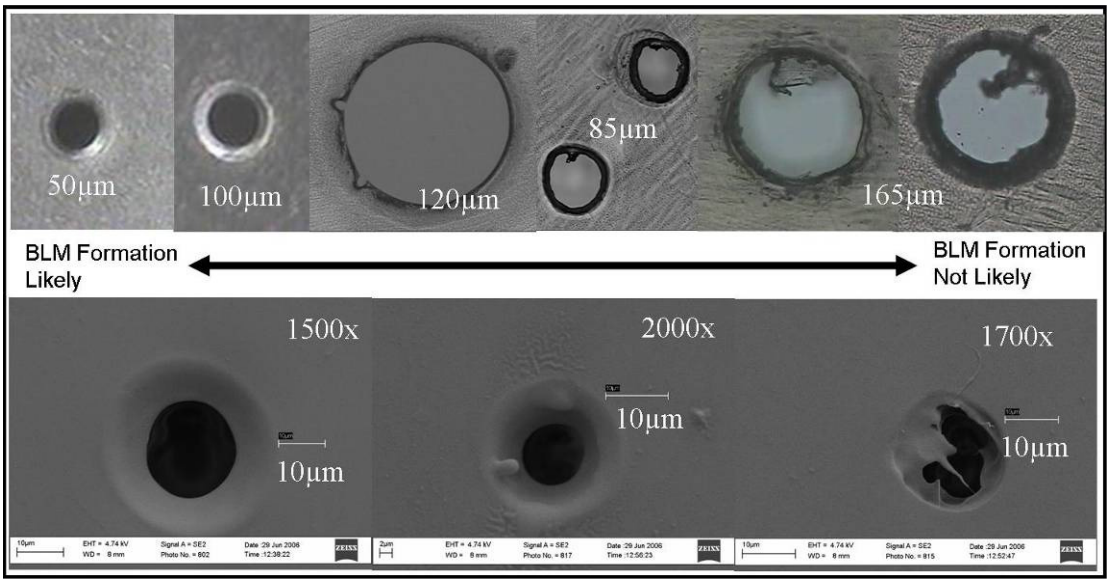

Figure 54: The good (left), the bad (middle), and the ugly holes (right). Images of holes burned in PTFE and PVDC collected by bright field microscopy (top), and SEM images of holes burned in PVDC (bottom).

Film Hole Burner

After reviewing the literature, a thermal formation technique with preference to using a hot needle was down-selected because of the following reasons. 1) Hot needle approaches were common in the literature [20, 47, 65, 94]. 2) The research group at NIST uses the hot needle apparatus with relative ease and it offers a great starting point because the holes created are known to form BLMs. 3) One can reverse engineer the existing device and build a new apparatus with the options that one needs, and 4) Having the NIST expert who has experience making holes with this technique is a great benefit.

In order to create holes in PVDC supporting film, a hot needle device was constructed and is known as the Film Hole Burner. Shown in Figure 55a, the Film

Hole Burner consists of a converted probe station (Cascade Microtech RF-1), which is typically used as a test platform for MEMS devices. The Film Hole Burner utilizes Tungsten probe needles held stationary in a vertical position by a pin vise as shown in Figure 55c. Ni-Cr wire is wrapped around the needle and is potted by an electrically insulative, but thermally conducting ceramic epoxy. A thermocouple is placed in the ceramic potting for temperature feedback. The recipe for making such needles is discussed later.

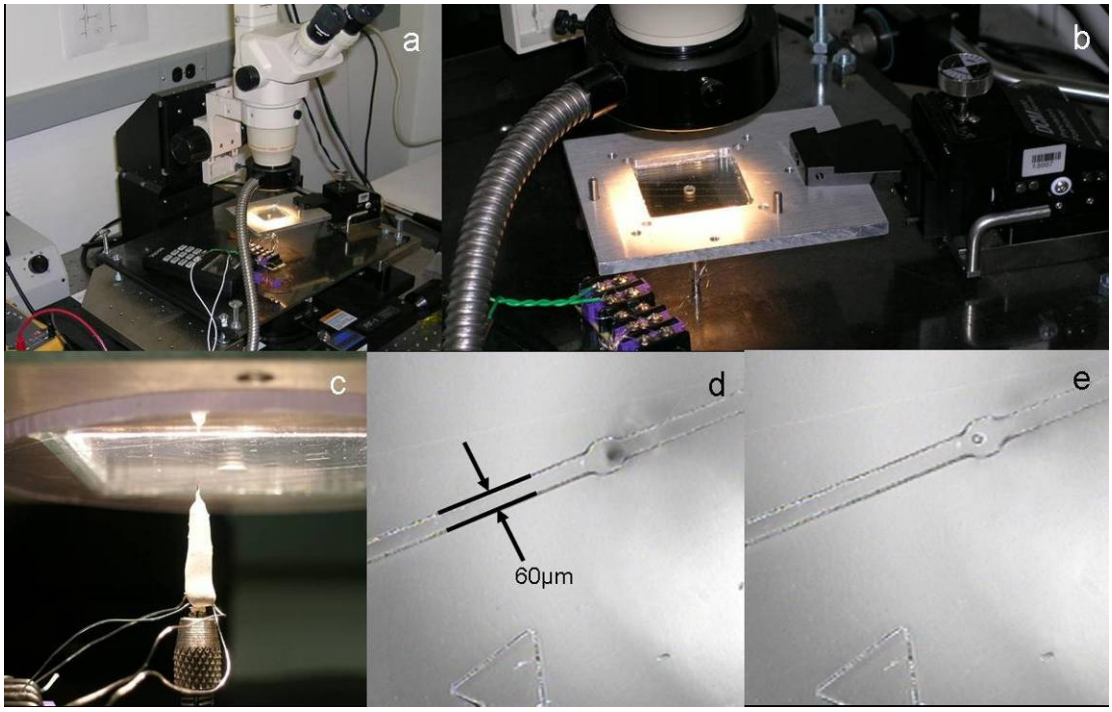

Figure 55: Film hole burner setup for fabricating holes in the supporting film. (a) The overall setup, (b) Detail of the XYZ manipulator portion, (c) Hot needle detail, (d) and (e) Microchannel shown pre- and post-hole burning operation, respectively. Shadow in (d) is hot needle located just below PVDC film out of focus. Hole in (e) is ~20 µm in diameter (125x).

The film hole burner utilizes a stereomicroscope (Olympus SZ60) for close up imaging of the support film. A XYZ manipulator is used to hold the PC imprint and to precisely locate the needle underneath. The XYZ manipulator can be seen in Figure 55b. Figure 55d and e show a microchannel close up at pre- and post-hole

formation, respectively. A simple control circuit is used to heat the needle up to a desired temperature. A thermocouple (Type E, Omega) is used for temperature feedback.

It should be noted that the Film Hole Burner can create holes in PVDC or PTFE film without problems. The only difference is that PTFE melts at (327 ºC) 620 ºF where as PVDC melts at a much lower temperature, (172 ºC) 342 ºF. At higher temperatures required for PTFE, the needle lifetime is much shorter (<5 holes). Failure mechanisms are Ni-Cr wire burn out or needle tip oxidation buildup. If using the needles to create holes in PVDC, the needle lifetime is much longer.

When creating holes at the BLM formation site, the sharpest probe needle (tip radius = 2.5 µm) available is utilized (Terra Universal, P/N 9111-01). For creating the feed thrus, a larger needle is used (tip radius = 25.4 µm, Terra Universal, P/N 9111-03).

Hole Forming Procedure

The procedure for making holes in the support film is quite easy, but takes practice. The process starts with a bottom PC imprint with the PVDC film already attached as shown in Figure 55d. Using the microscope, the needle is located beneath the exact position that the BLM hole is desired. The needle is then heated and the film is lowered down until the needle tip breaks through the opposing film surface. After break through, the needle direction is quickly reversed and cooled. The hole is then checked for size using a calibrated recticle. As mentioned before, the process becomes easier by practicing as it takes “three hands” to operate the system: One hand working the microscope focus, the second hand working the XYZ manipulator,

and the third working the film burner on/off switch. Prior to making holes in good devices, a series of practice trials should be conducted so to dial in the desired hole diameter (i.e. applied voltage level to the needle).

When forming the feed thrus, an identical procedure is used with one exception. After the hot needle has pierced the film, the needle needs to be moved back and forth so that the feed thru is wider. Creating a feed thru is more like milling a slot as opposed to drilling a hole. A higher temperature is also used so the needle stays hot has the heat is wicked away by thermal milling operation.

Hot Needle Construction for Hole Burner

The process for hot needle construction is depicted in Figure 56. Frame A illustrates the wire wrapping zone. It is very important to stay within this area as the bottom length of the needle is the grip-able length for the pin vise and the top length needs to remain clear for hole creation. Typically, a set of 5 needles are fabricated at once since the entire process takes about a day. Prior to wire wrapping, the needles are cleaned with IPA. A very light coating of ceramic epoxy (Omega Coat 600, P/N OB-600) is applied to insulate the needle from the first wrapping of Ni-Cr wire. The ceramic is mixed according to manufacturer's instruction. Once applied, the part is cured vertically in a vacuum oven at 80 ºC for ½ hour. Next, a 6 inch piece of Ni-Cr wire (Omega, 30 AWG, P/N NI80-010-50) is wrapped upward (approximately 5 turns) starting from the bottom; leaving about 2 inches of wire at the end for electrical connections later. The wire is then covered with ceramic potting, as shown in Frame D, followed curing in the vacuum oven again at 80 ºC for ½ hour. Next, the wire is wrapped down the needle (5 turns), a shown in Frame E. If done correctly, two

inches of wire should be left over for electrical connections. Another coat of ceramic potting is applied followed by another cure cycle. Now, a type E thermocouple is wrapped around the assembly as shown in Frame G. The assembly is completed with a final ceramic potting coat followed by a cure of ½ hour and 1 hour at 80 ºC and 100 ºC, respectively.

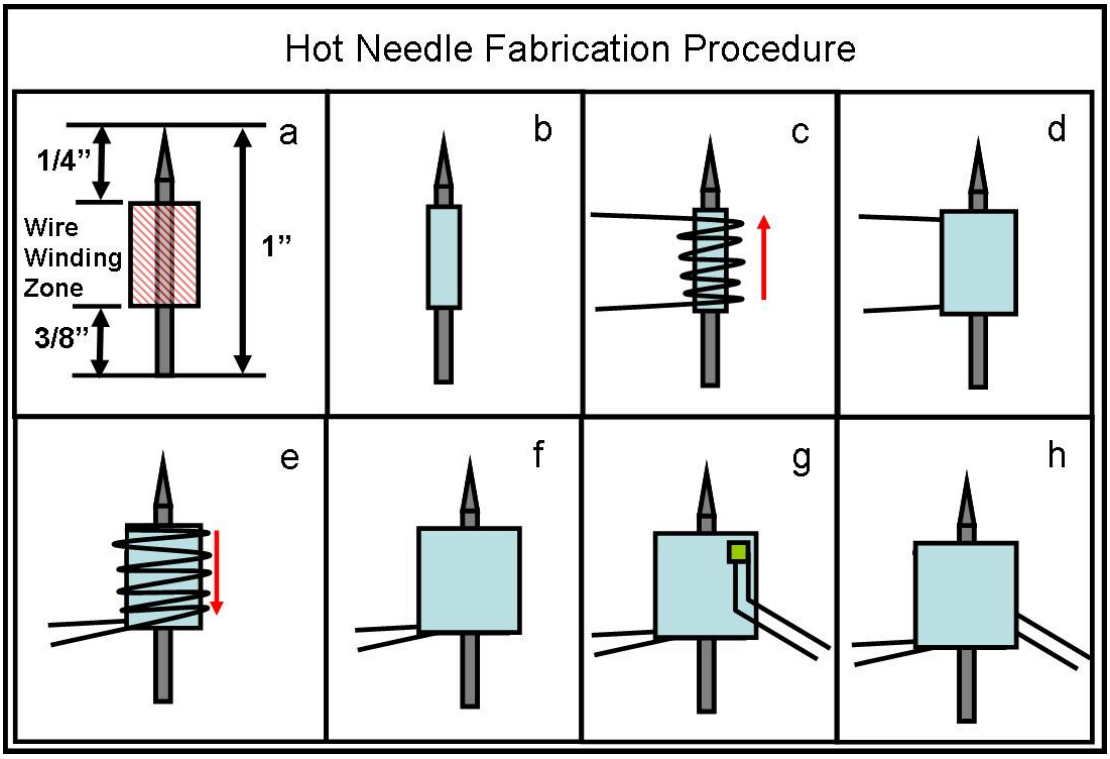

Figure 56: Needle fabrication procedure. See text for details.

Appendix B

Ag/AgCl Thin Film Electrode Fabrication

This appendix provides details on BLM micro-device fabrication, part 2 of 3. Specifically covered in this appendix is Ag/AgCl electrode fabrication.

In past micro-device designs, such as the one shown in Figure 25, electrical contact to the outside world was made by inserting commercially bought sintered Ag/AgCl electrode wires (203 μm OD, A&M Systems, WA) into a via hole previously drilled in the PC wafer. The electrode was then anchored and sealed by the tightening of a Nanoport (Upchurch Sci, WA) compression fitting around the wire. This method allows quick measurements, but it is not without problems: 1) Sealing of the wires is problematic since the sintering process yields wire that is not of constant diameter. A secondary operation using PDMS to seal the electrode in the Nanoport is required. 2) Device performance will suffer because the commercial wire electrodes can only be placed so close to the BLM formation site due to physical limits (e.g. Nanoport size, electrode size, etc). An alternative way to make electrical measurements on chip was needed.

One solution is to fabricate the Ag/AgCl electrodes as a part of device construction, thus integrating the electrodes. This not only would solve the problems associated with the commercially bought electrodes, but it would be another step closer to demonstrating an integrated lab-on-a-chip system. The process discussed below is an adaptation of the one developed by Dr Polk et al. of NIST (Gaithersburg, MD) [95]. While the key fabrication steps are still the same, modifications were

required to adapt the process to polymer substrates. Thanks to Dr. Polk for his consultation during the adaptation.

Ag/AgCl Reference Electrodes

Ag/AgCl electrodes were chosen for a few reasons: 1) The chemistry at the electrode solid/liquid interface is known and reversible. In presence of a solution containing chloride anions, an Ag/AgCl electrode experiences the following reaction: $AgCl\ (s) + e^- \leftrightarrow Ag(s) + Cl^-\ (aq)$, where the chemical reaction is driven left or right depending on the direction of applied electron flow. The reduction half cell reaction at the cathode is: $Ag^+ + e^- \rightarrow Ag(s)$ and the oxidation half cell reaction at the anode is: $Ag^+ + Cl^- \rightarrow AgCl(s)$. In words, electrons traveling down the cathodic AgCl trace reduces a small amount of AgCl and release Cl^- into solution. In the reverse direction, Cl^- anions travel to the opposing electrode interface and oxidize thus forming solid AgCl in return for giving up the electron which travels up the anodic AgCl trace, and 2) Reference electrode provide a way to relate measured signals to fixed potential (reference) since only potential differences can be measured between two electrodes [96].

Ag/AgCl Electrode Fabrication Overview

After application of the PVDC support film, the bottom PC wafer is ready for electrode construction. Layers of Cr, Au, and Ag are deposited via thermal evaporation with nominal thickness of 100 Ang, 100 Ang, and 1000 Ang, respectively. Metal patterning is done by mechanically fixing a brass shadowmask prior to metal evaporation. After the shadowmask is removed, electroplating of additional Ag on top of the evaporated Ag is performed to build up the Ag amount.

Finally, the Ag traces are chloridized to complete the Ag/AgCl electrodes. This procedure is depicted in Figure 27, which is located in Chapter 3.

Shadowmask Generation

A shadow masking technique is utilized to pattern the metal layers for three reasons. 1) Metal patterning post-evaporation would be detrimental due to plastic-to-solvent compatibility issues. For example, photoresist liftoff is another common way to pattern metallic layers but this way would not be advisable because most photoresist developers attack PC. 2) Using a wet chemical process would most likely remove the PVDC supporting film, which is just held in place by electrostatic attraction. 3) The electrode traces are very small in area compared to the device total area. Depositing multiple metal layers on your device to just remove a high percentage of it afterward is not very logical. Shadow masking helps to keep device field uncontaminated. Lastly, the mask can be lifted off after the evaporation process thus revealing patterned metal layers with no further processing. Thus, it essentially combines two steps in one; the deposition and patterning of metal layers.

Shadowmasks are constructed from alloy 260 brass sheet shim stock that is 7 mils thick (McMaster, NJ, P/N 9011K6) and are machined using the Protomat95s CNC router (LPKF, OR). The process starts with mounting the brass shim stock to a sacrificial underlayment, as shown in Figure 57a. In this case, the underlayment, 1/16 inch thick PC and is affixed with double-sided tape. Next, the brass shim is loaded into the CNC router. The LPKF router can machine up to six shadowmasks at a time. Machining instructions for the LPKF router are created using CircuitCAM and BoardMaster Software (LPKF, OR). Details regarding use of the software packages

are beyond the scope of this appendix, fortunately both software packages are easy to learn.

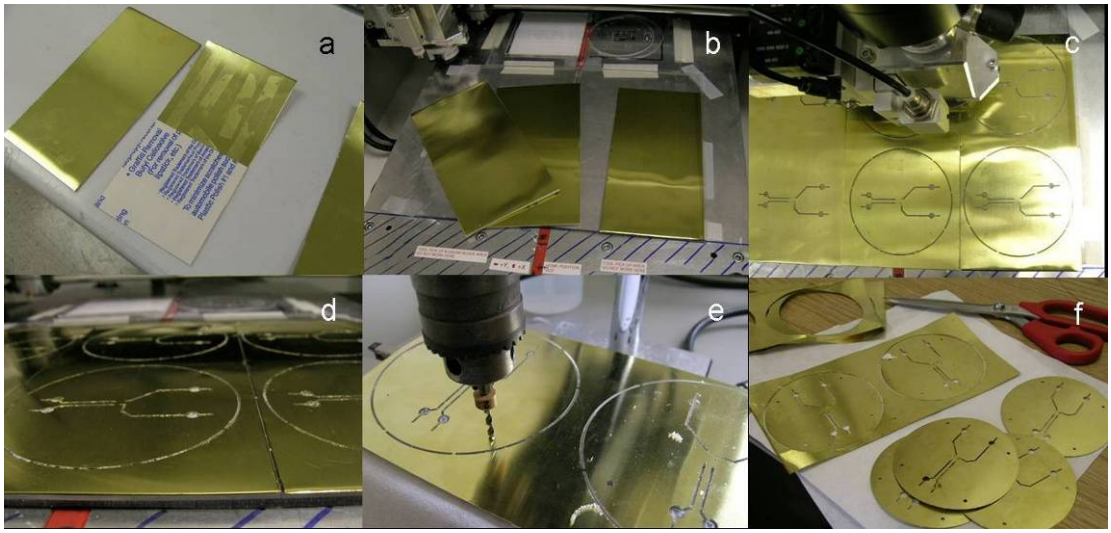

Figure 57: Shadowmask generation steps in pictures. (a) Mounting brass shim stock to sacrificial underlayment, (b) Loading into CNC router, (c) Milling the masks, (d) Masks post-milling, (e) Drilling periphery mounting holes, and (f) Cutting out final product.

After the machining is finished, the brass/PC assembly is removed from the LPKF router table. A secondary machining operation is then performed by drilling the mounting holes around the shadowmask periphery to 2.35 mm (3/32 inch) in diameter, see Figure 57e. The final step is to remove the brass shadowmasks from the PC underlayment and then to cut the shadowmasks out from the surrounding scrap with heavy duty scissors. Optional sanding of the mask faces can be performed with 800 and 1200 grit sandpaper to remove any machining burrs.

Metal Deposition via Thermal Evaporation

Metal deposition is performed using the CVC thermal evaporator located inside the NIST Advanced Measurements Laboratory's (AML) Nanofab Cleanroom. The CVC evaporator is large enough to evaporate metal onto six wafers at a given time. In addition, the CVC evaporator can deposit up to four different metals during

each run. For these above reasons, the CVC is a perfect choice for metal deposition over, say sputtering which can only deposit a single metal on a single wafer on a given run. Before the actual evaporation process is discussed, a method to hold the aforementioned shadowmasks to the corresponding polymer wafers during evaporation will be detailed next.

Wafer Holder Assembly

Prior to metal evaporation, the bottom PC wafers need to be assembled onto a wafer holder. The wafer holder serves a few purposes: 1) It allows a mechanical means to hold the polymer wafers inside the evaporator so that metal deposition can occur uniformly. 2) It allows six polymer wafers to be placed inside the evaporator at one given time, thus increasing process efficiency, and 3) It allows a mechanical means to place the brass shadowmasks in precise location on each polymer wafer prior to evaporation.

The wafer holder physically consists of 1/8 inch thick aluminum sheet stock cut into a 13.5 inch diameter circle, as shown in Figure 58a. A rectangular cut out exists around the wafer holder's periphery which sole purpose is to not block the crystal oscillator when the holder is placed inside the evaporator. In loading the wafer holder, the PC wafers are placed on the wafer holder first followed by the shadowmasks. Six 2 inch diameter holes are also cut into the wafer holder so that one can double check the shadowmask alignment after everything is assembled.

Each polymer wafer is loaded onto the wafer holder by using four No. 0-80 x ½ inch socket head cap screws and four 2 washers, see Figure 58b. The four screw/washer combinations pass through the holes in the wafer holder and then mate

up with the four tapped mounting holes in each polymer wafer. After tightening the wafer down to the holder, the four screws will extend proud of the obverse polymer surface and will become the mounting studs for the shadowmasks. Wafer location and orientation, when placed on the wafer holder, is purely subjective. Of course, the PVDC side of the polymer wafers need to be placed outward so that the metals are deposited on the right surface.

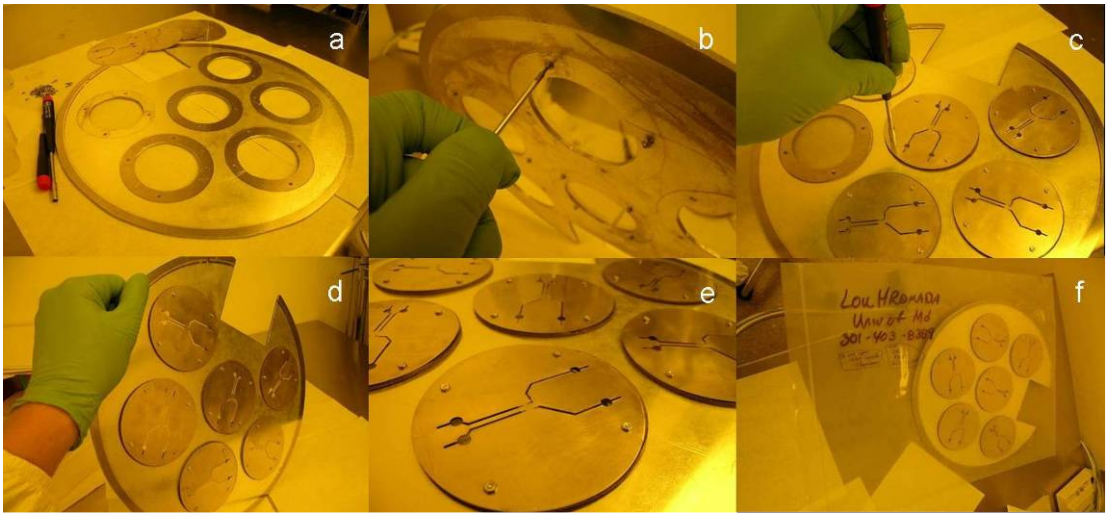

Figure 58: (a) Mounting the PC wafers onto the wafer holder. Substrate holder and masks, (b) Mounting the PC wafers, (c) Mounting the shadowmasks, (d) All the wafers and masks mounted, (e) Close-up, and (f) Wafers bagged ready for the evaporator.

Once all six wafers are loaded onto the holder, the brass shadowmasks are mounted next. Shadowmask orientation is critical so care must be taken to get proper electrode location based on the chip design. Each shadowmask has four clearance holes so the mask just slides down over the four screws previously inserted. Four No. 0 nuts are then threaded onto the No. 0 screws and tightened to complete the shadowmask mounting. Figure 58c-e show shadowmask mounting in detail. Once the procedure is complete, the entire wafer holder assembly can be bagged to keep everything clean until metal deposition occurs in the evaporator as seen in Figure 58f.

Metal Evaporation

The CVC evaporator is shown in Figure 59a below. When the system is vented and the bell jar raised, see Figure 59b, the populated wafer holder is placed at the tower top as indicated by the red arrow. The green arrow shows where the evaporation boats and source metals are placed. A close up of the metal sources is shown in Figure 59c, whereas Figure 59d and e show the wafer holder pre- and post-evaporation. Note the rectangular cut out of the wafer holder is oriented so not to block the crystal oscillator of the CVC evaporator.

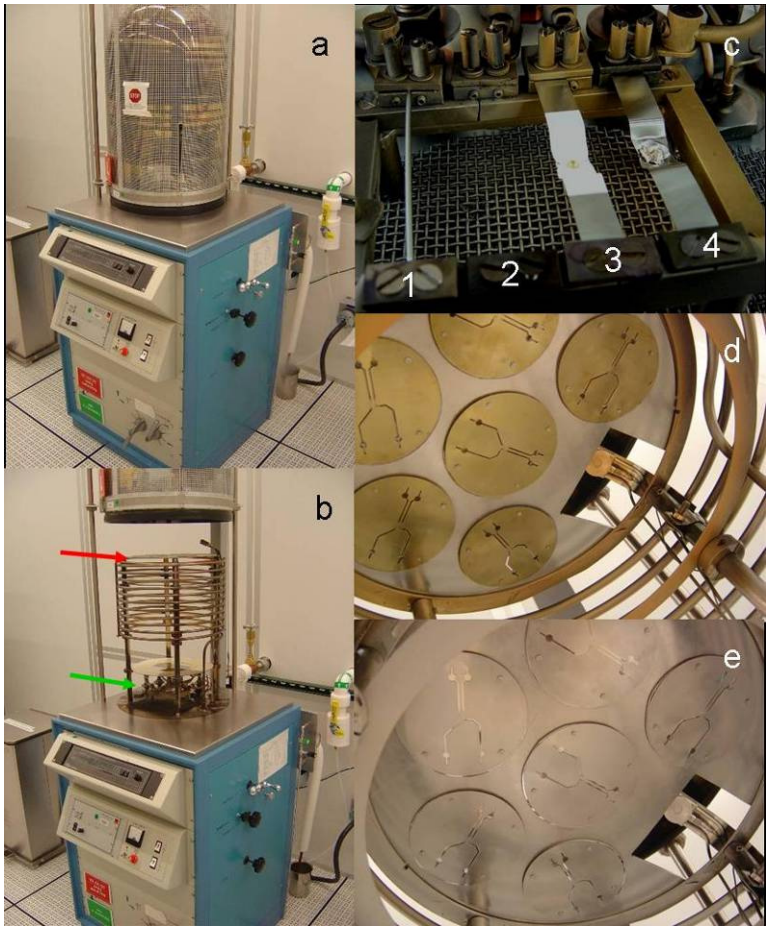

Figure 59: Metal evaporation steps in pictures. (a) The CVC thermal evaporator, (b) Evaporator with bell jar open to reveal metal source boats (green arrow) and target area (red arrow) where the PC wafer holder sits, (c) Close-up of deposition metals, (d) Wafer holder pre-evaporation looking up inside the evaporator, and (e) Wafer holder post-evaporation.

Documenting the actual CVC operation procedure is beyond the scope of this appendix, but details of the evaporation process are documented in Table X below. First, Cr is evaporated to a target thickness of 100 Angstroms. Next, Au is evaporated to a target thickness of 100 Angstroms followed by Ag at 1000 Angstroms. Material densities and Z-ratios are listed since this information is required by the crystal oscillator to determine metal thickness as the evaporation process runs real time. Additional information, such as current drawn, dial settings and deposit rates, is included for reference.

Table X: Typical CVC Evaporator Settings for Metal Deposition

Metal	Density (gm/cc)	Z-ratio	Current (Amps)	Dial Setting	Target Thickness (Ang)	Deposit Rate (Ang/Sec)
Cr	7.2	0.305	5	6	50	3.0
Au	19.3	0.381	9	10	60	0.5
Ag	10.5	0.529	5	6	1000	5 – 6

Wafer Holder Disassembly

After metal evaporation, the polymer wafers must be removed from the wafer holder. This process is simply just the reverse of placing the wafers onto the wafer holder, as illustrated in Figure 60. First, the shadowmasks are removed by unscrewing all of the No. 0 nuts. Next, each polymer wafer is removed by unscrewing the four No. 0-80 screws originally used to anchor the wafers to the wafer holder. Care should be taken not to damage the newly created electrode traces. The wafers are immediately placed in a wafer boat and backfilled with N_2 gas, which helps reduce Ag oxidation prior to Ag electroplating.

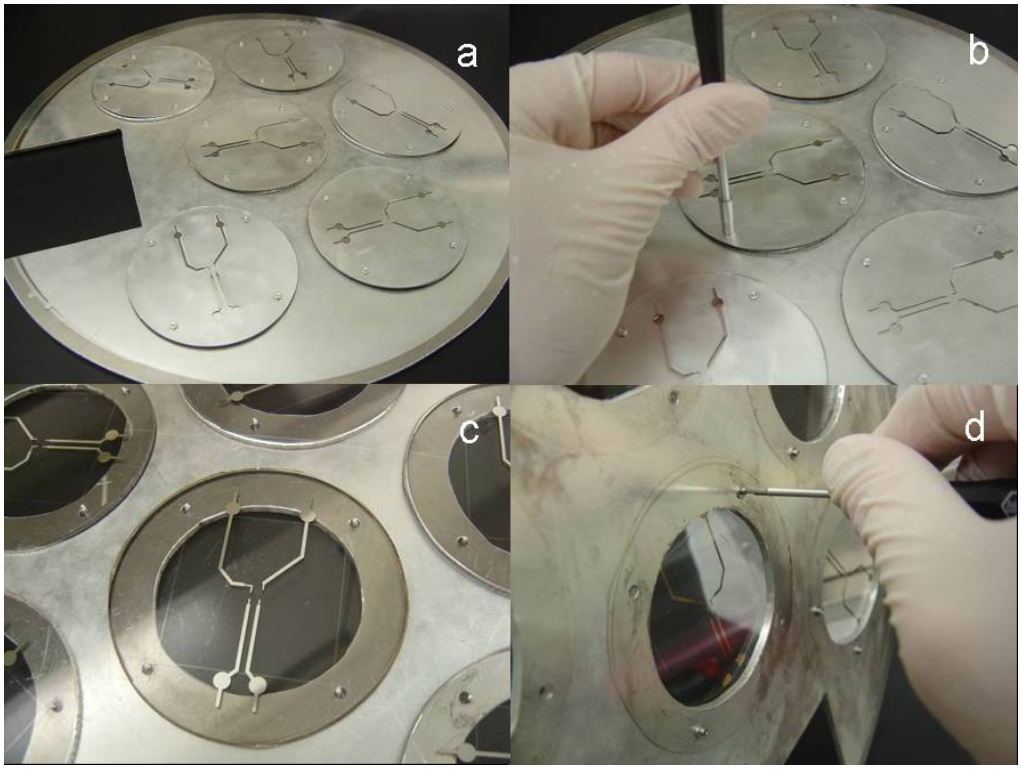

Figure 60: Removing wafers post-evaporation in pictures. (a) Wafer holder just after evaporation, (b) Removing the shadowmasks, (c) Close-up of a wafer after shadowmask removal showing electrode traces, and (d) Removing the wafers from the wafer holder.

Ag Electroplating

The next step in electrode construction is to electroplate additional Ag on top of the previously evaporated Ag. This additional silver is required to increase electrode lifetime, since silver chloride slowly dissolves in water. Even though the solubility constant (1.8×10^{-8}) for silver chloride is very low in water, the initial amount of silver chloride (order of pL) enclosed inside the microchannel is not much to begin with.

Electroplating Jig

To actually perform the electroplating, a jig was constructed to aid in the process. This jig, shown in Figure 61 and 62a, consists of a ½ inch thick PC base

plate into which two vertical rods are placed. The vertical rods act as anchors to which horizontal swing and down arms are affixed. At the end of one down arm, both a counter electrode and reference electrode are located. The counter electrode was constructed from Pt wire finely coiled to increase its stiffness and surface area while in the electroplating bath. The reference electrode is a commercial bought AgCl electrode (A&M Systems, WA). The other down arm holds a Cu probe which contacts the Ag trace that is to be electroplated. Thumbscrews, located at each joint of the swing arms, can be loosened to manipulate both electrodes and Cu probe into any position necessary for Ag electroplating. Figure 62b shows a close-up view of both the counter and reference electrode submerged in the electroplating bath. The Cu probe on the right makes contact with one end of an Ag trace.

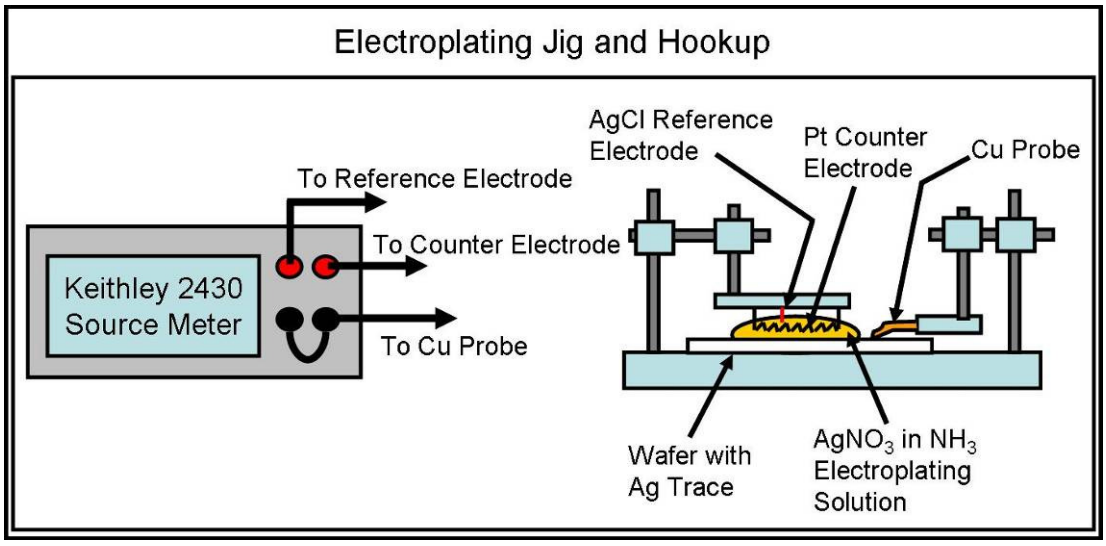

Figure 61: Electroplating jig (right) consists of a base plate on which the polymer wafer is placed. A volume of electroplating solution is piped over the Ag trace to be electroplated. The counter and reference electrodes are then submerged into the electroplating solution. The Cu probe makes contact with the Ag trace end on the wafer to complete the circuit. Information to hookup the Keithley 2430 source meter is provided on left.

A Keithley 2430 1kW pulsing source meter is used to power the electroplating process. Connecting the source meter to the electroplating jig is illustrated in Figure 61. The 4 wire sense terminal (upper left, red) on the Keithley gets connected to the AgCl reference electrode. The Input/Output terminal (upper right, red) gets connected to the Pt coiled counter electrode. Both ground (lower, black) terminals run to the Cu probe. When setting up the Keithley source meter, first set the unit to 4 wire sense mode by hitting the following button sequence:

- Configure, Measure V, Enter, 4 wire (edit →), enter, exit.

Next, the current magnitude needs to be set.

- Source I, edit ←, range ↑ until I_{src} is in mA range, edit →, 16mA, enter.

Finally, make sure the clamping voltage is 21 Volts (default).

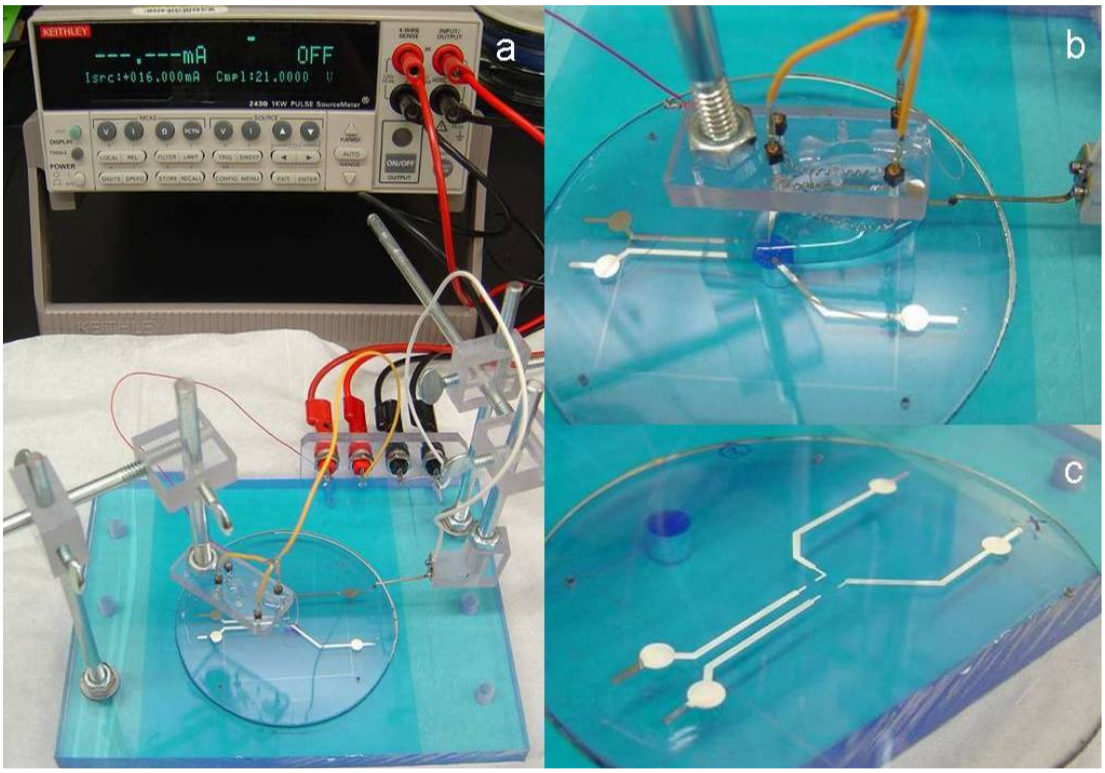

Figure 62: Electrode electroplating steps in pictures. (a) Electroplating setup, (b) Close-up of electroplating jig in action. Note, the yellow wires lead to the Pt counter electrode, and (c) Completed white electroplated Ag traces.

Electroplating Operation

The electroplating operation starts with placing the polymer wafer with newly evaporated Cr, Au, and Ag traces face up on the electroplating jig's base plate. First, locate the Cu probe and then lower it onto the edge of a desired Ag trace to be electroplated. Next, pipe ~0.7 mL of 0.35 M $AgNO_3$ in aqueous 1 M NH_3 over the Ag trace, being sure to cover the entire trace just up to the Cu probe but not touching the Cu probe. Because the PVDC is hydrophobic, the electroplating solution will puddle up and will not spread. Next, the Pt counter and AgCl reference electrode is carefully lowered into the electroplating solution, being careful not to bottom out on the Ag trace below. Be sure that both electrodes are submerged. Also, double check to make sure that the electroplating solution is still covering the entire Ag trace, especially where the microchannel will be.

Once everything is set up, the last step is to apply the current for a fixed amount of time. The amount of current and time was determined based upon how much Ag mass needed to be electroplated via Faraday's constant. Faraday's constant represents the amount of electric charge in one mole of electrons, and can be represented by the following equation: $F = N_A * Q$, where F is Faraday's constant (9.65×10^4 Coulombs/mol), N_A is Avogadro's number (6.02×10^{23} mol^{-1}) and Q is the charge on an electron (1.602×10^{-19} Coulombs). Trials were performed on test samples to ensure proper electroplating thickness (~1 μm) and plating uniformity across the entire trace. The outcome of the test trials yielded values for current density and electroplating time (0.33 mA/mm^2 and 25 seconds, respectively), which can be used electroplate any size trace regardless of area.

For the present electrode design, each Ag trace area is approximately equal therefore the applied current is equal based upon the current density found above. However, electroplating time was increased so as to increase the Ag thickness to just under 2 μm. Sequential bonding tests showed that the increase in Ag trace thickness lessened the likelihood of electrode failure due to thermal-induced cracking across trace's width. Current electroplating operation performed at 16 mA for 40 seconds. The traces are electroplated one at a time, clockwise for convenience. As the electroplating process occurs, the Ag trace will turn white. After each trace is electroplated, the electroplating solution is removed. The wafer is cleaned with DI water and then carefully blown dry with N_2, so not to remove the PVDC film. When proceeding to the next Ag trace to electroplate, the procedure starts over by positioning the Cu probe, piping on fresh electroplating solution, submerging the Pt counter electrode, etc. A newly electroplated wafer is shown in Figure 62c.

Electrode Chloridizing

The final step in electrode construction is chloridizing the portions of the Ag traces that will be exposed in the microchannels. Electrode chloridization is relatively simple and all of the Ag traces can be done at once by using aqueous Ferric Chloride ($FeCl_3$). When the $FeCl_3$ is applied to the Ag traces, a spontaneous oxidation reaction will occur according to the following equation:

$$FeCl_3 + Ag \rightarrow AgCl + FeCl_2$$

The above reaction then self terminates once the AgCl layer becomes thick enough to shield the remaining Ag from oxidizing, which takes approximately one minute.

First, a ¼ inch thick PTFE donut with a ½ inch diameter hole is centered on the electrode tips and then is gently placed onto the PC substrate. The PTFE donut keeps the $FeCl_3$ solution pooled up over the electrode tips instead of spreading along the Ag traces, which are hydrophilic compared to the hydrophobic PVDC film. Using a pipette, pipe the aqueous $FeCl_3$ (30 mM, 0.7 mL) onto the hole of the PTFE donut. After one minute, any remaining $FeCl_3$ solution can be removed using a pipette. Be careful not to touch the electrode traces or the PVDC surface with pipette tip or device damage could occur. Also, be careful removing the PTFE donut so not to scratch the Ag traces. Finally, rinse the wafer using DI water for 20 seconds. The chloridizing process is summarized in Figure 63.

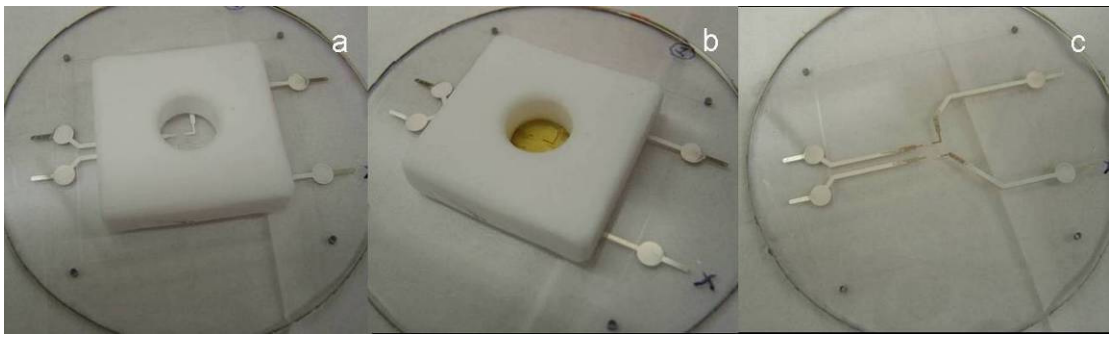

Figure 63: Electrode chloridization steps in pictures. (a) PTFE donut resting on Ag traces, (b) Ferric chloride solution applied over trace tips, and (c) Completed Ag/AgCl traces. Note, the pinkish color of the AgCl tip.

Electrode Cracking

During process development, electrode cracking was prevalent after device bonding. Strain induced during heating due to thermal expansion coefficient mismatches between the PVDC film and metal traces is the likely cause of cracking. Considerable effort was performed in improving the Ag/AgCl electrode fabrication with the goal of minimizing major cracking that would render a device un-useable for testing. Under the current fabrication process, discussed above, minor cracking is

still occurs but rarely will the crack cross the entire trace width breaking trace continuity.

To reduce cracking during device thermal bonding, the following causes were identified and the following solutions were implemented: 1) PVDC film spanning microchannels without PC support on either side always produced cracking where the electrode met the PC interfaces. Supporting the PVDC film with at least one PC wafer beneath reduced PVDC film sag and hence the possibility of cracking. Sandwiching the PVDC film on both sides by PC wafers reduces cracking and is recommended. 2) Cracks are created between material junctions where evaporated Ag meets electroplated Ag, as shown in Figure 64. Originally, only the evaporated Ag trace tips were electroplated and chloridized where the tip would protrude into the microchannel. Transmission microscopy clearly identified gaps that formed after thermal bonding. The solution was to electroplate the entire Ag trace and not just the trace tip. No cracking problem exists between AgCl and the plated Ag, so chloridizing only the electrode tips is still performed. 3) Hairline cracking was prevalent in the plated Ag trace after bonding especially after changes in trace dimensions, as shown in Figure 65. Changing electrode shadowmask design to include fillets and to avoid sharp inside corners remedied this issue. 4) Cracking of Ag traces in random places along the trace length. The solution was to plate the Ag traces longer (25 seconds to 40 seconds at same current), thus increasing the Ag trace thickness to resist strain-induced cracking. This proved to make a dramatic reduction in random cracking, and finally 5) Via holes previously drilled in PC wafer for

electrical connections to the Ag/AgCl trace would rub through or cause cracking of trace at interface. This solution is discussed later on in Figure 72.

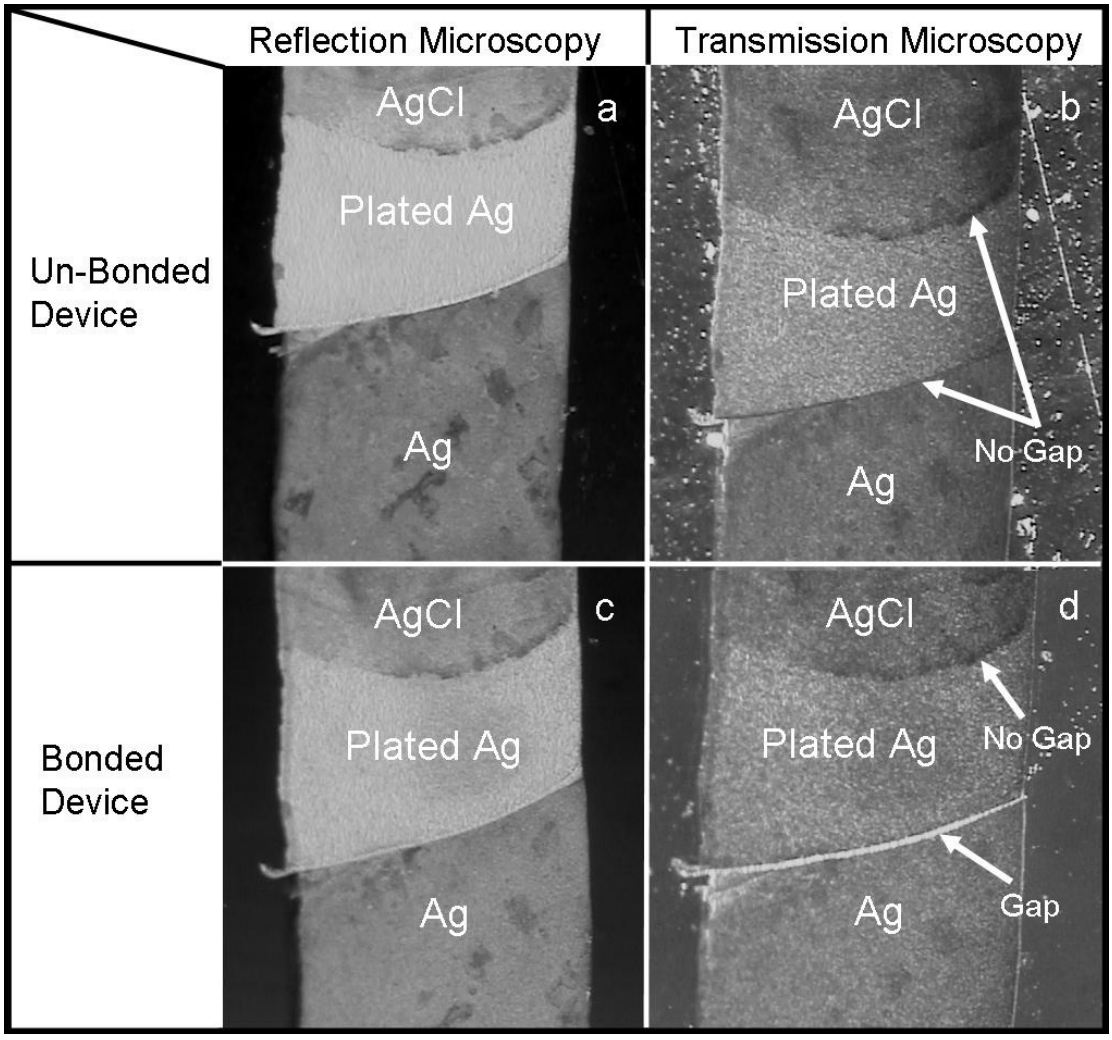

Figure 64: Pictures of cracking between material junctions of Ag/AgCl electrode traces. (a) and (c) Identical electrode trace before and after device bonding under reflection microscopy. Gaps between material junction not clearly visible in bonded case. (b) and (d) Same electrode before and after device bonding under transmission microscopy. Gap between evaporated Ag and Plated Ag in bonded case is now noticeable.

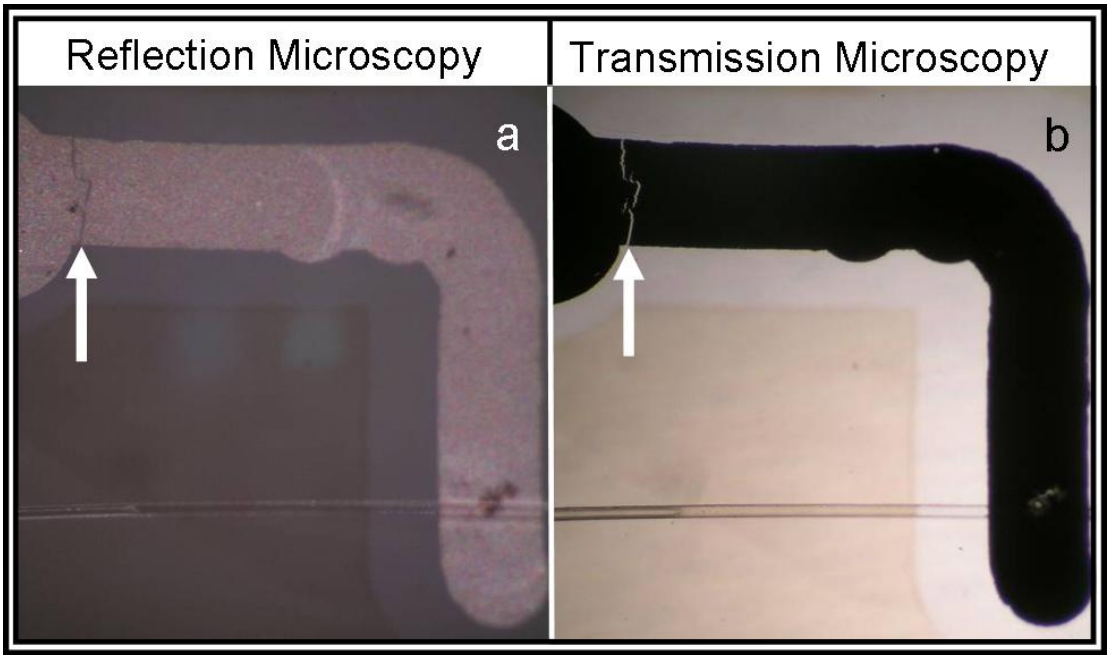

Figure 65: Pictures of Ag/AgCl electrode hairline cracking. (a) Crack across entire trace width as indicated by arrow under reflection microscopy. (b) Identical electrode trace with crack illuminated by transmission microscopy.

Appendix C

Final Assembly and Post-Bonding Operations

This appendix provides details on BLM micro-device fabrication, part 3 of 3. Topics covered in this appendix are: 1) assembling the micro-devices, 2) bonding of the micro-devices and 3) post-bond operations to get the chip ready for testing.

Device Alignment and Assembly

In prior steps in the fabrication process, work has been done to each wafer half independently. It is at this point, the two wafer halves finally come together to form some semblance of a microfluidic device. Since this design has imprinted features on both wafer halves, a wafer-to-wafer alignment is required for the device to function properly. This section summarizes not only the process of device alignment, but it discusses how the alignment is held until the bonding process is complete.

Device Alignment Jig

Due to the difficulties trying to align features of micron order over a 5 cm square area, a jig was created to aid in the process. Current design tolerances allow misalignment up to 15 μm before the device is not useable. Fortunately, alignment within 5μm can readily be achieved with this alignment jig. Below in Figure 66, a schematic of the alignment jig is shown.

The alignment jig consists of two halves, a top and bottom plate. Both plates, made from aluminum, move independently from each other. An opening in the jig's top plate permits the user to view the alignment event via the probe station microscope. In turn, the imprinted wafers are affixed to the alignment jig's top and bottom plate using mounting screws. Once the wafers are anchored, the alignment jig

plates are then placed on a Cascade Probe Station as shown in Figure 67a. The bottom plate fixes to the probe station's wafer stage while the top plate fits in the probe table's circular inset. The probe station's inherent translational and rotational movements allow fine movements of the alignment jig's top and bottom plate, thus the two wafer halves can be moved independently into precise alignment. Once alignment is achieved, the probe station table is lowered to contact the two wafers and then the wing nuts are tighten to lock the device's position. After the wing nuts are tightened, the alignment jig can be removed from the probe station in unison so that spring pins can be inserted at the drill press. The spring pins hold device alignment after removal from the alignment jig until the bond cycle is complete.

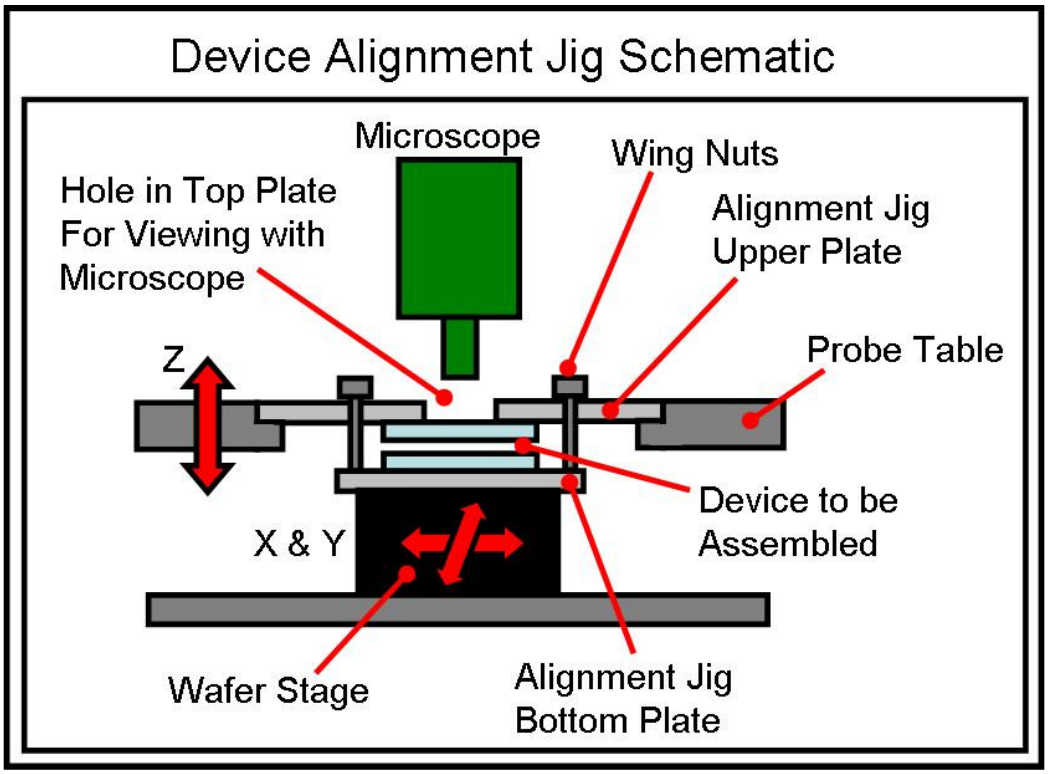

Figure 66: Schematic showing elements of the alignment jig used to align and assemble the two wafer halves that form the final device.

Alignment Procedure

The alignment procedure starts with attaching one wafer to the jig's bottom plate using four socket head cap screws (No. 0-80 x ½ inch), while the mating wafer is attached to the top plate using another four cap screws as shown in Figure 67b and c. Naturally, the imprinted sides of the wafers face outward. The arrows shown on the top and bottom plate aid the user when aligning the wafers since rotational orientation must be observed. Remove any blue dicing tape and clean the wafers with the ionizing N_2 air gun. Quickly, rough align and mate the two wafers together just so the wafer stay clean until fine alignment can be achieved. Tighten the wing nuts temporary until the alignment jig is placed on the probe station.

Now that the wafers are loaded, the jig plates are mounted onto the Cascade probe station. Loosen the wing nuts and lift the probe table up so a gap is formed between the two wafers. This gap allows the wafers to move independently without touching. Alignment is performed by moving the wafer stage (X-Y-θ) until the bottom wafer mates up with the top wafer attached to the jig's top plate. Lower the probe table to mate the wafers once desired position is achieved. After the wafers are aligned and mated, tighten the four ¼-20 wing nuts. Remove the alignment jig from the probe station and go to the miniature drill press for spring pin insertion.

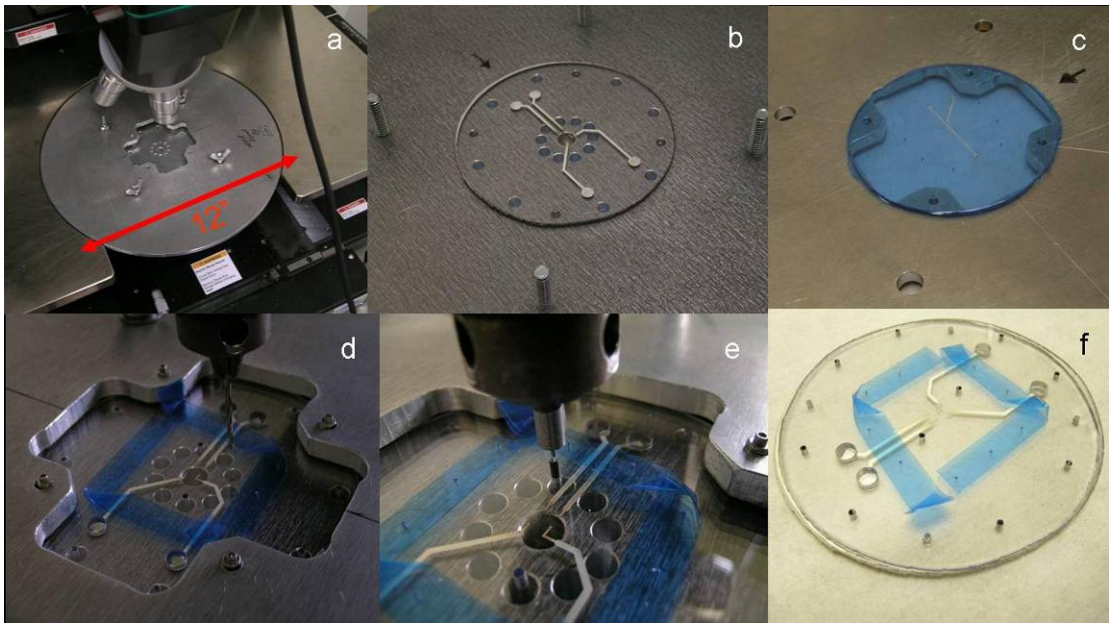

Figure 67: Device alignment and assembly steps in pictures. (a) Alignment jig shown on Cascade probe station, (b) PC wafer with PVDC and electrodes shown being loaded on bottom plate, (c) Mating PC wafer mounted on top plate, (d) Post-alignment holes are drilled for spring pins, (e) Spring pins being inserted, and (f) Final wafer ready for bonding.

At the miniature drill press, drill eight alignment holes using a No. 52 drill bit. The eight alignment holes are located around the device periphery and are indicated by blue circles in Figure 51d. The Φ1.5 mm x 4 mm spring pins (McMaster, NJ, P/N 91611A076) are then pressed into place by using a homemade tool that is mounted in the chuck of the drill press. The homemade spring pin tool, constructed from mild steel, is designed to press the spring pins just below the PC surface so as not to damage the glass plates in the hot press bonding jig (discussed later). Figure 67e shows a spring pin being pressed into the device using the insertion tool. After all eight spring pins are inserted; the assembled device can be removed from the alignment jig. This is accomplished by removing the eight small socket head cap screws followed by the four wing nuts. Finally, Figure 67f shows the aligned device

after being removed from the alignment jig. The device is now ready for bonding which is discussed next.

Device Thermal Bonding

This section discusses the bonding procedure that holds the assembled micro-devices together and seals the microchannels. As much detail as possible has been provided below, since it is well known that the resulting product (i.e. bond strength, amount of film sag inside the microchannel) is very sensitive to process parameter variation. The procedure given below, if followed correctly, will yield a satisfactory device ready for testing. It is assumed that persons following this procedure are familiar with equipment associated with thermal bonding.

Bonding Setup

This procedure utilizes the same equipment and jigs (hot press and embossing fixture) as discussed in Appendix A with one exception. Instead of a patterned Si master template, a blank Si wafer is placed in the lower embossing fixture. This blank Si wafer ensures that the bonded device will remain smooth and optically clear while still allowing temperature measurement via the embedding thermocouple. To aid in bonding and to minimize alignment shift due to press shear, a release film consisting, nominally 50 µm-thick PTFE film, is placed between the micro-device and lower plate of the embossing jig.

Bonding Recipe

The hot press is run under temperature control, where all temperature measurements are read from the lower embossing jig's thermocouple. At the beginning of each bonding run, the press platens are programmed for a 155 °C (311

F) setpoint. Warm-up period takes approximately ten minutes. At a reading of 80 °C (176 °F), place the cleaned assembled micro-device on the lower embossing jig plate making sure the device is centered on the blank Si wafer. Slowly close the press entirely and load the device with 700 lbs (72.7 psi). At 115 °C (240 °F), increase loading to 2700 lbs (280.6 psi). When the temperature reaches 141 °C (286 °F), start water cooling the press. While cooling, keep the loading constant until the temperature reads 90 °C (194 °F) and cease water cooling. Wait until temperature reads 80 °C (176 °F) before opening press to retrieve bonded device. The process can then be repeated with cycle times of approximately 25 minutes. See Figure 68 for pictures.

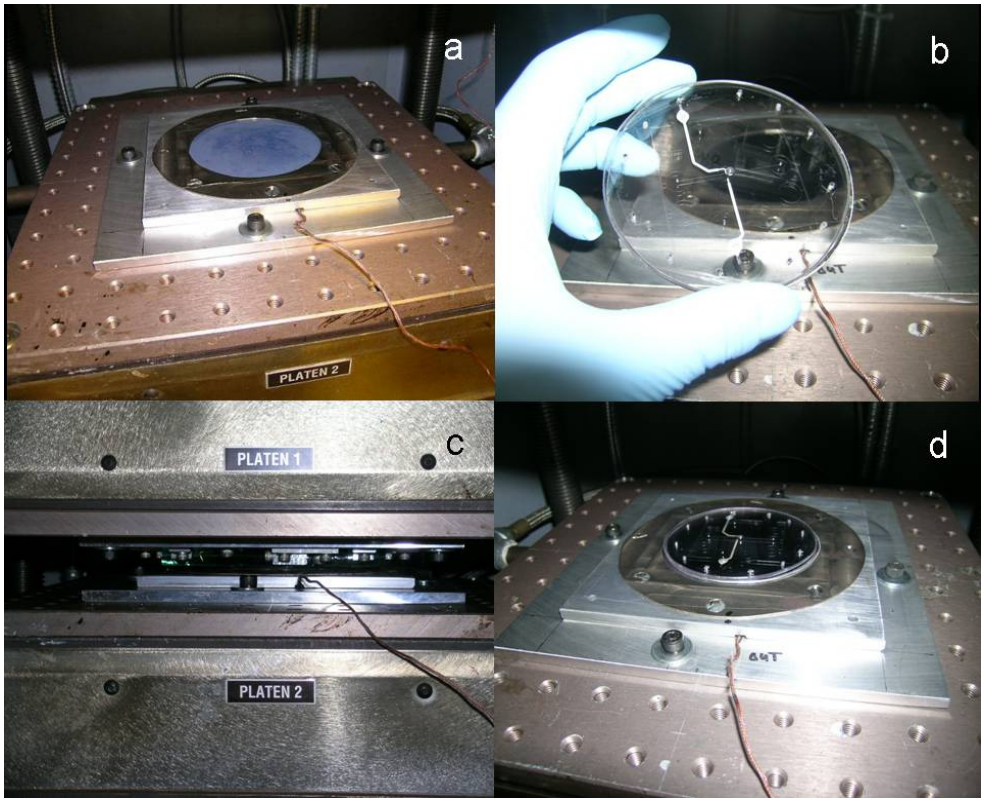

Figure 68: Device bonding in pictures. (a) Bottom embossing jig loaded with blank Si wafer covered with PTFE release film, (b) Clean assembled device ready for bonding, (c) Device being bonded in hot press, and (d) Newly bonded device ready for removal from hot press.

Bonding Issues

The above optimized bonding recipe resulted from many trials. Many issues, such as loss of wafer alignment, PVDC film sealing microchannels, leaky microchannels, microchannel reflow, and poor bondline strength were prevalent during early device bonding. Table XI reports possible causes and solution to the common issues associated with thermal device bonding.

Post-Bonding Operations

This final section discusses all of the fabrication operations that are performed on bonded chips so testing can then occur. There are three major operations: 1) Cutting the chip out of its now useless surrounding, 2) Inserting interconnects for fluid I/O, and 3) Making electrical I/O connections with the Ag/AgCl electrodes. Each operation will be discussed in turn.

Chip Extraction

The process has finally reached the point where the device can be cut out. Once extracted from its now useless surroundings, the chip will be approximately 5 cm (2 inch) square. A band saw is used to extract the chip by following the chip outline which was previously imprinted into the PC substrates. The chip outline is shown in Figure 51. Figure 69a shows the band saw blade mid-course traversing the chip outline, whereas Figure 69b shows a chip completely cut out. Note, blue dicing tape is applied to the bottom side (not shown here for clarity) to avoid scratching the PC surface prior to testing. Blue dicing tape is also used to cover the inlet reservoirs to avoid dust contamination of the microchannels. Lastly, the chip edges are

deburred and then the entire chip is cleaned with the N_2 gun prior to subsequent operations.

Table XI: Common Issues Associated with Thermal Device Bonding

Bonding Issue	Possible Cause	Solution
Loss of Alignment	1) Bonding Temperature Too High 2) Excessive Shear Force During Bonding 3) Device Sticks to Bonding Plates 4) Using Too Few Spring Pins	1) Do Not Exceed Max Temperature (141°C) 2) Check Hot Press Platen Parallelism 3) Use PTFE Release Film 4) Use Min 8 Pins to Hold Alignment
PVDC Sags; Sealing Microchannel	1) Bonding Temperature Too High 2) Excessive Bonding Pressure 3) Bonding Pressure Too Low 4) Microchannel Width too Large	1) Do Not Exceed Max Temperature (141°C) 2) Do Not Exceed Max Bonding Pressure (280.6 psi) 3) Increase Bonding Pressure to Reported 4) Microchannel Width Must Be < 100 µm
Leaky Microchannels or Poor Seal Around Electrodes	1) Bonding Temperature Too Low 2) Bonding Pressure Too Low 3) Debris Between PC Wafers	1) Increase Temperature to Reported 2) Increase Bonding Pressure to Reported 3) Use N_2 Ionizing Gun to Clean Wafers Prior to Assembly
Microchannels Reflow	1) Bonding Temperature Too High 2) Bonding Pressure Too High	1) Do Not Exceed Max Temperature (141°C) 2) Do Not Exceed Max Bonding Pressure (280.6 psi)
Poor Bondline Strength	1) Bonding Temperature Too Low 2) Bonding Pressure Too Low 3) Debris Between PC Wafers	1) Increase Temperature to Reported 2) Increase Pressure to Reported 3) Use N_2 Ionizing Gun to Clean Wafers Prior to Assembly
Electrode Cracking	See Appendix B on Electrode Cracking	

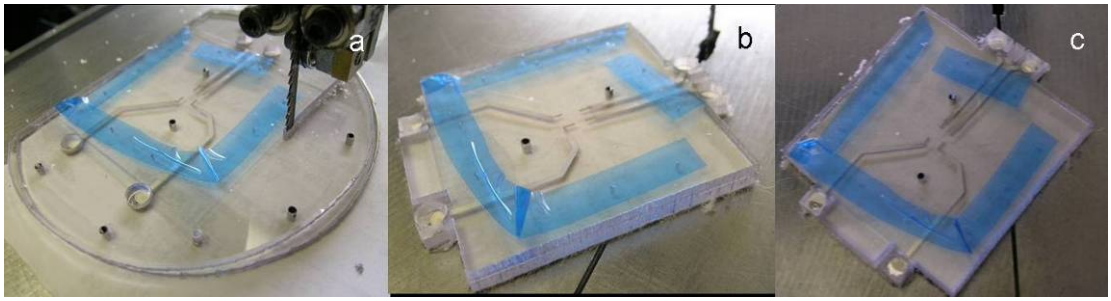

Figure 69: Chip extraction in steps. (a) First, the band saw is used to cut the chip out, (b) The chip after extraction, and (c) the extracted micro-device after deburring.

Chip Fluid Interconnects Using Hypodermic Needle Tubing

This section summarizes the procedure to utilize hypodermic needle tubing as chip interconnects for fluid I/O. This method eliminates the need for Nanoports (Upchurch Scientific, WA), as small lengths of hypodermic needle are interference fit into a mating hole of specific size making leak proof connections to the chip. Once the needles are installed, common Upchurch parts (e.g. unions, capillary tubing, etc) can be used to complete the fluid circuit to syringes, etc.

Hypodermic Needle Tubing

Needles utilized are from raw needle tubing stock which is obtainable, pre-cut to length, through preferred vender, Hamilton Syringe (Reno, NV). Syringe needles come in many sizes. For microfluidic connections, gauge 22 (P/N 21022A) needle tubing is desirable for the following reasons: 1) This gauge can withstand enough compressive force to allow the needle to be press fit into a mating hole without the needle buckling. 2) The needle outer diameter is compatible with common Upchurch parts (as mentioned earlier), thus off-shelf fittings and connectors can still be used, and 3) This needle gauge comes in a thick-walled version (gauge 22s, P/N 21038A) which reduces the dead volume when pumping fluids into the chip. The reduced

inner diameter of the 22s gauge needle essentially mimics press fitting a much smaller needle (e.g. gauge 30) into the hole, which would buckle under the compressive force required. Table XII, below, lists the critical dimensions of gauge 22 needle tubing.

Table XII: Critical Dimensions for Gauge 22 Needle Tubing

Needle Gauge	Outer Diameter (mm / inch)	Inner Diameter (mm / inch)	Min / Max Unit Volume (µL/cm)	Min / Max Unit Volume (µL/in)
22	0.7110 – 0.7237 mm 0.0280 – 0.0285 in	0.3940 – 0.4321 mm 0.0155 – 0.0170 in	1.22 – 1.47	3.09 – 3.72
22s	Same as Above	0.1400 – 0.1781 mm 0.0055 – 0.0070 in	0.154 – 0.249	0.39 –0.63

Device Mating Hole Size

The goal is to interference fit the needle into the mating hole which is bored into the polymer substrate. By definition of interference fit, the needle diameter must be larger than that of the mating hole in the polymer. The needle diameter is fixed since a gauge 22 (or 22s) needle was selected above, thus leaving the mating hole diameter to be determined. The mating hole diameter must be a maximum size of 0.7110 mm (0.028 inch), which is the minimum needle diameter accounting for dimensional tolerances. Of course, drilling a hole of this size would not produce a desirable result. Leakage will most likely occur when pumping fluids into the device, or even worst, the needle will just pop out from pumping pressure buildup. In addition, drill chuck runout must be accounted for when sizing the mating hole. For example, picking a 0.70 mm drill bit, while smaller than the minimum needle diameter, is a poor choice. If the drill press has a .025 mm (.001 inch) runout, the final hole diameter (0.725 mm) would be larger that the maximum needle diameter.

Another point to consider is the degree of interference fit (the size difference between the needle and hole) obtainable between the mating parts. Typically, both parts are considered but in this case, the degree of interference fit will depend mainly on the polymer's ductility since the needle's material is substantially stiffer and stronger. PC, a plastic noted for its toughness, can withstand a higher degree of interference fit compared to PMMA, which is more brittle. Needless to say, the best way of figuring out the mating hole size is just to experiment with different hole sizes and to see what works.

Hole sizes are limited to the standard drill bits available. Drill bits just smaller than the needle tubing are (largest to smallest):

1) 0.70 mm (0.0276 inch)
2) No. 71 (0.66 mm / 0.026 inch)
3) 0.65 mm (0.0256 inch)
4) No. 72 (0.635 mm / 0.025 inch)

It was determined that holes drilled smaller than with a No.72 bit were too small due to excessive wall shaving when fitting the needle, thus only the above need to be considered. A quick way to determine a preliminary mating hole size is to take a piece of scrap plastic (PC, PMMA, or COC) and to drill a few holes of each size. After deburring the holes, take a few needles and using the fit procedure (discussed later) insert them into holes of differing diameters. By practicing pressing needles into the scrap plastic, mating holes that are too small or too big will be immediately identifiable by sight and feel. If too big, the needle will pull out with minimal effort, if too small, the needle will shave the interior wall producing debris. Check the results under a microscope. If there are a few hole diameters that could be feasible,

insert the needles and do not remove them immediately. As time passes, the strain placed on the plastic holes will relax. If the plastic is overstressed, radial cracking will result about the hole's circumference. Cracks can appear quickly after pressing the needle in (COC and PMMA) or after a day (PC). Radial cracking of the plastic can be stress relieved by a subsequent heat treatment after fitting the needles into the plastic.

If a suitable hole size is determined from the scrap plastic test, the next step is to try it out on a microfluidic chip. Doing this is a must as the preliminary hole size may not work when implemented and the hole size must be further adjusted. Things to look for are leakage around needle while pumping fluids in and/or bondline delamination. If no problems exist, then the prefect hole size has been found.

In summary, the following drill sizes have been determined for PC, PMMA, and COC:

Table XIII: Drill Sizes for Needleports in Different Plastics

Polymer	Drill Size	Heat Treatment
PC	No.71 or .65 mm	No
PMMA	0.7 mm	Yes
COC	0.7 mm	Yes

Notes: 1) The miniature drill press was used when drilling holes. Another drill press will have different chuck runout, which will alter results. 2) Only preliminary hole drilling in scrap plastic was used to determine the PMMA and COC hole size. Needle ports have not been tried in bonded PMMA or COC devices to date. 3) Heat treatment of PMMA and COC are a must from preliminary work to avoid severe radial cracking. Heat treatment consisted of placing plastic part with inserted needles immediately into a pre-heated oven at 85 % T_g for 1 hour. 4) Don't

forget to deburr the mating hole because it helps center the needle when press fitting into the chip. 5) If after needle insertion, bondline delamination continues to occur, then bondline strength may not be sufficient to allow using needle port connections. Try to increase the bondline strength, via UV-Ozone surface treatment, if possible.

Needle Preparation

The needles, composed of stainless steel alloy 304, are drawn many times during the fabrication process making the needle tubing tough to cut due to material strain hardening. Abrasive tools, such as cut off wheels and files, can be used to size needle tubing to length, if needed. Regardless of whether the needle tubing was pre-cut or not, all needle ends need to be sanded, deburred and polished. This step is very important or the sharp needle edges will shave the walls of the mating hole, thus leaving undesirable plastic shavings in your microchannel reservoir. Finally, cleaning the needles' internal bore is a necessity to rid all debris and machining oils from fabrication prior to insertion.

The first step in detailing the needles is to make sure that the ends are square to the length. A fixture has been created from an aluminum scrap piece and a few Upchurch Nanoports that holds three needles simultaneously see Figure 70d. This fixture aids the user in holding the needles perpendicular to the sandpaper when sanding the ends. A pin vise can be used to alternately hold a single needle, but takes longer. Start with 600 grit wet/dry sandpaper, followed by 800 grit, and then working up to 1200 grit. Apply light pressure and blow off the debris every few strokes with the N_2 gun to avoid clogging the needles. Inspect the needles under the microscope

before proceeding to the next grit size. The needle end should appear like the one in Figure 70b when complete.

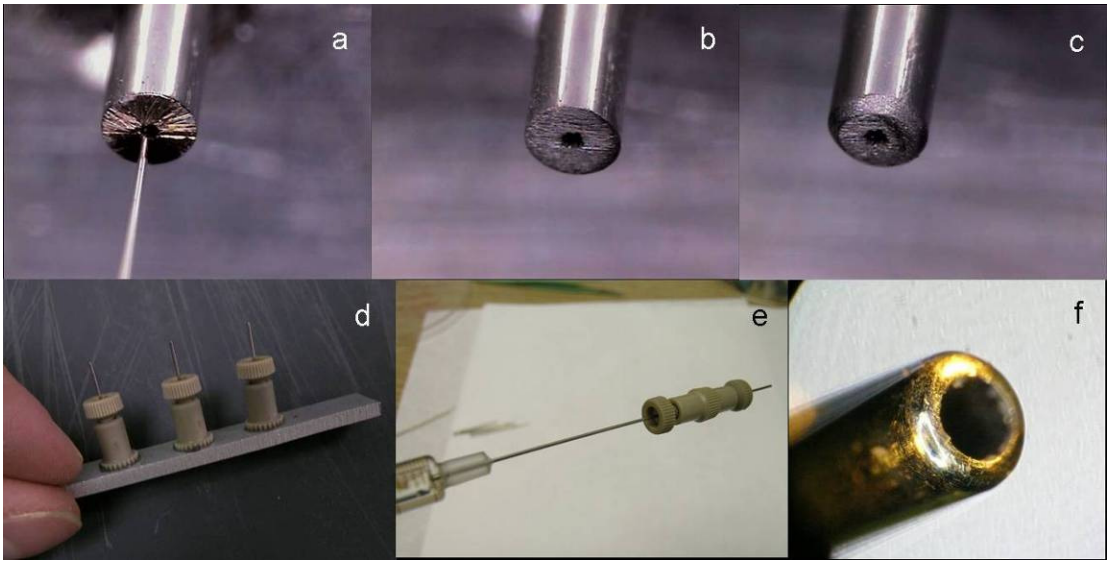

Figure 70: Needle preparation in pictures. (a) Raw gauge 22s needle from Hamilton Syringe, (b) After sanding needle square to length, (c) After rounding the edge, (d) Needle sanding fixture, (e) Cleaning the needles, and (f) Gauge 22 needle pre-cleaned for comparison.

The next step is to break the edges on the needle ends to avoid shaving the mating holes' interior bore. This is done by putting the needle in a pin vise and one at a time, sand the edge down by holding the pin vise at a 45 degree angle to the sandpaper. Apply light pressure and twist the pin vise while taking long strokes up and down the sandpaper. After a few strokes on 1200 grit sandpaper, blow off the dust and inspect under the microscope. The final needle end should look like the one show in Figure 70c.

The final step in needle preparation is cleaning. Cleaning can be performed by utilizing a Hamilton 500 µL syringe with an Upchurch union interface, as shown in Figure 70e. The needle, to be cleaned, can be inserted into the open union end and then the syringe can be used to pass cleaning fluids through the needle. First, 100 µL of acetone is passed through the needle and then 100 µL of IPA followed by 100 µL

DI water. Finally, N_2 is blown through the needle to remove any excess liquid. Additional cleaning in an ultrasonic bath is recommended.

Needle Insertion

After the needles have been prepared and the mating holes have been drilled and deburred, the needles can be inserted into the micro-device. A device to aid in press fitting the needles into the micro-devices had to be developed. The device consists of a Mitutoyo digital dial indicator and a miniature Jacobs drill chuck. The digital dial indicator aids in determining how far the needle has been pressed into the chip, while the miniature drill chuck grips the needle tubing firmly without slippage. Together, the press fit device goes into the chuck of a larger Ryobi drill press, where the press fitting is performed. An additional aluminum backing plate sits on the drill press worktable which aids in providing support. Blue dicing tape covers the backing plate to keep the underside of the device from getting scratched or marred.

Start by placing the needle to be press fit into the miniature Jacobs drill chuck and tighten. Clean the needle end with N_2 to remove any lingering debris, which could get into the micro-device. Remove the blue dicing tape covering the mating hole in the micro-device and place the chip on the backing plate, as shown in Figure 71a. Raise the drill worktable until the dial indicator arm comes in contact with the backing plate but the needle is just shy of touching the device surface. Next, a reference datum needs to be established so the needle insertion depth is known.

This is accomplished by lowering the needle to the chip's surface slowly just next to the hole where the needle will be inserted. Hold in place with light downward force and reset the dial indicator to zero. The needle end is now referenced to the

chip's top surface. Next, raise the needle just a tad and center the needle to the mating hole. Slowly, lower the needle toward the mating hole. Allow the chip to "float" until the needle centers itself in the mating hole. Once centered, hold the device manually while pressing the needle into the chip with the opposing hand. Slowly press the needle into the chip until the dial indicator reads the approximate desired depth. As a rule of thumb, needles should be inserted no more than 75-90% of polymer thickness. Trying to hit the exact bottom of the mating hole risks local device delamination due to overshooting. Local chip delamination could occur at 90% depth insertion, which in this case, the depth should be reduced to 75 or 80% in future needle insertions. Delamination can also be prevented by loosening the chuck while keeping a downward pressure on the inserted needle.

After hitting the desired depth, raise the miniature chuck upward. Now attached to the needle, the chip will raise off the backing plate. Carefully, loosen the miniature drill chuck's grip on the needle and let the chip fall back down to the backing plate. Lower the drill press worktable straight downward to withdraw the remaining needle from the miniature drill chuck. Figure 71d and e shows a needle that has just been inserted into a PC device. Finally, Figure 71c demonstrates the many ways the now inserted needles can be connected to the outside world. Needles longer than 25.4 mm (1 inch) can be purchased, inserted into the chip, and then bent any direction (e.g. 90 degrees) for more convenient connections. The downside is that once the needles are bent, they cannot be reused.

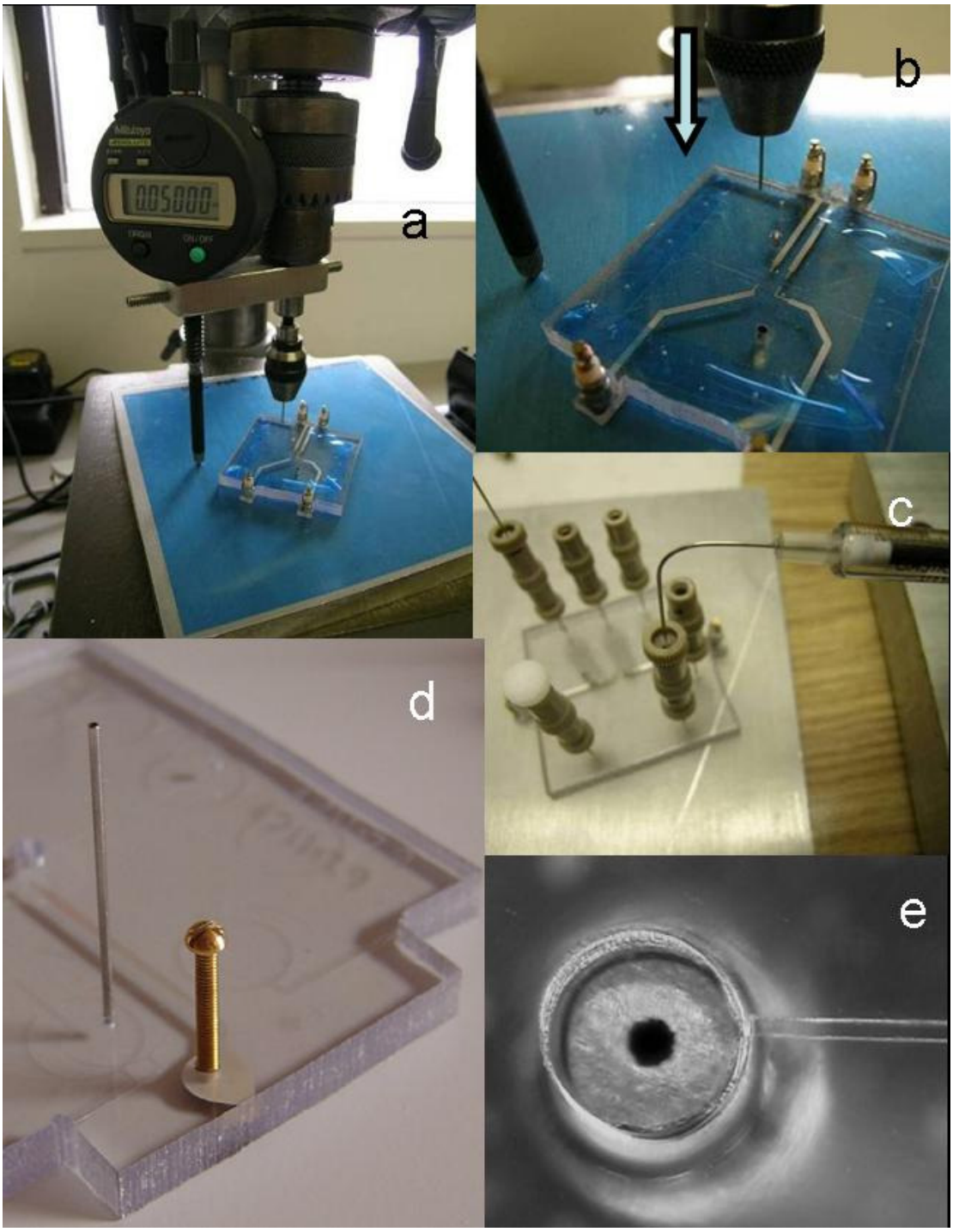

Figure 71: Needle insertion in pictures. (a) Press fit device consisting of miniature chuck and digital dial indicator, (b) Pressing a needle into a micro-device, (c) Possible connections with Upchurch fittings, (d) Micro-device post needle insertion, and (e) Close-up of inserted needle and microchannel (e).

Electrode Terminals

This section discusses the design aspects and then summarizes the procedure to make reliable electrical I/O connections to the previously fabricated on-chip Ag/AgCl electrodes. Once the electrode terminals are attached, chip fabrication is complete and ready for testing.

Design Methodology

Being that the Ag/AgCl traces are nominally 2 μm thick, care must be taken to avoid electrode damage until chip fabrication is complete. A distinct challenge associated with fragile thin film electrodes is how to make reliable connections to the external electrical circuitry. This section discusses possible electrode terminal designs, the results of prototype testing, and finally the down selected design.

Three electrode terminal designs, as shown in Figure 72, were originally thought of and implemented for prototype testing. The first design shown utilizes typical Cu wire which is merely held in place by an application of Ag conductive epoxy. The second design takes an external threaded stud and threads it into the bottom PC wafer. As the stud bottoms out, the stud bottom makes physical contact with the Ag trace and thus electrical contact is made. In both designs thus far, a thru hole is made in the upper PC piece so that enough clearance is achieved to allow access for Ag epoxy application and/or tools for stud seating. The last design utilizes a small machine screw which is threaded into a mating hole in the top PC piece. Similar to the second design, electrical contact is made when the screw bottoms out.

As each design was prototyped and tested, it became obvious that certain designs were not desirable. For instance, the bonded Cu wire in Design 1 would tend

to delaminate the PVDC film from the underlying PC. The PVDC film could not support the rotational moment created by the cantilevered Cu wire even though an AWG 30 wire was used. Better performance was achieved with Design 2, but problems still existed with having to drill through the Ag trace (and PVDC film) so that the male stud could be anchored. It was decided that drilling into the Ag trace should be avoided. After trying the third design, it clearly became the best design because it was simple. Design 3 has one drawback; chip delamination occurs if the screw is over tightened.

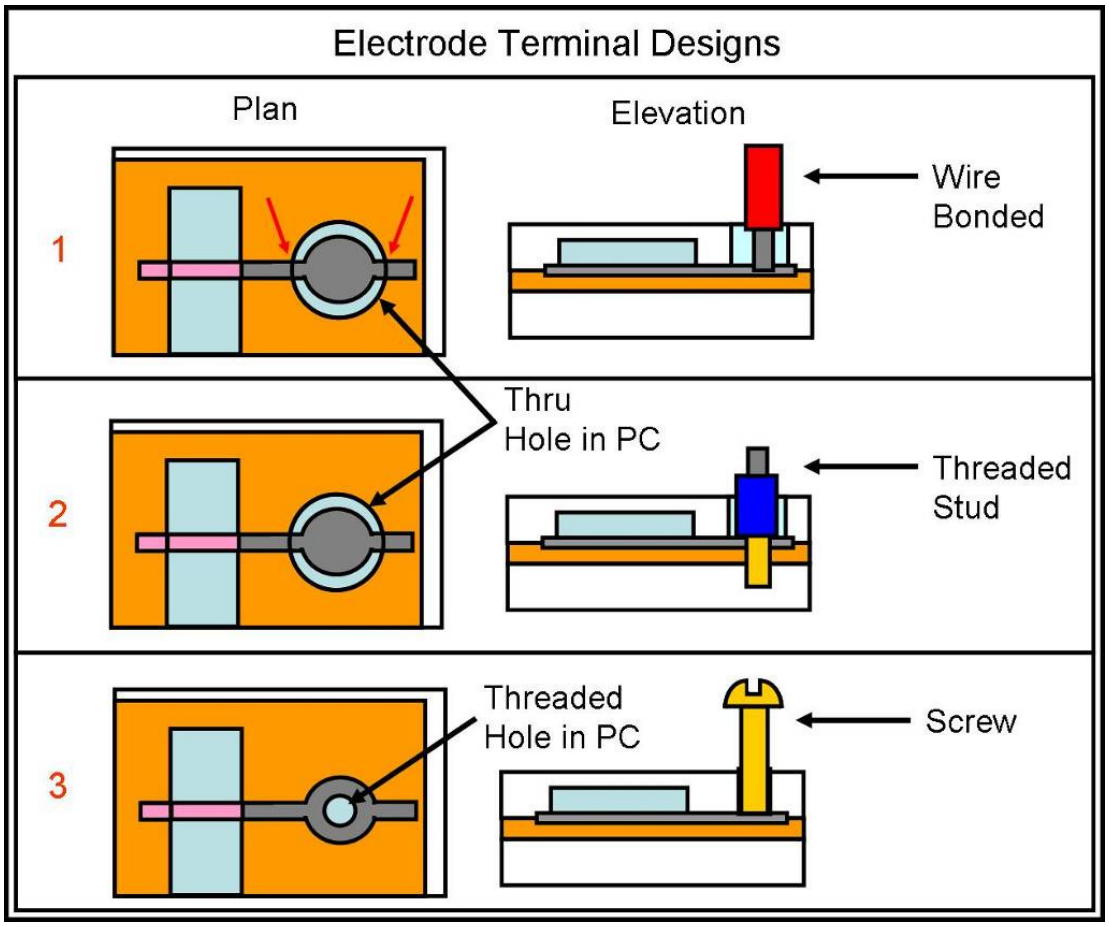

Figure 72: Electrode terminal designs. Design 1 consist of a wire bonded to the Ag trace using epoxy. Design 2 utilized a threaded stud seated against the Ag trace, and the final design utilizes a screw that bottoms out when inserted into a threaded hole. Design 3 was ultimately chosen.

Another critical issue that was common to all designs should be mentioned. Through holes drilled (and deburred) into the upper PC piece would always lead to cracking of the Ag trace after thermal bonding. Through holes larger than the Ag bond pad (e.g. Designs 1 and 2) would always rub through the Ag trace as indicated by the red arrows in Figure 71. Through holes smaller than the Ag bond pad (e.g. Design 3) still produced cracking but trace continuity would rarely be broken entirely because cracks rarely went totally around the hole's circumference. To improve the reliably and performance of Design 3, Ag conductive grease is injected into the threaded hole prior to screw insertion. The Ag grease fills all voids and bridges any gaps produced by thermal bonding. In summary, the risk of total Ag trace loss due to cracking was found to be minimized by using smaller holes in conjunction with Ag grease application. Design 3 was down-selected as the method to make external connections to the thin film Ag electrodes.

Terminal Mounting

After cutting out the device and inserting the needle port fluid interconnects, the electrode terminals can then be populated. The electrode terminals in this case are brass machine screws 0-80 x ½ inch (McMaster, NJ, P/N 92482A275). Brass screws were selected for improved electrical conduction versus stainless steel or carbon steel screws. The screw length is arbitrary but ½ inch was utilized for ease of clipping and reliably holding alligator leads.

A preparation step must be performed on the brass screw terminals prior to use. The bottom of the threaded portion must be grinded flat orthogonal to the screw length. Raw screws have a ridge on their bottom side which could damage the trace

and/or prevent full contact with the electrode trace. To complete this operation, a simple jig is made to hold the screws perpendicular while sanding the bottom surface. Sand using 600 and 1200 grit sandpaper until the screws are smooth and shiny.

After the screws have been prepared, there are two steps required to ready the mating BLM devices. First, the holes where the terminal screws are going to be threaded into must be checked for any visible debris leftover from the threading and deburring operations. Debris can cause the terminal screw not to contact the electrode properly, so the removal of any debris is critical. Lastly, a conductive media, either Ag grease or epoxy, must be piped into the thread hole prior to screwing in the terminal. While both the Ag grease and epoxy is acceptable, the grease is easier to work with since the lack of setup time allows relaxed terminal application. The Ag conductive grease aids in making a fail-proof electrical contact between the Ag thin film trace and the electrode screw terminal. In addition, any cracking of the thin film electrode due to thermal stresses near the terminal threaded hole will be bridged by the Ag grease. Packing Ag grease into the terminal threaded hole is simply done by manual means with aid of a microscope.

The screw terminals are finally ready for mounting. While keeping the screw perpendicular to the device, start threading the screw in place. As the screw tightened, the Ag grease will be drawn down towards the Ag thin film electrode by the piston action of the screw. As the screw nears the hole bottom, care must be taken not to over tighten the screw too much or device delamination will occur. Observing under the microscope while tightening the screw will aid in knowing when

the terminal mounting operation is complete. Finally, wipe away any leftover Ag grease on the device that squeezed out.

Terminal screws can be reused by removing them from spent devices. The Ag grease can be removed by an IPA wash along with a manual wiping operation. Prior to reuse, the screw bottoms should be lightly abraded with 1200 grit sandpaper to eliminate any surface oxidation which could increase electrical resistance if not removed.

Appendix D

UV-Ozone Surface Treatment

This appendix discusses the UV-Ozone surface treatment performed to the top and bottom PC wafers prior to BLM micro-device array chip assembly. The goal this surface treatment was to hydrophilize the microchannel surfaces thus improving fluidic control, especially when injecting lipid solution for BLM formation.

UV-Ozone Fundamentals

UV-ozone surface treatment is a simple process only requiring an UV lamp emitting the right wavelengths for polymer surface activation. The UV wavelengths of interest are 184.0 nm and 253.7 nm. The former wavelength, 184.0 nm is absorbed by atmospheric O_2 and generates ozone, O_3, whereas the latter wavelength, 253.7 nm, is absorbed by O_3 and broken back down into O_2 thus completing a cycle of ozone generation and depletion. Polymers also absorb the UV light and chemical bonds can be broken on the polymer surface resulting in oxidation reactions occurring with the ambient O_2 and O_3 discussed earlier. These oxidation reactions leave the polymer surface activated thus changing its hydrophobicity and contact angle. More information on UV-ozone surface treatment fundamentals can be found in [97].

UV-Ozone Surface Treatment Process

UV-ozone surface treatment consists of placing the polymer surface to be treated inside a commercial UV-ozone cleaner for an allotted time and then measuring the contact angle, which changes with degree of surface activation. A Novascan PSD UV/O surface cleaner [98] was utilized to conduct UV-ozone surface

treatment on the BLM micro-device array chip. The bottom PC wafer with applied PVDC film and the top PC wafer were subjected to various UV-ozone surface treatment times. Table XIV provides contact angle information for a water droplet on the polymer surface that has been UV-ozone treated for various times. Contact angle information provided in this table was obtained via a goniometer immediately after UV/O treatment, under the following conditions: 1) without a quartz mask covering the polymer surface, 2) the Novascan UV/O cleaner lamp was warmed for 5 minutes, and 3) the lamp-to-polymer surface was the standard distance in all cases.

Table XIV: Average Contact Angle versus UV-Ozone Surface Treatment Time

UV-Ozone Surface Treatment Time	Bottom PC Wafer with PVDC Film	Top PC Wafer
Native (no UV-O)	88.5º ± 2.5º	99.5º ± 1.5º
8 minutes	63º ± 10º	--
10 minutes	--	23.3º ± 3.5º

The UV-ozone treatment times reported in Table XIV were the results of time trial experiments. These times are used in UV-Ozone treatments of the BLM micro-device chips, if necessary. Note PVDC cannot be surface treated longer than 8 minutes because the film becomes brittle and does not achieve high bondline strength after thermal bonding. In addition, PVDC film must be irradiated at a distance to avoid thermal strains that can cause the film to curl off the PC substrate. UV-O treatment also causes yellowing of both polymers.

Masking Options

Recent work by Childs et al. [99] showed that PDMS surfaces can selectively UV-O treated by utilizing quartz photolithography masks. This knowledge led to patterning of PVDC film for satisfactory substrate adhesion of the Ag/AgCl

electrodes. In addition, the mating areas of the top PC wafer are also UV-O surface treated for leak-proof seals around the Ag/AgCl electrodes.

Two masking plans, see Figure 73, were devised where Plan A is a lightfield mask and Plan B is a darkfield mask. Each masking technique has advantages and disadvantages. For example, Plan B leaves the entire PVDC field untreated, thus the subsequent thermal bonding procedure does not need modification, whereas Plan A requires modification of the thermal bonding procedure. Both plans were tried, but ultimately Plan B was used since it did not change further fabrication procedures down the line.

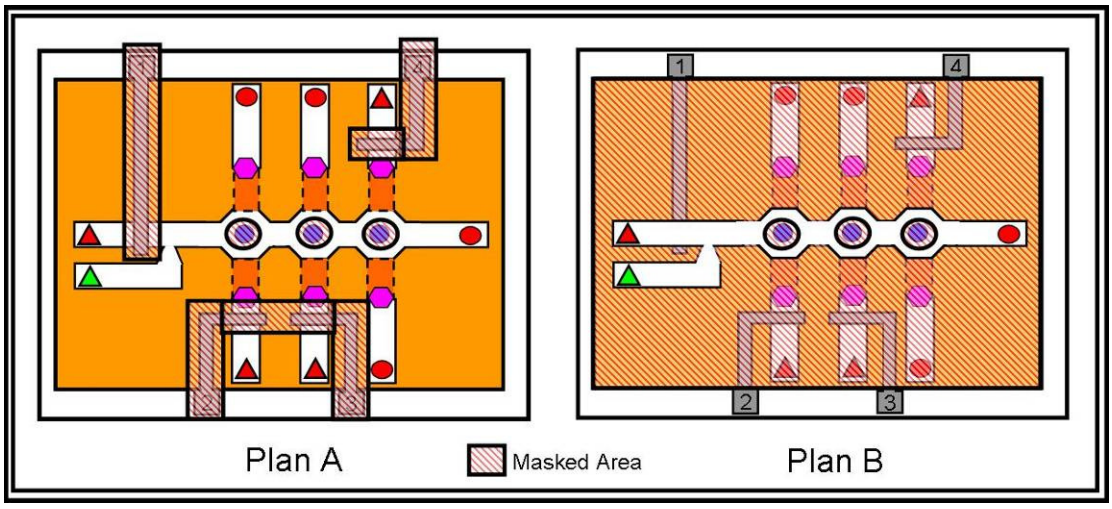

Figure 73: UV-Ozone masking options for the BLM micro-device array chip. Left, Plan A proposes to mask the PVDC film where the Ag/AgCl electrodes and BLM formation sites are located. Right, Plan B proposes to mask the entire PVDC surface and BLM formation sites only. UV-Ozone surface treating the PVDC film and mating PC surface requires modification to the device thermal bonding procedure.

UV-Ozone Results

Results of the UV-Ozone surface treatment are shown below in Figures 74 and 75. The first figure shows a PC wafer that was masked (Plan A approach) and then UV-O treated for 12 minutes. The treatment time is different then listed in Table

XIV because an additional 2 minutes is required if a quartz mask is used to pattern surfaces. Distinct hydrophobic and hydrophilic areas are pronounced when DI water is piped onto the PC surface as shown in Figure 74.

The bottom PC wafer with PVDC film can be UV-O treated before or after Ag/AgCl electrode fabrication. In Figure 75, Ag/AgCl electrodes were fabricated first on native PVDC film and then masked to prevent detrimental UV-O effects to the electrodes (UV light breaks down AgCl). Areas of surface treatment can be seen where the ferric chloride solution was piped earlier during electrode tip chloridization.

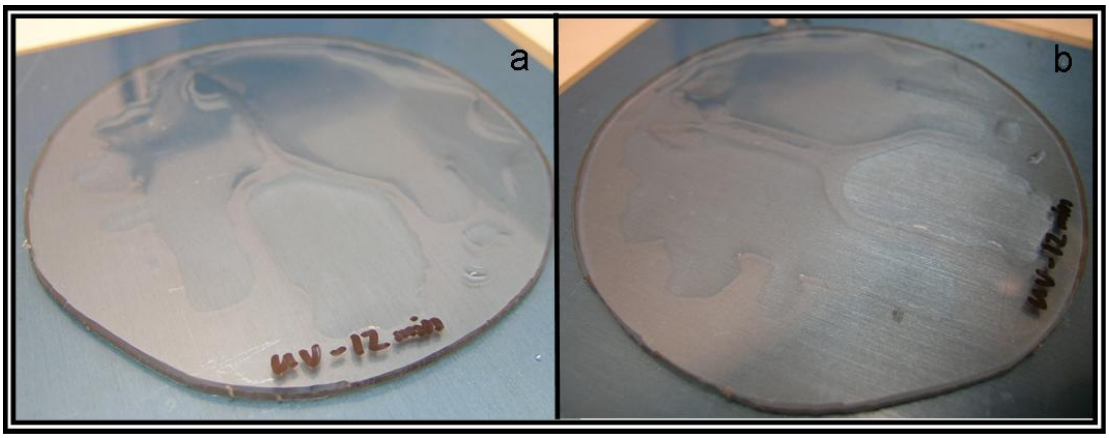

Figure 74: Top PC wafer UV-Ozone treated for 12 minutes. A quartz mask, Plan A approach, was used to mask the electrode trace areas thus preventing hydrophilization of the PC surface beneath. DI water was piped onto the PC surface to reveal the native hydrophobic areas.

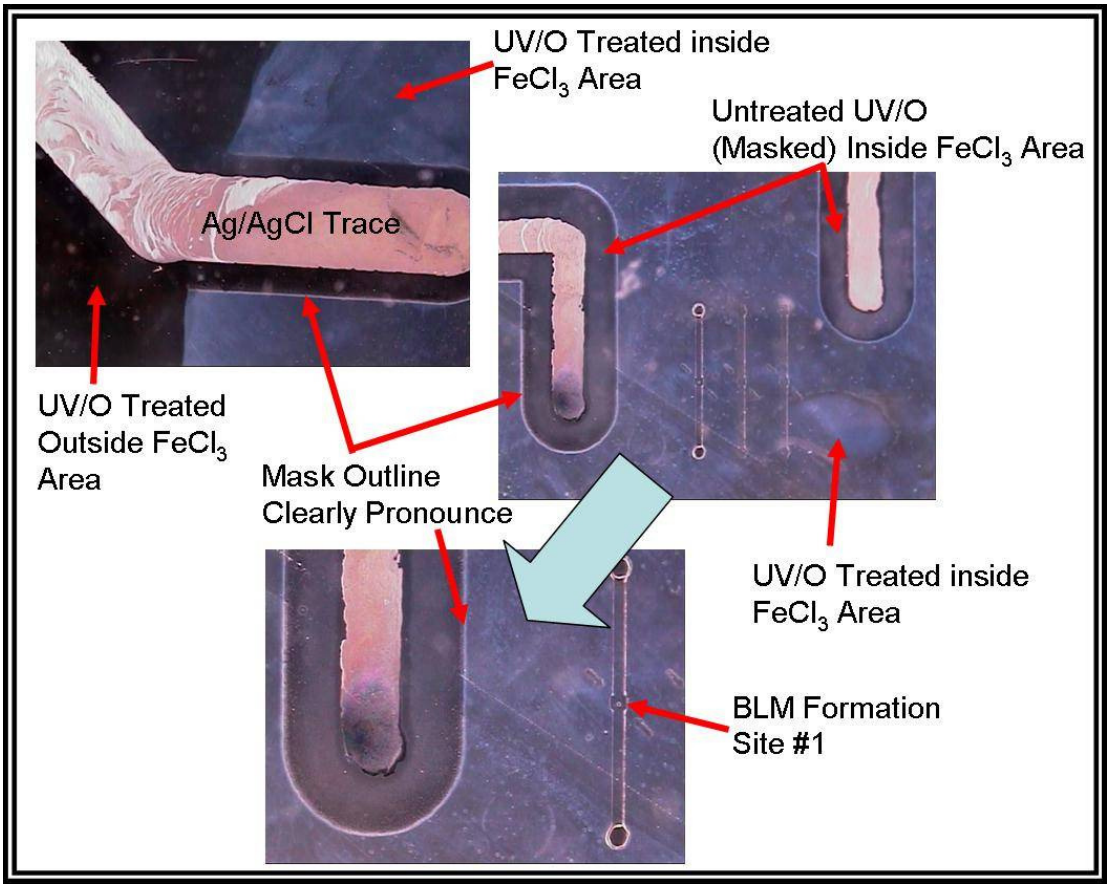

Figure 75: Bottom PC wafer with PVDC film UV-Ozone treated for 8 minutes. A quartz mask, Plan A approach, was used to mask electrodes which were previously fabricated on the native PVDC film. After treatment, the area where the $FeCl_3$ solution was applied for electrode trace chloridization is now apparent.

Appendix E

Pump-inator 2006 Software

This appendix provides an overview to a piece of software created specifically for this research. *Pump-inator 2006* was coded and compiled in *Visual BASIC 2005*, thus it is a stand alone executable program that can be installed on any PC. This software was created due to the need for remote actuation of three PHD 2000 syringe pumps (Harvard Apparatus) inside the Faraday cage. Other commercial software packages available at the time had issues that made them undesirable to use for this application. For instance, one program ran inside *LabVIEW*, which made for very slow communication between the syringe pumps and PC. Moving fluids inside a micro-device need not have syringe pump control with such lag time in actuation. Other canned programs would only run a single pump at a time. Lastly, the biggest disadvantage of all the existing canned programs was that once you sent a command signal (i.e. update pump speed, etc) to the pump, there was no feedback to guarantee that the signal was: 1) sent to the pump and 2) the pump accepted the command and updated its settings. The *Pump-inator 2006* program automatically confirms all commands set to the pumps.

Initialization of *Pump-inator 2006* brings up a startup menu (Figure 76) where the user selects how many syringe pumps are connected to the PC and the serial port options. After the pump configuration and serial port options are selected, the user hits the initialize button. The program then verifies that the syringe pumps are connected and establishes communication, if all the settings are correct.

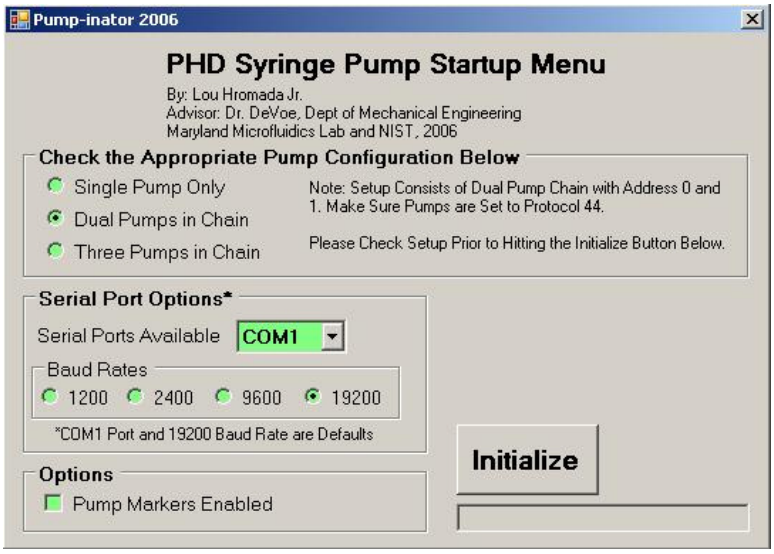

Figure 76: Startup menu for *Pump-inator 2006*.

Next, the main form of the *Pump-inator 2006* program appears. A screen capture for a two pump configuration is shown in Figure 77 below. Located on the main form are multiple frames each with specific tasks. For instance, the "Pump 0" frame houses controls that do three tasks: 1) Allows the user to start/stop the pump and to change the pump's mode (i.e. infuse/refill). 2) Allows the user to enter and send new pump parameters, such as syringe diameter, infuse rate, refill rate, to the pump. 3) Allows the user to verify that sent commands were accepted by the syringe pumps, and 4) Automatically keeps track of current pump conditions and alerts the user with warnings, as necessary.

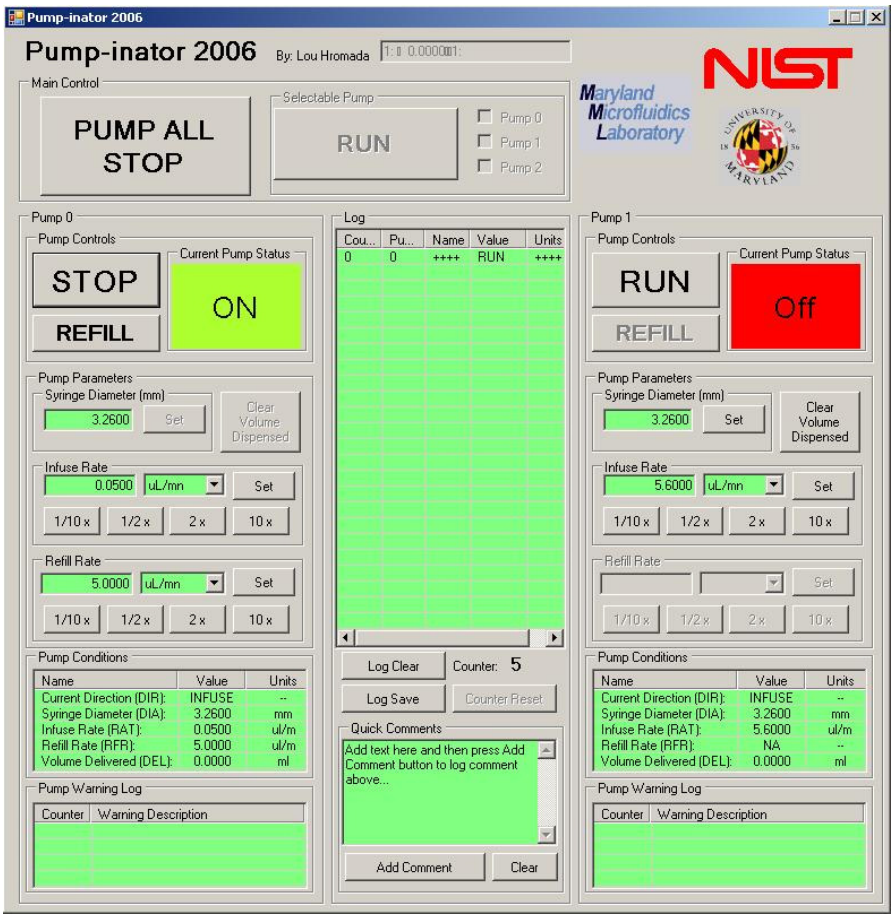

Figure 77: *Pump-inator 2006* main form activated for two syringe pumps. See text for details.

One last feature worth mentioning on *Pump-inator 2006* is the pump marker option. Pump markers are forms that can be placed on top of other windows, such as microscope video feed, so that pump conditions can be seen real time. The idea is that experiments can be recorded with a screen capture software (i.e. *Snag it 8*) and upon playback all key pieces of information will be available for analysis apriori. A log window, which keeps track of past pump commands and current pump conditions, can also be recorded. Figure 78, below, shows a screen capture of a BLM micro-device being tested. Here, the *Pump-inator 2006* pump markers and log window provides instant pump conditions as fluids are being pumped through the micro-device.

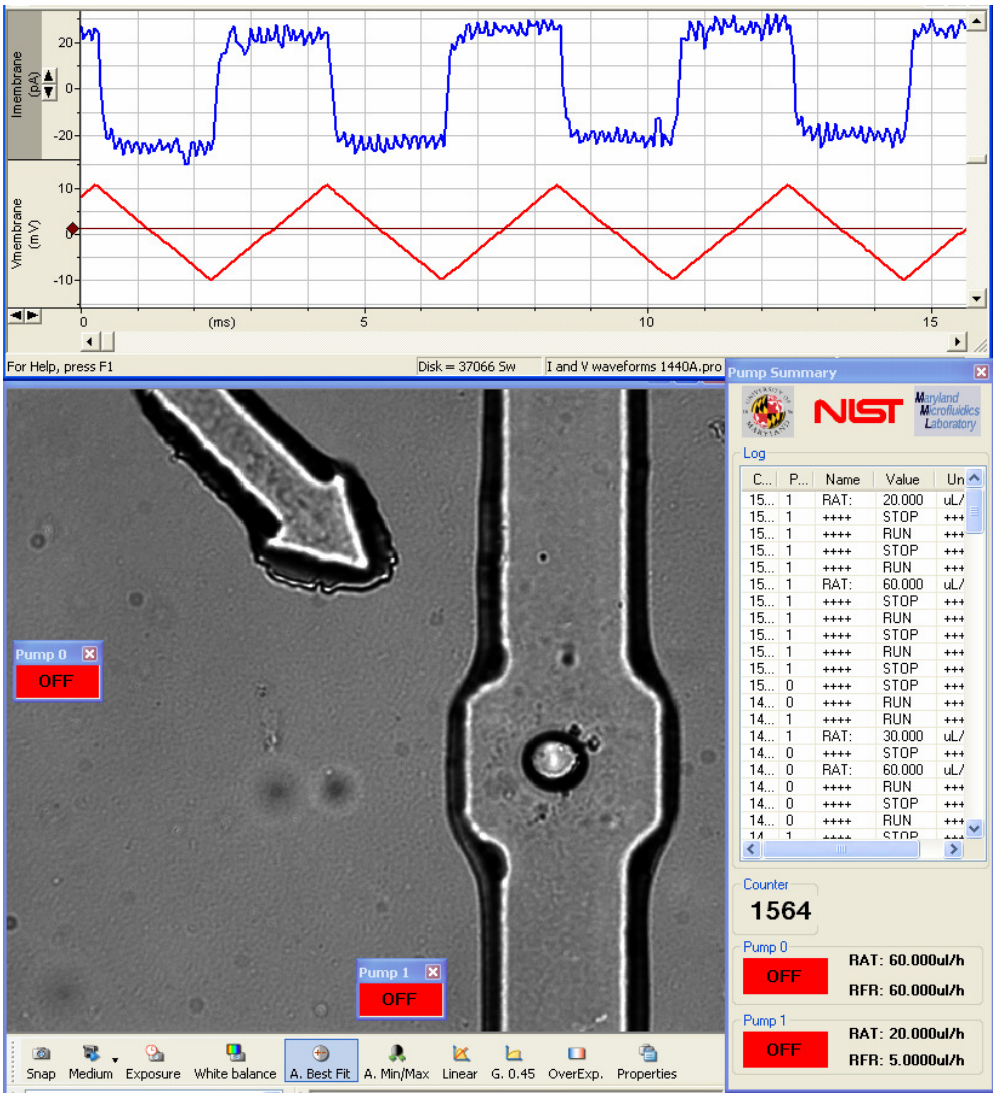

Figure 78: Pump marker option available with *Pump-inator 2006*. See text for details.

Endnotes

1. Singer, S.J. and G.L. Nicolson, *Fluid Mosaic Model of Structure of Cell-Membranes.* Science, 1972. **175**(4023): p. 720-731.
2. Jacobson, K., E.D. Sheets, and R. Simson, *Revisiting the Fluid Mosaic Model of Membranes.* Science, 1995. **268**(5216): p. 1441-1442.
3. Kasianowicz, J.J., et al., *Simultaneous Multianalyte Detection with a Nanometer-Scale Pore.* Analytical Chemistry, 2001. **73**(10): p. 2268-2272.
4. Henrickson, S.E., et al., *Driven DNA Transport into an Asymmetric Nanometer-Scale Pore.* Physical Review Letters, 2000. **85**(14): p. 3057-3060.
5. Chandler, E.L., et al., *Membrane Surface Dynamics of DNA-Threaded Nanopores Revealed by Simultaneous Single-Molecule Optical and Ensemble Electrical Recording.* Langmuir, 2004. **20**(3): p. 898-905.
6. Kasianowicz, J.J., et al., *Characterization of Individual Polynucleotide Molecules Using a Membrane Channel.* Proceedings of the National Academy of Sciences of the United States of America, 1996. **93**(24): p. 13770-13773.
7. Kasianowicz, J.J., *Nanopores - Flossing with DNA.* Nature Materials, 2004. **3**(6): p. 355-356.
8. Sutherland, T.C., et al., *An Analysis of Mismatched Duplex DNA Unzipping Through a Bacterial Nanopore.* Biochemistry and Cell Biology-Biochimie Et Biologie Cellulaire, 2004. **82**(3): p. 407-412.
9. Rhee, M. and M. Burns, *Nanopore Sequencing Technology: Research Trends and Applications.* Trends in Biotechnology, 2006. **24**(12): p. 580-586.
10. Movileanu, L. and H. Bayley, *Partitioning of a Polymer into a Nanoscopic Protein Pore Obeys a Simple Scaling Law.* PNAS, 2001. **98**(18): p. 10137-10141.
11. Krasilnikov, O., C. Rodrigues, and S. Bezrukov, *Single Polymer Molecules in a Protein Nanopore in the Limit of a Strong Polymer-Pore Attraction.* Physical Review Letters, 2006. **97**(1): p. 0183011-4.
12. Howorka, S., et al., *A Protein Pore with a Single Polymer Chain Tethered within the Lumen.* Journal of American Chemistry Society, 2000. **122**(11): p. 2411-2416.
13. Sanchez-Quesada, J., et al., *Single DNA Rotaxanes of a Transmembrane Pore Protein.* Angewandte Chemie, 2004. **43**: p. 3063-67.
14. Khulbe, P., M. Mansuripur, and R. Gruener, *DNA Translocation Through Alpha-Hemolysin Nanopores with Potential Application to Macromolecular Data Storage.* Journal of Applied Physics, 2005. **97**: p. 1043171-1043176.
15. Ashkenasy, N., et al., *Recognizing a Single Base in an Individual DNA Strand: A Step Toward DNA Sequencing in Nanopores.* Angewandte Chemie, 2005. **44**: p. 1401-1404.
16. Howorka, S., S. Cheley, and H. Bayley, *Sequence-Specific Detection of Individual DNA Strands Using Engineered Nanopores.* Nature Biotechnology, 2001. **19**: p. 636-639.
17. Astier, Y., O. Braha, and H. Bayley, *Toward Single Molecule DNA Sequencing: Direct Identification of Ribonucleoside and Deoxyribonucleoside*

5'-Monophosphates by Using an Engineered Protein Nanopore Equipped with a Molecular Adapter. Journal of American Chemistry Society, 2006. **128**: p. 1705-1710.
18. Murphy, R. and M. Muthukumar, *Threading Synthetic Polyelectrolytes Through Protein Pores.* Journal of Chemical Physics, 2007. **126**(5).
19. Eray, M., et al., *Highly Stable Bilayer-Lipid Membranes (Blms) Formed on Microfabricated Polyimide Apertures.* Biosensors & Bioelectronics, 1994. **9**(4-5): p. 343-351.
20. Mueller, P., et al., *Methods for Formation of Single Bimolecular Lipid Membranes in Aqueous Solution.* Journal of Physical Chemistry, 1963. **67**(2): p. 534-7.
21. Tien, H.T. and A.L. Ottova, *Supported Planar Lipid Bilayers (s-BLMs) as Electrochemical Biosensors.* Electrochimica Acta, 1998. **43**(23): p. 3587-3610.
22. Tien, H.T. and A.L. Ottova, *From Self-Assembled Bilayer Lipid Membranes (BLMs) to Supported BLMs on Metal and Gel Substrates to Practical Applications.* Colloids and Surfaces a-Physicochemical and Engineering Aspects, 1999. **149**(1-3): p. 217-233.
23. Huang, C., T.E. Thompson, and L. Wheeldon, *Properties of Lipid Bilayer Membranes Separating 2 Aqueous Phases - Formation of Membrane of Simple Composition.* Journal of Molecular Biology, 1964. **8**(1): p. 148.
24. White, S.H., *Formation of Solvent-Free Black Lipid Bilayer Membranes from Glyceryl Monooleate Dispersed in Squalene.* Biophysical Journal, 1978. **23**(3): p. 337-347.
25. Mayer, M., et al., *Microfabricated Teflon Membranes for Low-Noise Recordings of Ion Channels in Planar Lipid Bilayers.* Biophysical Journal, 2003. **85**(4): p. 2684-2695.
26. Wonderlin, W.F., A. Finkel, and R.J. French, *Optimizing Planar Lipid Bilayer Single-Channel Recordings for High-Resolution with Rapid Voltage Steps.* Biophysical Journal, 1990. **58**(2): p. 289-297.
27. Suzuki, H., et al., *Planar Lipid Bilayer Reconstitution with a Micro-Fluidic System.* Lab on a Chip, 2004. **4**(5): p. 502-505.
28. Suzuki, H., et al. *Planar Lipid Membrane Array for Membrane Protein Chip*. in *Proceedings of the 17th IEEE International Conference on MEMS*. 2004. Maastrict.
29. Suzuki, H., et al. *Planar Lipid Bilayer Chip for Electrophysiological Analysis of Membrane Proteins*. in *8th International Conference on Miniaturized Systems for Chemistry and Life Sciences*. 2004. Malmo, Sweden.
30. Suzuki, H., et al. *Formation Process of Planar Lipid Bilayer Observed by Confocal Microscopy*. in *Proceedings of the 3rd Annual International IEEE EMBS Special Topic Conference on Microtechnologies in Medicine and Biology*. 2005. Kahuku Oahu Hawaii.
31. Suzuki, H., et al., *Electrophysiological Recordings of Single Ion Channels in Planar Lipid Bilayers Using a Polymethyl Methacrylate Microfluidic Chip.* Biosensors & Bioelectronics, 2007. **22**: p. 1111-1115.

32. Suzuki, H., et al., *Highly Reproducible Method of Planar Lipid Bilayer Reconstitution in Polymethyl Methacrylate Microfluidic Chip.* Langmuir, 2006. **22**(4): p. 1937-1942.
33. Funakoshi, K., H. Suzuki, and S. Takeuchi. *Lipid Bylayer Formation By Contacting Monolayers*. in *9th International Conference on Miniaturized Systems for Chemistry and Life Sciences*. 2005. Boston Massachusetts.
34. Morgan, H., et al. *Artificial Lipid Bilayers in a Microfabricated System*. in *8th International Conference on Miniaturized Systems for Chemistry and Life Sciences*. 2004. Malmo Sweden.
35. Sandison, M.E. and H. Morgan. *Polymer Microfluidic Devices for the Formation and Investigation of Artificial Bilayer Lipid Membrane (BLM) Systems*. in *9th International Conference on Miniaturized Systems for Chemistry and Life Sciences*. 2005. Boston, Massachusetts.
36. Sandison, M.E. and H. Morgan, *Rapid Fabrication of Polymer Microfluidic Systems for the Production of Artificial Lipid Bilayers.* Journal of Micromechanics and Microengineering, 2005. **15**(7): p. S139-S144.
37. Zagnoni, M., et al. *Controlled Delivery of Calcium Gated MthK Channels into an On-Chip Bilayer Lipid Membrane For Electrophysiology Measurements*. in *10th International Conference on Miniaturized Systems for Chemistry and Life Sciences*. 2006. Tokyo, Japan.
38. de Planque, M.R.R., et al., *Controlled Delivery of Membrane Proteins to Artificial Lipid Bilayers by Nystatin-Ergosterol Modulated Vesicle Fusion.* IEE Proceedings -- Nanobiotechnology, 2006. **153**(2): p. 21-30.
39. Malmstadt, N., et al., *Automated Formation of Lipid-Bilayer Membranes in a Microfluidic Device.* Nanoletters, 2006. **6**(9): p. 1961-65.
40. Malmstadt, N., et al. *Lipid Bilayer Membrane Formation by Solvent Extraction in a Microfluidic Channel*. in *10th International Conference on Miniaturized Systems for Chemistry and Life Sciences*. 2006. Tokyo, Japan.
41. Unger, M., et al., *Monolithic Microfabricated Valves and Pumps by Multilayer Soft Lithography* Science, 2000. **288**: p. 113-116.
42. Studer, V., et al., *Scaling Properties of a Low-Actuation Pressure Microfluidic Valve.* Journal of Applied Physics, 2004. **95**(1): p. 393-398.
43. *The Planar Lipid Bilayer Workstation*. [cited 2007 March 26]; Available from: http://www.harvardapparatus.com/wcsstore/ConsumerDirect/images/site/hai/techdocs/BS4_H_6.pdf.
44. Instruments, W. *Planar Lipid Bilayer Workstation*. [cited 2007 March 26]; Available from: http://www.warneronline.com/product_info.cfm?name=Planar%20Lipid%20Bilayer%20Workstation&id=1094.
45. Sharma, V., et al., *Poloxamer 188 Decreases Susceptibility of Artificial Lipid Membranes to Electroporation.* Biophysical Journal, 1996. **71**(6): p. 3229-3241.
46. Troiano, G.C., et al., *The Reduction in Electroporation Voltages by the Addition of a Surfactant to Planar Lipid Bilayers.* Biophysical Journal, 1998. **75**(2): p. 880-888.

47. Finkelstein, A., *Bilayers: Formation, Measurements, and Incorporation of Components*, in *Methods in Enzymology*, S. Fleischer and L. Packer, Editors. 1974, Academic Press: New York. p. 489-501.
48. *The Port-a-patch NPC-1*. [cited 2007 March 26]; Available from: http://www.nanion.de/pdf/port-a-patch.pdf.
49. *Bilayer Recordings with the Port-a-patch*. [cited 2007 March 26]; Available from: http://www.nanion.de/pdf/NanionNotes5.pdf.
50. Sondermann, M., et al., *High-Resolution Electrophysiology on a Chip: Transient Dynamics of Alamethicin Channel Formation.* Biochimica et Biophysica Acta, 2006. **1758**: p. 545-551.
51. Fertig, N., et al., *Microstructured Glass Chip for Ion-Channel Electrophysiology.* Physical Review E, 2001. **6404**(4): p. 0901.
52. Fertig, N., R.H. Blick, and J.C. Behrends, *Whole Cell Patch Clamp Recording Performed on a Planar Glass Chip.* Biophysical Journal, 2002. **82**(6): p. 3056-3062.
53. Brueggemann, A., et al., *Ion Channel Drug Discovery and Research: The Automated Nano-Patch Clamp Technology.* Current Drug DiscoveryTechnologies, 2004. **1**(1): p. 91-96.
54. Brueggemann, A., et al., *High Quality Ion Channel Analysis on a Chip with the NPC Technology.* ASSAY and Drug Development Technologies, 2003. **1**(5): p. 665-673.
55. *The Patchliner, NPC-16*. [cited 2007 March 26]; Available from: http://www.nanion.de/pdf/patchliner.pdf.
56. *Personal Communication between Joseph Robertson and Author, April 10.* 2007.
57. Cooper, G., *The Cell, A Molecular Approach*. 2nd ed. 2000: ASM Press.
58. Karp, G., *Cell and Molecular Biology, Concepts and Experiments*. 3rd ed. 2002: Wiley and Sons.
59. Pollard, T. and W. Earnshaw, *Cell Biology*. 2002: Saunders.
60. Niles, W.D., R.A. Levis, and F.S. Cohen, *Planar Bilayer-Membranes Made from Phospholipid Monolayers Form by a Thinning Process.* Biophysical Journal, 1988. **53**(3): p. 327-335.
61. *Phosphatidylcholine*. 2006 [cited 2006 June 6]; Available from: http://www.avantilipids.com/SyntheticPhosphatidylcholine.asp.
62. Voet, D., J. Voet, and C. Pratt, *Fundamentals of Biochemistry*. 2001: Wiley.
63. Mueller, P., et al., *Reconstitution of Cell Membrane Structure in Vitro and Its Transformation into an Excitable System.* Nature, 1962. **194**(4832): p. 979
64. Mueller, P., et al., *Reconstitution of Excitable Cell Membrane Structure in Vitro.* Circulation, 1962. **26**(5): p. 1167.
65. Montal, M. and P. Mueller, *Formation of Bimolecular Membranes from Lipid Monolayers and a Study of Their Electrical Properties.* PNAS, 1972. **69**(12): p. 3561-3566.
66. Bezrukov, S., et al., *Dynamics and Free Energy of Polymers Partitioning into a Nanoscale Pore.* Macromolecules, 1996. **29**: p. 8517-8522.

67. Misakian, M. and J.J. Kasianowicz, *Electrostatic Influence on Ion Transport through the Alpha-HL Channel.* Journal of Membrane Biology, 2003. **195**(3): p. 137-146.
68. Misakian, M., et al., *Frequency Response of Alternating Currents through the Staphylococcus Aureus Alpha-Hemolysin Ion Channel.* Bioelectromagnetics, 2001. **22**(7): p. 487-493.
69. Bhakdi, S. and J. Tranumjensen, *Alpha-Toxin of Staphylococcus-Aureus.* Microbiological Reviews, 1991. **55**(4): p. 733-751.
70. Song, L.Z., et al., *Structure of Staphylococcal Alpha-Hemolysin, a Heptameric Transmembrane Pore.* Science, 1996. **274**(5294): p. 1859-1866.
71. Menestrina, G., *Ionic Channels Formed by Staphylococcus-Aureus Alpha-Toxin - Voltage-Dependent Inhibition by Divalent and Trivalent Cations.* Journal of Membrane Biology, 1986. **90**(2): p. 177-190.
72. Bezrukov, S. and J.J. Kasianowicz, *Structure and Dynamics of Confined Polymers*, J.J. Kasianowicz, M. Kellermayer, and D.W. Deamer, Editors. 2002, Kluwer, Dordrecht, Netherlands. p. 117-130.
73. Halverson, K., et al., *Anthrax Biosensor, Protective Antigen Ion Channel Asymmetric Blockade.* Journal of Biological Chemistry, 2005. **280**(40): p. 34056-34062.
74. Polypure. *Moodisperse PEG Derivatives for Advanced Applications*. 2007 [cited April 6 2007]; Available from: http://www.polypure.no//content/view/53/72/.
75. Robertson, J., et al., *Single Molecule Mass Spectrometry in Solution Using a Solitary Nanopore.* Proceedings of the National Academy of Sciences of the United States of America, 2007. **In Press**.
76. *Ion Channel Reconstitution*, ed. C. Miller. 1986, New York: Plenum Press.
77. White, S.H., *Analysis of Torus Surrounding Planar Lipid Bilayer Membranes.* Biophysical Journal, 1972. **12**(4): p. 432-445.
78. Vandenbe.Hj, *A New Technique for Obtaining Thin Lipid Films Separating 2 Aqueous Media.* Journal of Molecular Biology, 1965. **12**(1): p. 290.
79. Tien, H.T., *Black Lipid Membranes in Aqueous Media - Interfacial Free Energy Measurements and Effect of Surfactants on Film Formation and Stability.* Journal of Physical Chemistry, 1967. **71**(11): p. 3395-3401.
80. White, S.H., et al., *Formation of Planar Bilayer Membranes from Lipid Monolayers - Critique.* Biophysical Journal, 1976. **16**(5): p. 481-489.
81. Hanke, W. and W. Schlue, *Planar Lipid Bilayers: Methods and Applications*. Biological Technique Series. 1993, London: Academic Press.
82. Jain, M., *The Bimolecular Lipid Membrane*. 1972, New York: Van Nostrand Reinhold.
83. Korn, E., *Methods in Membrane Biology: Volume 4, Biophysical Approaches*, ed. E. Korn. 1975, New York: Plenum Press.
84. Anrather, D., et al., *Supported Membrane Nanodevices.* Journal of Nanoscience and Nanotechnology, 2004. **4**(1-2): p. 1-22.
85. Lide, D., *Handbook of Chemistry and Physics*. 83rd ed, ed. D. Lide. 2002: CRC.

86. Labs, L.B. *Alpha Toxin from Staphylococcus Aureus*. 2007 [cited 2007 April 8,]; Available from: http://www.listlabs.com/.
87. *Personal Communication between John Kasianowicz and Author, November 21*. 2006.
88. Aksimentiev, A. and K. Schulten, *Imaging Alpha-Hemolysin with Molecular Dynamics: Ionic Conductance, Osmotic Permeability, and the Electrostatic Potential Map.* Biophysical Journal, 2005. **88**(6): p. 3745-3761.
89. Sartori, R. and e. al., *Binding of Electrolytes to Poly(Ethylene Oxide) in Aqueous Solutions.* Macromolecules, 1990. **23**: p. 3878-3881.
90. *Personal Communication between Joseph Robertson and Author, April 12*. 2007.
91. *Personal Communication between Joseph Robertson, John Kasianowicz and Author, April 12*. 2007.
92. Eppendorf. *Eppendorf FemtoJet Microinjectors*. 2007 [cited 2007 April 7,]; Available from: http://www.eppendorfna.com/products/ecet_femtojet_de.asp.
93. Brydson, J., *Plastics Materials*. 7th ed. 1999, Oxford: Butterworth-Heinemann.
94. Sherman-Gold, R., *The Axon Guide for Electrophysiology & Biophysics Laboratory Techniques*. 1993, Axon Instruments.
95. Polk, B.J., et al., *Ag/AgCl Microelectrodes with Improved Stability for Microfluidics.* Sensors and Actuators B-Chemical, 2006. **114**(1): p. 239-247.
96. Geschke, O., H. Klank, and P. Tellemann, *Microsystem Engineering of Lab-on-a-Chip Devices*. 2004: Wiley-VCH.
97. Vig, J., *UV / Ozone Cleaning of Surfaces.* Journal of Vacuum Science Technology A, 1985. **3**(3): p. 1027-1034.
98. *PSD Series UVOzone Cleaning and Sterilization* [cited 2007 April 23]; Available from: http://www.novascan.com/products/psd_uvozone.php.
99. Childs, W., et al., *Masterless Soft Lithography: Patterning UV/Ozone-Induced Adhesion on Poly(dimethylsiloxane) Surfaces.* Langmuir, 2005. **21**: p. 10096-10105.

Bibliography

Abstracts, Conferences, and Journals

Aksimentiev, A. and K. Schulten, *Imaging Alpha-Hemolysin with Molecular Dynamics: Ionic Conductance, Osmotic Permeability, and the Electrostatic Potential Map.* Biophysical Journal, 2005. 88(6): p. 3745-3761.

Anrather, D., et al., *Supported Membrane Nanodevices.* Journal of Nanoscience and Nanotechnology, 2004. 4(1-2): p. 1-22.

Ashkenasy, N., et al., *Recognizing a Single Base in an Individual DNA Strand: A Step Toward DNA Sequencing in Nanopores.* Angewandte Chemie, 2005. 44: p. 1401-1404.

Astier, Y., O. Braha, and H. Bayley, *Toward Single Molecule DNA Sequencing: Direct Identification of Ribonucleoside and Deoxyribonucleoside 5'-Monophosphates by Using an Engineered Protein Nanopore Equipped with a Molecular Adapter.* Journal of American Chemistry Society, 2006. 128: p. 1705-1710.

Bezrukov, S. and J.J. Kasianowicz, *Structure and Dynamics of Confined Polymers*, J.J. Kasianowicz, M. Kellermayer, and D.W. Deamer, Editors. 2002, Kluwer, Dordrecht, Netherlands. p. 117-130.

Bezrukov, S., et al., *Dynamics and Free Energy of Polymers Partitioning into a Nanoscale Pore.* Macromolecules, 1996. 29: p. 8517-8522.

Bhakdi, S. and J. Tranumjensen, *Alpha-Toxin of Staphylococcus-Aureus.* Microbiological Reviews, 1991. 55(4): p. 733-751.

Brueggemann, A., et al., *High Quality Ion Channel Analysis on a Chip with the NPC Technology.* ASSAY and Drug Development Technologies, 2003. 1(5): p. 665-673.

Brueggemann, A., et al., *Ion Channel Drug Discovery and Research: The Automated Nano-Patch Clamp Technology.* Current Drug DiscoveryTechnologies, 2004. 1(1): p. 91-96.

Brydson, J., Plastics Materials. 7th ed. 1999, Oxford: Butterworth-Heinemann.

Chandler, E.L., et al., *Membrane Surface Dynamics of DNA-Threaded Nanopores Revealed by Simultaneous Single-Molecule Optical and Ensemble Electrical Recording.* Langmuir, 2004. 20(3): p. 898-905.

Childs, W., et al., *Masterless Soft Lithography: Patterning UV/Ozone-Induced Adhesion on Poly(dimethylsiloxane) Surfaces.* Langmuir, 2005. 21: p. 10096-10105.

Cooper, G., *The Cell, A Molecular Approach*. 2nd ed. 2000: ASM Press.
de Planque, M.R.R., et al., *Controlled Delivery of Membrane Proteins to Artificial Lipid Bilayers by Nystatin-Ergosterol Modulated Vesicle Fusion.* IEE Proceedings -- Nanobiotechnology, 2006. 153(2): p. 21-30.

Eray, M., et al., *Highly Stable Bilayer-Lipid Membranes (Blms) Formed on Microfabricated Polyimide Apertures.* Biosensors & Bioelectronics, 1994. 9(4-5): p. 343-351.

Fertig, N., et al., *Microstructured Glass Chip for Ion-Channel Electrophysiology.* Physical Review E, 2001. 6404(4): p. 0901.

Fertig, N., R.H. Blick, and J.C. Behrends, *Whole Cell Patch Clamp Recording Performed on a Planar Glass Chip.* Biophysical Journal, 2002. 82(6): p. 3056-3062.

Finkelstein, A., *Bilayers: Formation, Measurements, and Incorporation of Components*, in *Methods in Enzymology*, S. Fleischer and L. Packer, Editors. 1974, Academic Press: New York. p. 489-501.

Funakoshi, K., H. Suzuki, and S. Takeuchi. *Lipid Bylayer Formation By Contacting Monolayers*. in *9th International Conference on Miniaturized Systems for Chemistry and Life Sciences*. 2005. Boston Massachusetts.

Geschke, O., H. Klank, and P. Tellemann, *Microsystem Engineering of Lab-on-a-Chip Devices*. 2004: Wiley-VCH.

Halverson, K., et al., *Anthrax Biosensor, Protective Antigen Ion Channel Asymmetric Blockade.* Journal of Biological Chemistry, 2005. 280(40): p. 34056-34062.

Hanke, W. and W. Schlue, *Planar Lipid Bilayers: Methods and Applications*. Biological Technique Series. 1993, London: Academic Press.

Henrickson, S.E., et al., *Driven DNA Transport into an Asymmetric Nanometer-Scale Pore.* Physical Review Letters, 2000. 85(14): p. 3057-3060.

Howorka, S., et al., *A Protein Pore with a Single Polymer Chain Tethered within the Lumen.* Journal of American Chemistry Society, 2000. 122(11): p. 2411-2416.

Howorka, S., S. Cheley, and H. Bayley, *Sequence-Specific Detection of Individual DNA Strands Using Engineered Nanopores.* Nature Biotechnology, 2001. 19: p. 636-639.

Huang, C., T.E. Thompson, and L. Wheeldon, *Properties of Lipid Bilayer Membranes Separating 2 Aqueous Phases - Formation of Membrane of Simple Composition.* Journal of Molecular Biology, 1964. 8(1): p. 148.

Ion Channel Reconstitution, ed. C. Miller. 1986, New York: Plenum Press.

Jacobson, K., E.D. Sheets, and R. Simson, *Revisiting the Fluid Mosaic Model of Membranes.* Science, 1995. 268(5216): p. 1441-1442.

Jain, M., *The Bimolecular Lipid Membrane*. 1972, New York: Van Nostrand Reinhold.

Karp, G., *Cell and Molecular Biology, Concepts and Experiments*. 3rd ed. 2002: Wiley and Sons.

Kasianowicz, J.J., et al., *Characterization of Individual Polynucleotide Molecules Using a Membrane Channel.* Proceedings of the National Academy of Sciences of the United States of America, 1996. 93(24): p. 13770-13773.

Kasianowicz, J.J., et al., *Simultaneous Multianalyte Detection with a Nanometer-Scale Pore.* Analytical Chemistry, 2001. 73(10): p. 2268-2272.

Kasianowicz, J.J., *Nanopores - Flossing with DNA.* Nature Materials, 2004. 3(6): p. 355-356.

Khulbe, P., M. Mansuripur, and R. Gruener, *DNA Translocation Through Alpha-Hemolysin Nanopores with Potential Application to Macromolecular Data Storage.* Journal of Applied Physics, 2005. 97: p. 1043171-1043176.

Korn, E., *Methods in Membrane Biology: Volume 4, Biophysical Approaches*, ed. E. Korn. 1975, New York: Plenum Press.

Krasilnikov, O., C. Rodrigues, and S. Bezrukov, *Single Polymer Molecules in a Protein Nanopore in the Limit of a Strong Polymer-Pore Attraction.* Physical Review Letters, 2006. 97(1): p. 0183011-4.

Lide, D., *Handbook of Chemistry and Physics*. 83rd ed, ed. D. Lide. 2002: CRC.

Malmstadt, N., et al. *Lipid Bilayer Membrane Formation by Solvent Extraction in a Microfluidic Channel*. in *10th International Conference on Miniaturized Systems for Chemistry and Life Sciences*. 2006. Tokyo, Japan.

Malmstadt, N., et al., *Automated Formation of Lipid-Bilayer Membranes in a Microfluidic Device.* Nanoletters, 2006. 6(9): p. 1961-65.

Mayer, M., et al., *Microfabricated Teflon Membranes for Low-Noise Recordings of Ion Channels in Planar Lipid Bilayers.* Biophysical Journal, 2003. 85(4): p. 2684-2695.

Menestrina, G., *Ionic Channels Formed by Staphylococcus-Aureus Alpha-Toxin – Voltage-Dependent Inhibition by Divalent and Trivalent Cations.* Journal of Membrane Biology, 1986. 90(2): p. 177-190.

Misakian, M. and J.J. Kasianowicz, *Electrostatic Influence on Ion Transport through the Alpha-HL Channel.* Journal of Membrane Biology, 2003. 195(3): p. 137-146.

Misakian, M., et al., *Frequency Response of Alternating Currents through the Staphylococcus Aureus Alpha-Hemolysin Ion Channel.* Bioelectromagnetics, 2001. 22(7): p. 487-493.

Montal, M. and P. Mueller, *Formation of Bimolecular Membranes from Lipid Monolayers and a Study of Their Electrical Properties.* PNAS, 1972. 69(12): p. 3561-3566.

Morgan, H., et al. *Artificial Lipid Bilayers in a Microfabricated System*. in *8th International Conference on Miniaturized Systems for Chemistry and Life Sciences*. 2004. Malmo Sweden.

Movileanu, L. and H. Bayley, *Partitioning of a Polymer into a Nanoscopic Protein Pore Obeys a Simple Scaling Law.* PNAS, 2001. 98(18): p. 10137-10141.

Mueller, P., et al., *Methods for Formation of Single Bimolecular Lipid Membranes in Aqueous Solution.* Journal of Physical Chemistry, 1963. 67(2): p. 534-7.

Mueller, P., et al., *Reconstitution of Cell Membrane Structure in Vitro and Its Transformation into an Excitable System.* Nature, 1962. 194(4832): p. 979.

Mueller, P., et al., *Reconstitution of Excitable Cell Membrane Structure in Vitro.* Circulation, 1962. 26(5): p. 1167.

Murphy, R. and M. Muthukumar, *Threading Synthetic Polyelectrolytes Through Protein Pores.* Journal of Chemical Physics, 2007. 126(5).

Niles, W.D., R.A. Levis, and F.S. Cohen, *Planar Bilayer-Membranes Made from Phospholipid Monolayers Form by a Thinning Process.* Biophysical Journal, 1988. 53(3): p. 327-335.

Polk, B.J., et al., *Ag/AgCl Microelectrodes with Improved Stability for Microfluidics.* Sensors and Actuators B-Chemical, 2006. 114(1): p. 239-247.

Pollard, T. and W. Earnshaw, *Cell Biology*. 2002: Saunders.

Rhee, M. and M. Burns, *Nanopore Sequencing Technology: Research Trends and Applications.* Trends in Biotechnology, 2006. 24(12): p. 580-586.

Robertson, J., et al., *Single Molecule Mass Spectrometry in Solution Using a Solitary Nanopore.* Proceedings of the National Academy of Sciences of the United States of America, 2007. In Press.

Sanchez-Quesada, J., et al., *Single DNA Rotaxanes of a Transmembrane Pore Protein.* Angewandte Chemie, 2004. 43: p. 3063-67.

Sandison, M.E. and H. Morgan, *Rapid Fabrication of Polymer Microfluidic Systems for the Production of Artificial Lipid Bilayers.* Journal of Micromechanics and Microengineering, 2005. 15(7): p. S139-S144.

Sandison, M.E. and H. Morgan. *Polymer Microfluidic Devices for the Formation and Investigation of Artificial Bilayer Lipid Membrane (BLM) Systems*. in *9th International Conference on Miniaturized Systems for Chemistry and Life Sciences*. 2005. Boston, Massachusetts.

Sartori, R. and e. al., *Binding of Electrolytes to Poly(Ethylene Oxide) in Aqueous Solutions.* Macromolecules, 1990. 23: p. 3878-3881.

Sharma, V., et al., *Poloxamer 188 Decreases Susceptibility of Artificial Lipid Membranes to Electroporation.* Biophysical Journal, 1996. 71(6): p. 3229-3241.

Sherman-Gold, R., *The Axon Guide for Electrophysiology & Biophysics Laboratory Techniques*. 1993, Axon Instruments.

Singer, S.J. and G.L. Nicolson, *Fluid Mosaic Model of Structure of Cell-Membranes.* Science, 1972. 175(4023): p. 720-731.

Sondermann, M., et al., *High-Resolution Electrophysiology on a Chip: Transient Dynamics of Alamethicin Channel Formation.* Biochimica et Biophysica Acta, 2006. 1758: p. 545-551.

Song, L.Z., et al., *Structure of Staphylococcal Alpha-Hemolysin, a Heptameric Transmembrane Pore.* Science, 1996. 274(5294): p. 1859-1866.

Studer, V., et al., *Scaling Properties of a Low-Actuation Pressure Microfluidic Valve.* Journal of Applied Physics, 2004. 95(1): p. 393-398.

Sutherland, T.C., et al., *An Analysis of Mismatched Duplex DNA Unzipping Through a Bacterial Nanopore.* Biochemistry and Cell Biology-Biochimie Et Biologie Cellulaire, 2004. 82(3): p. 407-412.

Suzuki, H., et al. *Formation Process of Planar Lipid Bilayer Observed by Confocal Microscopy*. in *Proceedings of the 3rd Annual International IEEE EMBS Special Topic Conference on Microtechnologies in Medicine and Biology*. 2005. Kahuku Oahu Hawaii.

Suzuki, H., et al. *Planar Lipid Bilayer Chip for Electrophysiological Analysis of Membrane Proteins*. in *8th International Conference on Miniaturized Systems for Chemistry and Life Sciences*. 2004. Malmo, Sweden.

Suzuki, H., et al. *Planar Lipid Membrane Array for Membrane Protein Chip*. in *Proceedings of the 17th IEEE International Conference on MEMS*. 2004. Maastrict.

Suzuki, H., et al., *Electrophysiological Recordings of Single Ion Channels in Planar Lipid Bilayers Using a Polymethyl Methacrylate Microfluidic Chip.* Biosensors & Bioelectronics, 2007. 22: p. 1111-1115.

Suzuki, H., et al., *Highly Reproducible Method of Planar Lipid Bilayer Reconstitution in Polymethyl Methacrylate Microfluidic Chip.* Langmuir, 2006. 22(4): p. 1937-1942.

Suzuki, H., et al., *Planar Lipid Bilayer Reconstitution with a Micro-Fluidic System.* Lab on a Chip, 2004. 4(5): p. 502-505.

Tien, H.T. and A.L. Ottova, *From Self-Assembled Bilayer Lipid Membranes (BLMs) to Supported BLMs on Metal and Gel Substrates to Practical Applications.* Colloids and Surfaces a-Physicochemical and Engineering Aspects, 1999. 149(1-3): p. 217-233.

Tien, H.T. and A.L. Ottova, *Supported Planar Lipid Bilayers (s-BLMs) as Electrochemical Biosensors.* Electrochimica Acta, 1998. 43(23): p. 3587-3610.

Tien, H.T., *Black Lipid Membranes in Aqueous Media - Interfacial Free Energy Measurements and Effect of Surfactants on Film Formation and Stability.* Journal of Physical Chemistry, 1967. 71(11): p. 3395-3401.

Troiano, G.C., et al., *The Reduction in Electroporation Voltages by the Addition of a Surfactant to Planar Lipid Bilayers.* Biophysical Journal, 1998. 75(2): p. 880-888.

Unger, M., et al., *Monolithic Microfabricated Valves and Pumps by Multilayer Soft Lithography* Science, 2000. 288: p. 113-116.

Vandenbe.Hj, *A New Technique for Obtaining Thin Lipid Films Separating 2 Aqueous Media.* Journal of Molecular Biology, 1965. 12(1): p. 290.

Vig, J., *UV / Ozone Cleaning of Surfaces.* Journal of Vacuum Science Technology A, 1985. 3(3): p. 1027-1034.

Voet, D., J. Voet, and C. Pratt, *Fundamentals of Biochemistry*. 2001: Wiley.

White, S.H., *Analysis of Torus Surrounding Planar Lipid Bilayer Membranes.* Biophysical Journal, 1972. 12(4): p. 432-445.

White, S.H., et al., *Formation of Planar Bilayer Membranes from Lipid Monolayers – Critique.* Biophysical Journal, 1976. 16(5): p. 481-489.

White, S.H., *Formation of Solvent-Free Black Lipid Bilayer Membranes from Glyceryl Monooleate Dispersed in Squalene.* Biophysical Journal, 1978. 23(3): p. 337-347.

Wonderlin, W.F., A. Finkel, and R.J. French, *Optimizing Planar Lipid Bilayer Single-Channel Recordings for High-Resolution with Rapid VoltageSteps.* Biophysical Journal, 1990. 58(2): p. 289-297.

Zagnoni, M., et al. *Controlled Delivery of Calcium Gated MthK Channels into an On-Chip Bilayer Lipid Membrane For Electrophysiology Measurements*. in *10th International Conference on Miniaturized Systems for Chemistry and Life Sciences*. 2006. Tokyo, Japan.

Verbal Discussions

Personal Communication between John Kasianowicz and Author, November 21. 2006.

Personal Communication between Joseph Robertson and Author, April 10. 2007.

Personal Communication between Joseph Robertson and Author, April 12. 2007.

Personal Communication between Joseph Robertson, John Kasianowicz and Author, April 12. 2007.

Web Resources

"Bilayer Recordings with the Port-a-patch" [cited 2007 March 26]; Available: http://www.nanion.de/pdf/NanionNotes5.pdf.

"Eppendorf. Eppendorf FemtoJet Microinjectors" 2007 [cited 2007 April 7,]; Available: http://www.eppendorfna.com/products/ecet_femtojet_de.asp.

"Instruments, W. Planar Lipid Bilayer Workstation" [cited 2007 March 26]; Available http://www.warneronline.com/product_info.cfm?name=Planar%20Lipid%20Bilayer%20Workstation&id=1094.

"Labs, L.B. Alpha Toxin from Staphylococcus Aureus" 2007 [cited 2007 April 8,]; Available: http://www.listlabs.com/.

"The Patchliner, NPC-16" [cited 2007 March 26]; Available: http://www.nanion.de/pdf/patchliner.pdf.

"Phosphatidylcholine. 2006" [cited 2006 June 6]; Available: http://www.avantilipids.com/SyntheticPhosphatidylcholine.asp.

"The Planar Lipid Bilayer Workstation" [cited 2007 March 26]; Available: http://www.harvardapparatus.com/wcsstore/ConsumerDirect/images/site/hai/techdocs/BS4_H_6.pdf.

"The Port-a-patch NPC-1" [cited 2007 March 26]; Available: http://www.nanion.de/pdf/port-a-patch.pdf.

"Polypure. Moodisperse PEG Derivatives for Advanced Applications 2007" [cited April 6 2007]; Available: http://www.polypure.no//content/view/53/72/.

"PSD Series UVOzone Cleaning and Sterilization" [cited 2007 April 23]; Available: http://www.novascan.com/products/psd_uvozone.php.